



Università Politecnica delle Marche
Corso di Dottorato in Ingegneria Civile, Ambientale, Edile e Architettura
Curriculum in Ingegneria Civile, Ambientale, Edile e Architettura

Experimental and numerical study on the full scale behaviour of micropiles under lateral loading

Ph.D. Dissertation of:
Maria Chiara Capatti

Advisor:

Prof. Luigino Dezi

Curriculum supervisor:

Prof. Stefano Lenci

XXIX cycle

Università Politecnica delle Marche
Dipartimento di Ingegneria Civile, Edile, Architettura
Via Brecce Bianche — 60131 - Ancona, Italy

Acknowledgements

I'd like to express my deep gratitude to *Alseo srlu*, based in Osimo (AN), for having provided the micropiles and the technical support during all the experimental study; the kindness of Marco Valori, who granted the space for the tests, and the tireless efforts of geologists L. Del Maschio and S. Sanchi, are also deeply acknowledged.

The precious reading of the thesis reviewers, Profs. Francesco Silvestri and Daniele Zonta, has been truly appreciated.

I'm sincerely grateful to Francesca Dezi for her guidance throughout those years, and I wish to thank all the staff of department DICEA for the help, the advices and the suggestions provided along the way.

Finally, the most heartfelt acknowledgment is forwarded to my parents, for their constant love, support and encouragement.

Contents

Acknowledgements	iii
Contents.....	v
List of Figures	ix
List of Tables.....	xv
Abstract	1
Sommario	3
Chapter 1. Introduction	5
1.1. Problems Statement	5
1.2. Thesis Objectives.....	9
1.3. Organization of the thesis	9
Chapter 2. Soil Structure Interaction	11
2.1. Introduction	11
2.1.1. Direct approach.....	12
2.1.2. Substructure approach.....	12
2.2. Review of models for Soil Pile Structure Interaction	14
2.2.1. Beam on Elastic Foundation Method.....	14
2.2.2. Elastic Continuum Method	17
2.2.3. Finite Element Method Approach.....	20
2.3. Pile groups effects	21
2.3.1. Approximate methods for the interaction of pile groups.....	21
2.3.2. Pile group complete interaction analysis.....	29
2.3.3. Theoretical and numerical investigation on the dynamic performance of battered piles groups	32
2.4. Numerical studies on micropiles and micropiles groups	33

Chapter 3. Full Scale Tests on Pile and Micropiles.....	35
3.1. Introduction	35
3.2. Full Scale Field Test on Traditional Piles.....	35
3.2.1. Field Lateral Load Test on Single Piles	35
3.2.2. Field Lateral Load Test on Pile Groups	38
3.2.3. Field Dynamic Test on Piles	42
3.3. Previous experimental studies on micropiles.....	50
Chapter 4. Experimental program.....	53
4.1. Introduction	53
4.2. Site Characterization and Field Tests Set Up	54
4.2.1. Geological Description of the Site	54
4.2.2. Geophysical Characterization of the Site	55
4.2.3. Geotechnical Description of the Site.....	55
4.3. Micropiles.....	58
4.4. Instrumentation.....	65
4.4.1. Transducers	65
4.4.2. Signal Conditioners and Data Acquisition System	75
4.5. Ambient Vibration Tests	76
4.6. Impact Load Tests	78
4.7. Two Way Horizontal Cyclic Load Tests	81
4.8. Free Vibration Tests	85
4.9. Forced Vibration Tests	87
Chapter 5. Results.....	91
5.1. Introduction	91
5.2. Single Micropiles.....	97
5.2.1. Ambient vibration tests	97
5.2.2. Impact Load Tests.....	99
5.2.3. Two-way cyclic loading.....	109
5.2.4. Free Vibration Tests.....	117

5.3.	Micropiles group	125
5.3.1.	Ambient vibration Tests.....	125
5.3.2.	Impact Load Tests.....	126
5.3.3.	Forced Vibration Tests.....	130
Chapter 6.	Soil-Micropile Interaction Modelling.....	137
6.1.	Introduction	137
6.2.	Analytical model	137
6.2.1.	Recall on the model	137
6.2.2.	Adaptation of the model for test simulations	148
6.2.3.	Results of impact load tests on single vertical micropiles.....	151
6.2.4.	Results of impact load tests on micropiles group.....	153
6.2.5.	Analytical and experimental impedance functions	154
6.3.	ABAQUS model.....	155
6.3.1.	Linear model	155
6.3.2.	Non linear model.....	163
6.3.3.	Results of numerical simulation of impact load tests.....	166
6.3.4.	Results of numerical simulation of free vibration tests	169
Chapter 7.	Main Conclusions.....	173
References	175
Appendix A.	Experimental Data	189
A.1.	Free Vibration Tests on P1.....	189
A.2.	Free Vibration Tests on P2.....	197
A.3.	Ambient Vibration Test on inclined micropile group.....	205
A.4.	Repetitions of Stepped Sine tests on micropiles group.....	207
A.5.	Repetitions of Stepped Sine tests on micropiles group.....	211

List of Figures

Figure 1-1 Some micropiles configuration types (after Frank, 2006).....	8
Figure 1-2 Damages of battered piles during the 1989 Loma Prieta earthquake: (a) at the port of Oakland; (b) at the port of San Francisco (after SEAOC, 1991).....	8
Figure 1-3 (a) Preferential damage to front batter piles of Rio Banano bridge;	8
Figure 2-1 Dynamic system: a) direct method of analysis with finite-element mesh of soil and artificial boundary and b) substructure unbounded soil with global dynamic stiffness in substructure method of analysis (Wolf, 1994)	13
Figure 2-2 Graphical definition of p and y: (a) elevation of section of pile; (b) earth pressure distribution prior and (c) after to lateral loading; typical family of p-y curves with depth (Reese and Sullivan, 1980)	15
Figure 2-3 (a) Force displacement hysteresis loop and complex p-y curves; (b) Artificial hysteresis loop with a gap (Nogami et al., 1992)	18
Figure 2-3 One and two-dimensional radiation damping models: (a, b) 1-D Model of Berger et al (1977); (c) Plane-strain model of Novak et al. (1974); (d) Plane-strain model of Gazetas and Dobry (1984)	19
Figure 2-4 Pile group unit load transfer method (from Bogard and Matlock, 1983).....	23
Figure 2-5 Vertical and horizontal dynamic pile interaction factors as a function of dimensionless frequency a_0 (from Kaynia and Kausel, 1982).....	24
Figure 2-6 Normalized horizontal and vertical dynamic stiffness and damping of a 4x4 pile group (from Kaynia and Kausel, 1982).....	25
Figure 2-7 Generalized pile head / free-field transfer function I_u for kinematic interaction (Fan et al., 1991).....	26
Figure 2-8 Schematic of three step procedure for computing pile-soil-pile interaction (from Makris and Gazetas, 1992).....	27
Figure 2-10 Substructuring method for seismic soil-pile superstructure interaction analysis (after Gazetas et al., 1993).....	28
Figure 2-11 Cone (a) and double cone (b) models (from Wolf et al., 1994)	29
Figure 3-1 Criteria for predicting p-y curves for (a) short time static loading, (b) equilibrium under initial cyclic loading and (c) reloading after cyclic (Matlock et al., 1970)	37
Figure 3-2 P-y curves developed from static and cyclic lateral load tests on pile in stiff clay (Reese et al., 1975).....	37
Figure 3-3 Field group test results indicating preferential load distribution to leading piles (Holloway et al., 1982).....	41
Figure 3-4 Field pile group load test results depicting; a) cyclic degradation of resistance; b) distribution of load by row (Brown et al., 1987).....	41
Figure 3-5 Dynamic pile response vs frequency (in rpm) from forced vibration tests: a) linear response; b) nonlinear response due to removal of supporting soil near pile head (Petrovski and Jurokovski, 1973)	44
Figure 3-6 Field pile forced vibration test set up (Scott et al., 1982).....	44

Figure 3-7 Field pile forced vibration test and earthquake observation: a) test set up and seismometer arrangement; b) forced vibration tests results illustrating influence of lateral support condition; c) structure to free field transfer function for three backfill cases; d) observed and computed response spectra for seismic event (Kobori et al., 1991)	47
Figure 3-8 Impact load tests (a) and free vibration tests (b) performed by Dezi et al (2012, 2013, 2016) on three near-shore steel pipe piles vibro-driven into soft marine clay	49
Figure 3-9 Four installed micropiles (a) and lateral load test setup (b) in the experimental campaign carried out by Abd Elaziz and El Naggat (2014).....	51
Figure 4-1 Excerpt of the geological map of Osimo (from ISPRA, sheet 293, or. 1:10000)	56
Figure 4-2 (a) Stratigraphic model, (b) V_s profile.....	56
Figure 4-3 Directional velocity spectra and HVSR diagram of the investigated field	57
Figure 4-4 q_c and f_s profile with reference to the portion of soil interested by micropiles..	57
Figure 4-5 Tube a manchètte	59
Figure 4-6 Plan view of the testing field.....	59
Figure 4-7 Insertion of an instrumented micropile into a grouted borehole.....	60
Figure 4-8 Packer for high pressure injections.....	61
Figure 4-9 Execution of high pressure injections.....	61
Figure 4-10 View of micropiles after high pressure injections	62
Figure 4-11 Single vertical micropiles	63
Figure 4-12 Inclined micropiles group.....	64
Figure 4-13 Strain gages disposition on instrumented inclined and vertical micropiles	66
Figure 4-14 a) Adopted strain gages; b) Half bridge configuration.	67
Figure 4-15 Subsequent steps of installation of strain gauges	68
Figure 4-16 Displacement transducers with mechanical supports.....	70
Figure 4-17 Instrumented hammer.....	71
Figure 4-18 a) Hydraulic jack; b) power pack with pressure transducer	72
Figure 4-19 Electro-mechanic vibrodyne.....	72
Figure 4-20 Performance of adopter vibrodyne, equipped with light masses	73
Figure 4-21 (a) Signal conditioner HBM MGC plus; (b) DAQ device NI 9234.....	75
Figure 4-22 Spider8 of HBM.....	75
Figure 4-23 (a) Disposition of accelerometers on P1/P2 for ambient vibration tests; (b) view from the top, during an acquisition.	76
Figure 4-24 Disposition of accelerometers on the group cap for ambient vibration tests ..	77
Figure 4-25 Example of impact load on micropiles group: a) Time History;	78
Figure 4-26 (a) Typical configuration of horizontal impact load test on single micropiles; (b) during a test in the original configuration, and (c) with the pipe extension.	79
Figure 4-27 Disposition of accelerometers on the group cap for impact load tests.....	80
Figure 4-28 Impact configuration on the group cap for impact load tests.....	80
Figure 4-29 Configuration for 2-way cyclic loading on pile P1 and P2.....	82
Figure 4-30 Arrangement for 2-way cyclic loading on P2.....	83
Figure 4-31 Details of the coupling between screwing device and reaction pile during test on P1.....	83
Figure 4-32 Arrangement for 2-way cyclic loading on P1.....	84
Figure 4-33 Details of the coupling between the load cell and pile P1.....	84
Figure 4-34 Calibrated pins adopted for snap back tests, and corresponding tensile failure forced.....	85

Figure 4-35 System adopted for the application of the release on P2.....	86
Figure 4-36 Details: shackle/eyebolt system, calibrated pin, and pile head instrumentation.	86
Figure 4-37 Dynamic force-frequency curves in the vibrodyne configuration.....	88
Figure 4-38 Forced vibration tests: (a) no added mass; (b) with added masses.....	89
Figure 4-39 Acquired instruments (a), and (b) selection of acquired SGs according to different test configuration	89
Figure 5-1 Peak picking method of modal analysis: (a) FRF modulus plot; (b) Resonance detail; (c) Real part of a single mode plot; (d) Imaginary part of single mode plot.....	93
Figure 5-2 Receptance (magnitude and phase plots) for undamped single degree of freedom system	94
Figure 5-3 Plots of real and imaginary parts of FRF for damped SDOF system.....	95
Figure 5-4 Results of ambient vibration tests for (a) injected vertical micropiles, (b) simply grouted vertical micropile, (c) inclined injected micropile, along x and y direction in free head configuration.....	98
Figure 5-5 Results of ILTs for single micropiles in free head configuration along dir x ..	100
Figure 5-6 Results of ILTs for (a) injected micropiles, and (b) simply grouted micropiles, along x and y direction in configuration B.....	101
Figure 5-7 Results of ILTs for P1 at difference depth (strain gage signals)	103
Figure 5-8 Results of ILTs for P2 at difference depth (strain gage signals).....	103
Figure 5-9 First fundamental frequency evaluated from strain gauges signals for	104
Figure 5-10 Damping evaluated from strain gauges signals for P1 (a) and P2 (b).....	104
Figure 5-11 Time histories and Stockwell transform of 3 strain gage signals	105
Figure 5-12 Schematic interpretation of SGs signals during impact load tests	106
Figure 5-13 Normalized values close to the first resonance of (a) curvature (experimental and fitted values); (b) deformed shape for P1 and P2.....	107
Figure 5-14 Experimental impedance functions of single vertical micropiles: real (a) and imaginary (b) parts of P1 and P2	108
Figure 5-15 Derivation of simplified micropile head rotation	109
Figure 5-16 L1, pile head displacement for micropiles P1 and P2 for the monotonic load	110
Figure 5-17 L2, pile head displacement for micropiles P1 and P2 for the monotonic load	110
Figure 5-18 Θ , approximated head rotation for P1 and P2 for the monotonic load.....	110
Figure 5-19 Gap at the end of the first loading cycle on P1	111
Figure 5-20 Strains profile at different loading levels	112
Figure 5-21 L2, pile head displacement for vertical micropiles over cycles.....	114
Figure 5-22 L1 pile head displacement for vertical micropiles over cycles.....	114
Figure 5-23 Θ , micropile head rotation for vertical micropiles over cycles	114
Figure 5-24 Stiffness ratio vs. number of cycles and corresponding degradation parameter (slope of the fitting line in the log-log graph) at increasing displacement step: (a, b) step 1; (c, d) step 2; (e, f) step 3; (g, h) step 4; (i, l) step 5	115
Figure 5-25 Trend of β_s for different values of the ratio y/y_{max} for P1 and P2	116
Figure 5-26 Displacements (a) and acceleration (b) time histories registered during a free vibration tests (F4-T2) on micropile P2; (c) S-Transform of acceleration.....	118
Figure 5-27 Variation with time of local spectrum	119

Figure 5-28 Profile of strains just before the release for the 4 force levels in (a) 1 st series and (b) 2 nd series (pile P1).....	120
Figure 5-29 Profile of strains at the end of the free vibrations test for the 4 force levels in (a) 1 st series and (b) 2 nd series (pile P1).....	121
Figure 5-30 Profile of strains just before the release for the 4 force levels in (a) 1 st series and (b) 2 nd series (pile P2).....	122
Figure 5-31 Profile of strains at the end of the free vibrations test for the 4 force levels in (a) 1 st series and (b) 2 nd series (pile P2).....	123
Figure 5-32 Investigation via ambient vibration tests of the residual dynamic properties after free vibration tests on P1 (x and y axis).....	124
Figure 5-33 Investigation via ambient vibration tests of the residual dynamic properties after free vibration tests on P2 (x and y axis).....	124
Figure 5-34 Results of Ambient Vibration Tests on micropiles group.....	125
Figure 5-35 Results of ILTs on micropiles group: (a) along x and (b) y direction	126
Figure 5-36 Mechanism for undertaking horizontal loading and moment of inertial origin, in vertical and inclined piles groups. Vectors indicate forces imposed by the cap on the piles while dashed lines correspond to the virtual location of the cap if the axial displacements of the piles are ignored.	128
Figure 5-37 Experimental impedance functions of micropiles group: real (a) and imaginary (b) parts along x and y directions.....	129
Figure 5-38 Results of Stepped Sine tests along x axis for increasing value of $K(\alpha)$	131
Figure 5-39 Results of Stepped Sine tests along y axis for increasing value of $K(\alpha)$	131
Figure 5-40 Superficial soil cracks around the pile	132
Figure 5-41 Effect of repetition of the same stepped sine tests ($K(\alpha) = 23.4 \text{ N/Hz}^2$, y axis)	132
Figure 5-42 Results of Stepped Sine tests along x axis for increasing value of in terms of horizontal and vertical accelerations	133
Figure 5-43 Results of Stepped Sine tests along y axis for increasing value of in terms of horizontal and vertical accelerations	133
Figure 5-44 Investigation via impact load tests of the residual dynamic properties after forced vibration tests on micropiles group along x (a) and y (b) direction.....	134
Figure 6-1(a) Pile group with inclined piles; (b) foundation subjected to interaction forces and (c) soil subjected to propagating seismic waves and interaction forces.....	138
Figure 6-2 Displacements at point i due to forces applied at point j	143
Figure 6-3 Pile group model	146
Figure 6-4(a) Schematic representation of the analytical model used to reproduce impact tests and (b) main properties of soil and micropile	150
Figure 6-5 (a) Schematic representation of the analytical model used to reproduce impact tests on the inclined micropile group and (b) main properties of soil and micropiles	150
Figure 6-6 Configuration A: comparison between experimental and analytical results for a impact load in frequency domain (FRF of micropile head acceleration) and time domain (time history) on P1 (a, b) and P2 (c,d).....	151
Figure 6-7 Configuration B: comparison between experimental and analytical results for a impact load in frequency domain (FRF of micropile head acceleration) and time domain (time history) on P1 (a, b) and P2 (c,d).....	152

<i>Figure 6-8 Configuration C: comparison between experimental and analytical deformation profiles at the first fundamental frequency, due to impact load test for P1 (a) and P2 (b)</i>	152
<i>Figure 6-9 Comparison between experimental results of impact load tests on micropiles group and analytical simulation along x (a) and y (b) directions</i>	153
<i>Figure 6-10 Experimental and theoretical impedance functions (real and imaginary parts) for the single vertical micropiles for P1 (a) and P2 (b)</i>	154
<i>Figure 6-11 Experimental and theoretical impedance functions (real and imaginary parts) for the micropiles group along x (a) and y (b) directions</i>	154
<i>Figure 6-12 Schematic view of the 3D FE linear model (a) and main geotechnical properties of soil and micropile (b)</i>	155
<i>Figure 6-13 Relationship between damping ratio and frequency (for Rayleigh damping)</i>	157
<i>Figure 6-14 Schematic view of the model calibrated on impact load tests, and of element used for pile, soil and quiet boundaries</i>	158
<i>Figure 6-15 Infinite Element: a) positioning of the second node; b) examples of an acceptable and an unacceptable two-dimensional infinite element</i>	161
<i>Figure 6-16 Schematic view of the 3D FE nonlinear model (a) and main geotechnical properties of soil and micropile (b)</i>	164
<i>Figure 6-17 Pile domain in non-linear model</i>	164
<i>Figure 6-18 Soil domain in non-linear model</i>	165
<i>Figure 6-19 Contact pressure-clearance relationship for “hard” contact</i>	166
<i>Figure 6-20 Comparison between experimental and simulated FRF of impact load test (a) and corresponding acceleration time history (b) for P1 in configuration A</i>	167
<i>Figure 6-21 Comparison between experimental and simulated FRF of impact load test (a) and corresponding acceleration time history (b) for P1 in configuration B</i>	167
<i>Figure 6-22 Comparison between experimental and simulated strain profile close to resonance at 25 Hz in terms of real component of FRF at increasing depth, for P1</i>	168
<i>Figure 6-23 Subsequent steps of a simulated free vibration test (F1_P1 on micropile P2): (a) initial moments of the loading step; (b) advanced phase of the loading; (c) detail of the detachment between soil and micropile; (d) view from the top of the free vibrations after the release, with double side detachment</i>	170
<i>Figure 6-24 Comparison between numerical and experimental result in terms of displacement registered at the pile head in the quasi static-loading phase</i>	171
<i>Figure 6-25 Comparison between numerical and experimental result in terms of acceleration registered at the pile head after the release</i>	171

List of Tables

<i>Table 4-1 Synthetic scheme of the tests carried out.....</i>	<i>54</i>
<i>Table 4-2 Geotechnical properties of superficial alluvial layer.....</i>	<i>58</i>
<i>Table 4-3 Properties of materials and sections of micropiles</i>	<i>62</i>
<i>Table 4-4 Performance of adopted vibrodyne, equipped with light masses</i>	<i>74</i>
<i>Table 4-5 Stepped sine configuration carried out during forced vibration tests</i>	<i>88</i>
<i>Table 5-1 Fundamental frequencies of single micropiles determined via AVTs.....</i>	<i>99</i>
<i>Table 5-2 Fundamental frequencies and damping of single micropiles</i>	<i>100</i>
<i>Table 5-3 Fundamental frequencies and damping of single micropiles</i>	<i>101</i>
<i>Table 5-4 Fundamental frequencies of P1 and P2 before and after snap back tests.....</i>	<i>124</i>
<i>Table 5-5 Fundamental frequencies and damping of micropiles group via ILTs.....</i>	<i>127</i>
<i>Table 5-6 Fundamental frequencies of micropiles group from stepped sine tests.....</i>	<i>132</i>
<i>Table 5-7 Fundamental frequencies of P1 and P2 before and after snap back tests.....</i>	<i>135</i>

Abstract

Micropiles have been increasingly used in the last decades, both as new foundation system for buildings in seismic zone, and for the retrofit of existing structures damaged by earthquakes. Hence, it is essential to enhance the knowledge of the dynamic behaviour of micropiles under horizontal loading.

Dealing with traditional piles, the topic of soil-pile dynamic interaction is investigated by means of 3-D finite element models or theoretical approaches, whose results are extremely sensitive to many geometrical and mechanical parameters. Results of small and full scale tests are extremely precious to validate and calibrate both theoretical and numerical models. In particular, small-scale tests allow a higher flexibility in the application of dynamic forces, while full-scale in-situ tests have the advantage of accounting for the actual soil behaviour, and for the real boundary and interface conditions. Furthermore, their results represent a keystone for the calibration of numerical models and help in developing new simplified approaches able to represent the true behaviour of the soil-pile system. The available literature on dynamic in-situ tests on deep foundations is limited, and many unresolved questions still remain, such as the behaviour of piles and pile groups under large deformations, and the influence of execution stages and foundation configuration. The latter points are particularly crucial in the case of micropiles, which are often installed with a certain angle of inclination and completed with high pressure injections along the embedded shaft.

Despite their growing use, few results exist of static and cyclic lateral load tests on micropiles, and dynamic field tests data are almost absent; thus, an experimental campaign is carried out, that includes both two single vertical micropiles and a group of 4 inclined micropiles embedded in alluvial soils. One of the vertical micropiles is simply grouted, while the others have been also grouted with high pressure injections throughout valves a-manchèttes placed along the steel core of the shaft. The two vertical micropiles and one of the inclined micropiles are permanently instrumented with strain gages along the shaft; traditional execution steps are modified to allow the installation of strain gauges in laboratory, and the steps of sensors protection, transportation from lab to field, micropiles installation and execution of grouting and high pressure injections are carried out with special care in order to avoid as much as possible damage to strain gages.

Different testing techniques are adopted, to evaluate the dynamic behaviour of the single micropiles and of the micropile group under small to large deformations. In particular, ambient vibration tests, impact load tests and free vibration tests are performed on the vertical micropiles, while ambient vibration tests, impact load tests and forced vibration tests are performed on the group. Moreover, two-way cyclic horizontal load tests are performed on the single vertical micropiles to evaluate the evolution of micropile head horizontal stiffness with the number of cycles, and with the development of phenomena related to non-linearity (among all, the detachment at the interface between the micropile and the soil). Results are presented in terms of fundamental frequencies, damping and modal shapes obtained from accelerometers at the pile head and strain gages permanently

installed along micropiles shaft. Displacements of the micropiles head during cyclic load tests and free vibration tests are also shown. Finally, impedances functions are experimentally derived for both the single micropiles and the group.

The experimental data are then compared with numerical results obtained exploiting different models, properly calibrated: a 3-D approach for the dynamic interaction analysis of vertical and inclined micropile groups proposed by Dezi et al. (2009, 2016), is here adopted to simulate impact load tests on the single micropiles and on the group. Moreover, two 3-D finite element models are developed in a general-purpose Finite Element code, having different properties in terms of soil, pile and interface behaviour, to evaluate the response of micropiles in the linear and nonlinear range, under dynamic horizontal forces.

Keywords: Micropiles, Battered piles, Dynamic Soil-Foundation Interaction, Dynamic Identification Techniques, Soil-Pile Gap

Sommario

Negli ultimi decenni si è assistito ad un crescente utilizzo dei micropali, sia come fondazioni di nuove costruzioni in zona sismica, che per il retrofit di fondazioni danneggiate di edifici esistenti. È dunque essenziale rafforzare la conoscenza del loro comportamento dinamico sotto carichi orizzontali.

Per quanto riguarda i pali tradizionali, il tema dell'interazione dinamica palo-terreno è generalmente investigato per mezzo di modelli 3D agli elementi finiti o tramite approcci teorici, i cui risultati sono estremamente sensibili ai parametri geometrici e meccanici in gioco. I risultati di prove in piccola e grande scala sono dunque assai preziosi per validare e calibrare questi modelli teorici o numerici.

In particolare le prove su prototipi in piccola scala permettono una maggiore flessibilità nell'applicazione del carico dinamico, mentre le prove eseguite in-situ su pali in vera grandezza hanno il vantaggio di tenere in conto il reale comportamento del terreno, e delle effettive condizioni al contorno e all'interfaccia. I loro risultati, oltre ad essere fondamentali per la calibrazione di modelli numerici, possono rappresentare un punto di partenza per lo sviluppo di modelli semplificati che siano in grado di rappresentare il reale comportamento del sistema palo-terreno. Lo stato dell'arte su prove in sito eseguite su fondazioni profonde è limitato e permangono diverse questioni aperte, come il comportamento di pali singoli e in gruppo sotto grandi deformazioni, nonché l'influenza delle modalità esecutive e della configurazione. Gli ultimi due aspetti sono particolarmente importanti per i micropali, che vengono spesso installati con un certo angolo di inclinazione e completati con iniezioni ad alta pressione lungo il fusto.

Nonostante il loro crescente utilizzo, esistono pochi risultati specificatamente riguardanti prove di carico statico e ciclico su micropali, mentre prove di natura dinamica sono sostanzialmente assenti. Per colmare questa lacuna, è stata affrontata una campagna sperimentale che riguarda sia due micropali singoli verticali che un gruppo di quattro micropali inclinati realizzati in un deposito di natura alluvionale.

Uno dei micropali verticali è semplicemente trivellato, mentre gli altri sono stati completati con iniezioni ad alta pressione attraverso valvole di non ritorno posizionate lungo il fusto del micropalo. Entrambi i pali singoli verticali ed uno dei pali inclinati del gruppo sono permanentemente strumentati con estensimetri lungo il fusto; per permettere l'installazione dei sensori in officina, le tradizionali modalità esecutive sono state leggermente modificate e le fasi di protezione degli estensimetri, di trasporto dall'officina al sito, di installazione dei micropali, di getto e di esecuzione delle iniezioni ad alta pressione sono state realizzate con cura estrema per evitare il più possibile il danneggiamento dei sensori.

Nel corso della sperimentazione sono state utilizzate diverse tecniche sperimentali al fine di valutare il comportamento dinamico di micropali singoli ed in gruppo nel campo delle piccole, medie e grandi deformazioni. In particolare sui micropali singoli sono state eseguite prove di vibrazione ambientale, prove di impatto, prove in condizioni di vibrazioni libere. Sul gruppo sono state eseguite prove di vibrazione ambientale, prove di impatto e prove in condizioni di vibrazioni forzate. Inoltre sono state eseguite sui micropali singoli

prove di carico ciclico a doppia via, per valutare l'evoluzione della rigidità orizzontale della testa del palo con il numero di cicli e con il conseguente sviluppo di fenomeni tipicamente non lineari (tra tutti, il distacco all'interfaccia tra micropalo e terreno circostante). I risultati delle prove dinamiche sono presentati in termini di frequenze fondamentali, smorzamento e forme modali ottenute dagli accelerometri sulla testa del palo e dagli estensimetri disposti lungo il fusto. Vengono mostrati anche gli spostamenti della testa dei micropali acquisiti durante le prove di carico ciclico e le prove in condizioni di vibrazioni libere. Infine, vengono proposte le funzioni di impedenza derivate sperimentalmente sia per i micropali verticali che per il gruppo.

I dati sperimentali sono confrontati con i risultati numerici ottenuti da diversi modelli opportunamente calibrati: dapprima l'approccio 3D per l'interazione dinamica cinematica ed inerziale di gruppi di pali verticali o inclinati proposto da Dezi et al. (2009, 2016) è stato utilizzato per simulare le prove di impatto sui micropali singoli verticali e sul gruppo di pali inclinati. Successivamente, con un codice commerciale agli Elementi Finiti, sono stati sviluppati e calibrati due modelli, caratterizzati da diverse caratteristiche in termini di proprietà del terreno, del micropalo e dell'interfaccia micropalo-terreno e che permettessero di stimare il comportamento dei micropali in campo lineare e non lineare sotto forze dinamiche orizzontali.

Keywords: Micropali, Pali Inclinati, Interazione Dinamica Terreno-Fondazione, Tecniche di Identificazione Dinamica, Gap Palo-Terreno

Chapter 1.

Introduction

1.1. Problems Statement

A micropile is a small-diameter (less than 300 mm), drilled and grouted replacement pile, typically reinforced. It is generally 7.5 or more meters in length and 300-1000 kN in load-carrying capacity. Micropiles undoubtedly offer many advantages (FHWA, 2005): firstly, their installation cause minimal disturbance to adjacent structures, soil, and environment, so they can be installed in access-restrictive spaces and in all soil types and ground conditions and where minimal disturbance to the existing structure is permissible; furthermore, since the installation procedure causes minimal vibration and noise and can be used in conditions of low headroom, micropiles are often used to underpin existing structures. Specialized drilling equipment is often required to install the micropiles from within existing basement facilities.

The use of micropiles to strengthen foundations of building dates back to the post war era and the reconstruction of cities in Italy. Since their conception in the 1950's by dr. Fernando Lizzi (Lizzi, 1991), they have been increasingly used for several purposes: generally, they are used as for underpinning of existing foundations, however, recently, they have been frequently adopted for many other applications such as foundation support, soil settlement problems, bearing capacity problems, slope stabilization and deep excavations (Mascardi, 1982; Laefer, 1999; Bruce et al., 1997). Moreover, they have also been exploited for the seismic retrofitting and protection method to new and old structures which have suffered seismic damage (see Pearlman et al., 1993; Taylor et al., 1998; Zelenko et al., 1998; Misra et al., 1999; Juran et al, 2001; Shahrour and Juran, 2004). In the last decades, micropile technology has been evolving significantly, and nowadays it is considered a very attractive solution for the structural and seismic retrofitting of bridges, churches and other ancient cultural heritage and modern structures in many seismic areas.

In Italy, mainly two technologies are adopted for micropiles. The original *palo Radice* or *root pile* is a small diameter, cast in place reinforced drilled pile, commonly designed to achieve a capacity in the range of 100-200kN. Casing fitted with a tungsten bit is drilled into the ground to the full depth of the pile. The drilling fluid (either water or bentonite mud) is injected inside the casing and flows in the annular space between the casing and the soil carrying away soil cuttings. After drilling and placing the reinforcement (a single bar or a small cage) sand cement mortar is pumped by means of a *tramie* pipe from the bottom of the hole, displacing away the drilling fluid. During the withdrawal of the casing, a pressure is applied to the grout, which is typically in the range of 0.3 to 1 MPa (it is limited by the capacity of the soil to maintain a grout-tight seal around the casing during its withdrawal).

Another micropile technology is presently available, sometimes referred to as Tubfix. In this case a steel tube with no return valves (*tube a manchèttes*), is positioned in the hole and the annular space between the tube and the hole wall is filled from the bottom with neat cement grout. A similar grout is injected at a pressure of 2 to 8 MPa using a double packer inside the tube a manchèttes, so that specific horizons can be treated, if necessary, several times. For this reason, Tubfix micropiles are also known as IRS (*Injection Répétitive et Sélective*), while Radice can be classified as IGU (*Injection Globale et Unitaire*). At the end of the injection stage, the steel tube is filled with grout. The load is mainly resisted by the steel tube. Capacity in the range of many hundreds to over 1000 kN may be achieved for Tubfix technology.

Since micropiles are designed not only to bear the ultimate load but even to limit the displacement of a structure, especially when they are used for retrofitting and rehabilitation of existing foundations, it is fundamental for micropile design to predict the complete load-displacement behaviour. The current design practice for micropiles is in fact based upon either the methods developed for large diameter drilled shafts and ground anchors or simplistic interpretation of micropile load tests similar to the approach used for analyzing tieback anchors. However, construction methods, structural characteristics of micropiles as well as soil-micropile interaction phenomena can be significantly different, so that the methods and parameters adopted for drilled shafts and ground anchors are not directly applicable. Hence, some authors performed numerical studies on micropiles under static, cyclic and dynamic lateral loading. On the other hand there are only a limited number of small/full scale experiments on micropiles. A review of those numerical and experimental researches is provided in Chapters 2 and 3, respectively.

A crucial aspect to be considered is that many different configurations can be adopted for micropiles implementation (Figure 1-1): micropiles can be connected vertically, but even in inclined forms around and below the foundations. In fact, by using the same type of equipment used for ground anchor and grouting projects, micropiles can be installed at any angle below the horizontal (battered micropiles). Besides, by adopting a network configuration, micropiles start to behave like tree roots, increasing the overall resistance. Inclined piles are able to resist higher lateral loading by exploiting their axial behaviour but, from the observations of past case histories, the behaviour of inclined large-diameter piles turns out to be ambiguous.

During 1989 Loma Prieta earthquake ($M_w = 6.9$) several port wharfs in which raked piles were used suffered important damages: the Public Container Wharf at the 7th street Terminal in the Port of Oakland was made with square concrete battered piles, and when the fill behind the wharf liquefied the poor tension connection to the deck failed (Figure 1-2a); on the other hand almost all the vertical piles remained undamaged. A similar type of failure was observed in the battered piles supporting the concrete wharf at the nearby Matson terminal, with additional damage to the back row of vertical piles. At the Oakland Outer Harbor Pier 7, the prestressed concrete batter piles failed near or at the connection to the pile cap.

In San Francisco, the Ferry Plaza pier experienced tensile failure at the connection of the deck to the prestressed concrete batter piles, with some of the piles punching the slab. Such failures, in any case, were most probably due to inadequate reinforcement in the top of the piles and to improper connection of piles to their caps (Figure 1-2b).

The Costa Rica earthquake ($M_w = 7.5$) caused severe damages over a wide area, including liquefaction-related collapse of several pile-supported bridges. For instance, the front batter piles of the Rio Banano bridge suffered flexural and shear damage whereas the vertical piles at the rear showed less damage (Figure 1-3a). An analogous type of damage was observed in the inclined piles supporting the abutments of the Rio Viscaya Bridge leading to large rotation and collapse of the deck. Again, the mode of failure of the batter piles suggests that damage resulted from the insufficient design of the pile-to-cap connection (Figure 1-3b).

In 1994 the Northridge earthquake ($M_s = 6.8$) produced a ground surface acceleration causing severe damage to the APL terminal in POLA. Battered piles suffered from pull out and chipping of concrete at the pile caps.

The main reasons mentioned to be real or perceived drawbacks are summarized by Giannakou et al. (2010): the appearance of *parasitic* bending stresses on the piles due to soil settlement after the earthquake or to soil consolidation; the presence of large cyclic forces at the pile cap; the reduction in bending moment capacity due to seismically induced high tensile force; undesirable permanent rotation of the cap when the inclination of the piles is not symmetric; the increased structural shear with respect to buildings on vertical piles, due to the higher stiffness of the system.

In truth, in the very last years, many studies on the seismic response of batter piles and micropiles (Sadek and Shahrour, 2004 and 2006; Gerolymos et al., 2008; Padron et al., 2009; Carbonari et al., 2017) have shown that the response of well designed batter piles not only have a good performance for themselves, but that they can also be beneficial for the structure they support. Furthermore, case histories referring to Maya Wharf in the Kobe 1995 earthquake and the Landing Road Bridge in the Edgumbe, New Zealand 1987 earthquake have highlighted the successful performance of battered piles.

Focusing specifically on micropiles, Bruce et al. (2005) show that *“inclined piles should not be used for transmitting lateral loads to the soil, but if such piles are used, they must be safely designed to carry axial and bending loads.”*, while Sadek and Isam (2004), by means of numerical analyses, proved that *“inclination of micropile improves micropiles performance with respect to seismic loading. The inclination allows a better mobilization of the axial stiffness of micropiles and consequently leads to a decrease in both shearing forces and bending moment induced by seismic loading”*. It is worth remembering that inclined micropiles, if well designed, give very attractive results in reducing liquefaction, while vertical do not (Bruce et al, 2005).

Nonetheless, the use of inclined piles is still not recommended by modern European codes. For instance, French Seismic Code AFPS 1990 states definitely that *“inclined piles should not be used to resist seismic loads”*, while the seismic Eurocode EC8/part 5 states that *“It is recommended that no inclined piles be used for transmitting lateral loads to the soil. If, in any case, such piles are used, they must be designed to carry safely axial as well as bending loading”*. Finally, the Italian code NTC 2008, reports the same limit for the use of inclined piles and add: *“In those cases in which it is necessary to make use of inclined piles, they should be designed to withstand stresses derived from the analysis of soil-foundation system in seismic conditions”*.

An important issue that should receive attention is that most of the studies concerning behaviour of micropiles (vertical or inclined) are essentially linear and thus adequate for the description of small displacements behaviour.

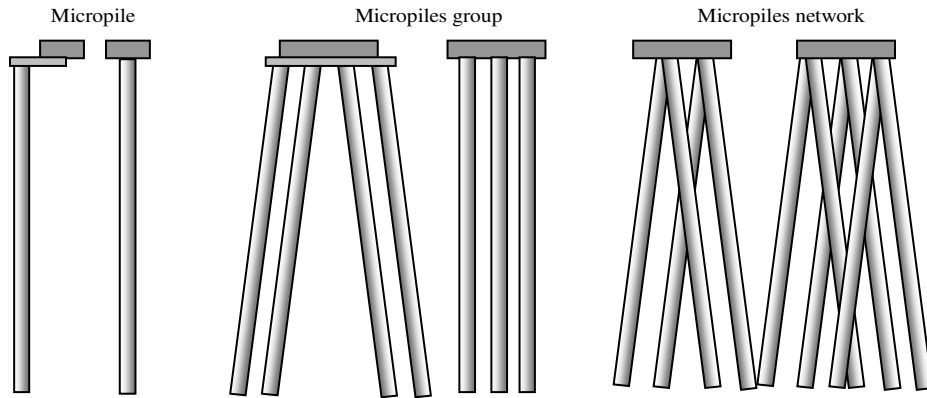


Figure 1-1 Some micropiles configuration types (after Frank, 2006)

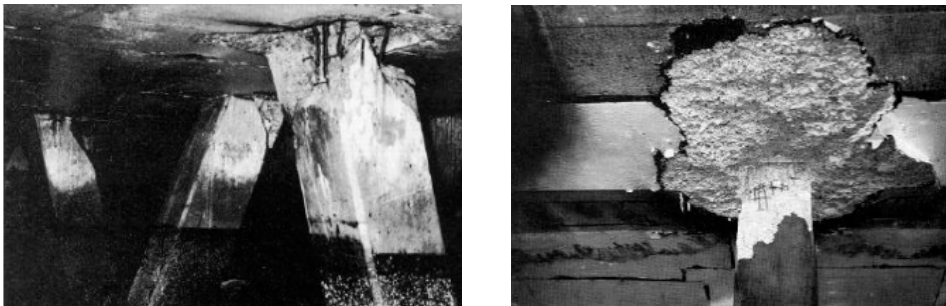


Figure 1-2 Damages of battered piles during the 1989 Loma Prieta earthquake: (a) at the port of Oakland; (b) at the port of San Francisco (after SEAOC, 1991)



Figure 1-3 (a) Preferential damage to front batter piles of Rio Banano bridge; (b) failure of Rio Viscaya Bridge Piles, during the 1991 Costa Rica earthquake (after Priestley et al., 1991)

At larger displacements, micropiles and micropiles group are supposed to behave in a non linear fashion (changing dramatically their dynamic stiffness and damping) because of soil non-linearity at high strain, pile separation (gapping), slippage and friction. Hence, to strengthen the knowledge of the seismic behaviour of vertical and batter micropiles in a wide strains range and to correct misconception often provoked by bad design of such foundation systems, analytical and numerical models, based on experimental data, should be developed and validated.

1.2. Thesis Objectives

This thesis is the result of an experimental investigation carried out on vertical and inclined micropiles. The experimental study proceeded from several needs:

- As already stated, there is a modest number of full scale tests performed directly on micropiles under horizontal loadings, and most of them consider static or cyclic load, while dynamic field tests data are substantially absent. Hence, the first aim of this study is that of point out the influence, on the horizontal dynamic behaviour of micropiles, of the execution techniques and configuration (i.e. high pressure injections, micropiles inclination, and restraint condition at the micropile head).
- Experimental data represent a precious instrument to verify whether numerical and analytical model specifically developed for traditional piles are able to account for the dynamic behaviour of micropiles; in addition they are fundamental to develop new simplified methods.
- The experimental program wants to investigate the system behaviour under different loading conditions (cyclic and dynamic, in the small, medium and very large strains range), in order to point out the characteristics of non linear phenomena interesting the soil-micropile system and the features of cyclic degradation.
- By comparing their dynamic behaviour with that of vertical piles, the research tries to put some light on the dynamic response of inclined piles; results are then compared with those obtained from an existing analytical model developed for inclined piles group.
- Finally, the experimental work hereinafter described comprises several techniques for the dynamic identification of systems, recently adopted in some areas of mechanical and civil engineering. To the author knowledge some of them have never been applied for the investigation of Soil Structure interaction problems, and the results are encouraging.

1.3. Organization of the thesis

In the present chapter, an introduction to the developed themes and the explanation of the objectives of the thesis are provided.

In Chapter 2 the current state of art on Soil Structure interaction is reported, including past numerical and analytical studies on piles and micropiles.

In Chapter 3 a review of the previous experimental campaigns performed on the dynamic behaviour of foundation on piles and pile groups under horizontal loading is presented with

special focus on full-scale field tests. A specific session is dedicated to small and full scale tests on micropiles.

Chapter 4 discusses the experimental program: firstly, the site characterization, based on laboratory and in-situ tests, is reported; then, the instrumentation of piles, carried out with particular care to prevent any damage related to micropile installation and high pressure injection is described. Finally, the different procedures carried out during the two campaigns (ambient vibration, impact load, free vibration, forced vibration and 2-way cyclic load tests) are described.

In Chapter 5 results are reported, with considerations regarding the influence of execution techniques, micropiles inclination, and the development of phenomena related to non linearity in the medium to high strain level tests.

Chapter 6 presents the simulation of the micropile-soil system behaviour by means of different approaches. First of all, an analytical model for the analysis of kinematic and inertial interaction for vertical and inclined piles groups in layered deposits is adopted. Then a 3-D Finite Element model is developed with a commercial general purpose code, and different modelling techniques are employed to investigate the behaviour of micropile-soil system in the linear and non linear field. Comparisons between numerical and experimental results are discussed.

Finally, Chapter 7 collects the main observations prompted out by this research.

Chapter 2.

Soil Structure Interaction

2.1. Introduction

The aim of a Soil Structure Interaction (SSI) analysis is to investigate the dynamic response of a structure interacting with the soil, and subjected to a time varying-load or to a dynamic excitation introduced through the soil (due, for example, to seismic waves). The dynamic behaviour of the structure cannot be studied independently of the wave propagation into the soil since, when the wave reaches the structure, part of it is scattered away, part of it is stored in the structure, and then it is re-injected in the soil or dissipated. The relevance of the study of SSI effects is straightforward for many fields of interest. For instance, when the dynamic motion is of seismic nature, the interaction between the structure and the soil foundation produces a modification (in terms of amplitude, frequency content and duration) of the seismic input at the base of the structure with respect to the free field motion (i.e. the motion far from any building). This modification produces the lengthening of the fundamental period of the structure and an increase of overall damping so that neglecting SSI effects is often assumed to be conservative; unfortunately, local seismic effects in conjunction with SSI may be detrimental for the seismic performance of certain structures (because of resonance effects, for instance), so that the perception of conservative design assumption is not always truthful (Mylonakys and Gazetas 2000); some of the modern seismic codes (Eurocode EC8, Italian NTC 2008) have recognized that under certain conditions SSI may significantly affect the seismic response of structure and suggest accounting for the flexibility of the soil foundation system in the superstructure design. The determination of SSI effects is also considered extremely important within the energy field and particularly for the offshore wind market. The actual trend is in fact to develop wind farms with higher capacity generators and in deeper waters, challenging the current offshore design procedures and involving the choice of adequate support structures for offshore wind turbines. In the design of offshore wind support structures fatigue derived from combined wind and wave loading is one of the critical issues. The potential of structural resonance with dynamic forces due to wind loading would result in large amplitude stresses and subsequent accelerated fatigue. For this reason, in practice, the wind turbine support structure is designed by setting the tower fundamental resonance between the blade passing and the rotor frequency. In addition, the overall damping of the structure has an important impact on the fatigue damage, since the amplitude of vibrations at resonance is inversely proportional to the damping ratios (Devriendt et al., 2012).

Effects of SSI have been extensively studied by many researchers. A general introduction can be found in Wolf (Wolf, 1985), where the soil is considered linear or linear equivalent and the SSI problem is treated in the frequency domain. This approach is often adopted since it allows a resolution in terms of superposition of simpler problems, but for strong motion excitation soil exhibit strongly inelastic behaviour, which is hardly estimated with a linear viscoelastic approximation. The full consideration of the non-linear character of the soil has to be performed in the time domain, as described by Wolf (1988). Concerning seismic problems, Kausel (1974) pointed out the necessity to consider not only the deformations of the soil due to the inertia forces in the structure (axial forces, base shear and overturning moment), but also the effect of a rigid foundation on a train of travelling seismic waves, that filters out high frequency components of the translational motions and generates rotational motions (in general rocking and torsion). Whitman introduced the terms inertial and kinematic interaction to distinguish these two types of effects. Later researchers confirmed the potential importance of kinematic interaction effects, especially for embedded foundations. Furthermore, Prof. J.P. Wolf (1985, 1994, and 2004) exhaustively dealt with the problem of dynamic SSI, identifying the main features of SSI in the increase of flexibility and effective damping (both due to energy radiation and material hysteresis) of the global system, in variation between foundation input motions and free-field ground motions and, finally, foundations deformations.

Methods that can be used to evaluate the above effects can be divided into direct and substructures approaches. In the former, the soil, the foundation system, and the structure are included into the same global model and analysed together, while in a substructure approach the SSI problem is separated into distinct parts, then combined to formulate the complete solution.

2.1.1. Direct approach

The direct approach provides the complete solution and represents the best way to perform 3D non-linear analyses in time domain. The entire system can be modelled in the direct approach with Finite Element Methods (FEM), Boundary Elements method (BEM) or mixed BEM-FEM approaches. In FEM models the far field domain is also explicitly modelled by means of artificial boundary that must be introduced to model the infinite (Figure 2-1), and that should include specific formulation to approximate the boundary conditions, avoiding the reflections of the outwardly propagating waves. The radiation conditions must be formulated on the artificial boundary that further assumes the role of transmitting boundary. Among other formulation of transmitting boundaries, the most known are the ones of Lysmer and Kuhlemeyer (1969), and Kausel (1988). The direct method can be performed also by separating the phase of estimation of the free-field motion (ground response analysis) from the phase of analysis of the whole structure-pile-soil system (i.e. when Beam on Linear on Non Linear Winkler Foundation method is used for the analysis).

2.1.2. Substructure approach

In the substructure method, the artificial boundary can be chosen to coincide with the structure soil-interface as shown in Figure 2-1b so that the two substructures, a bounded domain (consisting of the structure) and an unbounded domain (the soil extending to

infinity), can be modelled independently. The bounded domain can be modelled by means of the Finite Element method, with the possibility of including non-linear relation; on the other hand, the unbounded domain must be regular (i.e. a layered half space) and linear. Under such conditions analytical solutions that satisfy exactly the radiation condition formulated at infinity may be calculated. With these fundamental solutions (Green's functions) a boundary-integral equation can be formulated, called the boundary-element method in discretized form, to calculate the interaction force-displacement relationship in the nodes located on the structure-soil interface. This dynamic stiffness, global in space and time, represents the rigorous boundary condition able to model the unbounded soil. The force-displacement relationships of the soil together with the discretized equations of motion of the structure represent the final system of equations of the total dynamic system. The substructure method thus permits each substructure to be analysed by the best suited computational technique.

According to the substructure approach, two distinct analyses have to be performed: the kinematic interaction analysis (performed in the soil-foundation sub domain) and inertial interaction analysis (in the structural sub-domain). Under the condition of linear behaviour, analyses are performed in the frequency domain, since properties of the soil are frequency dependent. As a result, the generalized motion experienced by the structure, traditionally known as Foundation Input Motion (FIM), as well as the dynamic impedance function (i.e. the complex valued force-displacement relationship at the interface) are determined. Then Inertial interaction analysis of the structure on compliant base (due to impedance functions) and subjected to FIM at the base, can be performed. Combination of these two responses provides the response of the system.

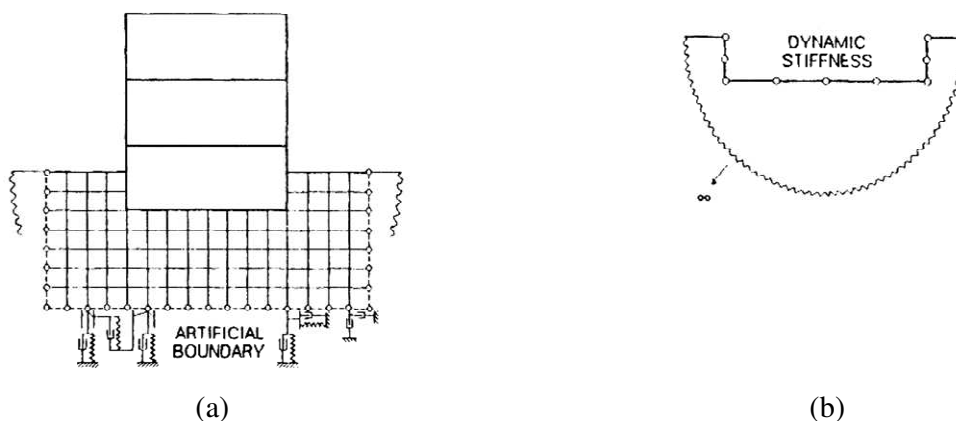


Figure 2-1 Dynamic system: a) direct method of analysis with finite-element mesh of soil and artificial boundary and b) substructure unbounded soil with global dynamic stiffness in substructure method of analysis (Wolf, 1994)

2.2. Review of models for Soil Pile Structure Interaction

A review of analytical methods for the evaluation of soil-pile-structure interaction under lateral loads is presented in the following section. As described by Poulos and Davis (1980) and Fleming et al. (1992), there are three major approaches for the load-deflection prediction of laterally loaded piles; these will be discussed hereinafter.

2.2.1. Beam on Elastic Foundation Method

By accepting Winkler's foundation assumption that each layer of soil responds independently to adjacent layers, a beam and a discrete springs system may be adopted to model a pile under lateral loading. Despite the fact that this assumption ignores the shear transfer between layers of soil, it is a popular and effective method for static and dynamic lateral pile response analyses. It consists in discretizing the soil-pile contact into a number of points where combinations of springs and dashpots represent the soil-pile stiffness and damping at each particular layer. These soil-pile springs may be linear elastic or non-linear; p-y curves typically used to model non-linear soil-pile stiffness have been empirically derived from field tests (Figure 2-2). In advanced applications, capabilities for soil-pile gapping, cyclic degradation, and rate dependency are also provided. A singular disadvantage of a beam-on-Winkler-foundation model is the two-dimensional simplification of the soil-pile contact, which ignores the radial and three-dimensional components of interaction. Exploiting the Baranov assumption, likely the extension of the well-known Winkler model to dynamic loading, transient excitations may be also analysed. Actually, for dynamic loadings, "free-field" soil acceleration time histories are usually computed in a separate site response analysis, double integrated to obtain displacement time histories, and then externally applied to the soil-pile springs.

Dezi et al. (2010) proposed a static equivalent approach to estimate the maximum kinematic interaction effects on piles subjected to lateral seismic excitation. Closed-form expressions are reported for the evaluation of the maximum free-field soil movements and for the computation of maximum pile shear force and bending moments. Firstly, modal analysis, combined with a suitable damped response spectrum, is used to evaluate the maximum free-field response. Secondly, the pile is schematised as a Winkler's beam subjected to equivalent static forces defined according to soil vibration modal shapes and amplitude. The method may be applied by using response spectra suggested by National Standards or those obtained with accelerograms. The procedure proposed may be conveniently implemented in simple spreadsheets or in commercial finite element programs and easily used by practicing engineers. Method accuracy is demonstrated by comparing the results with those obtained with a more rigorous model. Good results may be achieved by considering only the first soil vibration mode making the procedure straightforward for practical design purposes. Among other models dealing with non-linear Winkler models (BNWF), the approaches of Nogami (1992) and Allotey and El Naggar (2008) are here recalled.

Nogami and coworkers developed a time-domain analysis focusing on a nonlinear zone around each pile under dynamic loading using p-y curves.

This was done using a pre-estimation factor to account for plastic deformations and opening of a gap at the pile-soil border. They also accounted for the group effect and the wave propagation away from the pile by introducing a far field element of three units in series, where each one has a spring and dashpot.

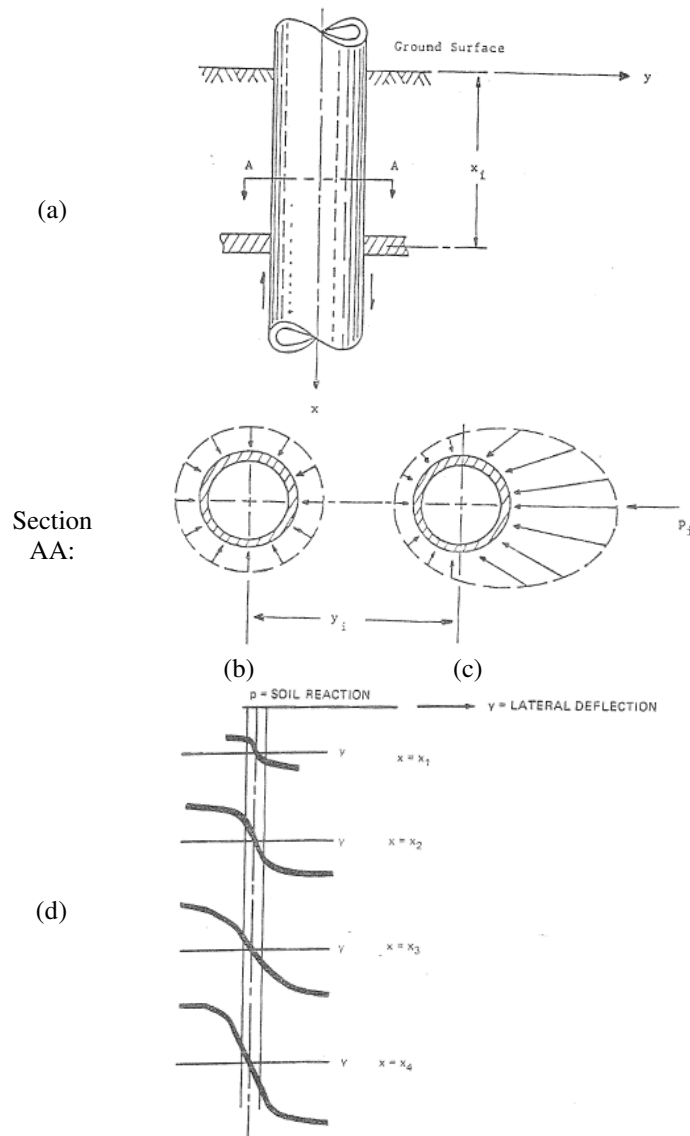


Figure 2-2 Graphical definition of p and y : (a) elevation of section of pile; (b) earth pressure distribution prior and (c) after to lateral loading; typical family of p - y curves with depth (Reese and Sullivan, 1980)

The near-field element accounts for the nonlinear soil behaviour in the vicinity of the pile shaft and the far-field element reproduces the elastic behaviour of the soil outside the region of strong nonlinear behaviour. Figure 2-3 shows a schematic view of the soil model proposed for the nonlinear sub-grade behaviour with near-field and far field element model. Years later, Allotey and El Nagggar (2008) developed a versatile dynamic BNWF model for the analysis of shallow and deep foundations. It is based on a degrading polygonal hysteretic model encompassing multilinear backbone curve with defined rules for loading, reloading and unloading. It accounts for cyclic soil degradation through simulating unloading-reloading behaviour, it can simulate gap formation and closing along the soil-pile interface for cohesive soils and reloading in the slack zone (by means of a strain-hardening curve) for cohesionless soils. In addition to cyclic soil degradation/hardening, the model can handle a reduced radiation damping due to increased soil non-linearity. The model is shown to be capable of representing various response features observed in SSI experiments. In addition, the predictions of the model for centrifuge tests of piles in weakening and partially weakening soil are shown to be in good agreement with the experimental results. The model has been developed as a stand-alone module then incorporated in commercial nonlinear structural analysis software SEISMOSTRUCT. Exploiting this module, Tombari et al (2013), evaluated the effect of soil non linearity and ground motion duration on the seismic response of bridge structures supported on extended pile shafts by performing Incremental Dynamic Analysis (IDA) in a two-step uncoupled procedure accounting for both site response and Soil-Pile-Structure interaction effects. In the 1st step, the free-field displacements within the soil deposit along the pile are defined by means of a linear-equivalent site response analysis. In the 2nd step, a fully-coupled SPSI analysis was performed using the BNWF model developed by Allotey and El Nagggar. The relevance of non-linear effects is investigated by comparing results with those obtained with a linear-equivalent model for SPSI.

Dealing with inclined piles, Carbonari et al (2016) presented an analytical model, based on the beam-on-dynamic Winkler foundation approach, for the evaluation of impedances and kinematic response of single inclined piles. The pile is modelled as an Euler-Bernoulli beam having a generic inclination and the soil-pile interaction is captured by defining soil impedances according to expressions available in the literature for viscoelastic layers undergoing harmonic vibrations of a rigid disk. The coupled flexural and axial behaviour of the pile is governed by a system of partial differential equations, with the relevant boundary conditions, that is solved analytically in terms of exponential matrices. The solution for piles embedded in layered soils is achieved according to the direct stiffness approach by using the analytical solutions derived for generic pile sections embedded in homogeneous soils. Expressions of both the soil-foundation impedance functions and the foundation input motion are derived. Some applications, including comparisons of results with those obtained from rigorous boundary element formulations, are performed to evaluate the model capabilities. Classical stiffness and damping coefficients, based on the propagation of shear and pressure waves in plane-strain condition, are used in the applications to account for the soil-pile interaction; anyway, different formulations can be easily implemented.

2.2.2. Elastic Continuum Method

The representation of the soil as a homogeneous elastic continuum has also been proposed for the analysis of the soil-pile interaction. The elastic continuum analytical method is based on Mindlin's (1936) closed form solution for the horizontal displacement caused by a horizontal point load within the interior of a semi-infinite elastic-isotropic homogeneous mass. The accuracy of these solutions is directly related to the evaluation of the Young's modulus and the other elastic parameters of the soil. Since Mindlin's solutions become singular when evaluating the displacement corresponding to the point where the load is located, integral solutions over a predefined area, representing a fraction of the pile surface, are used. These solutions are generally known as Green's Functions, and define the displacement field due to an assumed loading system (pattern) associated with the pile-soil interaction. This approach is limited in the sense that non-linear soil-pile behaviour is difficult to incorporate (the equivalent linear method is available), and it is more appropriately applied for small strains, steady state vibration problems. In addition, layered soil profiles cannot be accommodated, and only solutions for constant, linearly increasing, and parabolically increasing soil modulus with depth have been derived. True continuum models do have the advantage of intrinsically modelling the effects of radiation damping, namely the loss of energy in the soil-pile system due to out-going stress waves that travel from pile-soil interface to infinity, whereas discrete models must artificially simulate this energy dissipation mode.

Among other authors working on the elastic continuum approach, Berger et al. (1977) proposed a simplified approach, assuming that the pile cross section (that moves horizontally) only generates one dimensional (1D) P-waves travelling in the direction of shaking, and 1D SH waves travelling perpendicular to the pile (Figure 2-4a, b).

In 1974, Novak published the first of many papers dealing with pile dynamics, where he adopted a plane strain, complex transmitting boundary adjacent to the pile for solution of pile stiffness and damping coefficients. Novak presented an approximate continuum approach to account for soil-pile interaction assuming the soil to be composed by a set of independent horizontal layers of infinitesimal thickness, which extend to infinity. As each plane is considered independent, this model may be viewed as a generalized Winkler model. The planes are homogeneous, isotropic, and linearly elastic, and are considered to be in a plane strain state (the plane strain condition is equivalent to incorporating the Winkler assumption into the continuum model). Using Baranov's solution for the horizontal soil reaction to a rigid circular disc with harmonic horizontal displacement (representing a pile cross section), Novak formulated the differential equation of the damped pile in horizontal vibration (Figure 2-4c). He found the steady-state (particular) solution for harmonic motion induced through pile ends, and used this solution to find the dynamic stiffness of the pile head for different boundary conditions.

Gazetas and Dobry (1984) derived a method for substructuring the seismic soil-pile-structure problem into kinematic and inertial components from a parametric finite element study based on the work of Blaney et al. (1976). They proposed a simplified model for the evaluation of the radiation damping by assuming that compression-extension waves propagate in the two quarter planes along the direction of shaking, and that SH-waves propagate in the two quarters perpendicular to the direction of shaking (Figure 2-4d). For

the inertial interaction component, they described the pile head dynamic stiffness by a complex valued impedance function. The case of constant, linearly varying, and parabolically varying soil modulus were studied for single piles subjected to vertically propagating shear waves. The authors also considered the problem of dynamic pile response in layered soil profiles and described a method whereby static pile head stiffness was “corrected” to account for profiling, and the overall damping value was obtained from a weighted average of dashpot coefficients developed along the length of the pile. They also included a discussion of radiation damping models and proposed a simplified plane strain version. This model for radiation damping emanating from a laterally oscillating pile consisted of zones of waves travelling at the soil shear wave velocity V_s , and at Lysmer’s analogue velocity V_{La} . The authors made the important note that at frequencies less than the natural frequency (precisely the *cut off* frequency) of the system, there is no radiation damping. Gazetas (1991) made a complete survey of foundation vibration problems and included detailed design charts and equations for direct computation of pile head lateral and axial stiffness and damping coefficients in soil profiles characterized by constant, linearly varying, and parabolically varying soil modulus with depth.

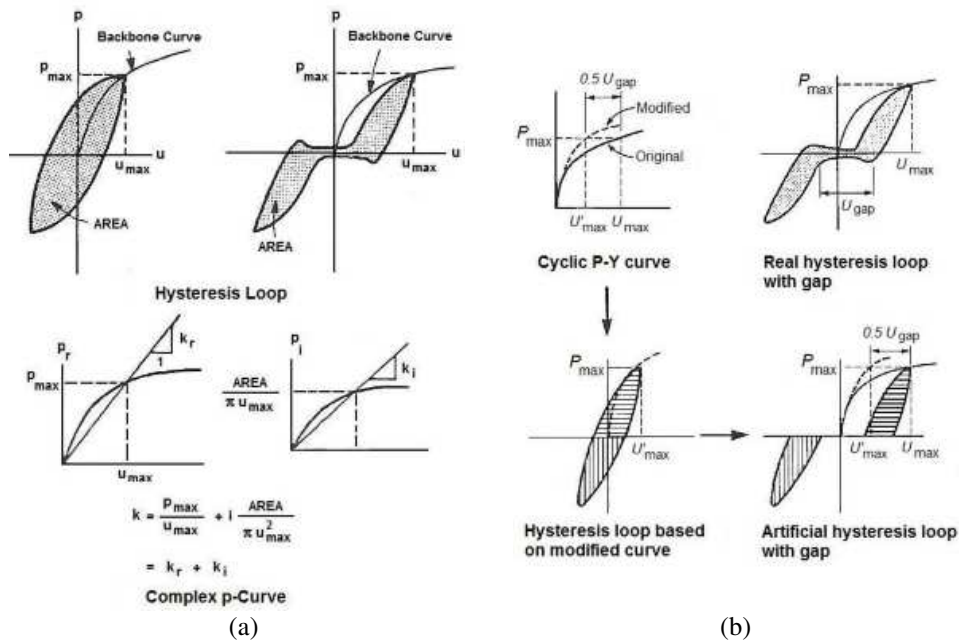


Figure 2-3 (a) Force displacement hysteresis loop and complex p-y curves; (b) Artificial hysteresis loop with a gap (Nogami et al., 1992)

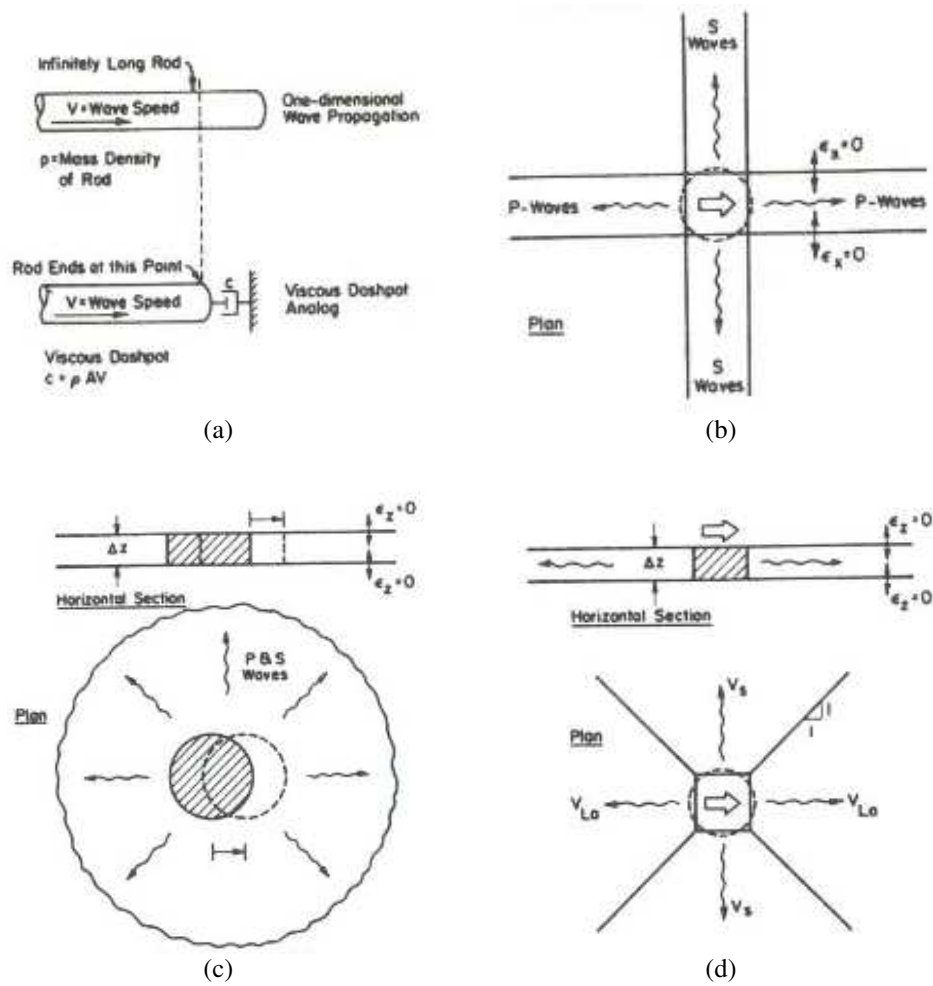


Figure 2-4 One and two-dimensional radiation damping models: (a, b) 1-D Model of Berger et al (1977); (c) Plane-strain model of Novak et al. (1974); (d) Plane-strain model of Gazetas and Dobry (1984)

2.2.3. Finite Element Method Approach

The finite element method potentially provides the most powerful means for conducting soil-pile-structure analyses, but it has not yet been fully realized as a practical tool. The advantages of a finite element approach include the capability of performing the soil-pile-structure analysis of pile groups in a fully-coupled manner, without resorting to independent calculations of site or superstructure response, or application of pile group interaction factors. It is of course possible to model any arbitrary soil profile, and to study 3D effects. Challenges to successful implementation of this technique lie in providing appropriate soil constitutive models that can model small to very large strain behaviour, rate dependency, degradation of resistance, and still prove practical for use. Special features to account for pile installation effects and soil-pile gapping should also be implemented.

Yegian and Wright (1973) implemented a finite element analysis with a radial soil-pile interface element that described the non-linear lateral pile response of single piles and pairs of piles to static loading. Blaney et al. (1976) used a finite element formulation with a consistent boundary matrix to represent the free-field, subjected to both pile head and seismic base excitations, and derived dynamic pile stiffness coefficients as a function of dimensionless frequency. Kuhlemeyer (1979a) offered efficient static and dynamic solutions for lateral soil-pile elastic response; Kuhlemeyer (1979b) used a finite element model of dynamic axially loaded piles to verify Novak's (1977) solution and a simplified method presented by the author. Angelides and Roesset (1981) extended Blaney's work with an equivalent linearization scheme to model non-linear soil-pile response. Randolph (1981) derived simplified expressions for the response of single piles and groups from a finite element parametric study. Dobry et al. (1982) made a parametric study of the dynamic response of head loaded single piles in uniform soil using Blaney's method and proposed revised pile stiffness and damping coefficients as a function of pile and soil Young's modulus. Lewis and Gonzalez (1985) compared field test results of drilled piers to a 3 D finite element study that included non-linear soil response and soil-pile gapping. Trochanis et al. (1988) investigated non-linear monotonic and cyclic soil-pile response in both lateral and axial modes with a 3 D finite element model of single and pairs of piles, incorporating slippage and gapping at the soil-pile interface. They deduced a simplified model accommodating pile head loading only. Koojiman (1989) described a quasi-3 D finite element model that substructured the soil-pile mesh into independent layers with a Winkler type assumption. Brown et al. (1987) obtained p-y curves from 3 D finite element simulations that showed only fair comparison to field observations. Wong et al. (1989) modelled soil-drilled shaft interaction with a specially developed 3-D thin layer interface element. Wu and Finn (1997a, b) presented a quasi-3-D finite element formulation with relaxed boundary conditions that permitted the dynamic elastic analysis of pile groups in the frequency domain and the dynamic non-linear analysis of pile groups in the time domain, showing a good comparison to more rigorous techniques, but at reduced computational cost.

2.3. Pile groups effects

The results of single soil-pile interaction analyses need to be extended to reflect the behaviour of pile group configurations. If piles are arrayed in groups with large pile-to-pile spacing (greater than 6 up to 8 pile diameters), pile group interaction effects are normally ignored for static loading. However, this may be an inaccurate approach for dynamically loaded piles, as much of the pile group interaction effects arise from wave energy reflected between neighbouring piles, which does not attenuate as rapidly as static loading pile group interaction. Pile group dynamic response is also a function of the loading; many of the group analysis methods that will be described address small strain elastic response, and few researchers have investigated non-linear pile group interaction. There is evidence however to suggest that pile group effects lessen with increasing soil-pile non-linearity, which inhibits wave energy transmission between piles.

The response of a pile group subjected to lateral loading and overturning moment is governed by the following main components:

- group rotation, inducing axial tensile/compressive forces, most severe at end piles;
- group translation and relative pile translations;
- individual pile head rotations at pile to cap connections;
- individual pile deflections and consequent bending moments.
- loading: static, cyclic, or dynamic; transient or steady state;
- relative soil-pile stiffness (more flexible piles experience greater interaction);
- group geometry, including individual pile cross sections and group spacing;
- head fixity, idealized as free head or fixed head, but in actuality an intermediate case;
- tip condition, either floating or end-bearing;
- superstructure mass and flexibility, which impart inertial loads to the pile group;
- pile cap embedment depth, stiffness and damping characteristics

The objectives of conducting a pile group analysis are to determine the following:

- pile group and individual pile deflections;
- individual pile head shear forces and moment distributions;
- impedance of the pile group;
- modifications to the input ground motion for superstructure analysis.

The state of the art is substantially divided into methods that derive quantities relevant for the pile group from those obtained for a single pile (i.e. by means of pile group dynamic interaction factors), and methods exploiting complete pile groups interaction analyses.

2.3.1. Approximate methods for the interaction of pile groups

Poulos (1971a,b) introduced the concept of pile group interaction factors. He used Mindlin's elasticity equations to solve for static stresses and displacements between pairs of piles due to horizontal point loads applied in an elastic half space. Poulos described interaction factors as the ratio between the displacement (rotation) of a pile due to an adjacent one and the displacement (rotation) of the pile itself subjected to its own loading.

He presented charts of factors for both fixed and free head piles subject to lateral and moment loadings as functions of pile flexibility, pile spacing, pile diameter, pile length, and departure angle (angle between piles and direction of loading). Analysis of groups was accomplished by superposition, calculating each pile's interaction with all other piles in the group, and ignoring the presence of intervening piles. Subsequently, his method has proved to underestimate pile group interaction at small pile spacings and overestimate interaction at large spacings. Poulos elaborated this method to include soil limit pressures, soil-pile axial slip, variation of soil modulus with depth, and batter piles in the computer code DEFPIG (Poulos, 1980). Randolph and Poulos (1982) presented a simplified flexibility matrix method for pile group response based on Poulos' axial interaction factors and Randolph's (1981) lateral interaction factors. In Poulos and Randolph (1983), these two methods are compared. Randolph (1986) also issued the pile group analysis program PIGLET, based on parametric finite element analyses.

Focht and Koch (1973) combined Poulos' elastic interaction factors with non-linear p-y analysis in a hybrid model to predict group deflections and shear load distributions. They conceived of pile group interaction to consist of two components, non-linear soil response close to the piles, and an elastic component at intermediate ranges between piles. The analysis procedure consisted of first computing a single pile mudline deflection from conventional p-y analysis, then computing a Poulos interaction factor-derived deflection at the mudline, the latter based on a low stress level in the soil. Individual pile deflections and shear forces were then estimated from integrating the plastic and elastic deformations, and the total group response was solved for. The variations of deflection and moment with depth on individual piles were then constructed from conventional p-y data modified by factors, accounting for the elastic components of interaction. The authors recognized the uncertainty in selecting values of soil modulus for elastic interaction, but it has proven to be a viable tool for pile group analysis under static and cyclic loading.

Bogard and Matlock (1983) introduced the modified unit transfer load method, which developed p-y curves for group piles by considering an imaginary pile with a diameter equal to the pile group diameter. As shown in Figure 2-5 the group pile p-y curve is constructed by summing the single pile deflection with the pile group soil mass deflection at a given soil pressure. This method was developed for static and cyclic loadings of a circular pile group in soft clay, and its extension to other group geometries and conditions is unproven.

O'Neill and Dunnavant (1985) surveyed static laterally loaded pile group interaction analyses, and compared the hind cast performance of four methods against a database of 16 pile group load tests. The methods evaluated included the Focht-Koch hybrid analysis, the Bogard-Matlock modified unit load transfer method, a plane strain interaction procedure, and the PILGP2R hybrid method, proposed by the authors. The plane strain interaction procedure consisted of analyzing stresses and displacements in an elastic layer produced by the displacement of a rigid embedded disk. Overall, the study showed the PILGP2R model to provide the best estimates of average behaviour of group piles, of initial group lateral stiffness, and load distribution, but it was found to under predict deflections and moments at high load levels.

Brown et al. (1987) performed cyclic lateral load tests on 3x3 pile groups in stiff clay and sand, and proposed the concept of p-multipliers to account for group effects. The p-multipliers are reduction factors applied to the p-y relationship computed for an individual

pile of the group. These reduction factors are a function of pile spacing and orientation to loading, and are implemented in the pile group analysis program GROUP (Reese et al., 1984).

Kaynia and Kausel (1982) derived dynamic interaction factors for floating pile group interaction analysis by combining a numerical integration for the evaluation of the influence coefficients with an analytical solution for the pile stiffness and flexibility matrices. This boundary element formulation computed Green's functions from imposed barrel and disk loads in a homogeneous soil medium, and used a consistent stiffness matrix to account for the far field. Their interaction factors were presented as complex-valued frequency dependent ratios of the dynamic displacement of pile i to the static displacement of pile j , due to a unit harmonic load on pile j . Vertical and horizontal interaction factors are shown in Figure 2-6 as a function of dimensionless frequency a_0 ($\equiv \omega d/V_s$, being ω the angular frequency, d the pile diameter, and V_s the shear wave velocity of the soil), demonstrating positive and negative group efficiencies (i.e. the horizontal - or vertical - displacement of pile 2 due to horizontal - or vertical - on pile 1).

Normalized dynamic stiffness and damping of a pile group for different spacing is shown in Figure 2-7, indicating the strong frequency dependence of dynamic group response. They also derived expressions for the distribution of forces over the pile group, which was shown to vary from static loading force distributions. Other important conclusions from this study were that the superposition technique is valid for dynamic pile group solutions (in homogeneous soil), pile groups are less influenced by near-surface ground conditions than isolated piles, group interaction effects are stronger for softer soil, and radiation damping increases with foundation size.

Sanchez-Saliner (1983) investigated single pile and pile group dynamic response. Using as indices the stiffness coefficients at the pile head predicted for static or dynamic axial and lateral loads, he compared the values computed by the methods of Poulos (1971), Penzien (1964), Kuhlemeyer (1979), Novak (1974), Blaney et al. (1976), and Novak and Nogami (1977).

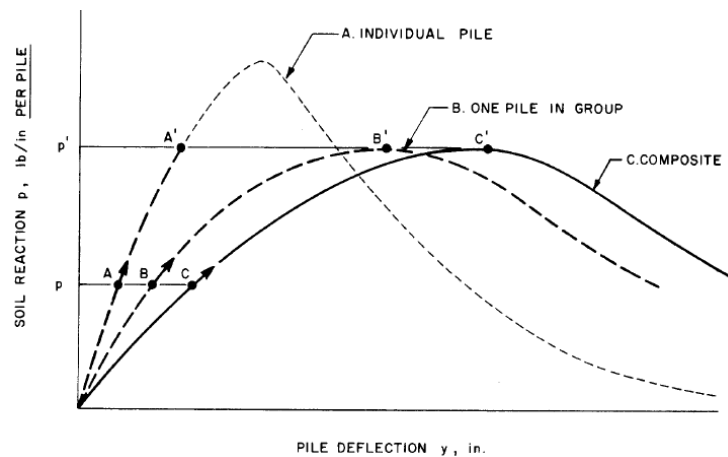


Figure 2-5 Pile group unit load transfer method (from Bogard and Matlock, 1983)

$$\frac{L}{d} = 15; \quad \frac{E_s}{E_p} = 10^{-3}; \quad \frac{\rho_s}{\rho_p} = 0.7$$

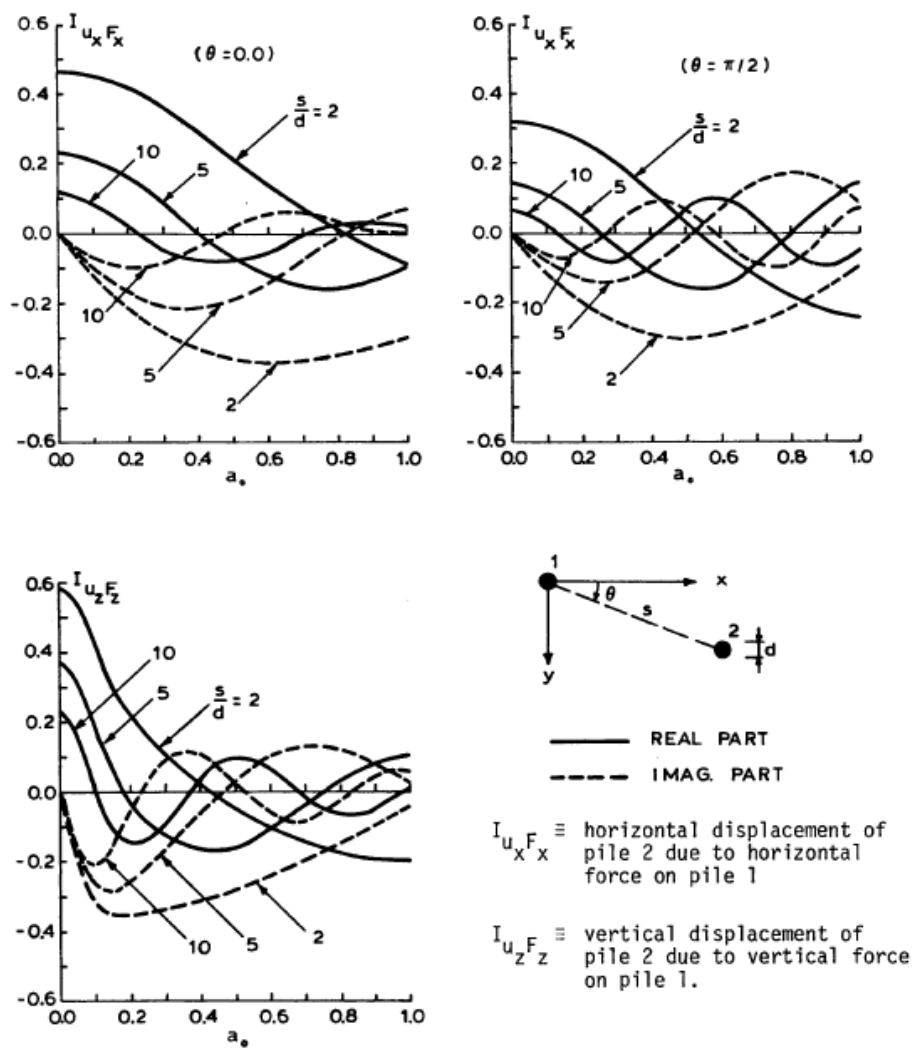


Figure 2-6 Vertical and horizontal dynamic pile interaction factors as a function of dimensionless frequency a_0 (from Kaynia and Kausel, 1982)

3x3 PILE GROUPS, FIXED-HEAD PILES

$$\frac{L}{d} = 15; \quad \frac{E_s}{E_p} = 10^{-3}; \quad \frac{\rho_s}{\rho_p} = 0.7$$

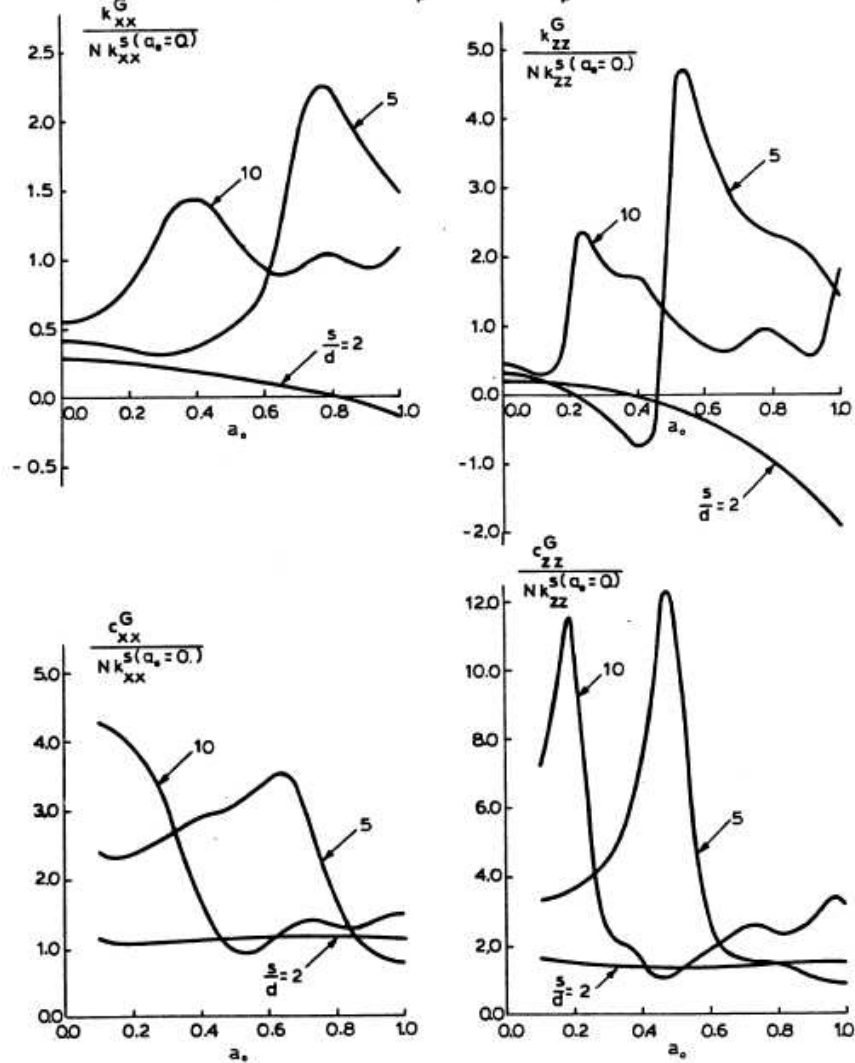


Figure 2-7 Normalized horizontal and vertical dynamic stiffness and damping of a 4x4 pile group (from Kaynia and Kausel, 1982)

For static lateral loads, Poulos' method was found to give lower stiffnesses and Kuhlemeyer's approach was found to give higher stiffnesses, with the other methods yielding similar intermediate values. For dynamic loads, Novak's Winkler assumption produced results comparable to Blaney's more sophisticated formulation. Sanchez-Salintero therefore extended the Winkler concept to an elasto-dynamic boundary element formulation for developing pile group interaction factors.

He contrasted point and disk pile approximations, and verified the validity of the superposition technique. The strong frequency dependence of pile group stiffness coefficients was noted, with the author concluding that the effects of soil non-linearity on pile group response may significantly affect the results.

Dobry and Gazetas (1988) presented a simplified method for calculating dynamic pile interaction factors in homogeneous soil by assuming that cylindrical wave propagation governs vibration of source piles and displacement of neighbouring piles. Fan and Gazetas (1991) studied pile group kinematic interaction effects, and as shown in Figure 2-8, the generalized pile head to free-field transfer function illustrates the pile group effect in filtering out high frequency components of motion. They found that pile group configuration and spacing have little influence on kinematic response, as pile head fixity and relative soil-pile stiffness play a stronger role.

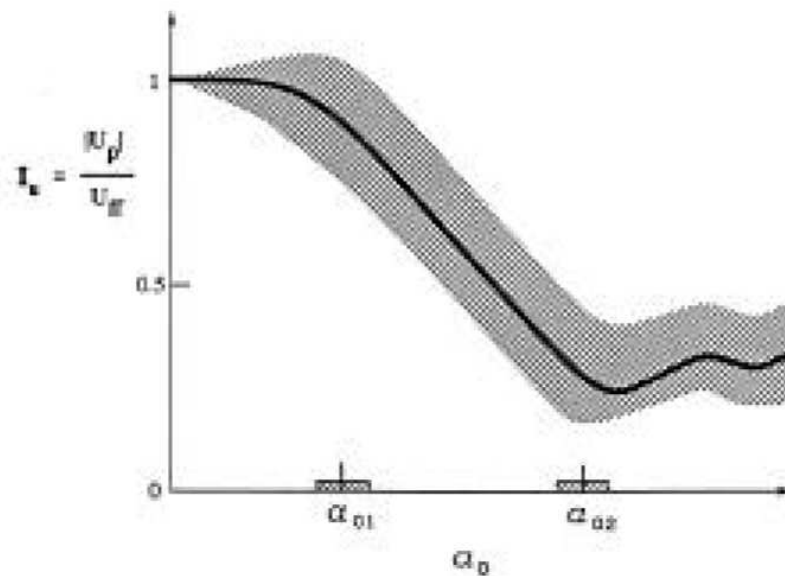


Figure 2-8 Generalized pile head / free-field transfer function I_u for kinematic interaction (Fan et al., 1991)

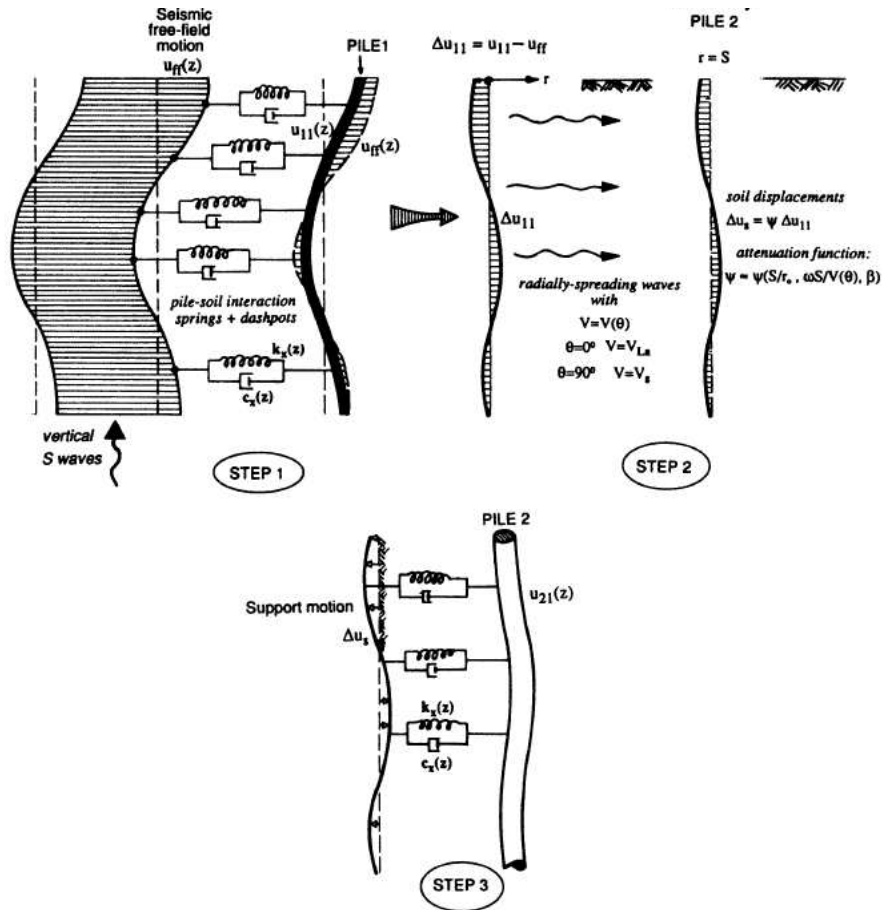


Figure 2-9 Schematic of three step procedure for computing pile-soil-pile interaction (from Makris and Gazetas, 1992)

Gazetas and Makris (1991) and Makris and Gazetas (1992) developed simplified methods of analysis for pile group axial and lateral dynamic response, respectively (Figure 2-9). Using a dynamic Winkler model, they found pile group effects to be more pronounced for inertial than kinematic loading.

The substructuring approach unifying the kinematic and inertial analyses is described in Gazetas et al. (1992), and is shown schematically in Figure 2-10. Mylonakis et al. (1997) applied this substructuring approach in an equivalent linear method to analyze pile supported bridge piers.

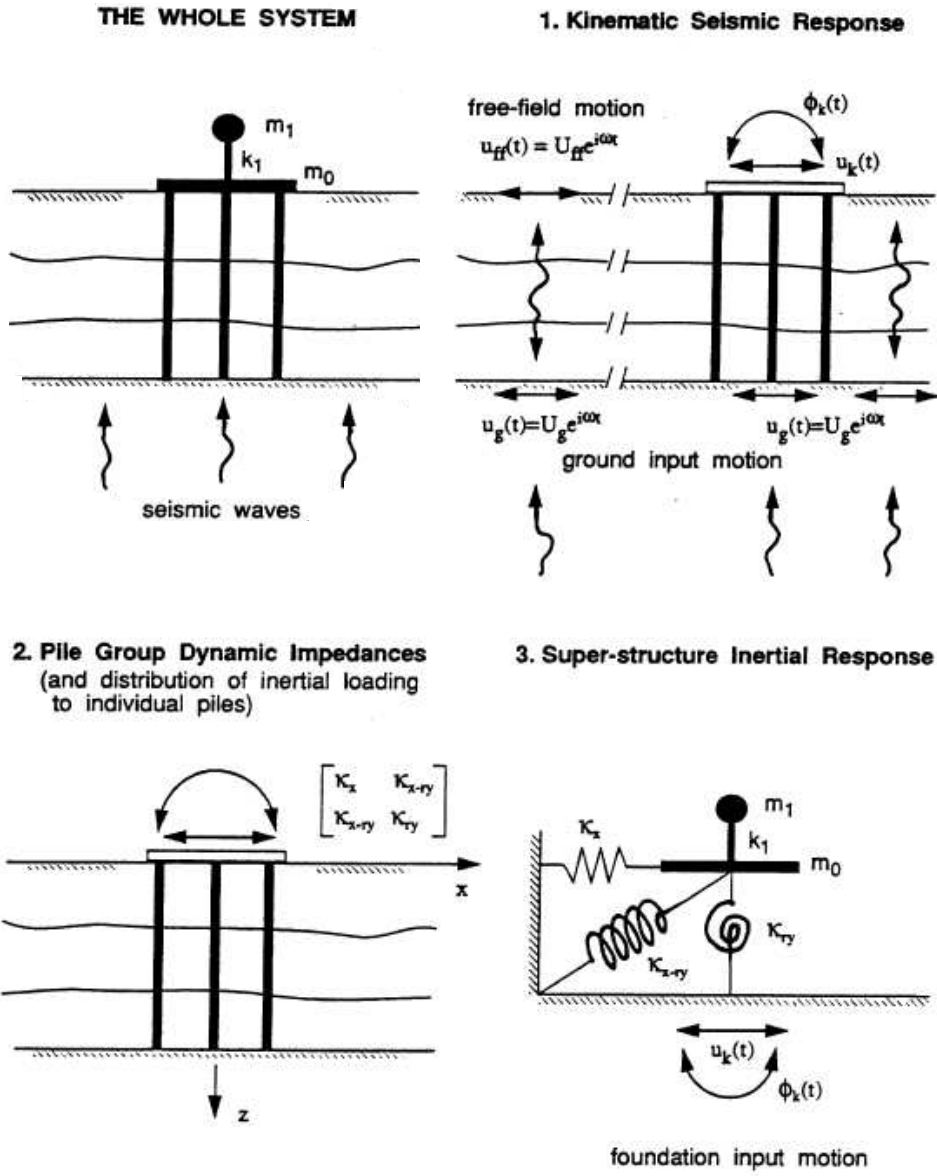


Figure 2-10 Substructuring method for seismic soil-pile superstructure interaction analysis (after Gazetas et al., 1993)

2.3.2. Pile group complete interaction analysis

Wolf and von Arx (1978) generalized the solution of Blaney et al. (1976) to publish the first pile group complete dynamic response analysis method. They considered a horizontally layered visco-elastic soil deposit with piles of equal diameter and length, either floating or end-bearing, in any group configuration. They used an axisymmetric finite element model to calculate the Green's functions producing the displacements at any point in the soil mass given a ring load applied at a discrete layer. The Green's functions were then used to compute the flexibility matrix of the soil at each frequency, and the dynamic stiffness matrix of the complete system was then assembled. The results displayed strong dependence on frequency, number of piles, and pile spacing. Wolf detailed procedures for calculating the dynamic stiffnesses of groups of battered piles.

Most recently, Wolf et al. (1992) described simplified but reasonably accurate cone models for single pile and pile group dynamic response. The cone model (Figure 2-11 a) is a simple physical representation of the unbounded soil in a dynamic soil-structure interaction analysis. Wolf has rearranged and extended the concept of the cone model (from Ehlers, 1942) to cover a complete range of dynamic excitations and physical situations. For each degree of freedom of the foundation, an equivalent rigid massless disk on the surface of a homogeneous half space is considered. The half space below the disk is modeled as a truncated semi-infinite cone with the same material properties: mass density, ρ , shear modulus, G , and Poisson's ratio, ν . The opening angle of the cone follows from equating the static-stiffness coefficient K of the cone to the closed-form solution of the disk on a half space. Wolf et al. (1993), expanded the concepts of the cone model to the analysis of pile foundations. In particular, a double cone model (Figure 2-11 b) is introduced to represent a disk in the interior of a homogeneous full space. The only change consists in doubling the static stiffness coefficient K of the disk. The double cone's displacement field defines approximate Green's function for use in a matrix formulation of structural mechanics. Wolf and Meek (1994) used the double cone model to determine the complex dynamic-stiffness matrix of a single layer. Cairo et al. (1999), adopted the double cone model to evaluate the impedance function of a pile embedded in a soil layer resting on rigid rock, and to analyze the pile group behavior.

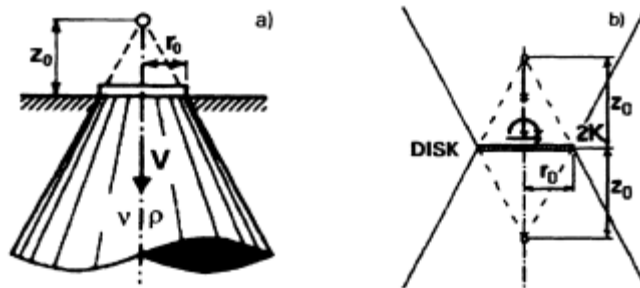


Figure 2-11 Cone (a) and double cone (b) models (from Wolf et al., 1994)

Kagawa (1983) used elastic wave propagation to compute soil displacements and reactions between pairs of piles for the derivation of pile group stiffness and damping coefficients. Both vertical and lateral interactions were considered, as well as pile head fixity condition. These values were found to be dependent on pile spacing, departure angle, and frequency. Dynamic pile group impedance efficiencies both in excess of and less than one were calculated.

Sheta and Novak (1982) investigated the effects of soil non-linearity on pile group axial dynamic response by means of including a cylindrical weak zone surrounding floating or end-bearing individual piles. El Sharnouby and Novak (1984) described a method of analysis of pile group interaction under static axial and lateral loading that yielded interaction factors, and was found to compare reasonably well with other accepted analyses. Mitwally and Novak (1987) presented complex, frequency dependent interaction factors for dynamic pile group response of offshore structures, with the recommendation that the equivalent linear method be employed to simulate non-linear soil-pile response. The authors evaluated the effects of including pile group interaction effects on the response of a pile-supported platform subjected to wave loading. El-Marsafawi et al. (1992) derived pile group dynamic interaction factors from a boundary integral formulation for floating and end-bearing piles in homogeneous or non-homogeneous soil deposits. They also verified the applicability of the superposition approach for the conditions studied, with some limitations. A set of translation, rotation, rototraslation coupling, fixed head, and vertical interaction factors were described in terms of amplitude and phase angle, a more convenient form for interpolation than real and imaginary stiffness terms. The authors concluded that the superposition method worked well except for cases of vertical response of stiff end-bearing piles, and the high frequency range for non-homogeneous soils.

El Naggar and Novak (1994a) described a non-linear model for dynamic axial pile response that consisted of a slip zone, an inner field, and an outer domain that simulated a variety of field test results with great success. El Naggar and Novak (1994b) presented chart solutions for pile group interaction factors derived from this model. Most recently, El Naggar and Novak (1995) described a dynamic non-linear time-domain Winkler soil-pile interaction model that allowed for both axial and lateral pile group response. The axial model consisted of a linear outer region and a non-linear inner field connected to the pile by a plastic slider allowing for soil-pile slip. The lateral response mode also consisted of inner and outer fields with formulations by Novak and Aboul-Ella (1978) and Novak and Sheta (1980) but with the addition of a directional gapping model. Interpile springs were used to model lateral and axial pile group effects. They found that non-linear foundation response is more pronounced for non-homogeneous soil profiles than homogeneous ones, and that the non-linear foundation behaviour decreases the structural damping ratio, but this is more than offset by the increase in foundation damping. They also concluded that dynamic pile group effects increase foundation damping, significantly for linear conditions, but to a lesser extent for non-linear conditions.

Nogami (1979) presented solutions for the dynamic axial response of pile groups in homogeneous soil profiles. Nogami and Konagi (1987) studied non-linear pile group axial response by incorporating slip at the soil-pile interface in a dynamic Winkler model. They found this non-linearity to reduce wave interference effects and suppress the frequency dependence of dynamic group response.

In addition to studying pile group interaction under static loading, Banerjee and co-workers have also investigated on pile group dynamic interaction effects. Banerjee and Davies (1980) compared the results of method of analysis for pile groups with b.e. formulation with the field data obtained from static load tests. Banerjee and Sen (1987) reported on boundary element formulations for pile group dynamic response. They also investigated the effects of a ground contacting massless pile cap, and found a marginal increase in pile head impedance of small floating pile groups, most pronounced for the damping component.

Makris and Badoni (1995b) followed their earlier work with a simplified method for analysis for pile groups subject to obliquely incident shear and Rayleigh waves, with spring and dashpot coefficients evaluated from the techniques described in Makris and Gazetas (1992). The method consisted of computing the difference between single “source” piles and free-field response, and propagating it to neighbouring “receiver” piles. By superposition, the pile group displacement, rotation, and individual pile head forces were obtained, incorporating both kinematic and inertial sources of loading. The results from this approximate method were found to compare very favourably to methods of Banerjee, and of Kaynia and Novak (1992).

Dezi et al. (2009) proposed a numerical model for the 3D kinematic interaction analysis of pile groups in layered soils. The numerical model is derived discretizing piles and soil in the vertical direction by considering a formal finite-element procedure based on the Lagrange-D’Alembert principle. The pile group is modelled by means of beam finite elements and the soil is assumed to be a horizontally layered half space. Both the piles and soil are considered to behave linearly. The pile-soil-pile interaction is taken into account in the frequency domain by considering the elastodynamic Green’s functions that make it possible to express the mutual interactions between all the piles of the group and the radiation problem consistently, without using the stepwise analysis generally adopted in the technical literature. The presence of a rigid cap is accounted for by constraining the displacements of the pile heads. This allows obtaining the impedances of the pile group and the motion at the cap necessary to study the inertial interaction with the superstructure in a straightforward manner. In particular, the procedure makes it possible to calculate all the components of the impedance matrix including the rocking-translation coupling.

Dezi and Poulos (2016) described kinematic seismic interaction analysis of square pile groups in homogeneous soil deposits, focusing on bending moments induced by the transient motion. Analyses were performed by means of a three-dimensional (3D) numerical procedure able to account for both pile-soil-pile interaction and radiation damping. The seismic motion was defined by an artificial accelerogram at the outcropping bedrock, and one-dimensional (1D) propagation analyses were performed to define the free-field motion within the deposits. An extensive parametric study was conducted to determine the effects of different variables, such as the soil properties, the bedrock location, the number of piles, and the pile spacing, on the dynamic response of pile-group foundations. Bending moments obtained from the analyses of the pile group, both at the pile head and at the interface separating soil layers, were normalized with respect to the single-pile bending moments, allowing for the proposal of a new design formula for the estimation of the kinematic bending moments in the most stressed pile of the group, starting from the knowledge of the single-pile response. The proposed formula was used, in conjunction with some simplified approaches that allow estimation of the single-pile

response, to evaluate bending moments in the analyzed pile groups. The adequacy of the formula for design purposes is also demonstrated.

2.3.3. Theoretical and numerical investigation on the dynamic performance of battered piles groups

Not a large amount of works focused on behaviour of inclined piles. Among others, Gerolymos et al. (2008) and Giannakou et al. (2010) reported proofs of beneficial role of inclined piles in visco-elastic soils by means of 3D FEM model. Padron (2010) obtained impedance functions of deep foundations with inclined piles, from a boundary element–finite element coupling model. More precisely, vertical, horizontal, rocking and horizontal–rocking crossed dynamic stiffness and damping functions of single inclined piles and 2×2 and 3×3 pile groups were presented, considering a homogeneous viscoelastic isotropic half-space, piles modelled as elastic compressible Euler–Bernoulli beams, and different configurations and inclinations for piles and piles group.

Dezi et al. (2015) proposed a numerical model for the dynamic analysis of pile groups with inclined piles in horizontally layered soil deposits. Piles are modelled with Euler-Bernoulli beams while the soil is supposed to be constituted by independent infinite viscoelastic horizontal layers. The pile-soil-pile interaction as well as the hysteretic and geometric damping is taken into account by means of two-dimensional elastodynamic Green's functions. Piles cap is considered by introducing a rigid constraint; the condensation of the problem permits a consistent derivation of both the dynamic impedance matrix of the soil-foundation system and the foundation input motion. These quantities are those used to perform inertial soil-structure interaction analyses in the framework of the substructure approach. Furthermore, the model allows evaluating the kinematic stress resultants in piles resulting from waves propagating in the soil deposit, taking into account the pile-soil-pile interactions. The model validation is carried out by performing accuracy analyses and comparing results in terms of dynamic impedance functions, kinematic response parameters and pile stress resultants, with those furnished by 3D refined finite element models. To this purpose, classical elastodynamic solutions are adopted to define the soil-pile interaction problem. The model results in low computational demands without significant loss of precision, compared with more rigorous approaches or refined finite element models.

The model was adopted by Carbonari et al. (2017) to investigate the seismic response of bridge piers founded on inclined pile groups in different soil deposits, evaluating effects of soil-structure interaction induced by different pile group geometries and piles inclinations. The significance of kinematic stress resultants in piles, the foundation filtering effect and the rotational component of the input motion due to the coupled roto-translational behaviour of the soil-foundation system are also investigated; to this purpose kinematic interaction analyses are performed and compared with results of complete soil-foundation structure analyses. These analyses revealed essential for the understanding of the general phenomena governing the dynamic response of the whole soil-foundation-superstructure systems. Results of numerical investigations highlight that conventional design approaches suggested by codes do not provide reliable predictions of the superstructure displacements and stress resultants.

2.4. Numerical studies on micropiles and micropiles groups

Focusing on finite elements analyses carried out on micropiles, one of the first works was the one of Kishishita et al. (2000), who performed a parametric 2-D FEM analysis of micropiles subject to earthquake input motions. The soil was modelled as linear and nonlinear. Different shear wave velocity profiles were considered for the linear soil models, corresponding to increasing stiffness of the soil. Moreover, four different types of piles were used: precast piles, cast-in-situ piles, high-capacity micropiles, and high-capacity raking micropiles. Two earthquake input motions were used in the analyses (the 1940 El Centro Earthquake and the 1995 Kobe Earthquake). In the nonlinear analysis, only the softest soil (with the lowest shear wave velocity) was used, but all the aforementioned four types of piles used in the linear case were considered. A modified Ramberg-Osgood (Ramberg and Osgood, 1943) model was used for the soil in the nonlinear case, a tri-linear model for the cast-in-situ piles, a modified Takeda (Takeda et al., 1970) model for the precast piles, and a bilinear model for high-capacity micropiles.

Shahrour et al. (2001) conducted a 3-D FEM analysis of micropiles using a finite element program, PECPLAS. They simulated a single micropile and a micropile group, embedded in a homogeneous soil layer overlaying a rigid bedrock and supporting a superstructure. Configurations adopted for the micropile group were: 1 x 3 micropiles, 3 x 3 micropiles, and 3 x 5 micropiles. The soil-micropile structure system was assumed to be elastic with Rayleigh material damping. The cross section of the micropile was assumed to be square. The superstructure was modelled as a single degree-of-freedom system. Periodic conditions were imposed at lateral boundaries for the displacement field. A harmonic acceleration was applied at the base of the soil mass with its frequency equal to the fundamental frequency of the soil.

Ousta and Shahrour (2001) performed similar analyses on saturated soils. The analyses were carried out using the (u-p) approximation for the fluid-soil coupling (Zienkiewicz et al. 1980) and a cyclic elastoplastic constitutive relation that was developed within the framework of the bounding surface concept for representing nonlinear soil behavior. Single micropile, 2 x 2 micropile group, and 3 x 3 micropile group were modeled in the analyses. The micropiles were assumed to be linear elastic. The base of the soil layer was assumed to be rigid and impervious. Water table was assumed to exist at the ground surface.

Sadek and Shahrour (2004) used a similar model to investigate the influence of pile inclination on the seismic behavior of a micropile group. A 2 x 2 vertical micropile group and a 2 x 2 inclined micropile group with a 20° inclination to the vertical axis were used.

Wong (2004) performed a Finite Element modelling study of single micropile and micropile groups under both static and dynamic loading, with two constitutive soil models, i.e. a linear elastic and a bounding surface plasticity model. The micropile/soil interface was modelled either with perfect bonding or with frictional interface elements. For dynamic loading cases, a SDOF (single degree-of-freedom) superstructure was placed on top of the micropiles. Parametric studies were performed for various independent variables including load intensity, non-linearity of soil, and soil stiffness for the static case; and soil non-linearity, input motion intensity, frequency contents of input motion, and the natural period of the superstructure for the dynamic case. The static and dynamic behaviour of micropiles was studied by examining the effects of aforementioned independent variables on the deflections and bending moments along the micropile length.

Turan et al. (2012) numerically studied the effect of pile-cap connectivity condition and of the characteristics of the supported superstructure on the lateral response of micropile supported foundations. A 3D non-linear finite element model is developed using ABAQUS. The Ricker Wavelets were used in the analysis. Nonlinear soil behaviour was modelled using a Mohr-Coulomb plasticity model and constant Rayleigh damping. The results indicated that the dynamic characteristics of the superstructure have a significant impact on the bending moments of micropiles. The results also indicated that the use of hinged-head connectivity resulted in significant reductions in the maximum bending moments. Such assumption also resulted in a uniform distribution of bending moments among the micropiles within the group.

2.5. Remarks about Soil-Structure Interaction modelling

The state-of-the-art review proves that a lot of research effort has been devoted in the last decades to enhance the predictive capability of SSI analysis models, by means of approaches characterized by increasing degree of refinement. However, most of these models are supposed to reproduce the response of traditional medium- to small-diameter piles, without considering the executive procedures (for example, repeated high pressure injections), the real behaviour of interfaces (soil-pile and reinforcement-grout interfaces), and the configuration (above all, the inclination of micropiles).

One of the objective of this thesis is to verify whether traditional SSI approaches are able to acceptably reproduce the response of real in-situ micropiles, by comparing the experimental data obtained by means of in-situ tests on single vertical micropiles and inclined micropiles group with results provided by existing analytical and numerical models, properly adapted. The comparison can also be considered as a starting point for the development of new simplified approaches, able to take into account the effects of execution techniques, real interfaces behaviour, micropiles inclination, under dynamic and cyclic loading conditions.

Chapter 3.

Full Scale Tests on Piles and Micropiles

3.1. Introduction

Several field and laboratory tests have been performed in the last century, in order to validate and calibrate numerical and analytical methods relevant for the description of the load-deformation behaviour of soil-pile systems. Field and laboratory tests on the soil-pile interaction are both important to improve the knowledge of SSI phenomena, as they are characterized by different and complementary features. Laboratory tests allow for the application of any kind of loading conditions and, due to their high flexibility, are suitable for parametric studies in a controlled environment. On the other hand, in full scale in-situ tests the load can be applied from the top of the system (this implies, for instance, that kinematic interaction effects may be registered on the *not-loaded* piles only); however, real scale experiments offer the advantages of using real soil, real piles, and real soil-pile stress conditions. In the following, a comprehensive review of full scale soil-pile experimental studies is provided, for piles embedded in cohesive soil.

3.2. Full Scale Field Test on Traditional Piles

This section reports selected case studies of static and dynamic lateral load tests on single traditional piles and pile groups dynamic tests published in scientific and technical literature.

3.2.1. Field Lateral Load Test on Single Piles

The first experimental studies that should be mentioned among others are those performed by Matlock (1970) in soft clay, and Reese et al. (1975) in stiff clay, since they still have great influence on engineering practice. In fact, they are codified in API design recommendations and their results may be used directly to define soil properties inside some computer software such as the OM624P and LPILE (which are worldwide adopted for the design of laterally loaded piles). The American Society for Testing Materials publishes standardized procedures for conducting such load tests under specification ASTM D-3966 (ASTM, 1997).

Matlock (1970) performed an integrated field and laboratory study considering static, cyclic, and post-cyclic lateral head loading of steel pipe piles (32.4 cm in diameter) embedded 12.8 m deep at two different soft clay sites at Lake Austin and Sabine, Texas.

The undrained shear strength of the soils at these two sites ranged from 14.3 to 38.3 kPa in the upper soil layers. Some crucial consideration can be drawn from his pioneering study:

- the soil resistance-pile deflection (p-y) relationship, shown in Figure 3-1, is highly nonlinear and inelastic, and such static and cyclic non linear soil-pile response is more evident at low depths, while approaches linear response at greater depths;
- for engineering purposes, the fundamental p-y relationship is independent of the pile head fixity (although pile forces are strongly related to fixity);
- after a large number of cycles of loading and degradation of resistance, the load-displacement response of the soil-pile system tends to stabilize (this is commonly referred to as *shakedown* condition);
- an important effect of cyclic loading is formation of a gap at the interface between pile and soil, with high transient pile forces developed while traversing the gap;
- response during reloading after cycling is governed by soil resistance which is reduced for deflections smaller than those previously attained.

Later, API sponsored a study for clay (O'Neill and Gazioglu, 1984), with the purpose to include the pile diameter effects in an alternative clay p-y procedure, known as Integrated Clay P-y Criterion. However, API did not adopt the proposed changes and the Matlock clay criterion remains the API recommended clay p-y procedure.

Reese et al. (1975) drove steel pipe piles (15.2 and 61 cm in diameter) into a stiff, fissured, overconsolidated clay deposit near Austin, Texas; they simulated conditions existing at the ocean floor by pre-excavating about 0.9 m the site, so that water impounded at the surface. Unconfined compressive strengths of 191.5 to 380 kPa were found at this site in the upper 6 m.

Reese found a more severe cyclic degradation of soil resistance in his tests than that observed by Matlock in soft clay; however, it should be observed that the impounded water could have contributed to scour of the soil in the soil-pile gap that opened during each cycle of loading, determining an increase of the resistance degradation. It is important to consider that the period of cyclic loading in these tests was in excess of 15 seconds, and the observed scour effect could be expected to vary with loading rate. P-y curves for a series of depths in static and cyclic loading are shown in Figure 3-2, with results presented for a series of depths; they reflect the tendency for the p-y relationships to become linear at depth.

Kramer (1991) performed full-scale lateral load tests on two instrumented steel piles driven in the silts of Deep River and other two in the Peats of Mercer Slough, in order to obtain information useful to develop p-y curves for those very specific soils. He found out that the response to laterally loaded piles in the Deep River silts and similar soft silts can be evaluated with the Integrated Clay Criterion. Input parameters can be determined as follows:

- cohesive strength, c , may be taken as the undrained strength, s_u , of the soil, which is determined through drilling, sampling, laboratory testing, CPT, Vane shear testing;
- stiffness/Strength Ratio, $E_s/c = 50$: the secant soil stiffness can be considered to be proportional to the cohesive strength of the soil;
- critical Strain, $\epsilon_c = 0.35 E_s/c$, is the axial strain at a deviator stress of one-half the maximum deviator stress in a triaxial compression test;
- soil degradability Factor, $F = 1$, is a measure of ductility of the soil in the development of its resistance to lateral pile movement

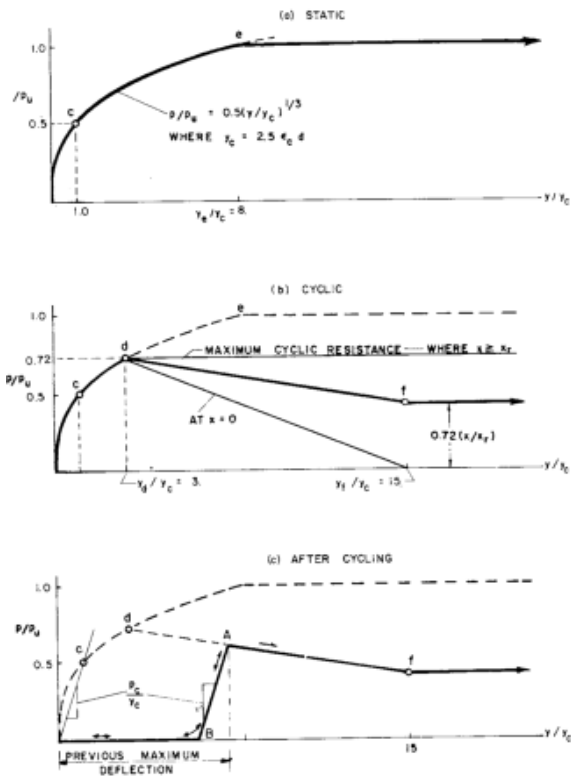


Figure 3-1 Criteria for predicting p-y curves for (a) short time static loading, (b) equilibrium under initial cyclic loading and (c) reloading after cyclic (Matlock et al., 1970)

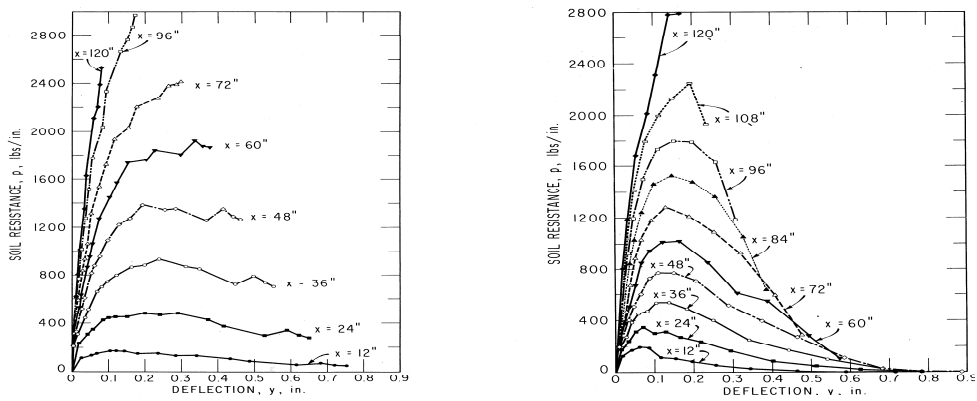


Figure 3-2 P-y curves developed from static and cyclic lateral load tests on pile in stiff clay (Reese et al., 1975)

Dunnivant and O'Neill (1989) performed cyclic tests a small steel pile, a large steel pile and reinforced concrete pile on natural, overconsolidated, saturated clays of the Beaumont formation. All tests were conducted with a water depth in the test pit of about 150 mm to simulate offshore or river- bottom conditions. Three loading series—"primary," "healing" and "sand"—were performed. P-y criteria were developed using the results of the primary series for the case of 100 loading cycles, while the healing series was performed after a gap had developed around the pile to investigate the effects of the lapse of time between major loading events. In the sand series, pile-soil gaps were filled with fine mortar sand to investigate changes in pile behaviour caused by filling the gaps.

Results prompted out the fact that significant degradation due to cyclic loading did not occur in the load-deflection curves until the head deflection reached about one percent of the pile diameter but, once started, did not appear to stabilize within 200 cycles. The rapid rate of degradation at larger deflections appeared to be associated with the formation of a permanent gap around the pile, intensified by hydraulic erosion. Rest periods between loadings after the opening of a gap between the pile and the soil resulted in weakened soil response, although this effect is not included explicitly in the proposed criterion, which appears particularly well-suited to the prediction of the behaviour of piles of very large diameter.

Khalili-Tehrani et al (2010) performed static two-way cyclic load tests on Cast-In-Drilled-Hole (CIDH) concrete pile in Hawthorne (California) clay in order to evaluate pile head fixity effects, by considering fixed pile, free head pile and a flagpole pile conditions. They found out that for the flagpole cases, the nonlinear top load versus the lateral displacement response was dominated by pile behaviour, and a distinct yield point existed that was associated with pile section yield. The response was ductile because the transverse reinforcement was sufficient to confine the core concrete and restrain buckling of the longitudinal reinforcement, given the low level of axial load. The load-displacement relationship for the fixed-head case displayed more pronounced nonlinearity because two plastic hinges formed at the pile-cap interface and at depth. The soil reactions against the pile were more strongly engaged than in the flagpole tests. Finally, the experimental p-y curves were compared with the API curves, which revealed that the experimental (back-calculated) p-y curves for the fixed-head and 1.8-m-diameter flagpole (free-head) piles had 100 and 60% larger capacities than the API curves, respectively. On the hand, the API and the back-calculated p-y curves for the 0.6-m-diameter flagpole pile were very similar, with the experimental curves having 20% less capacity.

3.2.2. Field Lateral Load Test on Pile Groups

Feagin (1937) performed field tests on groups of 9.8 m long timber piles at Lock and Dam No. 26, Alton, Illinois, in order to investigate the relative lateral resistance of vertical and battered piles; a lot of different configuration and orientation with the direction of loading were considered. The soil at this site was sandy alluvium, and the piles were installed by a combination of jetting and driving. The superior performance of battered piles under lateral load was clearly evident.

Highly discussed was the work of Kim and Brungraber (1976): they drove 2x3 groups of vertical and battered H-piles in cohesive soil. They compared the pile group per pile performance (in fixed head condition) to that of a single (free head) reference piles driven

nearby and computed pile group efficiencies in excess of unity, contrary to conventional notation. The bottom of the pile cap connecting the pile groups was cast against the ground surface: this potentially introduces a pile-cap base frictional contribution to the lateral resistance. As a response to their critics, Kim et al. (1979) published the results of a second series of tests where 4 in of soil beneath the pile caps had been excavated to avoid any frictional resistance. They concluded that the pile cap base friction contribution was significant for vertical pile groups, but negligible for battered pile groups.

An important result prompted out from the research of Holloway et al. (1982), that installed timber piles with the same construction techniques as originally used in the 1930's, and tested a 2x4 pile group to failure. They were the first to make the experimental observation of pile group "shadowing" effects, i.e. the preferential load carrying capacity of piles in front of the line of loading, thereby reducing load on piles at the rear of the line of loading. This load distribution is illustrated in Figure 3-3.

Meimon et al. (1986) analysed the group behaviour of driven steel pile in clay at Plancoet site under lateral monotonic and cyclic loading. During the cyclic loading, a soil reaction breakdown was recorded near the soil surface while the soil reaction increased at lower levels. The same phenomenon was obtained during the creep tests but smaller in amplitude. This confirms equivalence between creep behaviour and cyclic behaviour.

A large group effect was obtained: it increased with the load applied to the group and was influenced by the row position. The cyclic loading led to the homogenization of the pile efficiency factors. This could indicate a uniform degradation of the soil around the group.

Even Brown et al. (1987, 1988) provided detailed evidence of pile group effects by performing cyclic lateral load tests on 3x3 pile groups in stiff clay and sand, with the aim of developing p-y curve formulation for pile groups (Figure 3-4).

For pile in clay they observed that:

- the deflection under the load of the piles in the group is significantly greater than that of a single pile under a load equal to the average load per pile.
- the bending moments in the piles of the group are greater than those obtained for the single pile, and the maximum moments are shifted deeper. The greatest portion of the shear on the group is distributed to the piles in the front row, with successively less shear distributed to the middle and back rows.
- the maximum soil resistance for the piles in the group is greatly reduced as compared to that of the single pile for both static and cyclic loading, and this reduction is more important with depth.
- the results of the load measurements on individual piles within the group indicate that the load transferred to the individual pile was predominantly a function of the row-to-row position of a pile rather than the position of a pile in a direction normal to the direction of load.

For piles in sand, they observed that:

- even in this case, the deflection of the piles in the experimental group was significantly greater than that of a single pile under a load equal to the average load per pile.
- bending moments of the piles in the leading row were very similar to those for the isolated single pile under the same load per pile. The maximum bending moments in the trailing-row piles occurred at a greater depth and were larger for a given lateral load on those piles; the maximum bending moments for a given load on the

group occurred in the leading row piles, where the greater proportion of load is concentrated.

- cyclic loading in two directions had a relatively small effect on pile response relative to similar tests conducted in clays. Significant densification occurred in the sand and may explain the relatively small loss of soil resistance due to cyclic loading. It is probable that one-directional cyclic loading would have produced greater loss of soil resistance and less densification.
- the reduced group efficiency under lateral load was due principally to the effect of *shadowing*. Piles in the trailing rows had a greatly reduced soil resistance because of the influence of the piles in the leading row. The soil resistance of the piles in the leading row was only slightly reduced below that of the isolated single pile. The diminishing is more pronounced at depth.
- the loss of soil resistance in the piles of the leading row is less significant than trailing rows. A convenient way of expressing the loss in soil resistance due to group effect is with the use of a *p-multiplier*, a constant used to modify p-y curves for an isolated single pile.

Rollins et al. (1998) investigated pile group effects by testing a 3x3 group and a single pile consisting of 32.385 cm diameter concrete filled steel pipe piles spaced at 3d and driven 9 m into lightly overconsolidated layered silts, clays, and sands.

They found that the deflection of closely spaced pile group (spacing = 3 pile diameters) is 2-2.5 times more than the isolated single pile under the same average load; furthermore maximum load was distributed to the front row of piles, and more load was distributed to the back row than the interior piles, contrarily to Brown's findings. However, piles in all rows carried less load than the single isolated pile due to group effects. They also observed significantly higher (50-100%) bending moments in group piles than in the single pile at the same average load level, especially at higher load levels. By simulating the single pile behaviour with LPILE, they also noted that using a detailed soil profile rather than an averaged one produced better results. Finally they proposed p-multipliers for the studied soft soil site ranging from 0.6 for the front row piles to 0.4 for the interior and back piles (lower than those previously proposed by other researchers). The same authors kept on working on the topic with further experimentations on pile group in stiff clay (Rollins et al, 2006), according to which they made the following observations:

- average lateral load resistance was a function of pile spacing. Group interaction effects became progressively more important in reducing lateral soil resistance as pile spacing decreased from 5.65, to 4.4 to 3.3 pile diameters on centres;
- the leading row piles in the groups carried the greatest load, while the second and third row piles carried successively smaller loads for a given displacement. However, the fourth and fifth row piles, when present, carried about the same load as the third row piles. The back row piles often carried a slightly higher load than the piles in the preceding row;
- the lateral resistance was a function of row location within the group, rather than location within a row. This behaviour has been observed in other full-scale tests in clay, but is contrary to expectations based on the elastic theory which predicts that piles located on the edges of a row will carry more load than those located within the group;

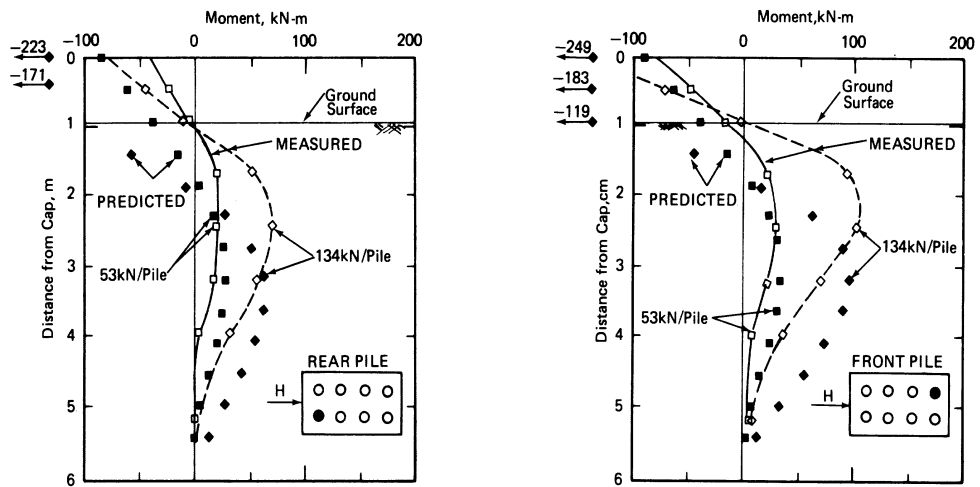


Figure 3-3 Field group test results indicating preferential load distribution to leading piles (Holloway et al., 1982)

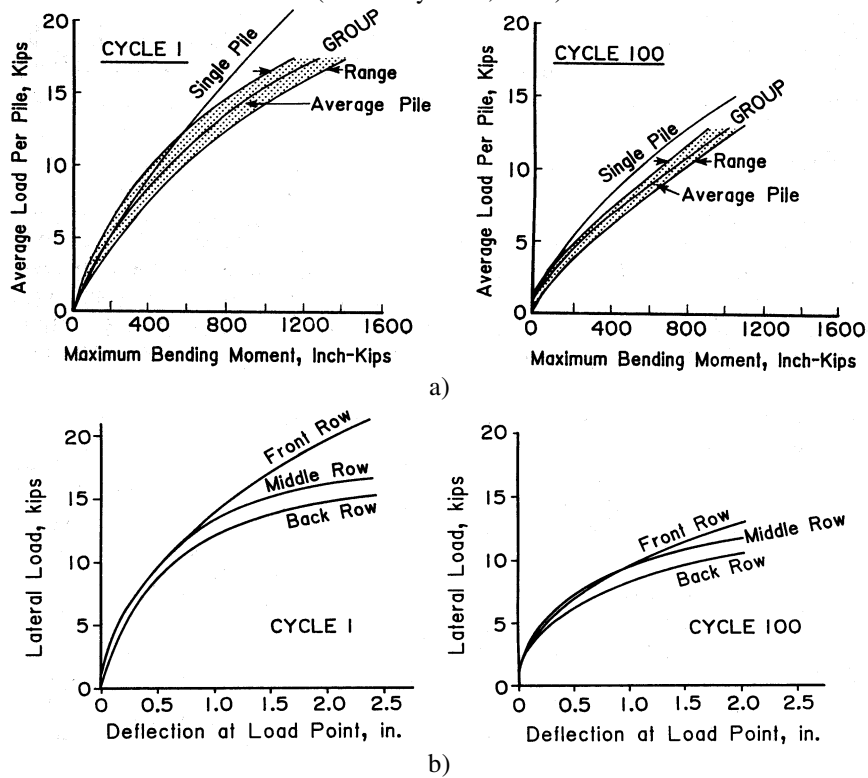


Figure 3-4 Field pile group load test results depicting; a) cyclic degradation of resistance; b) distribution of load by row (Brown et al., 1987)

- for a given load, the maximum bending moments in the trailing row piles were greater than those in the lead row due to group interaction effects, which essentially softened the lateral soil resistance against the trailing row piles relative to the leading row piles;
- cyclic loading reduced the peak load at the same deflection by about 15% after 15 cycles and about half of this reduction occurred after only one cycle. However, at deflections less than the peak, the reduction in lateral resistance was considerably greater due to gap formation.
- cyclic loading also led to increases of 14–30% in the maximum bending moment for a given load with the smallest increases in the single pile and lead row piles and the greatest increases in the trailing row piles.

3.2.3. Field Dynamic Test on Piles

In order to determine pile stiffness under dynamic loads, three classes of tests on full-scale piles and pile groups are generally performed in the field. They can be classified as 'impact load', 'free vibration' or 'forced vibration' tests. In any case, a mass may be fixed to the pile head to accentuate the resonant response and damping characteristics of the pile.

Free vibration (often termed as 'snap-back') tests consist of quickly releasing the pile from some imposed, initial lateral displacement, and measuring the free vibrations of the pile as it attempts to rebound to its original position. Pile stiffness and damping values can be derived from measurements of the free vibrations of the pile by the logarithmic decrement method.

Impact tests are a smaller strain version of a free vibration test, where an impact load, impressed to the pile by means of an instrumented hammer, generates free vibrations in the pile to be measured. A load cell is mounted on the hammer to record the impact load.

Forced vibration tests involve mounting an eccentric mass shaker to the pile head, whose motors spin eccentrically fixed masses, thereby inducing vibrations into the pile head. By adjusting the orientation, motor speed, and fixed mass, this test offers the flexibility of generating horizontal, vertical, or rocking vibrations over a range of frequencies and amplitudes. Electrodynamic oscillators are also employed in forced vibration tests, and can deliver much higher frequencies to the pile head than the mechanical type, which is limited to about 100 Hz. Soil-pile stiffness and damping can be interpreted directly from the experimental data resonance peak with the half-power bandwidth method. Comparisons of observed and predicted behaviour are good when the response remains linear and soil elastic properties are well-characterized. Conversely, when higher load levels generate nonlinear soil-pile response, the conventional models adopted for predicting the response are less accurate.

Alpan (1970) exerted an extensive experimental programme including the dynamic testing of a prestressed R.C. pile, fixed at its top against rotation, by inducing free oscillations from the records of which the damped natural frequency and the logarithmic decrement were obtained. In addition, slow lateral load tests with inclinometer measurement along the pile axis were conducted in order to enable the comparison of the measured dynamic response with that predicted on the basis of calculations utilizing the soil deformation parameters obtained from in-situ tests. The main conclusions drawn from the field test data and their

analysis were that free oscillation tests of piles in-situ can provide useful data for the evaluation of their dynamic response.

Petrovski and Jurokovski (1973) dynamically tested single piles and four pile groups of drilled shafts in loose sandy soil, with different conditions of pile cap embedment. The contrast between the linear and nonlinear response resulted in the degradation of stiffness and damping at increasing load levels, as shown in Figure 3-5.

Grib (1975) reports on field piles excited by a series of explosive charges timed to have “earthquake-like” characteristics. Grib’s results and analysis were not especially impressive, but his experimental method does hold promise as it overcomes the limitation of applying dynamic loads directly to the pile head, rather than through the free-field soil. This technique was also adopted by Rollins et al. (2015), who used blasting to induce liquefaction around auger-cast piles extending to 8.5, 12, and 14 m below ground at a site in Christchurch, New Zealand. Liquefaction led to negative skin friction and pile settlement. Skin friction following liquefaction was compared to pre-liquefaction values based on static load tests. Negative skin friction in the non-liquefied soil was equal to the positive skin friction. Contrary to common design assumptions, the negative skin friction in the liquefied sand was not zero. As excess pore pressure dissipated, the increased effective stress allowed negative skin friction to increase. After consolidation, the average negative skin friction was roughly equal to 50% of the positive skin friction which agrees with previous full-scale tests with driven steel piles. The average unit side resistance for the auger-cast piles was typically 50% to 70% of the unit side resistance predicted by design FHWA equations for drilled shafts.

Scott et al. (1982) conducted horizontal forced vibration and free vibration tests on an instrumented steel pipe pile driven into silty sand, and in a parallel study they modelled the observed field response in centrifuge tests. The extensive field instrumentation monitored pile bending moments, pile head displacement and acceleration, pore pressures in the surrounding soil, and ground surface velocity in the free-field (Figure 3-6). Maximum pile head accelerations reached 0.265 g, which unlike many smaller amplitude tests, is representative of strong-motion seismic loading. At higher loading levels, partial liquefaction was observed around the pile head, considerably reducing pile stiffness. Damping values were relatively small (1-7 %) and were observed to increase with the amplitude of pile motion, until the onset of liquefaction. Resonant frequencies observed in low level forced vibration and free vibration tests were considerably different.

Jennings et al. (1985) reported the dynamic tests conducted on a pair of 450 mm piles in diameter with 10 mm wall thickness, which were driven into saturated silty sands. Both piles were embedded 6.75 m below the ground surface. The piles were installed in the flood plain with the Hunt River about 1 km upstream from where the river discharges into Wellington Harbour, New Zealand. Two types of loading were applied to the piles, corresponding to dynamic tests and slow cyclic loads. Cyclic loads were applied by using the jack mounted between the piles 1.35 m above the ground level, and dynamic loads with a shaking machine mounted on top of one of the piles. Initial testing involved dynamic shaking of the test piles and was followed by slow cyclic loading at a rate of about one cycle per hour. Thus, clearly, there is a distinct natural frequency when the pile is loaded dynamically at low levels of excitation. By observing the ground surface during the loading, it was evident that high pore water pressures were generated adjacent to the pile shafts.

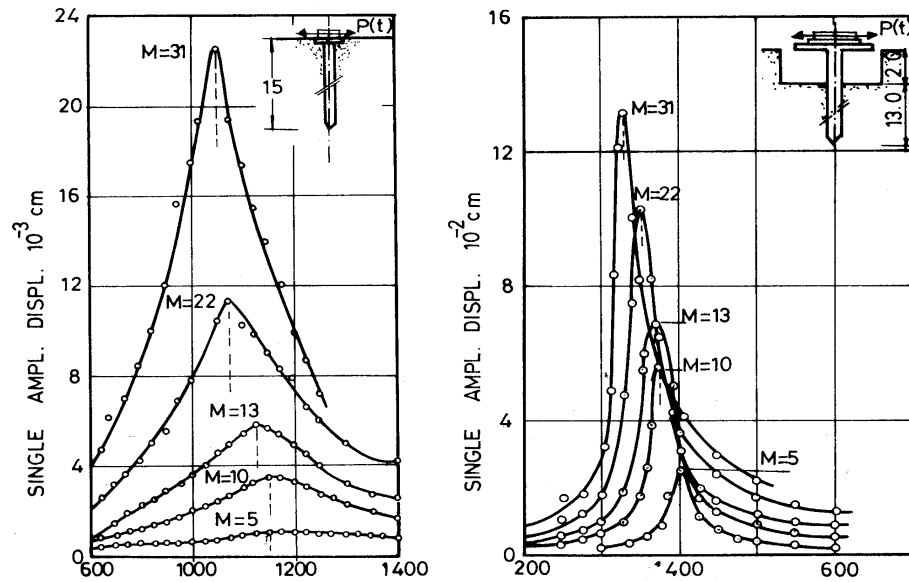


Figure 3-5 Dynamic pile response vs frequency (in rpm) from forced vibration tests: a) linear response; b) nonlinear response due to removal of supporting soil near pile head (Petrovski and Jurokovski, 1973)

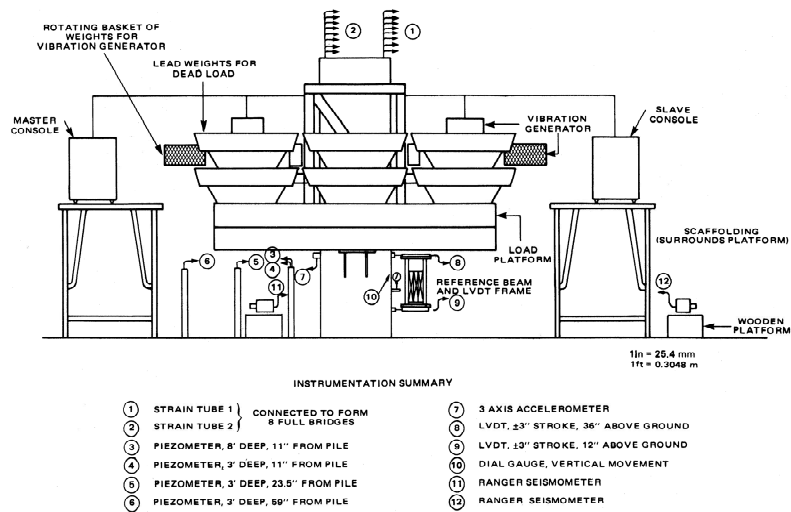


Figure 3-6 Field pile forced vibration test set up (Scott et al., 1982)

When piles are embedded in saturated sands, gapping cannot occur along the pile shaft but there is a dynamic degradation in the pile performance because of a reduction in stiffness of the sand as a consequence of the builds up in pore water pressure.

Ting (1987) computed p-y curves from the test results and compared them to API recommended curves, which were found to overestimate the observed stiffness due to the nonlinear response, gapping, and partial liquefaction that occurred.

Lam and Cheang (1995) released cyclic load test data from a second test program conducted at the same site in order to compare dynamic p-y curves with cyclic p-y curves; this proprietary information had remained unpublished for a number of years. Tests were made on a pile newly installed, and on a pile previously subjected to vibratory loading; the load-deformation measurements of the two piles were nearly identical, indicating that the prior vibratory load did not result in permanent changes to the soil-pile system. Free-head resistance to lateral loading was found to be greater than fixed-head resistance, due to the mobilization of additional frictional resistance in the free-head rotational deformation mode; the authors assert this mechanism contributes to the “diameter effect” observed by Stevens and Audibert (1979). The soil-pile stiffness under cyclic loading was in very good agreement with the low amplitude dynamic loadings, but nonlinear response under large amplitude dynamic loads reduced the apparent stiffness by 80 %. This was attributed to drained versus undrained soil behaviour in the two types of tests.

Crouse and Chang (1987) performed free vibration tests on vertical and battered concrete filled steel pipe pile-supported transformers with pile caps embedded in superficial loose, sandy, saturated soils. Observed resonant frequencies and damping values were less than those predicted by simplified numerical models by 10–30 %, and the low damping values in particular suggested suppressed pile cap-soil interaction. The authors observed that the site experienced peak ground accelerations of 0.06-0.1 g during the 1965 magnitude 6.5 Puget Sound earthquake, which may have induced settlement of the loose sandy soil away from contact with the pile cap. When ignoring cap embedment contact effects, predicted and observed values showed excellent agreement.

Blaney et al. (1987 and 1989) dynamically tested a 3x3 group of steel pipe piles driven into overconsolidated clay. The two publications report the results of vertical and horizontal forced vibration tests, respectively. A preliminary conclusion from the first study was that the average group pile frequency response was stiffer and more damped than that of an equivalent single pile. This was concluded to be related to wave interference in the group, but was cautioned not to be taken as an universal result, but as specifically dependent on the soil properties and pile spacing at this site. In contrast, under horizontal vibration, the average group pile frequency response was more flexible and less damped than that of an equivalent single pile. Numerical models incorporating the observed soil-pile gapping were found to more accurately capture the measured response.

Kobori et al. (1991) conducted an extensive series of tests on a pile group with different pile cap contact/embedment conditions that consisted of horizontal forced vibration tests and earthquake observations, in order to evaluate both inertial and kinematic interaction effects. The pile group was composed of four drilled shafts, and is shown schematically in Figure 3-7a. The three pile cap conditions included no contact, grouted contact with the soil surface, and complete backfilled embedment. The forced vibration test results are shown in Figure 3-7b, indicating the strong influence of backfill embedment on group stiffness; damping values were not tabulated. At the completion of the forced vibration tests, the

earthquake observations commenced; the maximum observed peak ground acceleration at the site was 0.08 g. Transfer functions of pile cap to free-field ground surface motions are shown in Figure 3-7c, with decreasing amplitude at resonant frequency with pile cap contact/embedment. Impedance functions for the three pile cap conditions were derived, and using two methods (SHAKE and a finite element method) to compute free-field input, the motion at the top of the block was computed and compared favourably with the observed records (Figure 3-7d).

Fuse et al. (1992) conducted forced vibration on pier over a foundation composed from 56 steel pipe piles, 50 m long and with a diameter of about 1.5 m embedded in a soil composed mainly from diluvial clay. The footing measured 32.5x27.5 m and the above pier had a sectional area of 5x5 m and a height of 34.4 m. The pier was partially submerged and the effect of the sea water was taken into account as added mass. Coupling resonant phenomena between the ground and the pier are conspicuously observed at the first and second natural frequencies. A simulation by the two-dimensional analyses model, FLUSH was carried out obtaining a good agreement between experimental and numerical results.

Tuzuki et al. (1992) performed an experimental parametric study on soil-pile interactions, considering the number of piles, pile spacing and pile arrangement. Four pile-soil-foundation models were made on a soft soil layer, and forced vibration tests were carried out using sinusoidal excitation (1-20 Hz); the amplitude of exciting force was applied as small as possible to obtain linear test results. The piles were made of prestressed high strength concrete (PHC) 0.6 m in diameter and 29 m in length and three different configurations were tested, with single pile, two piles and four piles. From the experimental data was found that the presence of another foundation near the tested one makes the latter more stiff, that the pile arrangement is very influent on the pile head condition, and that the passive foundation is more excited when is seated along the direction excitation (due to the different pattern of propagation).

Mizuno and Iiba (1992) reported a wide experimental campaign carried out on several pile groups (single pile, 2-pile group, 4-pile group and mat foundation) to investigate the effects of foundation type, number of piles, pile spacing, backfill and soil nonlinearity. Two different kinds of driven- pile were used, steel pipe piles and PHC, 6 m long and with different diameters. The result evaluated in terms of impedance functions show that: the effect of pile existence are remarkable in rotational and vertical impedance, thanks to axial resistance of the pile that increase the stiffness; stiffness of the pile foundation (per pile) becomes smaller with the number of pile, while damping is not much affected by the number of pile in low frequencies; backfill effects are remarkable at almost all frequencies, increasing both stiffness and damping; the effects of soil non linearity tends to decrease both real and imaginary parts of impedance functions.

Imamura et al. (1996) conducted forced vibration tests on both a single pile and a four-pile group, with different shaking patterns in order to investigate the nonlinear behaviour of the soil-pile system. Piles were made of precast centrifugally compacted concrete, with a diameter of 0.45 m and the length of 15.0 m. The results are expressed in terms of response curves, mode shape of vibration, the distributions flexural response and the impedance functions, this work represents a useful data for non linear behaviour of soil-pile system. It is remarked that the soil nonlinearity induced by a large strain has a great influence on the nonlinear response of single pile and that the gap developed by the separation at the pile-soil interface strongly affects the nonlinear response of pile groups.

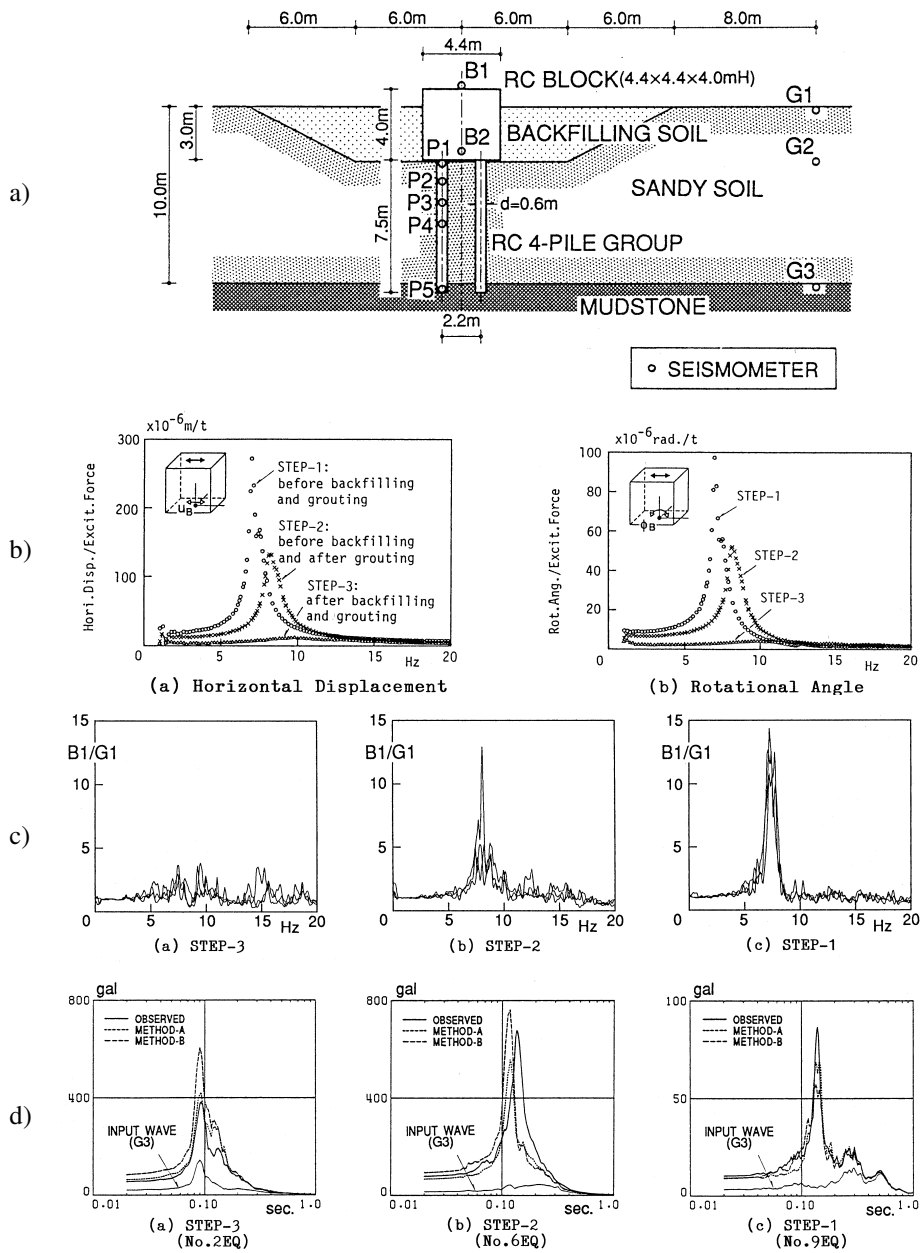


Figure 3-7 Field pile forced vibration test and earthquake observation: a) test set up and seismometer arrangement; b) forced vibration tests results illustrating influence of lateral support condition; c) structure to free field transfer function for three backfill cases; d) observed and computed response spectra for seismic event (Kobori et al., 1991)

Halling et al. (2000) conducted an experimentation on a 3x3 pile group and pile cap subjected to impact load and forced vibration test. The steel pipe piles with an outer diameter of 0.305 m and a length of about 9.1 m were embedded in a soft clay. The tests were conducted during different construction phases (single pile, group pile, group pile with cap) and repeated after static and statnamic test to study the substantial changes in dynamic characteristics subsequent to high strain induced in the system. The campaign shows a substantial change in natural frequency of the system (in particular a reduction) between the natural state and after it had been loaded using static or statnamic methods. This indicates the substantial effect that major loading can have on a foundation system even during a single event.

Shimomura et al. (2004) performed forced vibration tests twice in 1995 and 1996 and repeated the test on the same mock-up in another experiment in 2001. Three different models were tested, single pile, pile group (2x2 and 3x3), all composed by steel pipe piles (diameter of 0.4 m, length of 26.6 m and thickness of 9.5 mm) embedded in fine sand. Through the comparison of test results carried out in the different campaigns, an evaluation of temporal variations of the dynamic characteristics of the pile foundation has been obtained. By means of the resonance curves and the impedance functions obtained, an increase of the rigidity of soil around the piles has been evaluated, on the other hand, the soil subsidence surrounding the piles under foundations, about 0.25 m, was found by a subsequent measurement. An increase in the rocking stiffness more appreciable than that of the sway one has been observed.

Boominathan et Ayothiraman (2006) carried out a program of field lateral dynamic load tests on 33 piles of varying types-driven precast concrete, driven cast-in-situ concrete and bored cast-in-situ concrete at different petrochemical complexes in India. The results indicate that driven precast concrete piles have stiffnesses that are four to five times higher than those of driven cast in situ piles. Furthermore the natural frequency of the soil-pile system is significantly influenced by the size of the pile (diameter and length), the pile installation procedure, and stiffness of the top soil layers.

General conclusions that can be drawn from observations and comments on the presented test programs (selected from the literature) are:

- soil-pile dynamic response is highly site dependent;
- soil-pile dynamic response is frequency and load level dependent;
- soil-pile vertical stiffness is greater than soil-pile horizontal stiffness;
- pile cap embedment increases soil-pile dynamic stiffness and damping;
- soil-pile nonlinear response decreases both stiffness and damping;
- pile group effects are frequency, pile spacing, and site dependent, and are more pronounced for stiffness and less for damping;
- elastic continuum analytical models incorporating a “weak zone” around the pile, soil-pile gapping, and a parabolic variation of modulus with depth appear to provide a reasonably good level of accuracy for the cases studied.

Sa'Don (2010) in her PhD thesis dealt with a full-scale dynamic field tests data conducted in Auckland residual clay. An idealized soil profile and soil stiffness under small strain (i.e. shear modulus, G and shear wave velocity, V_s of the soil) determined from in situ testing, were used to model the single pile tests results. In particular, she tested four hollow steel pipe piles, each with an outside diameter of 273 mm and wall thickness of 9.3 mm installed at a site in Pinehill, Auckland. Static lateral loads were applied by using hydraulic jack,

while dynamic loads were applied using an eccentric mass shaker. The free vibration and snap-back tests were also performed by using instrumented sledgehammer and snap shackle as the quick release mechanism. The primary purpose of the pile testing was to measure the inertial response of piles in Auckland soils and to investigate how the soil stiffness decreases with increasing pile head excitation. An elastic continuum model developed on the basis of nonlinear Davies and Budhu (1989) equations, which enables the nonlinear behavior of the soil around the long elastic pile to be modelled using a simple expression of pile-head stiffness method, was validated on the experimental results.

Recently Dezi et al. (2012, 2013 and 2016) presented results of lateral impact load field tests and free vibration tests conducted on three near-shore steel pipe piles vibro-driven into soft marine clay. All piles are instrumented with accelerometers at the head, while one on them (the *source* pile) is also permanently instrumented with strain gauges and pore pressure transducers along the shafts. For what concerns impact load tests (Figure 3-8 (a)) two series of experiments are carried out, the first 1 week and the second 10 weeks after the vibro-driving. The variation in the dynamic behaviour in time, due to reconsolidation of soil subsequent to vibro-driving is discussed. The obtained results show the complex dynamic behaviour of the vibrating soil-water-pile system in terms of natural frequencies, damping and mode shapes. The horizontal dynamic impedance function of the whole system is derived from the experimental data over a wide frequency range and compared with that obtained from a numerical soil-pile interaction model. Features of pile-soil-pile interaction are also analysed through the analyses of accelerometric signals registered at the *receiver* piles head and a method for the in-situ derivation of shear wave velocity of the shallower soil layer is proposed. Finally, through the analysis of accelerometric signals registered during free vibration tests (Figure 3-8 (b)) with high force level, the development of nonlinearities is monitored. The results of experimental modal analyses, in terms of natural frequencies and damping ratios of the system, are presented and the complex dynamic behaviour of the vibrating soil water pile system and the pile-to-pile interaction are discussed at increasing force level. For a better reliability assessment of the system response in the range of linear behaviour, the results of free vibration tests at the lowest level of the applied loads are compared with those obtained from impact load tests.



Figure 3-8 Impact load tests (a) and free vibration tests (b) performed by Dezi et al (2012, 2013, 2016) on three near-shore steel pipe piles vibro-driven into soft marine clay

3.3. Previous experimental studies on micropiles

A limited number of small/full scale experiments on micropiles are available.

Yamane et al. (2000) conducted tests on various full scale micro-piles. Their aim was to study the vertical behaviour of micropiles, but they also performed lateral load tests on seven micropiles to study the bending capacity. Their study revealed that the micropile (steel pipes, grout, and thread-lugged bars) with coupling joints provided higher strength and stiffness as compared to the ones of an identical micropile without coupling joints.

Yang et al. (2000) tested a single reduced scale micro-pile installed in dry sand on a shaking table. Sinusoidal vibrations were applied in the horizontal direction. They observed that with weak base shaking (< 0.25 g), the micropiles follows the motion of the soil and the maximum bending moment occur near the sand surface, indicating that the inertial effects play an important role in micropile bending during shaking. On the other hand, during strong base shaking (> 0.25 g), the micropile did not follow the motion of the soil and the effects of the non-linear soil behaviour clearly affected the seismic micropile behaviour. Moreover, under strong base shaking, the maximum bending moments occurred near the pile bottom, which indicated that the micropile bending was dominated by the deformation of surrounding soil and the inertial effect from the pile head could be neglected. They finally commented that the frequency domain method might not be suitable and a time history analysis is needed for strong shaking or high excitation frequency.

Juran et al. (2001) tested a single reduced scale micro-pile, micropile groups, and micropile networks in the centrifuge, considering various micropile configurations, inclinations, number of micropiles, and loading levels. They found out that when the inclination of the micropile increased, the fundamental frequency increased.

The lateral performance of micro-pile groups and micro-pile networks was assessed in the field by Geosystems (2002). Different micropile numbers and configurations were installed and tested with different directions of lateral loading. Most of the micropiles installed were of the Ischebeck Titan type.

Abd Elaziz and El Nagggar (2014) performed two monotonic and six cyclic lateral load tests on four hollow bar micropiles (Figure 3-9 a,b) in stiff to very stiff silty clay to clayey silt, and the results were used to calibrate/verify a numerical model subsequently used in a numerical investigation. The observed load-displacement curves demonstrated that the micropile behaviour was flexible and was governed by the properties of soil along a depth equal to 10 times the pile diameter. The parametric study suggested that hollow bar micropiles can carry moderate lateral loads with proper reinforcement configurations and pile head fixity condition. During cyclic loading, the micropile head stiffness degraded initially as the number of load cycles increased. However, the stiffness reached a constant value after a specific number of cycles at the same load amplitude and at different cyclic load amplitudes.



(a)



(b)

Figure 3-9 Four installed micropiles (a) and lateral load test setup (b) in the experimental campaign carried out by Abd Elaziz and El Naggar (2014)

3.4. Remarks about full-scale tests on piles and micropiles

In the last decades, a lot of research effort has been put in the field of soil-pile dynamic interaction, as it can dramatically influence the dynamic response of the soil-foundation-structure system to horizontal dynamic loads. Accordingly, there is a need for experimental data from real scale tests, as they are extremely precious for the calibration of numerical or theoretical models adopted to investigate the problem. However, the state of the art on dynamic horizontal field study on deep foundations is poor (especially for what concerns Italian soil and the local executive techniques) and various phenomena need further investigations, such as the role of execution stages and construction techniques. This point is particularly crucial in the case of micropiles. Despite their growing use, results from static and cyclic lateral load tests on micropiles are limited and dynamic field tests data are almost absent; thus, an experimental campaign is carried out, that includes both two single vertical micropiles and a group of inclined micropiles. Several dynamic testing techniques are exploited and some of them have never been adopted before for the dynamic identification of micropiles.

Accordingly, this work represents a starting point for a deep investigation on the influence of geometrical, physical, mechanical, geotechnical and technological issues on the dynamic behaviour of micropiles under transient horizontal loading. As a matter of fact, this is a due premise for the optimization of the design and the execution of injected micropiles.

Chapter 4.

Experimental program

4.1. Introduction

The experimental field campaign described in the following includes both two single vertical micropiles and a group of 4 inclined micropiles embedded in alluvial soils. The field tests were undertaken in 2015 (however, the instrumented micropiles are still periodically monitored). The objectives of the experimental program are several. Among them, the main goals can be summarized as follows:

- the greatest part of the numerical models and analytical approaches developed in the past refers to traditional medium-to-large diameter piles; even in researches dealing specifically with micropiles, often investigations are limited to small diameter (simply bored and reinforced) piles, without taking into account common execution techniques. The applicability of those numerical and theoretical approaches for the investigation of real soil-micropile system should be verified.
- since most of the physical and numerical models studies on piles and micropiles do not take into account installation procedures, such as high pressure injections, nor the configuration (i.e. angle of inclination), the present study aims at the improvement of the knowledge of the dynamic and cyclic behaviour of micropiles, paying attention to the role of execution techniques and inclined configuration.
- many of the experimental techniques exploited in this study have been rarely (or never) adopted in the past to investigate foundations; therefore, one of the objectives is to verify their applicability, to validate their results and to compare different testing techniques.
- moreover, this research tries to investigate phenomena related with the development of non linearity in the soil-micropile system, by testing it under increasing loading levels.

Taking the cue from the scopes listed above, the experimental program regards small diameter cast-in-situ bored piles reinforced with a hollow-core steel bar. Two single vertical micropiles and a group of four inclined micropiles (connected by a rigid concrete cap at the head) are realized. At last, all micropiles (except one, which is left simply grouted) were completed by multi-step high pressure grouting at predetermined depths via valves and manchettes placed along the bar. The traditional execution stages were suitably modified to allow the preliminary permanent instrumentation of the hollow-core steel bar of the micropiles, and to limit damages of the sensors induced by mechanical stresses during the in-situ installation and the high pressure injection stages.

A schematic view of the testing procedures exerted on micropiles is reported in Table 4-1.

Table 4-1 Synthetic scheme of the tests carried out

System	Investigated strain range	
	Linear	Non linear
Simply Grouted Vertical Micropile	Ambient Vibration	Two-Way Cyclic Load
	Impact Load	Free Vibration
Injected Vertical Micropile	Ambient Vibration	Two-Way Cyclic Load
	Impact Load	Free Vibration
Inclined Micropiles Group	Ambient Vibration	Forced Vibration
	Impact Load	

It is appropriate to point out that the proposed classification is based on phenomenological evidences and it is not rigorous; for instance, under certain conditions, even impact load tests can induce slight evidence of non-linearity and the response of micropile-soil system can be slightly different than that observed by means of ambient vibration tests. However no appearance of permanent degradation or detachment visually comes from impact load tests and so it can be considered, at least grossly, as a test which acts in the linear field. After tests performed in the highly non linear field residual stiffness properties are checked by means of ambient vibration tests (for single micropiles), and impact load test (for micropiles group).

4.2. Site Characterization and Field Tests Set Up

In this section the geological and geotechnical description of the site in which the experimental program took place, and the main characteristics of the installed micropiles are provided.

4.2.1. Geological Description of the Site

The site chosen for the installation of the micropiles is placed in San Biagio (Osimo), an industrial zone nearby Ancona, in the centre of Italy. From a geomorphologic point of view, the area (marked with a red dot in Figure 4-1), rests above alluvial deposits sedimented by the Offagna Trench along its hydraulic left. The river-induced depression of the valley, with its axis developing approximately from NW to SE, is characterized by a flat valley-bottom whose amplitude grows toward the East direction, as a result of the lateral confluence with the valley modelled by the San Valentino Trench. The confluence of the two trenches generates the Scaricalasino Stream.

From a geological point of view the river basin is set above Plio-Pleistocene sediments of marine Facies made by mainly clayey litotypes, alternating with sandy little layers (of variable thickness), that are more frequent at the top of the series. For what concerns the

alluvial sediments deposited by the Offagna Trench, they are mainly constituted by clayey-silty, silty-sandy deposits originated from the dismantling of neighbouring hilly areas. The area is characterized by a flat morphology, placed at about 50 m above sea level.

The convergence of various alluvial basins allowed the development of several productive activities. The deposits of recent alluvial soils reach thickness higher than 15 ÷ 20 m. The area, placed close to the Offagna Trench, doesn't present criticisms with the exception of potential flooding.

The soil layer at the base of the hills surrounding the basin of the Offagna Trench, Monte Gallo and Santo Stefano, is represented by an alternation of loose sandy silts and clays above ochraceous sands, sometimes cemented. The underlying geological bedrock is represented by Pleistocene clays in angular unconformity.

4.2.2. Geophysical Characterization of the Site

Profile of the shear wave velocity V_s with depth and the fundamental period of the deposit have been evaluated from passive and active geophysical survey techniques: in particular, Multi-channel Analysis of Surface Waves (MASW), Extended Spatial AutoCorrelation (ESAC) and Horizontal to Vertical Spectral Ratio (HVSr) methods have been applied.

The micropiles shafts are embedded (for a length of 7.5 m) in a quite homogeneous and normally consolidated alluvial silty-clayey layer with poor mechanical properties, characterized by $V_s = 180$ m/s. The seismic bedrock (i.e. $V_s > 800$ m/s) is recognized at a depth of about 75 m from the ground level.

4.2.3. Geotechnical Description of the Site

Before the realization of the micropiles, mechanical properties of the deposit were investigated. Results of previous geotechnical surveys (both in situ and in laboratory) performed in close proximity were collected. In addition, a new borehole 15 m deep was realized nearby the testing area, from which undisturbed soil samples were extracted for the execution of laboratory tests. Summarizing, geotechnical data include:

- 2 static penetrometer tests (CPTs) to a depth of 20 m
- Laboratory tests on undisturbed soil samples (volumetric characteristics, Atterberg limits, unconfined compression test, direct shear test, oedometer test, unconfined undrained triaxial test)

Furthermore, an open standpipe piezometer was installed in situ, to allow for periodic readings of the groundwater level. GW level was checked before each pile test.

From the borehole layering, a lithological description of the deposit can be drawn. Under a 1 m-depth clayey-silty backfill soil, a brown, dry and crumbly colluvial organic soil (about 3 m thick) is found, having a medium-low consistency. 4 m under the ground surface, submerged in copious groundwater, light brown sandy silty soil can be found, having almost no consistency. At 8 m below the ground surface, the greyish colour of the soil suggests the presence of alluvial soils constituted by weathered, disrupted, transported and re-sedimented soil. This lithology is described as "silty clayey aggregate of recent alluvia", and it holds several water levels, suspended or trapped into layers with higher clayey components (aquiclude) alternating in layers with higher permeability (aquifer). At the bottom of the alluvial mattress the blue clays of the Lower Pleistocene crop up, showing a weathered uppermost layer covering a formation increasingly stiffer with depth. From the

borehole, it appears that the water table is about 3.5-4 m below the ground level, and 6 m below the ground level the borehole tends to close.

The relevant information for the stratigraphic and geophysical model are shown in Figure 4-2(a, b) and Figure 4-3. In Figure 4-4 and Figure 4-5 results from CPT tests and UU TXL on soil samples collected at 5 m in depth are reported, respectively; moreover, in Table 4-2 the main geotechnical properties of the first soil layer, obtained for specifically executed laboratory tests as well as data collected from local archives, are recalled.



Figure 4-1 Excerpt of the geological map of Osimo (from ISPRA, sheet 293, or. 1:10000)

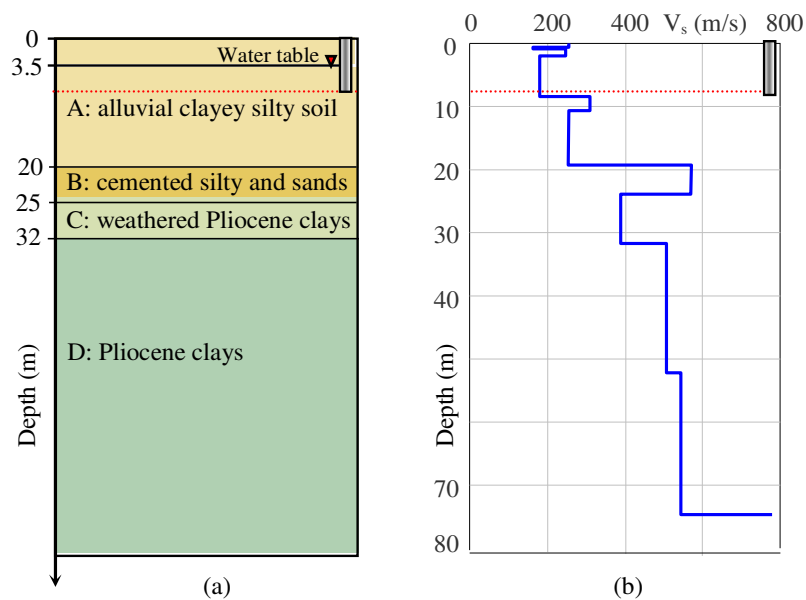


Figure 4-2 (a) Stratigraphic model, (b) V_s profile

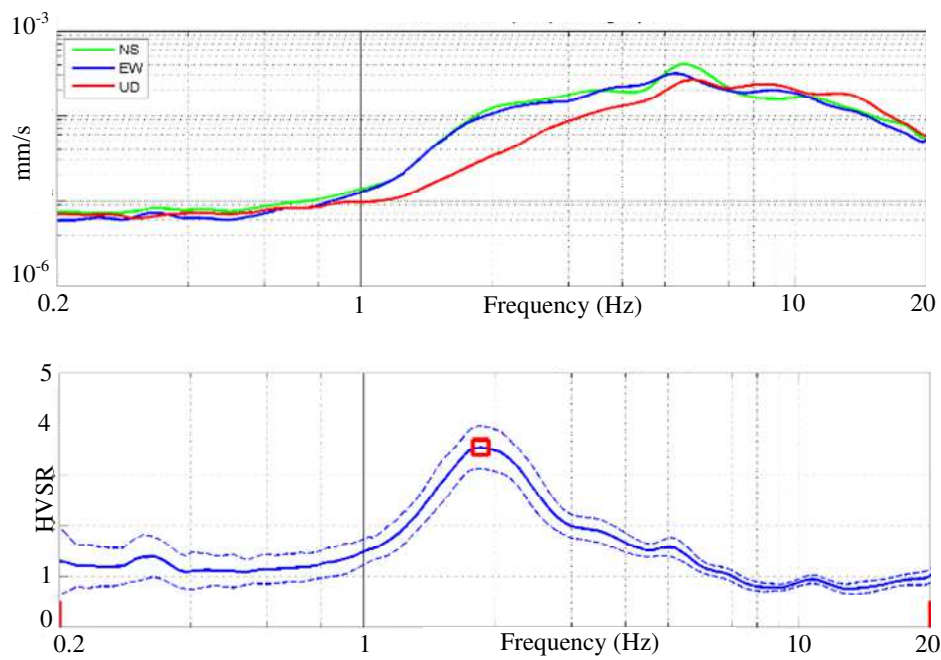


Figure 4-3 Directional velocity spectra and HVSR diagram of the investigated field

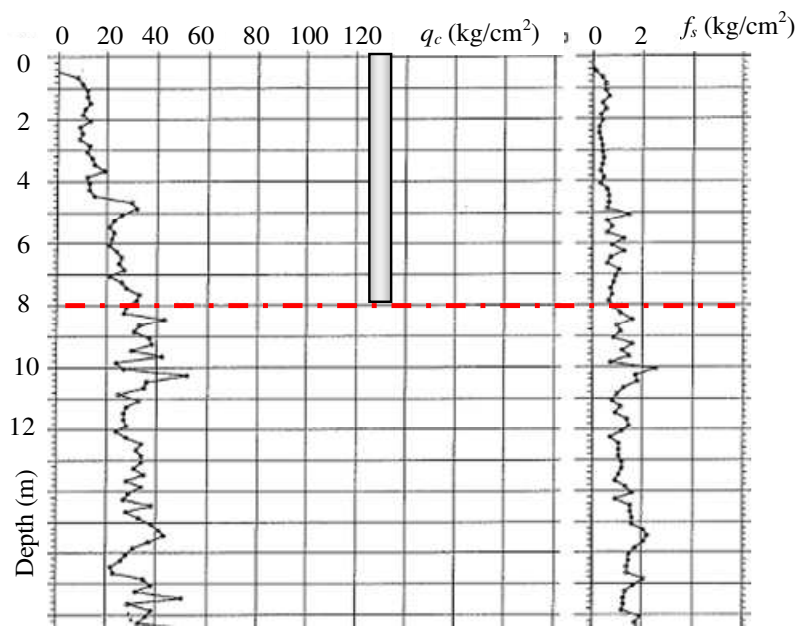


Figure 4-4 q_c and f_s profile with reference to the portion of soil interested by micropiles

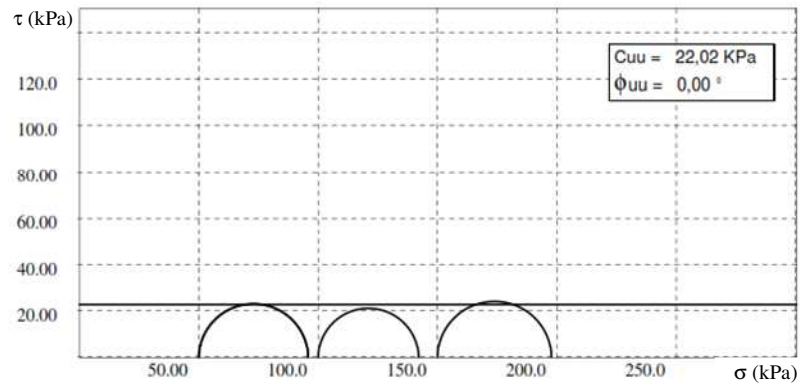


Figure 4-5 Undrained cohesion c_u from unconsolidated undrained triaxial test on undisturbed soil samples collected at a depth of 5 m.

Table 4-2 Geotechnical properties of superficial alluvial layer

<i>Unit weight (sat.)</i> γ	17-19	kN/m ³
<i>Unit weight (subm.)</i> γ'	7-9	kN/m ³
<i>Friction angle</i> φ'	24-26	°
<i>Effective cohesion</i> c'	0	kPa
<i>Undrained cohesion</i> c_u	20-40	kPa
<i>Liquid limit</i> ω_L	20-40	%
<i>Plastic limit</i> I_p	5-15	%
<i>Oedometric modulus</i> E_{oad}	2000-3000	kPa

4.3. Micropiles

In this experimental study, Tubfix technology has been investigated. In particular, micropiles reinforcement is constituted by 8 m long steel pipe bars, assembled through the junction of 4 elements (each element is 2 m in length). The outer diameter of the circular cross section of each pipe is 76.1 mm, and 6 mm thick. From the head of the micropiles, the 3rd and 4th elements are equipped with four 50 cm spaced valves a manchèttes for high pressure injections. The 4th element is also provided with a bottom plug for the grout injection at the micropile tip. Valves a manchèttes are realized by means of 2 small holes for each valve, covered by a rubber band that is fastened by steel rings welded at the valve end (Figure 4-6). Traditionally, elements are assembled in situ during the insertion of the hollow bar into the grouted borehole. In this experimental study, elements relevant for instrumented micropiles were assembled in lab to allow the proper installation of measuring

devices along the pipe. Once the sensors were mounted and zealously protected, the pipes were transported in situ for the installation. Firstly, six soil borings were drilled with a diameter of 170 cm and a length of 7.5 m. Two of them were vertical, while the remaining boreholes were realized with an angle of inclination equal to 15° with respect to the vertical axis. The inclination was given only around the x axis (along the y axis, with respect to the global reference system indicated in Figure 4-7, where a schematic plan view of the testing field is provided) in such a way that the configuration resulted symmetrical with respect to the z-x plane. Then, after the first grouting (with neat cement grout) of each borehole, the instrumented pipes were carefully inserted (Figure 4-8). The upper 50 cm of the pipes were left above the ground level to allow the execution of the lateral dynamic tests. After 48 hours from the first grouting, additional neat cement grout was injected via valves a manchèttes in one of the two vertical micropiles using a packer with double effect piston (Figure 4-9): when the packer was at the required depth, the grout was injected at a pressure of 6÷8 MPa. The cement slurry used for both the first and the secondary (selective) grouting had a water/cement ratio of 0.5. The quantity of cement slurry injected was calculated in order to obtain an equivalent diameter in the injected portion of the micropile equal to 2 times the diameter of the borehole. The elastic modulus of the concrete adopted for the micropiles execution (used for both the first grouting and the high pressure injections) was obtained from the results of ultrasonic tests. Properties of material and sections adopted in the study are summarized in Table 4-3.

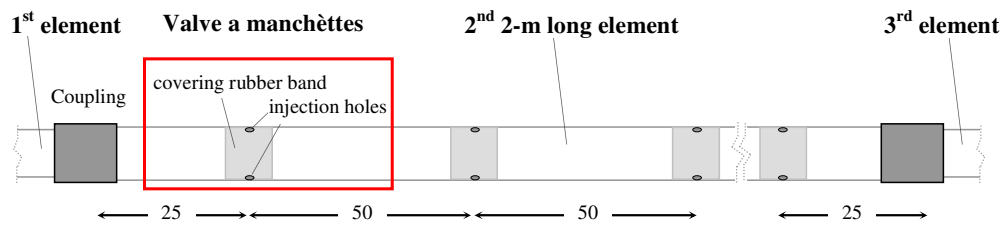


Figure 4-6 Tube a manchèttes

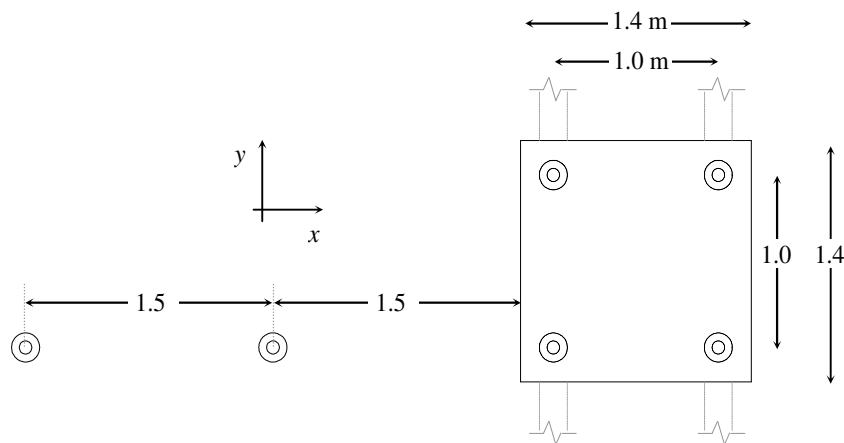


Figure 4-7 Plan view of the testing field

In Figure 4-10 a phase of the execution of high pressure injections is portrayed, and in Figure 4-11 the testing field just after high pressure injections is reported. In the following, the IRS micropile is referred to as P1, while the non-injected micropile as P2. All the inclined micropiles were realized with high pressure injections. In June 2016 (after preliminary testing on single inclined micropiles) a concrete cap was realized to connect the group. Separation between the cap and the soil surface is obtained by inserting a 5-cm thick layer of polystyrene between the cap and the soil that was subsequently removed after the hardening of the concrete. The final arrangements of the vertical micropiles and the inclined micropiles group are depicted in Figure 4-12 and Figure 4-13, respectively.



Figure 4-8 Insertion of an instrumented micropile into a grouted borehole



Figure 4-9 Packer for high pressure injections



Figure 4-10 Execution of high pressure injections



Figure 4-11 View of micropiles after high pressure injections

Table 4-3 Properties of materials and sections of micropiles

MATERIALS PROPERTIES			
Neat cement grout	<i>Young's modulus, E_c</i>	22000	MPa
	<i>Density, ρ_c</i>	1800	kg/m ³
	<i>Charact. cylinder compressive strength, f_{ck}</i>	20.75	MPa
	<i>Mean axial tensile strength, f_{ctm}</i>	2.3	MPa
Steel S355	<i>Young's modulus, E_s</i>	210000	MPa
	<i>Density, ρ_s</i>	7600	kg/m ³
	<i>Yield strength, f_{yd}</i>	355	MPa
SECTION PROPERTIES			
Section 1 (towering portion)	<i>Area*</i>	0.0161	m ²
	<i>Inertia*</i>	$8.9 \cdot 10^{-6}$	m ⁴
	<i>Density*</i>	1025	kg/m ³
Section 2 (simply grouted portion)	<i>Area *</i>	0.0341	m ²
	<i>Inertia*</i>	$4.8 \cdot 10^{-5}$	m ⁴
	<i>Density*</i>	1435	kg/m ³
Section 3 (injected portion)	<i>Area *</i>	0.1022	m ²
	<i>Inertia*</i>	$6.6 \cdot 10^{-4}$	m ⁴
	<i>Density*</i>	1678	kg/m ³

* Homogenised with respect to cement grout

SINGLE VERTICAL MICROPILES

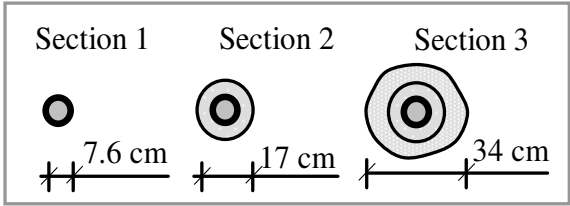
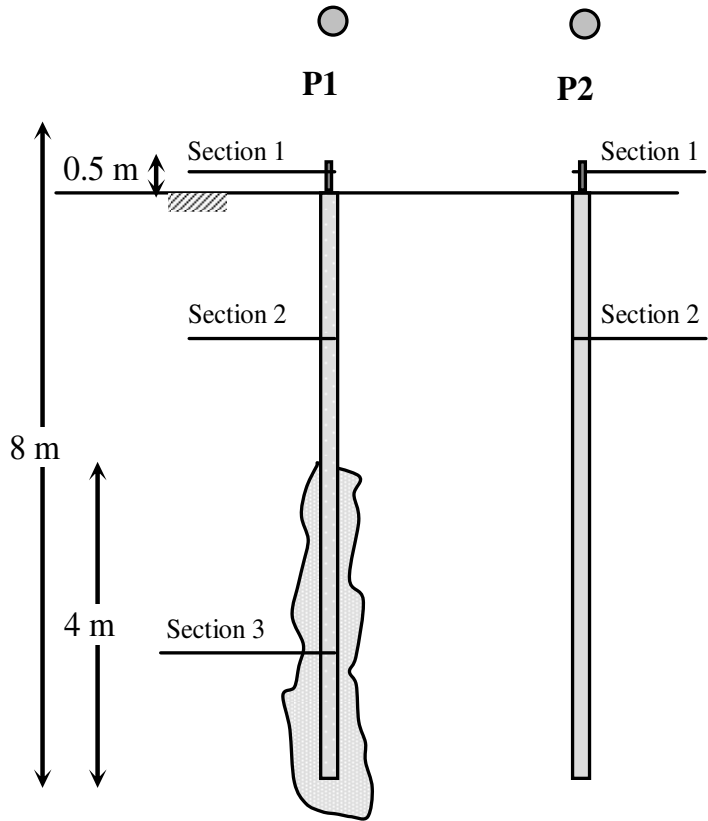


Figure 4-12 Single vertical micropiles

INCLINED MICROPILES GROUP

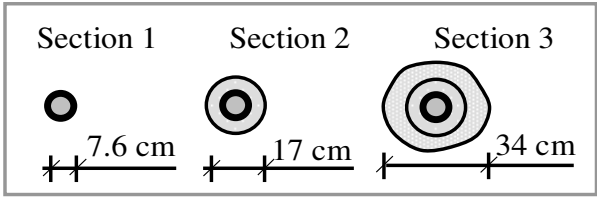
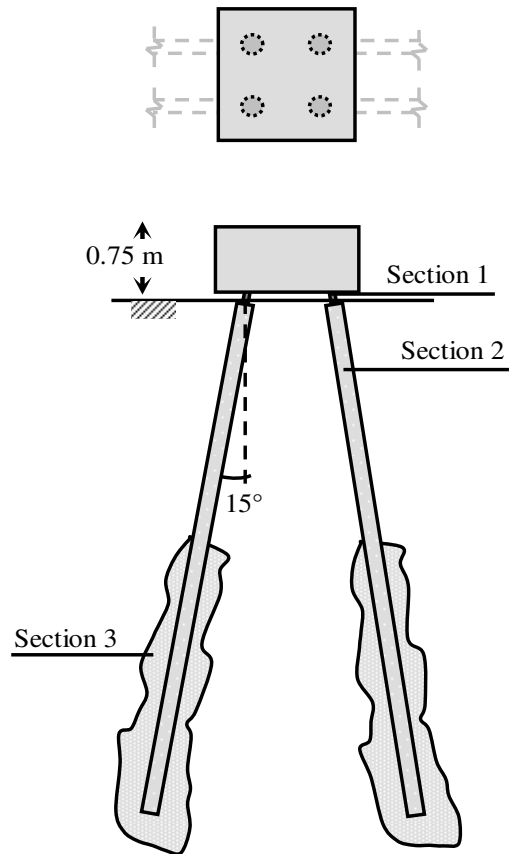


Figure 4-13 Inclined micropiles group

4.4. Instrumentation

The instrumentation used for the tests was mainly composed by transducers, excitation devices, signal conditioners and software for data acquisition and processing.

4.4.1. Transducers

Transducers are electrical devices able to convert a physical entity into an electrical one, usually a voltage. In particular, strain gages, accelerometers, geophones and displacement transducers were used.

Strain Gages

The instrumentation included permanently installed Strain Gages (SGs), in order to measure the longitudinal strains along the shafts during the dynamic loading. In particular, the steel cores of the vertical micropiles are instrumented with 14 SGs along a main alignment and with 2 SGs along two secondary verticals (18 SGs), while one of the inclined micropiles is equipped with 12 SGs along 3 main alignments (equally spaced along the cross sectional circumference) in order to distinguish the bending from the axial contribution in the total strain. The choice of the position of the sensors was suggested by the results of a preliminary soil-pile interaction analysis and is represented in Figure 4-14.

For the measurement of strains along the pile, strain gages KYOWA model KFGS are used (Figure 4-15a). In particular T rosettes with two measuring grids in common steel connected in a half-bridge configuration (Figure 4-15b) were used, in order to avoid the thermal effects. Each SG has a gage resistance of 120 Ohm and a gage length of 5 mm. The gage-factor of the lot package of strain-gages used is 2.01 with a maximum error of $\pm 1\%$.

The strain may be obtained from the output voltage by means of the following expression:

$$\varepsilon = \frac{4}{k \cdot B} \frac{V_o}{V_i} \quad (4.1)$$

where ε is the strain; B is the bridge factor; k is the gage-factor; V_o is the output voltage; V_i is the input voltage. In this case, according to the grid arrangement and the half-bridge configuration, the bridge factor is equal to

$$B = 1 + \nu = 1.3 \quad (4.2)$$

where ν is the Poisson's ratio of the specimen material ($\nu = 0.3$ for steel).

It is worth noting that, since cables connecting strain gages to the amplifier (MGC plus) are quite long (the length depending on the strain gage location along the pile), cable resistance should also be taken into account, since it is added to the resistance of the strain gage.

The actual strain value is obtained by multiplying the recorded one for the correction factor

$$\frac{R_{sg} + R_c}{R_{sg}} \quad (4.3)$$

where R_{sg} is the strain gage resistance and $R_c = \frac{\rho \cdot l}{S}$ is the cable resistance, in which ρ , l and S are the electrical resistivity, the length and the cable cross section, respectively

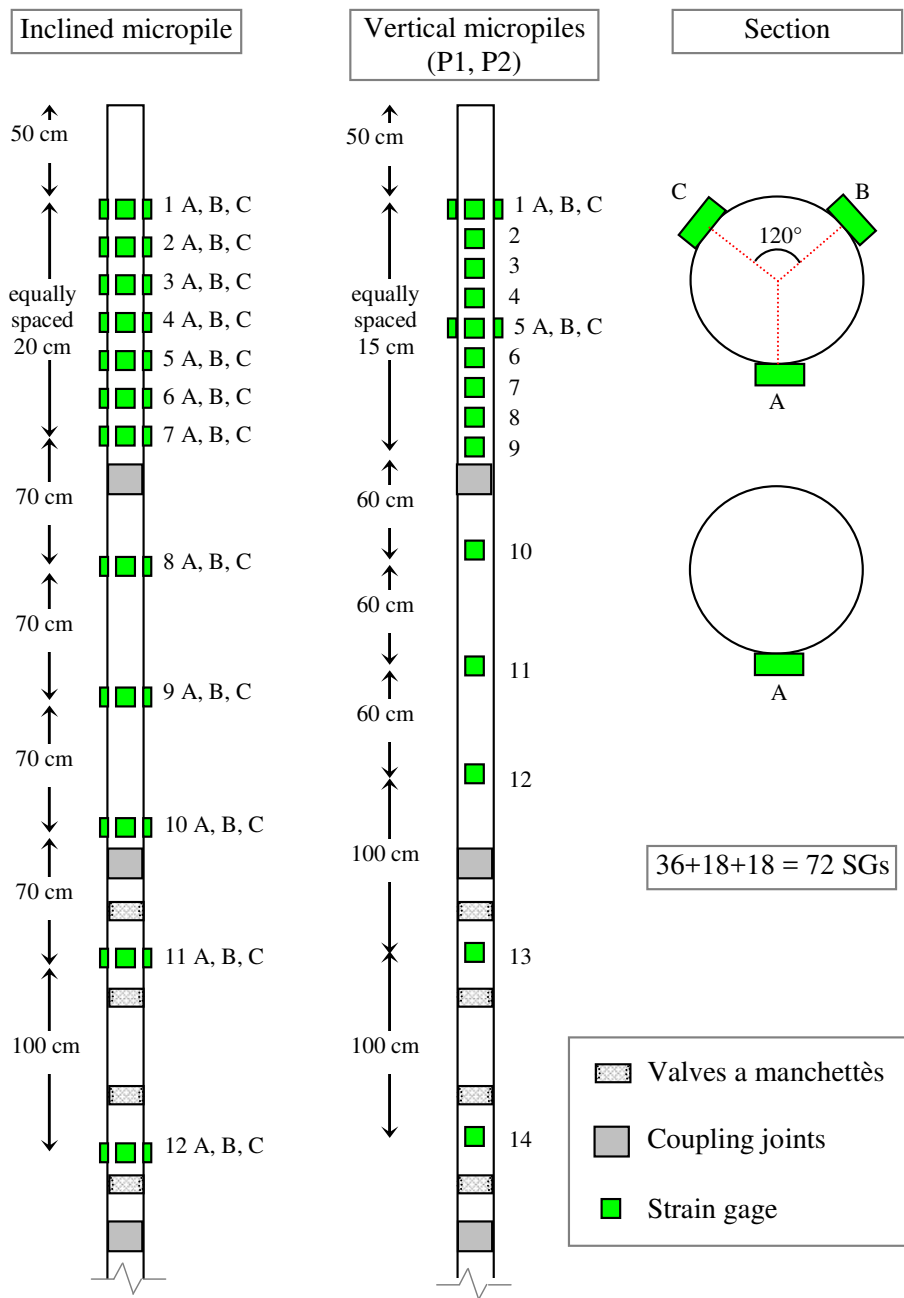


Figure 4-14 Strain gages disposition on instrumented inclined and vertical micropiles

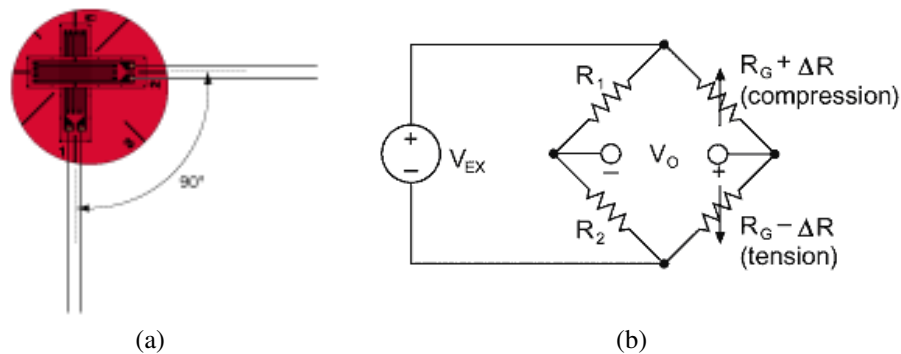


Figure 4-15 a) Adopted strain gages; b) Half bridge configuration.

Strain Gage Installation

Preliminary Soil-Micropile analyses have been performed to figure out where to place strain gages. Then, the installation of strain gages has followed standard procedures; once the pile elements have been assembled in laboratory, SGs have been mounted with the following steps:

1) Preparation of bonding surface

- removal of the rusty layer on the pile reinforcement surface with wire brush (a);
- first cleaning of the strain gage placement area by means of solvents, in order to avoid that grease could remain on the metal surface for the subsequent processing;
- smoothing of the strain gage placement area (about 10 cm wide) by means of a grinder provided with sandpaper discs and then manually with sandpapers of decreasing grit in order to obtain a flat and smooth level surface. For the final finishing 220 grit sandpaper is used;

2) Bonding of the strain gages:

- identification of the precise bonding place by means of a ballpoint pen;
- grooving of the bonding surface with two or three raps of fine sandpaper in order to create a minimal but functional roughness to the 'grip' of the glue;
- cleaning of the places with alcohol swabs and then with acetone swabs to remove fat and any impurities;
- positioning on a piece of Scotch tape the strain gage, with the polished side of the strain gage attached to the tape (since the opaque side will be subsequently attached to the pile).
- bonding of the strip of tape with strain gage in the position previously identified and marked with the pen (b);
- uplifting of the strain gage;
- spreading of the cyanoacrylate adhesive on the area (60 seconds after the previous operation), eliminating of the surplus adhesive through a Teflon spatula (Figure 4-16c);
- lowering of the strain gages and the relative solder terminal;

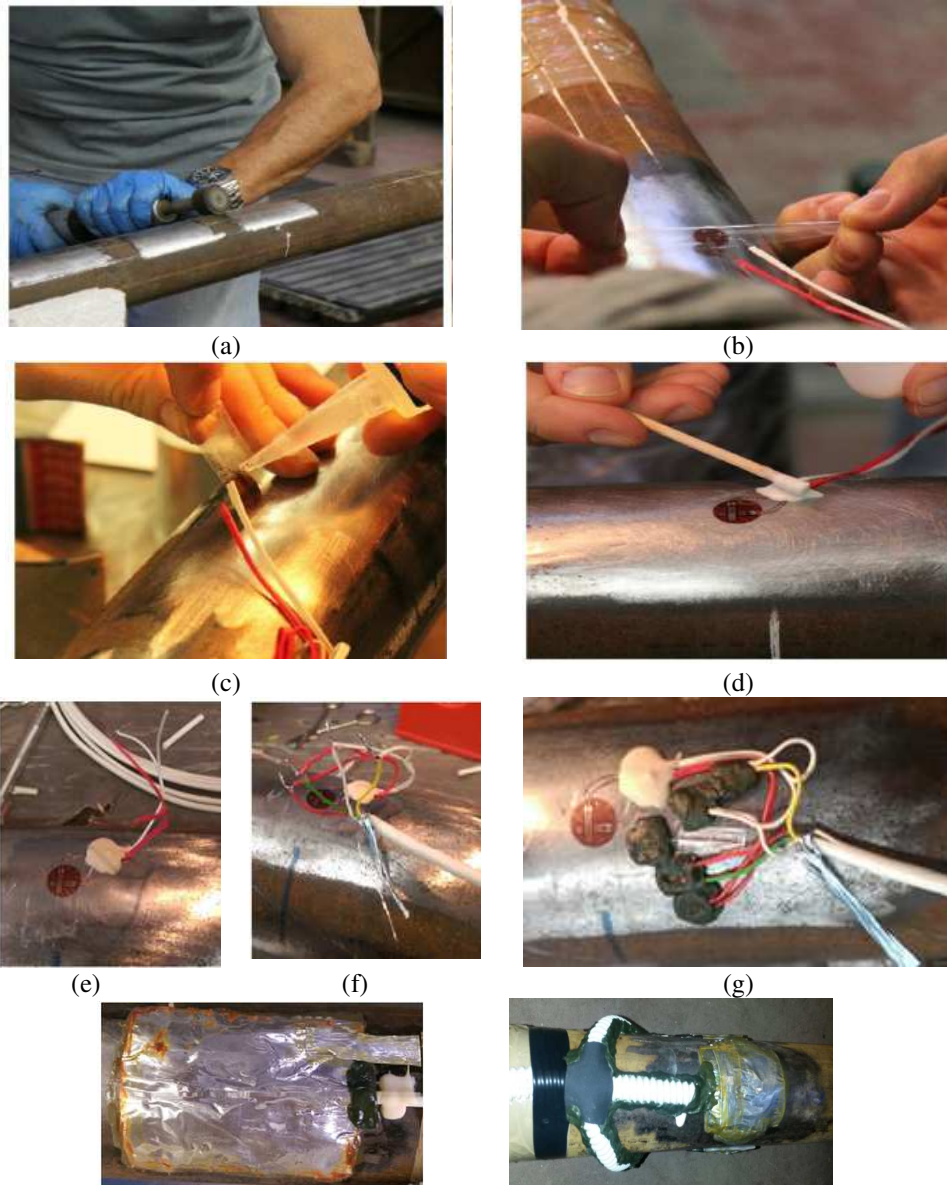


Figure 4-16 Subsequent steps of installation of strain gauges

- application of a uniform pressure on the instrument (i.e. by means of a rubber) for about 30 seconds to ensure an optimal bonding;
 - removing of the strip of tape used for temporary fixation of the strain gage;
 - check that all edges of the strain gage base are stuck, and ensure that any wrinkle, that might facilitate the entry of undesired substances and impurities, is absent;
 - fixing of the wires protruding from the strain gage with two component epoxy adhesives (
 - d):
- 3) Installation of connection wires:
- realization of the connection with little cables between the strain gage and the solder terminal (
 - e);
 - welding of the cables to the solder terminal (
 - f);
- 4) Protection of the measuring point and the wires:
- laying of a layer of polyurethane paint for a first protection;
 - application of a further protection by means of a device composed by a layer of about 3 mm of kneading compound coupled with an aluminium foil 0.05 mm thick(
 - g,h);
 - In addition, cables placed near valves a manchèttes are protected with high-resistance corrugated Polyethylene pipes (
 - i)

The technique adopted for the protection of the strain gages has proved to be very effective, since most of the sensors worked properly after the installation and the high pressure injections; moreover they kept on functioning throughout all the experimental study.

Accelerometers and geophones

Different types of accelerometers are adopted, depending on the accelerations induced by the different tests performed.

For ambient vibration tests, impact load tests on the pile group and for the acquisition of vertical acceleration of the cap during forced vibration tests, ICP (Integrated Circuit Piezoelectric) accelerometers, PCB 393B31, are adopted. They have a sensitivity of about 10 V/g, a frequency range ($\pm 10\%$) of $0.07 \div 300$ Hz, and a broadband resolution of $1 \mu\text{g}$ rms; in this case, accelerometers are mechanically connected to small plates bonded to the surface of interest by means of hot melt glue or quick-setting glue.

For impact load tests on the single micropiles, uniaxial piezoelectric accelerometer (Dytran 3097A3) is used, having a sensitivity of 500 mV/g, a frequency range ($\pm 5\%$) of $0.3 \div 5000$ Hz and a broadband resolution of $300 \mu\text{g}$ rms. This accelerometer can be mounted on the surface of the pile head (eventually smoothed with brush to remove any rusty layer) by means of permanent magnets. The connection method allows the accelerometers to work properly within a bandwidth larger than that of interest.

For snap back testing a ICP Dytran accelerometer with sensitivity 10 mV/g and a B&K 4508 (sensitivity 100 mV/g) are used, while for forced vibration tests in horizontal

directions B&K 4508 and PCB 353B43 accelerometers are adopted, having a sensitivity of 100 and 300 mV/g, respectively.

For ambient vibration tests on the cap of the micropile group also 2 synchronized geophones (velocimeters) of GEMINI 2 (produced by PASI) are adopted, instead of accelerometers, due to their higher sensitivity. GEMINI 2 has a natural resonance frequency of 2 Hz +/- 10%, and a sensitivity of 2 V/cm s⁻¹ (+/-5%).

Displacement Transducer

Two W50K HBM inductive transducers (Figure 4-17) are used to measure displacements during snap back test, forced vibration test and 2 way cyclic load tests. The sensitivity of the instrument is 80 mV/V with a full scale of ±50mm.

4.3.2 Excitation Devices

For impact load tests the PCB Piezotronics instrumented hammer have been used. The 086B50 type PCB Piezotronics instrumented hammer of 5.5 kg is used, with a steel head of 7.6 cm diameter and a wood handle 81 cm long (Figure 4-18).

The load cell, mounted on the hammer, is a piezoelectric transducer with the following technical characteristics:

- sensitivity (±15%) of 0.23 mV/N;
- peak force range ±22240 N;
- higher resonant frequency 5 kHz;
- non linearity of ±1%.

The hammer has a set of 4 polyurethane tips of different hardness: super soft (colour: gray, model: 084A30); soft (colour: brown, model: 084A31); medium (colour: red, model: 084A32); hard (colour: black, model: 084A33).

Tips of different hardness allow varying the pulse width and the frequency content of the input force. By fixing the input energy, a soft tip produces a wider pulse with a less high peak value than that relative to a hard; consequently, the frequency spectrum of the signal resulting from the soft tip is characterised by a shorter plateau. The soft tip is usually used when low frequencies should be considered while hard tips are used in problems characterised by higher frequencies. Usually the tip is chosen to obtain a reduction of the spectrum less than 10-20 dB at the higher frequency of interest. In this way, the energy is supposed to be equally distributed over all frequencies, up to the frequency of interest. The selection of the tip for the tests has been carried out after a series of trial impacts.



Figure 4-17 Displacement transducers with mechanical supports



Figure 4-18 Instrumented hammer

Hydraulic Jack

The hydraulic jack used for the snap-back test and for 2-way cyclic load tests is a prototype built in the Materials and Structures Testing Laboratory of Polytechnic University of Marche. It is able to apply a compression load up to 50 tons and a tension load up to 20 tons (Figure 4-19a). A pressure transducer has been mounted on the power pack to measure the oil pressure (Figure 4-19a), while the force is evaluated by means of a load cell installed on the hydraulic jack. The sensitivity of the load cell is 2 mV/V with a full scale of ± 200 kN.

Vibrator

The vibrator used for forced vibration tests is an electro-mechanical vibrations generator (*vibrodyne*), rigidly connected to the structure and able to provide forces (strictly sinusoidal and uniaxial) with maximum amplitude of 20 kN. As shown in Figure 4-20 the vibrodyne is characterized by 2 counter-rotating mechanical shafts, on which two identical wedge-shaped masses, are mounted. Two different set of masses, (light masses or heavy masses) can be adopted, depending on the combination of frequency and force needed. The mutual angular position of these two masses can be regulated when the machine is off.

The vibrodyne has a maximum weight of 3.5 kN (with heavy masses), the maximum force that can be supplied is 20 kN, while the maximum frequency that can be reached is 50 Hz.

The functioning principle is that the eccentric mass, rotating around an axis with a constant angular velocity ω , generates a centrifugal force that can be represented by a vector rotating in the plane orthogonal to the rotation axis, the amplitude of which can be obtained through the following relation:

$$|F| = m \times e \times \omega^2 = m \times e \times (2 \times \pi \times f)^2 = [m \times e \times (2 \times \pi)^2] \times f^2 \quad (4.4)$$

where m is the eccentric mass, expressed in kg; ω is the angular frequency in rad/s; f is the frequency expressed in Hz; e is the distance of the mass from the rotation axis (eccentricity) expressed in m; $|F|$ is the amplitude of the generated force expressed in N.

The eccentric mass obtained by means of the identical masses constrained to the peripheral rim of each disk; moving on the rim one of the two masses (mobile mass) with respect to the other (fixed mass) is possible to set the value of eccentricity from zero to, theoretically speaking, the value of the single mass.



Figure 4-19 a) Hydraulic jack; b) power pack with pressure transducer

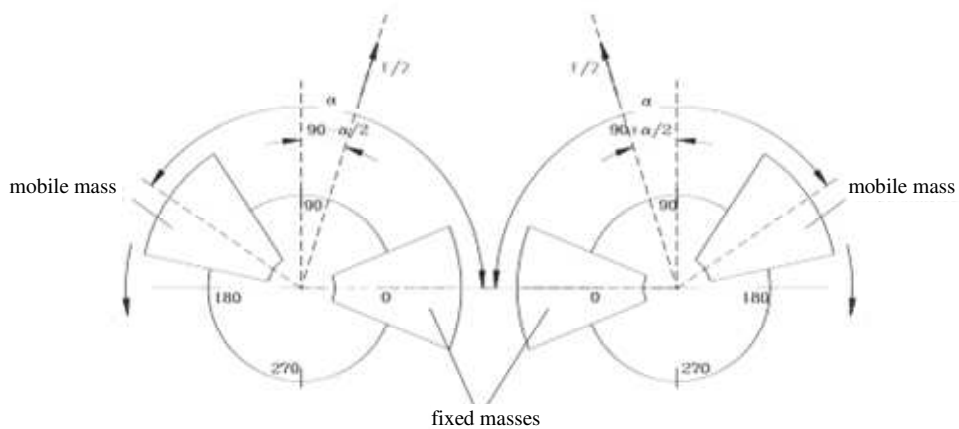


Figure 4-20 Electro-mechanic vibrodyne

The resulting force vector acts along the bisector of the angle formed by the two half-lines outgoing from the rotation centre and passing through the centre of gravity of the respective masses. In other words, the components orthogonal to the plane which contains the rotation axis of the counter-rotating force vectors are added together, those that lay on the plane containing the rotation axis of the counter-rotating force vectors cancel each other out.

The mechanical potential of the machine is defined by means of the *characteristic constant* that is indicated with C , is measured in N/Hz^2 and represents the maximum force that can be exerted by the machine at the frequency of 1 Hz if it were possible to overlap the masses in the same radius of the disk. The characteristic constant C groups together all the mechanical parameters of a certain machine equipped with determined eccentric masses, likely:

$$C = d \times n \times m \times e \times (2\pi)^2 \quad (4.5)$$

where d is the number of disks (in this case 2) and n is the number of the masses (in this case 2). Furthermore, the utilization constant of the machine is the ratio between the exerted force and the square of the frequency:

$$|F| = K(\alpha) \times f^2 \quad (4.6)$$

K, expressed in N/Hz^2 , is a function of the phase angle (α) between the masses, and it is related to the characteristic constant C through the following relationship:

$$K(\alpha) = C \times \cos(\alpha/2) \quad (4.7)$$

For the present application, the machine is equipped with lighter set of masse, that enables investigate a wider range of frequency; performances of the adopted vibrodyne under different masses configurations are reported in Figure 4-21 and in Table 4-4.

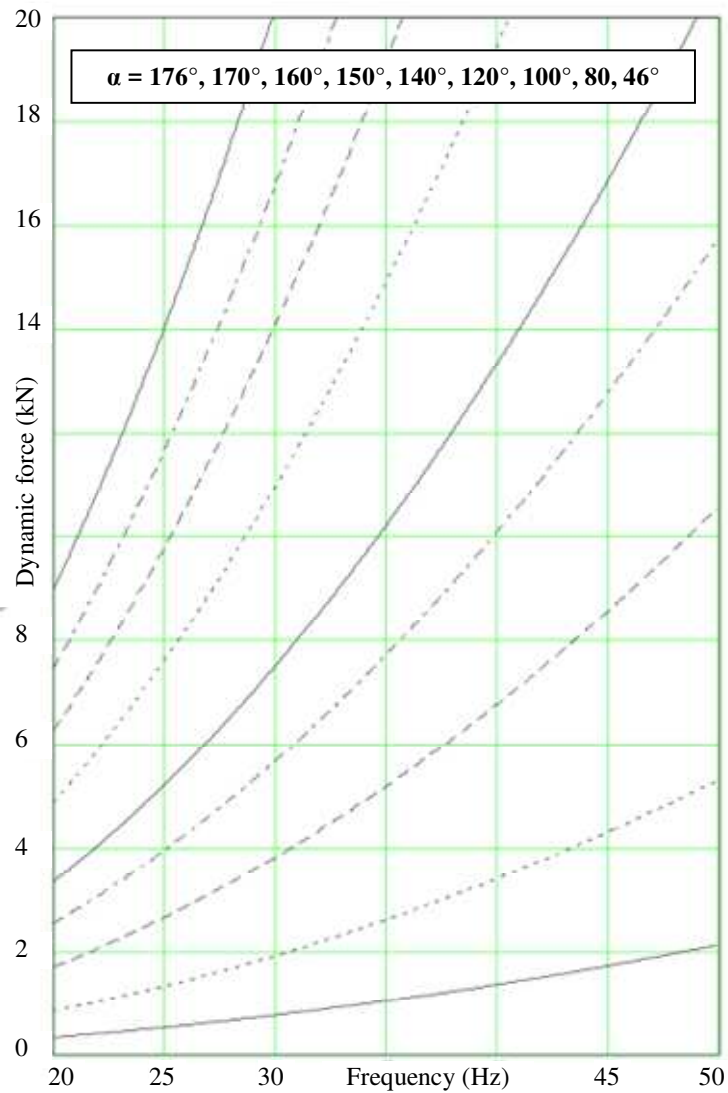


Figure 4-21 Performance of adopter vibrodyne, equipped with light masses

Table 4-4 Performance of adopted vibrodyne, equipped with light masses

α [°]	$90 - \alpha/2$ [°]	$90 + \alpha/2$ [°]	$K(\alpha)$ [N/Hz ²]	f_{max} [Hz]	α [°]	$90 - \alpha/2$ [°]	$90 + \alpha/2$ [°]	$K(\alpha)$ [N/Hz ²]	f_{max} [Hz]
30			23.6	29.1	106			14.7	36.9
32	74	106	23.4	29.2	108	36	144	14.3	37.4
34			23.3	29.3	110			14.0	37.8
36	72	108	23.2	29.4	112	34	146	13.6	38.3
38			23.1	29.5	114			13.3	38.8
40	70	110	22.9	29.5	116	32	148	12.9	39.3
42			22.8	29.6	118			12.6	39.9
44	68	112	22.6	29.7	120	30	150	12.2	40.5
46			22.4	29.8	122			11.8	41.1
48	66	114	22.3	30.0	124	28	152	11.4	41.8
50			22.1	30.1	126			11.1	42.5
52	64	116	21.9	30.2	128	26	154	10.7	43.3
54			21.7	30.3	130			10.3	44.1
56	62	118	21.5	30.5	132	24	156	9.9	44.9
58			21.3	30.6	134			9.5	45.8
60	60	120	21.1	30.8	136	22	158	9.1	46.8
62			20.9	30.9	138			8.7	47.8
64	58	122	20.7	31.1	140	20	160	8.3	49.0
66			20.5	31.3	142			7.9	50.0
68	56	124	20.2	31.5	144	18	162	7.5	50.0
70			20.0	31.6	146			7.1	50.0
72	54	126	19.7	31.8	148	16	164	6.7	50.0
74			19.5	32.0	150			6.3	50.0
76	52	128	19.2	32.3	152	14	166	5.9	50.0
78			19.0	32.5	154			5.5	50.0
80	50	130	18.7	32.7	156	12	168	5.1	50.0
82			18.4	33.0	158			4.7	50.0
84	48	132	18.1	33.2	160	10	170	4.2	50.0
86			17.8	33.5	162			3.8	50.0
88	46	134	17.5	33.8	164	8	172	3.4	50.0
90			17.2	34.1	166			3.0	50.0
92	44	136	16.9	34.4	168	6	174	2.5	50.0
94			16.6	34.7	170			2.1	50.0
96	42	138	16.3	35.0	172	4	176	1.7	50.0
98			16.0	35.4	174			1.3	50.0
100	40	140	15.7	35.7	176	2	178	0.9	50.0
102			15.3	36.1	178			0.4	50.0
104	38	142	15.0	36.5	180	0	180	0.0	50.0

4.4.2. Signal Conditioners and Data Acquisition System

The conditioning and amplification of the signals from strain gages, displacement transducers and load cells are carried out by means of HBM MGC plus of HBM (Figure 4-22(a)). After the external conditioning, the amplified signals are acquired by means of the same system used for accelerometers, likely DAQ devices NI 9234 (Figure 4-22b) and a laptop. In particular, NI 9234 of National Instruments is a 24-bit acquisition system with an input range of ± 5 V. The NI 9234 delivers 102 dB of dynamic range and incorporates Integrated Electronics Piezoelectric (IEPE) signal conditioning at 2 mA constant current for accelerometers. The four input channels simultaneously acquire at rates up to 51.2 kS/s. In addition, the module includes built-in anti-aliasing filters that automatically adjust to the selected sampling rate. NI Compaq DAQ is used to collect signal by several NI 9234 permitting the synchronization between the different modules.

The dynamic tests are acquired by means of specifically developed LABVIEW scripts: for the ambient vibration tests and forced vibration tests is simply a continuous acquisition system, while for impact load tests or snap back testing it includes a trigger, which allows catching the event considering a specific pre-trigger time and a fixed time length of measuring. For acquisitions that don't require synchronism among acquired data (as in the case of cyclic load test), Spider8 of HBM (Figure 4-23) is also adopted for the conditioning, amplification and acquisition of signals, and Catman 4.2 is used as real-time interface



Figure 4-22 (a) Signal conditioner HBM MGC plus; (b) DAQ device NI 9234



Figure 4-23 Spider8 of HBM

4.5. Ambient Vibration Tests

Ambient vibration tests allow the investigation of the dynamic response of various full scale structures in the elastic range, by acquiring the response of the system to natural vibrations (e.g. micro tremors, wind, anthropic activities, noise). To the authors knowledge ambient vibration tests have never been adopted to evaluate the dynamic properties of piles; however, in this experimental campaign, ambient vibration tests are performed on both the single micropiles and the micropiles group. In addition they are adopted to check the residual dynamic properties of the single verticals micropiles after medium to high strain level dynamic tests (snap back, forced vibration tests, 2-way cyclic load tests).

Single piles

For single micropiles in free head configuration, two accelerometers per micropile are positioned as shown in Figure 4-24 (a,b) (i.e. measuring along two orthogonal axis called x and y). ICP accelerometers, PCB 393B31, are adopted. They have a sensitivity of about 10 V/g, a frequency range ($\pm 10\%$) of $0.07 \div 300$ Hz, and a broadband resolution of $1 \mu\text{g}$ rms. A time length of about 1500 seconds and a sample frequency of 2048 Hz are used for the tests. Signals are suitably processed by means of traditional processing techniques:

- Elimination of those parts in which signal saturates
- Correction of the spurious trends, by fitting the signal with a polynomial function and subtracting that contribution.
- Application of a low-pass Butterworth filter (zero-phase digital filtering) with a frequency cut of 512 Hz in order to avoid aliasing phenomena during the subsequent process of resampling.
- Resampling of the signal at a frequency of 1024 Hz in order to make the successive analyses faster.

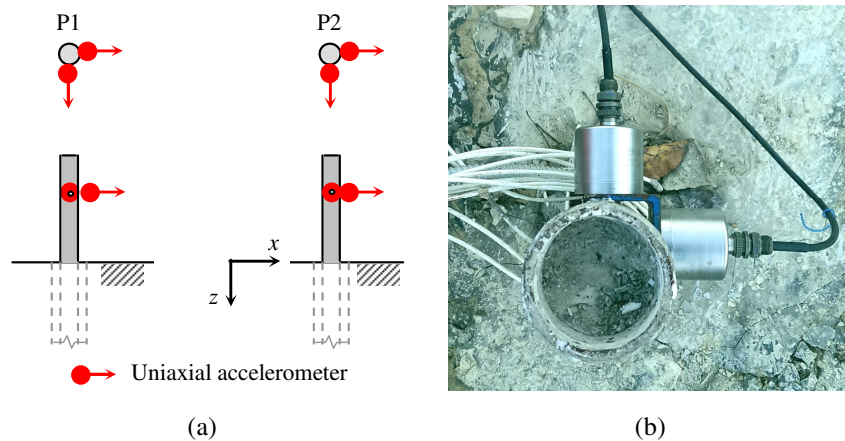


Figure 4-24 (a) Disposition of accelerometers on P1/P2 for ambient vibration tests; (b) view from the top, during an acquisition.

Micropiles group

For the group, seven uniaxial accelerometers (measuring along x , y or z axis) are positioned as shown in Figure 4-25 in order to allow for a proper recognition of the rocking motion coupled with the translational modes of vibration, and for any eventual roto-traslational mode in the horizontal plane.

Even in this case, ICP accelerometers, type 393B31 of PCB, are adopted. A time length of about 1500 seconds and a sample frequency of 2048 Hz are used for the tests. Signals are processed with the same techniques adopted for ambient vibration tests on single micropiles.

Moreover, ambient vibration test on the pile group are also performed by means of two triaxial synchronized geophones, placed in different configurations: a geophone is always placed in the ground (several meters away from the cap) while the other one at nodes 1, 2, 4 and at the centre of the cap. In any case a time length of about 1500 seconds and a sample frequency of 200 Hz are used for the tests.

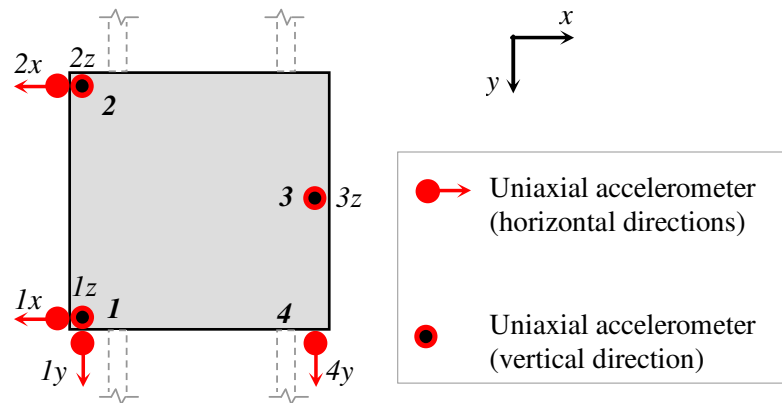


Figure 4-25 Disposition of accelerometers on the group cap for ambient vibration tests

4.6. Impact Load Tests

Impact load test performed with instrumented hammer is highly used in dynamic testing thanks to its execution simplicity. Moreover, it allows investigating a wide range of frequencies with few hammer blows and short acquisition times. However, since a low amount of input energy is supplied to the system at each frequency, they allow analysing the system behaviour only for very small strains and thus it is not suited to investigate system non-linearity which generally occur at higher strain levels. Figure 4-26a shows a typical time history of a medium intensity impact measured by the load cell of the hammer; the relevant frequency spectrum, reported in Figure 4-26b, may be assumed as flat in the frequency range of interest (up to about 200 Hz).

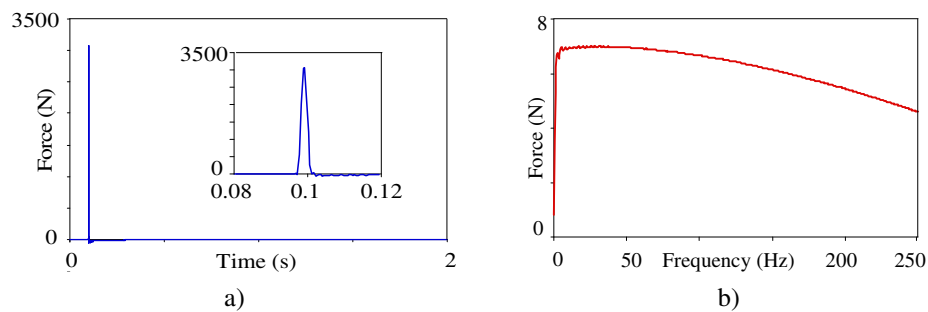
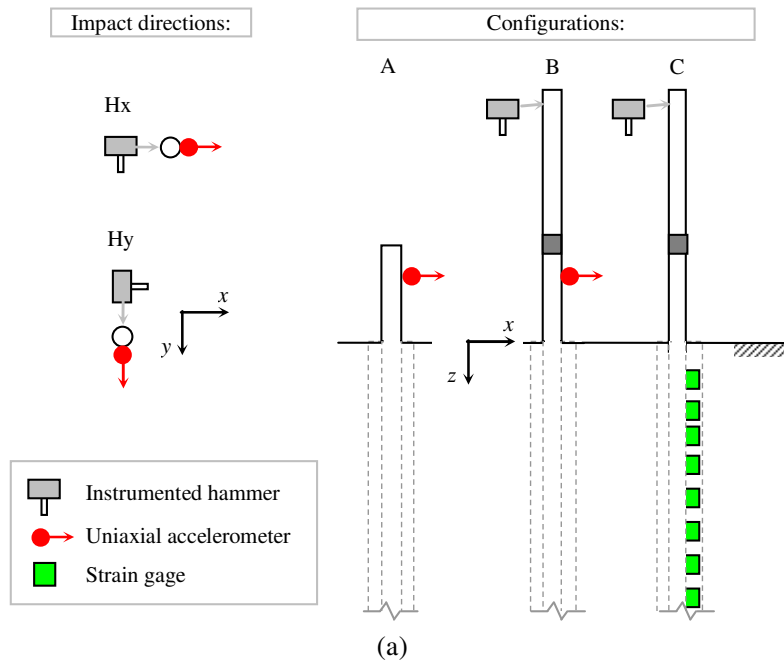


Figure 4-26 Example of impact load on micropiles group: a) Time History; b) Frequency Spectrum

Single vertical micropiles

Several configurations were considered for impact load tests performed on single vertical micropiles. Firstly, impacts were impressed at the top of micropiles head (configuration A). This configuration turned out to be not suitable for the investigation of strain gauges signals, since the force level was not enough high to induce readable strains along the shaft. Therefore, a 1-m long pipe extension was rigidly connected at the pile head by means of a joint; by impressing the hammer blows at the top of the pipe extension, it was possible to obtain higher force level with respect to configuration A. This arrangement is exploited for two configurations, hereinafter called B and C. In configuration B hammer blows were characterized by a limited force level to avoid the saturation of the accelerometer: given the input range of the DAQ device ($\pm 5V$), and the sensitivity of the adopted accelerometer (500mV/g) saturation occur at 10 g. In configuration C hammer blows were characterized by a higher force level in order to acquire the signal of strain gauges embedded in the soil. In configuration A the behaviour of micropiles has been investigated along the direction that would have been relevant for the strain gauges readings (however only accelerometers signals at the micropiles head provide significant values). For configuration B and C, impacts were executed along x and y orthogonal directions. At least 10 impacts for each configuration were imposed, in order to get a reliable averaged response.



(b)



(c)

Figure 4-27 (a) Typical configuration of horizontal impact load test on single micropiles; (b) during a test in the original configuration, and (c) with the pipe extension.

The accelerometers were applied to micropiles so that the signal was acquired along the same direction of the impact (Figure 4-27 (a, b, c)). A sampling frequency of 2048 Hz was chosen to achieve high resolution in time domain, and an acquisition time duration of 2 s was considered to investigate the entire duration of the micropile oscillation.

Micropiles group

For the group, seven uniaxial accelerometers (measuring along x , y or z axis) are positioned as shown in Figure 4-25 in order to allow for a proper recognition of the rocking motion coupled with the translational modes of vibration, and for any eventual roto-traslational mode in the horizontal plane. A schematic view of the accelerometer disposition is portrayed in Figure 4-28, while Figure 4-29 provides a reference to the hammer impacts that have been performed in x , y , and z direction. Having checked that the saturation of accelerometers signal isn't reached, ICP accelerometers, type 393B31 of PCB, are adopted. A sampling frequency of 2048 Hz is chosen to achieve high resolution in time domain, and an acquisition time duration of 2 s.

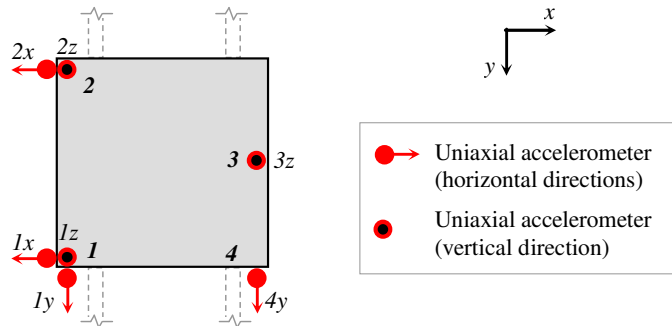


Figure 4-28 Disposition of accelerometers on the group cap for impact load tests

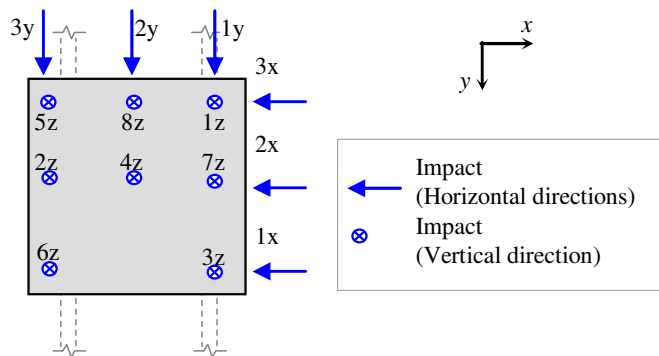


Figure 4-29 Impact configuration on the group cap for impact load tests

4.7. Two Way Horizontal Cyclic Load Tests

Horizontal cyclic load tests can be exploited to obtain the load-displacement behaviour of micropiles under horizontal loading, and to determine the degradation of pile head stiffness as the number of cycles increases. Two cyclic lateral load tests were performed on the vertical micropiles P1 and P2. Pile P2 is loaded along the y axis, while P1 is loaded along the x axis, as shown in Figure 4-30, according to the corresponding alignment of strain gages. For pile P2, an arrangement of four 1-m³ concrete blocks is adopted as contrast (Figure 4-31), while for pile P1 the reaction is represented by the other pile (according to the configuration known as *two-in-one*, Richards and Rothbauer, 2004). Thus, in this case, the two micropiles are loaded with the same amplitude, but in opposite directions. For both pile the force is applied by means of a hydraulic jack, which is capable of imparting both tension and compression. The force applies at about 180 mm from the ground surface; moreover, two transducers measure the pile head displacements at 30 mm from the top of the pile (hereinafter called L1), and at about 120 mm from the soil surface (L2). Both tests are carried out in displacement control, and in particular the displacement of the transducer which is closer to the soil surface (and to the point of force application) is considered. As a displacement limitation, several lateral interpretation criteria are taken into account (a complete review can be found in Chen and Lee 2010): among others the criterion proposed by Walker and Cox (1966) is considered, thus the load at 12.5 mm head displacement is taken as the interpreted failure load.

The setup, for P2 test, consists of several plates and joints: the load cell is screwed into the cylinder of the hydraulic jack, and on the other side, it is horizontally articulated with a plate, rigidly connected to the concrete reaction block. Furthermore an artisanal mechanism that allow for high precision bi-directional screwing is welded to a plate connected to the other side of the hydraulic jack. This is to have a higher control of the displacement imposed to the pile, since the hydraulic power unit is not precise enough in the first steps on the loading. Finally the screwing mechanism is inserted into a 3-holes plate, that is rigidly connected to the pile by means of a hooked bar embracing the pile, bolted to the plate (Figure 4-32). This complex coupling system can work in tension and compression and has the advantage that doesn't require in situ soldering (particularly dangerous because of the presence of strain gages wires). The same kind of connection is adopted for P1 cyclic load tests, in order to connect the load cell to P2 (the reaction pile), as shown in Figure 4-33, and the manual screwing mechanism to pile P1 (the studied pile). The arrangement of cyclic load tests carried out on P1 is portrayed in Figure 4-34. In this case, also the displacement of the reaction pile (at about 120 mm from the ground surface) is registered.

Before and after free vibration tests, ambient vibration tests are carried out on micropiles to evaluate the residual dynamic properties.

Monotonic load test (first branch)

The lateral monotonic field load tests represent free (pinned) head conditions (in other words, the micropile head is free to rotate). In accordance with ASTM D3966 (ASTM 2007) the quick maintained load tests procedure is adopted during the monotonic load tests (first branch of the load-displacement curve). The load is applied in steps such that the

controlled displacement of the pile head (at L2) is of 0.5 mm. Such precise control on the applied force is allowed by the adoption of the manual screwing mechanism. Once the 0.5 mm displacement increment is obtained, the load is kept constant for about 2.5 minutes before applying a new load increment. When a total displacement of 12.5 mm is obtained, then the increment is kept constant for about 10 minutes.

Cyclic load tests

After the first loading branch, the first full cycle is performed (i.e. unloading, reversal of load until a displacement equal to 12.5 mm is reached in the opposite way, and corresponding unloading). Only three complete cycles have been performed on P2, due to a malfunctioning of the hydraulic power unit (almost all the cyclic load test was performed by applying the load with the manual screwing mechanism, requiring a high physical effort and time consumption). On P1, five full load cycles are performed since, after the first refined cycle, the traditional loading via hydraulic power unit is adopted.

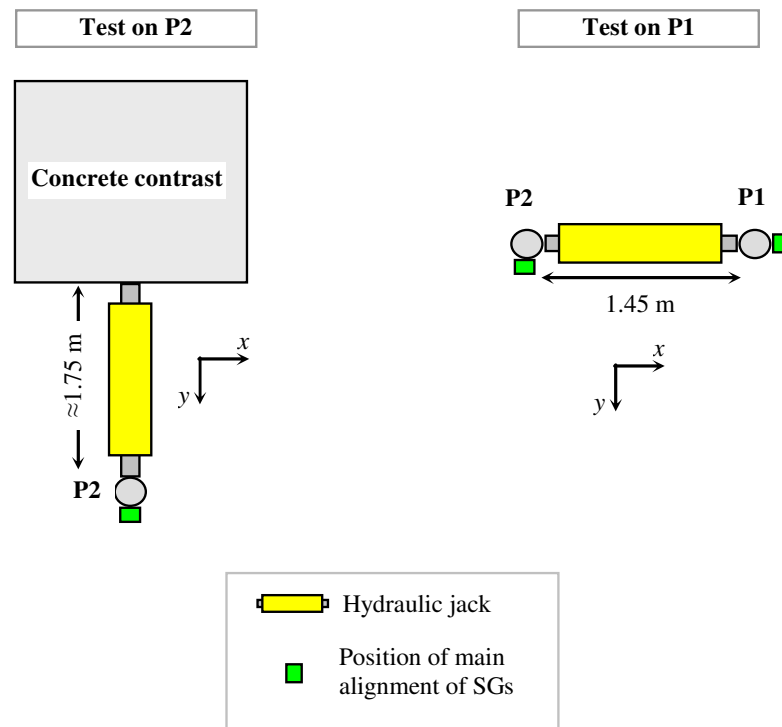


Figure 4-30 Configuration for 2-way cyclic loading on pile P1 and P2

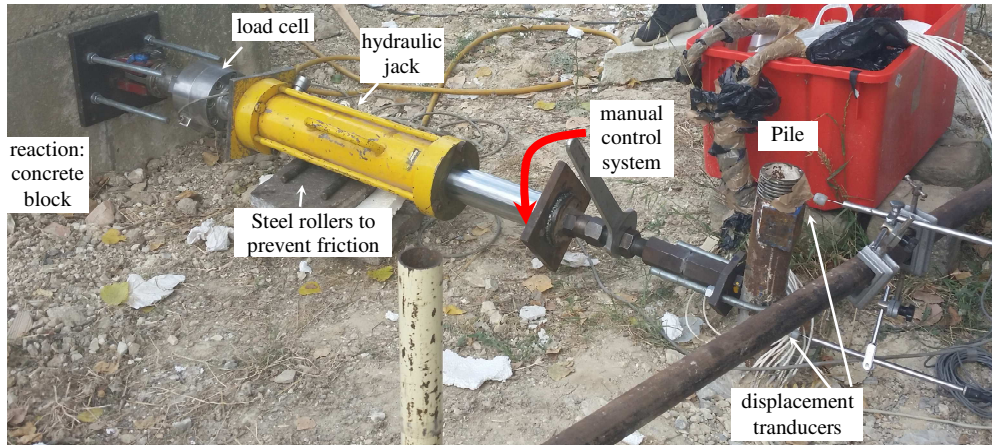


Figure 4-31 Arrangement for 2-way cyclic loading on P2



Figure 4-32 Details of the coupling between screwing device and reaction pile during test on P1



Figure 4-33 Arrangement for 2-way cyclic loading on P1



Figure 4-34 Details of the coupling between the load cell and pile P1

4.8. Free Vibration Tests

The free vibration test allows identifying the natural frequencies of soil-micropile system, its flexural deformed shapes and damping by studying the decrement of the vibrations. The free vibration test allows inducing stresses on the soil greater than the impact load test. These tests do not require a sophisticated instrumentation since the load may be applied with a standard hydraulic actuator. Here, the load is applied using the double acting hydraulic jack previously described, which has a capacity in tension of 20 t. As for cyclic load tests, the releases are carried out on both P1 (along x direction) and P2 (along y direction).

The quick release of the load is achieved thanks to “calibrated steel pins”. The calibrated pin consists of a steel element; the cross section of which is opportunely determined (Figure 4-35) so that it fails once a predetermined load is reached. After the pin failure, the micropile undergoes a number of steadily decreasing horizontal oscillation around its equilibrium position. As shown in Figure 4-36, the system adopted to put micropile under tension is similar to the one described for cyclic load tests for P1 and P2 respectively, except for the fact that the shear pin is placed between the jack and the pile, exploiting a specifically designed system of shackles and eyebolt (details in Figure 4-37).

The instrumentation comprises strain gages, displacement transducers with the same disposition as the one illustrated for cyclic loading, and two accelerometers (placed at the same height of the displacement transducers, but diametrically opposed in cross section). For pile P1 also the displacement of the reaction pile is monitored by means of a displacement transducer. Releases induced by four force (F) levels are investigated: 12 – 18 – 24 – 30 kN; for each force level, 2 tests (T) are carried out, for a total amount of 8 shear pins per pile. Before and after free vibration tests, ambient vibration tests are carried out on micropiles to evaluate the residual dynamic properties.







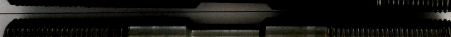
	T1	12 kN
	T2	
	T1	18 kN
	T2	
	T1	24 kN
	T2	
	T1	30 kN
	T2	

Figure 4-35 Calibrated pins adopted for snap back tests, and corresponding tensile failure forced

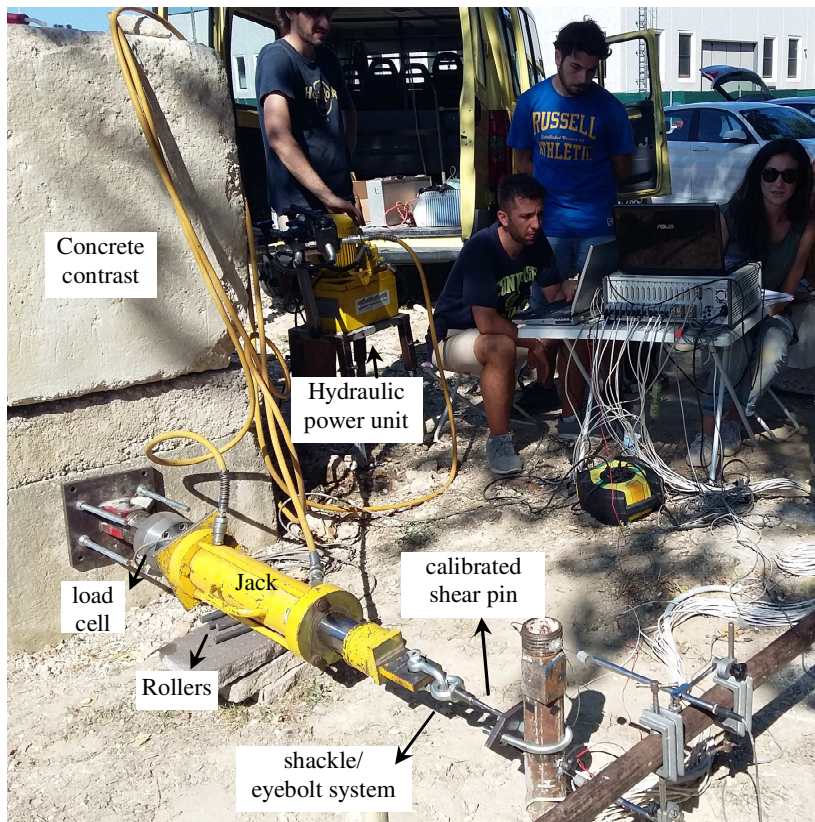


Figure 4-36 System adopted for the application of the release on P2



Figure 4-37 Details: shackle/eyebolt system, calibrated pin, and pile head instrumentation.

4.9. Forced Vibration Tests

Forced vibration test is the best technique to provide an input with high energy content and allows for an accurate assessment of the characteristics of the system also for highly damped modes that are not easy to catch with an impact load test or a snap back test (that usually excite mainly the first mode of vibration). However, the test has a long duration and is generally considered unattractive due to the cost of the rental or purchase of the shaker, and to its transportation. The forced vibration test can be carried out in two different ways, stepped-sine test and sine sweep test. In the stepped-sine testing the command signal supplied to the exciter is a discrete sinusoid with a fixed amplitude and frequency. In order to encompass a frequency range of interest, the command signal frequency is stepped from one discrete value to another in such a way as to provide the necessary density of points for the frequency response plot. In this technique, it is necessary to ensure that steady state conditions have been attained before the measurements are made. The sine sweep testing is the traditional method of the Frequency Response Function (FRF) measurement and involves the use of a sweep oscillator to provide a sinusoidal command signal, the frequency of which is varied slowly but continuously through the range of interest. As before, it is necessary to check that progress through the frequency range is sufficiently slow to check that steady-state response conditions are attained before measurements are made. If an excessive sweep rate is used, then distortions of the FRF plot are introduced. A way to check whether the sweep rate is suitable or not is to make the measurements twice, once sweeping up and the second time sweeping down through the frequency range. If the same curve results in the two cases, then the sweep rate is probably not excessive.

Forced vibration tests are performed by means of an experimental shaker (vibrodyne) on the pile group, with the stepped sine techniques. The vibrodyne can work with heavy or light masses, but, since with the heavy mass the investigable frequency range is reduced to less than 30 Hz, all tests are carried out with the light masses, which allow testing the system up to 50 Hz.

Several configurations are taken into account, by varying:

- direction of vibration (dir. x and y in the global reference system)
- $k(\alpha)$ of the machine (0.9, 4.2, 8.3, 23.4 N/Hz², as shown in Figure 4-38).
- masses of the cap (by means of 4 concrete blocks of about 70 kg, rigidly attached to the micropile group in a symmetrical configuration, as shown in Figure 4-39)

The configurations summarized in Table 4-5 are carried out.

During the tests several signals were acquired: 7 accelerometers on the cap (those measuring along the vertical axis have sensitivity 300 mV/g, and those measuring in the x/y directions have a sensitivity of 100 mV/g); 2 accelerometers on P1 and 2 on the ground near the cap, with a sensitivity of 10V/g and measuring along x and y axis; two displacement transducers measuring along the direction of loading, SGs placed on the instrumented inclined micropile (Figure 4-40a).

Tests indicated with number (2) are simply repeated, to check whether results are stable, while in those indicated with number (3) a different set of strain gages is acquired (Figure 4-40b). The acquired instrumentation is depicted in Figure 4-40 Before and after tests with the same $K(\alpha)$ along a direction, impact load tests along x and y axis are carried out on the micropiles group to evaluate the “post-shaking” dynamic properties.

Table 4-5 Stepped sine configuration carried out during forced vibration tests

	WITHOUT ADDED MASSES		WITH ADDED MASSES	
	<i>dir x</i>	<i>dir y</i>	<i>dir x</i>	<i>dir y</i>
	0.9	0.9	0.9	0.9
	0.9 (2)	-	0.9 (2)	0.9 (2)
	4.2	4.2		
K(α) (N/Hz ²)	4.2 (2)	4.2 (2)		
	8.3	8.3		
	8.3 (2)	8.3 (2)		
	23.4	23.4		
	23.4 (2)	23.4 (2)		
	23.4 (3)	23.4 (3)		

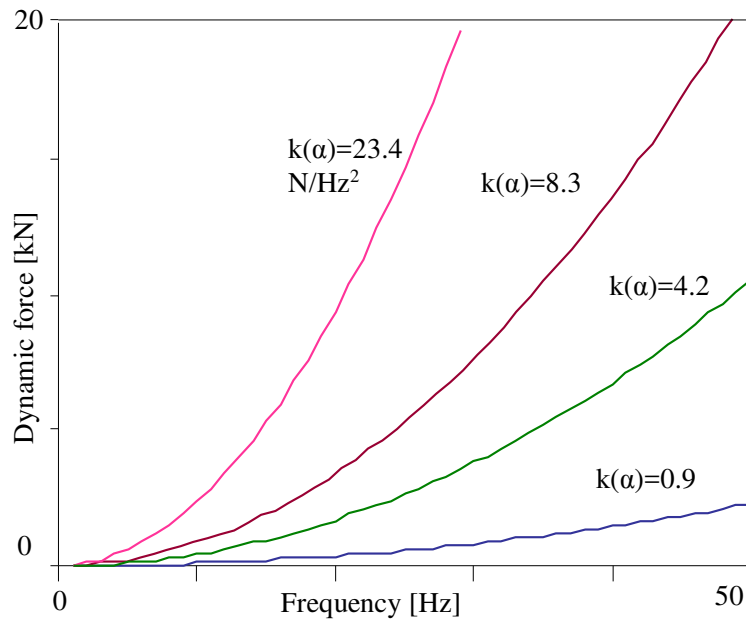


Figure 4-38 Dynamic force-frequency curves in the vibrodyne configuration adopted for forced vibration tests



Figure 4-39 Forced vibration tests: (a) no added mass; (b) with added masses

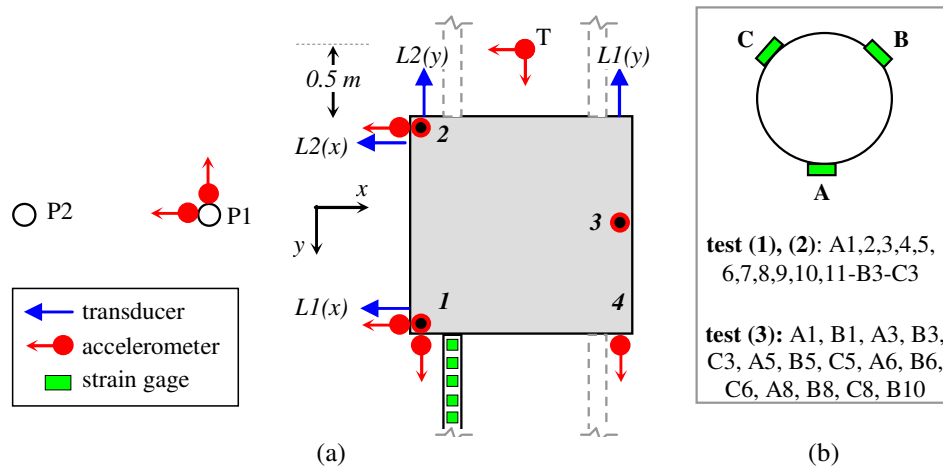


Figure 4-40 Acquired instruments (a), and (b) selection of acquired SGs according to different test configuration

Chapter 5.

Results

5.1. Introduction

In this chapter results of the test performed on single micropiles and micropiles group are presented and discussed.

Results of ambient vibration tests are here presented in terms of Power Spectral Density (PSD) function along x and y direction.

The PSD of a real, stationary signal $x(t)$ is the Fourier transform of the autocorrelation, i.e:

$$PSD(f) = \int_{-\infty}^{+\infty} R_x(\tau) e^{-2\pi i f \tau} d\tau \quad (5.1)$$

being R_x the auto-correlation function of the signal, f the frequency, and t the time; it describes the distribution of power into the frequency components that compose that signal.

On the other hand, results of impact load tests, free vibration tests and force vibration tests are presented in terms of Frequency Response Function (FRF) function of the registered signal along x and y direction, likely:

$$FRF(f) = \frac{X(f)}{Y(f)} \quad (5.2)$$

being $X(f)$ the Fourier transform of the output (i.e. accelerometer signal) and $Y(f)$ the Fourier transform of the input (i.e. hammer impact signal); in other words, it is a simple representation of the relationship between the input and the output of the studied system.

In general, this ratio is complex and it is characterized by both an amplitude ratio and a phase angle between the two sine waves.

This ratio can be expressed by means of several alternative forms:

- Receptance Frequency Response Function or $\alpha(\omega)$: the ratio between a harmonic displacement response X and the harmonic force F ;
- Mobility Frequency Response Function or $Y(\omega)$: the ratio between a harmonic velocity response V and the harmonic force F ;
- Inertance Frequency Response Function or $A(\omega)$: the ratio between a harmonic acceleration response A and the harmonic force F .

When considering sinusoidal vibration we have very simple relationship between displacement, velocity and acceleration, thus between receptance, mobility and inertance.

In fact:

$$x(t) = X e^{i\omega t} \quad (5.3)$$

and

$$v(t) = \dot{x}(t) = Ve^{i\omega t} = i\omega X e^{i\omega t} \quad (5.4)$$

so that

$$Y(\omega) = \frac{V}{F} = i\omega \frac{X}{F} = i\omega \alpha(\omega) \quad (5.5)$$

Thus

$$|Y(\omega)| = \omega |\alpha(\omega)| \text{ and } \theta_Y = \theta_\alpha + 90^\circ \quad (5.6)$$

Similarly,

$$A(\omega) = \frac{A}{F} = -\omega^2 \alpha(\omega) \quad (5.7)$$

FRFs are commonly represented in terms of modulus (and phase) of FRF versus frequency (Figure 5-2), or real and imaginary part of FRF versus frequency (Figure 5-3).

Moreover, there exist more alternatives by defining the functions in an inverse way, such as in terms of dynamic stiffness, the ratio between force and displacement.

Dealing with FRFs, the simplest approach to evaluate fundamental frequency, damping, and modal constant of the mode being analysed, is the so called *peak picking* or *peak amplitude method* (Ewins, 2000). In this method it is assumed that all the response can be attributed to the local mode and that any effects due to other modes can be ignored.

This is a method that adequately works for structures whose FRF exhibit well-separated modes which are not so lightly damped that accurate measurement at resonance are difficult to obtain but which, on the other hand, are not so heavily damped that the response at a resonance is strongly influenced by more than one mode. Although this limits the applicability of the method, it should be noted that in the more difficult cases, such approach can be useful to obtain an initial estimates to the required parameters.

The peak picking method can be applied by following the subsequent steps (Figure 5-1a, b):

- First, individual resonance peaks are detected on the FRF plot, and the frequency of the maximum response (or of one of the maximum responses) taken as the natural frequency of that mode.

$$f_r = \frac{\omega_r}{2\pi} = \frac{\omega(\max|H|)}{2\pi} \quad (5.8)$$

- Then, the local maximum value $|\hat{H}|$ of the FRF is noted and the frequency bandwidth of the function for a response level of $\frac{|\hat{H}|}{\sqrt{2}}$ is determined ($\Delta\omega$). The two points so identified as ω_a and ω_b , are the '*half power points*':

$$\omega_a, \omega_b = \omega \left(\left| \hat{H} \right| = \frac{|H|(\omega = \omega_r)}{\sqrt{2}} \right) \quad (5.9)$$

- The damping of the analysed mode can be estimated as:

$$\xi_r = \frac{\omega_b^2 - \omega_a^2}{4\omega_r^2} \approx \frac{\omega_b - \omega_a}{2\omega_r} \quad (5.10)$$

- Last, we may now obtain an estimate for the modal constant A_r of the mode being analysed by assuming that the total response in this resonant region is attributed to a single term in the general FRF series.

$$A_r = |\hat{H}| 2\xi_r \omega_r^2 \quad (5.11)$$

As already mentioned, the limitations of this method should not be forgotten. In particular, it must be noted that the estimates of damping and modal constant depend heavily on the accuracy of the maximum FRF level, $|\hat{H}|$.

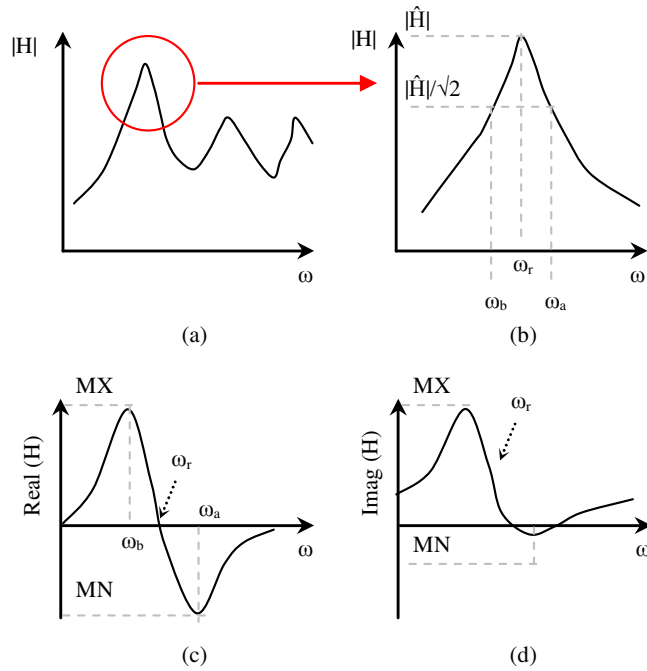


Figure 5-1 Peak picking method of modal analysis: (a) FRF modulus plot; (b) Resonance detail; (c) Real part of a single mode plot; (d) Imaginary part of single mode plot

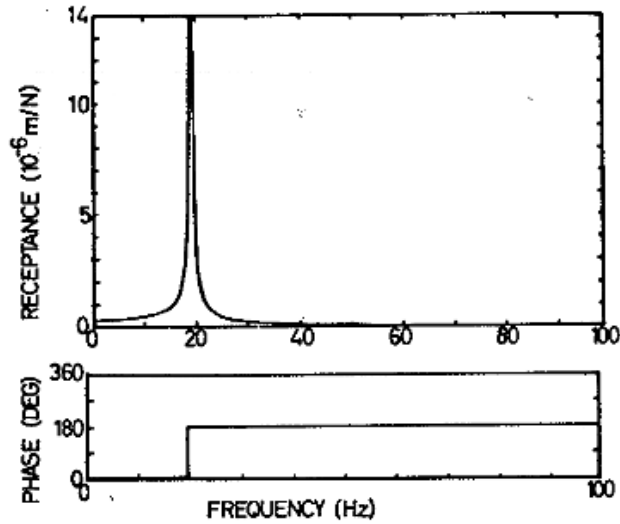


Figure 5-2 Receptance (magnitude and phase plots) for undamped single degree of freedom system

Unfortunately, most of the errors in measurements are concentrated around the resonance region and particular care must be taken with lightly damped structures where the peak value may rely entirely on the validity of a single point in the FRF spectrum.

Also, it is clear that only real modal constant (i.e. relevant for real modes, typical of proportionally damped structures), can be deduced by this method. Then, clearly, it should be considered that the single-mode assumption is generally not strictly applicable. In fact, even with well-separated modes, it is often found that the neighbouring modes contribute a lot to the total response at the resonance of the mode being analysed. However, this drawback can be overcome by working with a plot of the real part of the FRF (when considering the Receptance FRF), instead of the modulus plot. The position and values of the plot yield good estimates of the location of the half-power points. Furthermore, a more refined estimate of the natural frequency can be obtained from the midway point between the maximum and minimum of the imaginary plot (Figure 5-1 c, d).

Thus we can use:

$$A_r = \left(|MX| + |MN| \right) 2\xi_r \omega_r^2 \quad (5.12)$$

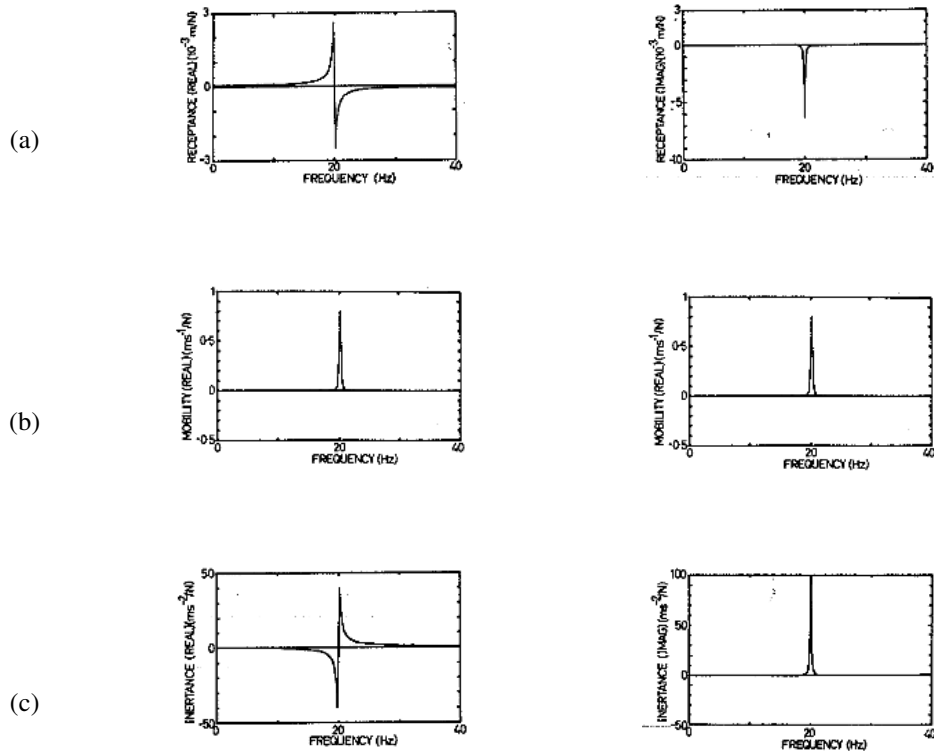


Figure 5-3 Plots of real and imaginary parts of FRF for damped SDOF system
 (a) Receptance; (b) Mobility; (c) Inertance.

For impact load tests and free vibration tests the so called S-transform will be adopted, in order to investigate some aspect of system non linearity and non stationarity of signals (conditions under which the applicability of traditional Fast Fourier Transform FFT is not verified). It has been developed for geophysical application by R. G. Stockwell (1996). Although the Fourier transform of the entire time series contains information about the spectral components in a time series, for a large class of practical applications, this information is inadequate. For instance, in an earthquake seismogram the first signal to arrive is the P (Primary) wave followed by other P waves travelling along different paths. The P arrivals are followed by the S (Secondary) waves and by higher amplitude dispersive surface waves. The amplitude of these oscillations can increase by more than two orders of magnitude within a few seconds of the arrival of the P. The spectral components of such a time series clearly have a strong dependence on time. In this case it would be desirable to have a joint time-frequency representation (TFR). The S-Transform provides a TFR with frequency-dependent resolution while, at the same time, maintaining the direct relationship, through time-averaging, with the Fourier spectrum.

There are several methods of arriving at the S transform, for instance it can be derived as the “phase correction” of the continuous wavelet transform (CWT). The CWT $W(\tau, d)$ of a function $h(t)$ is defined by

$$W(\tau, d) = \int_{-\infty}^{\infty} h(t)w(t-\tau, d)dt \quad (5.13)$$

where $w(t, d)$ is a scaled replica of the fundamental mother wavelet. The dilation d determines the “width” of the wavelet $w(t, d)$ and thus controls the resolution.

The S transform of a function $h(t)$ is defined as a CWT with a specific mother wavelet multiplied by the phase factor

$$S(\tau, d) = e^{i2\pi f\tau}W(\tau, d) \quad (5.14)$$

where the mother wavelet is defined as

$$w(t, d) = \frac{|f|}{\sqrt{2\pi}} e^{-\frac{t^2 f^2}{2}} e^{-i2\pi ft} \quad (5.15)$$

Note that the dilation factor d is the inverse of the frequency f .

The wavelet in Equation (5.15) does not satisfy the condition of zero mean for an admissible wavelet; therefore, Equation (5.14) is not strictly a CWT. Written out explicitly, the S transform is

$$S(\tau, d) = \int_{-\infty}^{\infty} h(t) \frac{|f|}{\sqrt{2\pi}} e^{-\frac{(t-f)^2 f^2}{2}} e^{-i2\pi ft} dt \quad (5.16)$$

If the S transform is indeed a representation of the local spectrum, one would expect a simple operation of averaging the local spectra over time to give the Fourier spectrum. It is easy to show that

$$\int_{-\infty}^{\infty} S(\tau, d)d\tau = H(f) \quad (5.17)$$

where $H(f)$ is the Fourier transform of $h(t)$.

Finally, for what concerns cyclic load tests, results focus on force-displacement relationship, and degradation parameters derived from the curves.

5.2. Single Micropiles

In this section results relevant for the response of single micropiles under loading of different nature and energy level, are reported. In particular ambient vibration tests, impact load tests (examining different configurations) and free vibration tests are exploited.

5.2.1. Ambient vibration tests

Ambient Vibration Tests (AVTs), performed by means of high sensibility accelerometers, are recently getting widely adopted by structural engineers to evaluate the dynamic properties of structures and infrastructures. However, to the author's knowledge, this procedure has never been taken into account for the identification of the dynamic properties of soil-micropile systems.

In this work, AVTs have been exploited to evaluate the dynamic properties of the single vertical micropiles. Tests are carried out at the end of the process of grout maturation, about one month after the execution of high pressure injections. Also the response of a single inclined micropile (before the execution of the concrete cap connecting the four inclined micropiles) has been investigated.

In Figure 5-4 results of AVTs performed on single micropiles in free head configuration are reported while the fundamental frequencies obtained from AVTs along x and y direction for the examined micropiles are summarized in Table 5-1.

Generally speaking, it can be seen that the natural frequencies of the single micropiles fall in a range of frequencies higher than that usually considered in seismic engineering; this is related to the absence of mass at the micropiles head.

By superposing PSD functions obtained along x and y axes for P1 (Figure 5-4a) it can be clearly observed that the dynamic responses along the two orthogonal directions are slightly different, especially in terms of fundamental frequencies. On the other hand, results for P2 are more similar in the two directions (Figure 5-4b). Moreover it can be noted that P1 is in general stiffer than P2 (in both directions).

The stiffening of the system can be attributed partly to the stiffening of the micropile itself (since its cross-section increases) but even to the compaction of the soil surrounding the injected portion of micropile (several bulbs are formed all around the pile, both displacing and compacting the soil). Moreover the stiffening seems to be more pronounced in the direction along which injections are performed. This can be explained by the fact that the 4 couples of injection holes of each 2-m long element of *tubes a manchèttes* are aligned along 2 generatrices diametrically opposite, as shown in Figure 4-6. It is worth noting that to allow a better interpretation of results, during the installation of the instrumented reinforcement bar the direction of injection and its normal have been aligned with the principal directions x and y adopted as global reference system.

For what concerns results relevant for the instrumented inclined injected micropile (P3) (Figure 5-4c), it can be found that the fundamental frequency along both x and y axis of the inclined micropile is higher than that registered not only for P2, but even for P1.

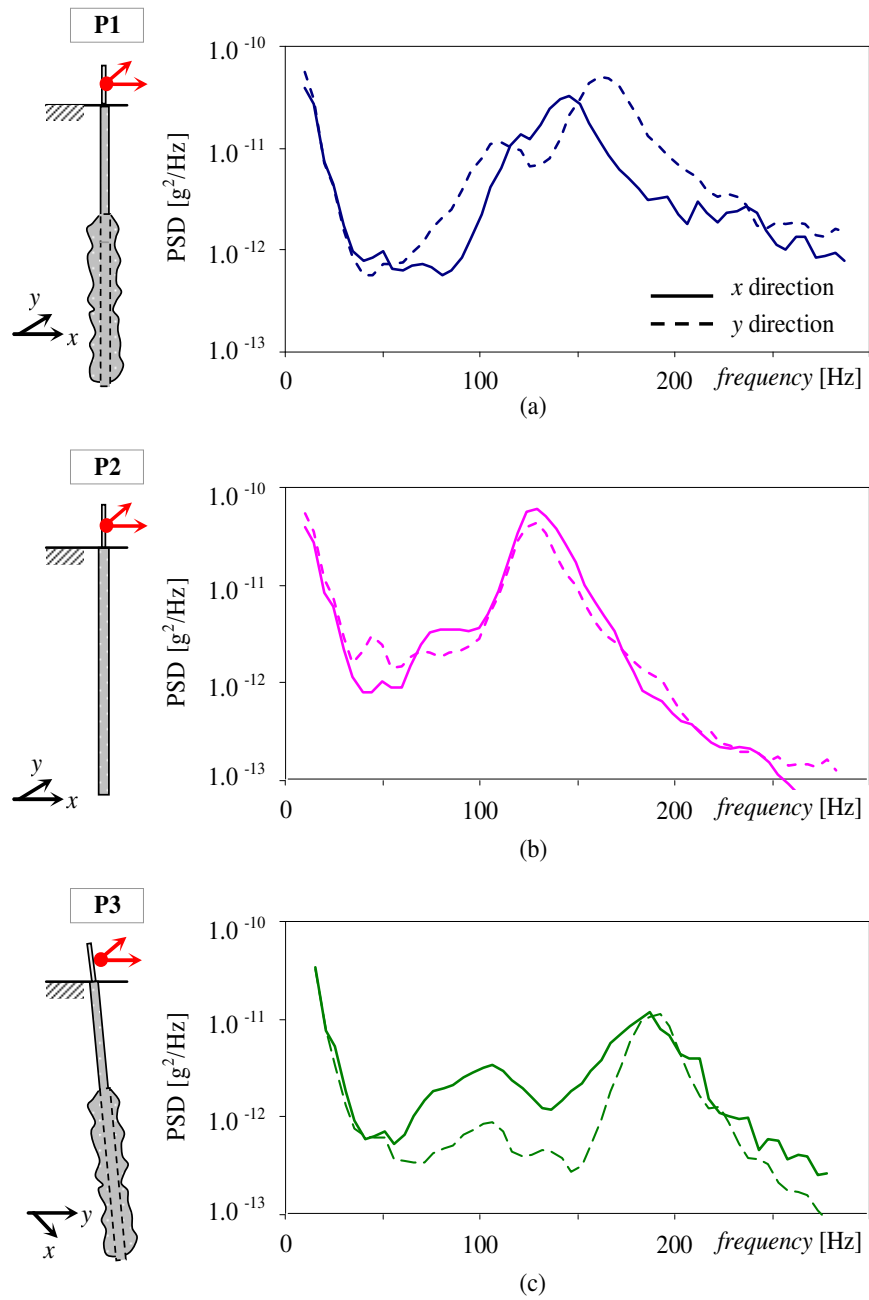


Figure 5-4 Results of ambient vibration tests for (a) injected vertical micropiles, (b) simply grouted vertical micropile, (c) inclined injected micropile, along x and y direction in free head configuration

Table 5-1 Fundamental frequencies of single micropiles determined via AVTs

	P1	P2	P3
x	146 Hz	131 Hz	192 Hz
y	166 Hz	131 Hz	197 Hz

This can be attributed to high pressure injections but even to the presence of the other 3 inclined injected micropiles nearby P3 and their effect on the surrounding soil.

As a general observation, AVTs have proven to be an effective and rapid test for the identification of the dynamic stiffness of soil-micropile system. Therefore, this technique has also been adopted for the identification of the “post-shake” dynamic properties of single micropiles at the end of high strain level tests.

5.2.2. Impact Load Tests

In the following, results relevant for different impact configurations are reported:

- configuration A: Impact Load Tests (ILTs) on micropiles without pipe extension, low impact intensity
- configuration B: ILTs on micropiles with pipe extension, low impact intensity
- configuration C: ILTs on micropiles with pipe extension, high impact intensity

Results of Impact Load Tests for single micropiles refer to the averaged values obtained from at least 10 impacts.

Configuration A

The comparison between averaged FRFs (calculated on micropile head acceleration) obtained for P1 and P2 (Figure 5-5), shows a difference between the behaviour of the injected and non-injected micropiles, as obtained from AVTs. In particular, the fundamental frequencies of the two systems (f_{P1} and f_{P2}) have a difference of about 12 Hz (Table 5-2).

Furthermore, from the time histories of the recorded accelerations a value of the damping coefficient (determined via half power bandwidth method) of about 12% is obtained for both micropiles in this test configuration.

With respect to fundamental frequencies obtained from AVTs, ILTs provide lower values due to higher strain range induced by the impact load test.

Configuration B

In this configuration, a 1-m long pipe extension is rigidly attached by means of a specific joint at the top the micropile head. By increasing the length of the system, fundamental frequencies decrease so that it is also possible to investigate the II mode of vibration of the micropile.

Coherently with results of AVTs, the comparison of averaged FRFs obtained considering impacts along x and y directions (Figure 5-6) shows that for the injected micropile a marked difference exists between the behaviour along the two orthogonal directions (again, the pile seems stiffer along the y direction), especially for the second mode, while the non-injected micropile doesn't show significant differences between the behaviour along the x axis and that along y axis. A synthesis of the obtained values of fundamental frequencies and damping for the first two modes of vibrations is presented in Table 5-3.

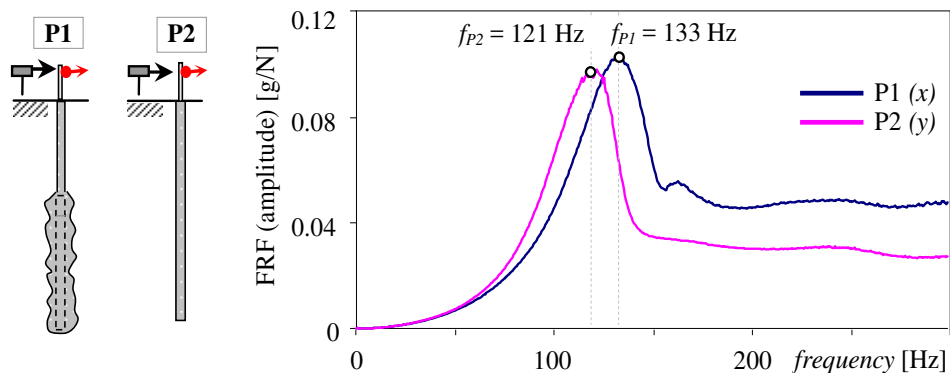


Figure 5-5 Results of ILTs for single micropiles in free head configuration along dir x

Table 5-2 Fundamental frequencies and damping of single micropiles via ILTs (configuration A)

	P1	P2
Fundamental frequency f_I	133 Hz	121 Hz
Damping ξ_I	0.122	0.118

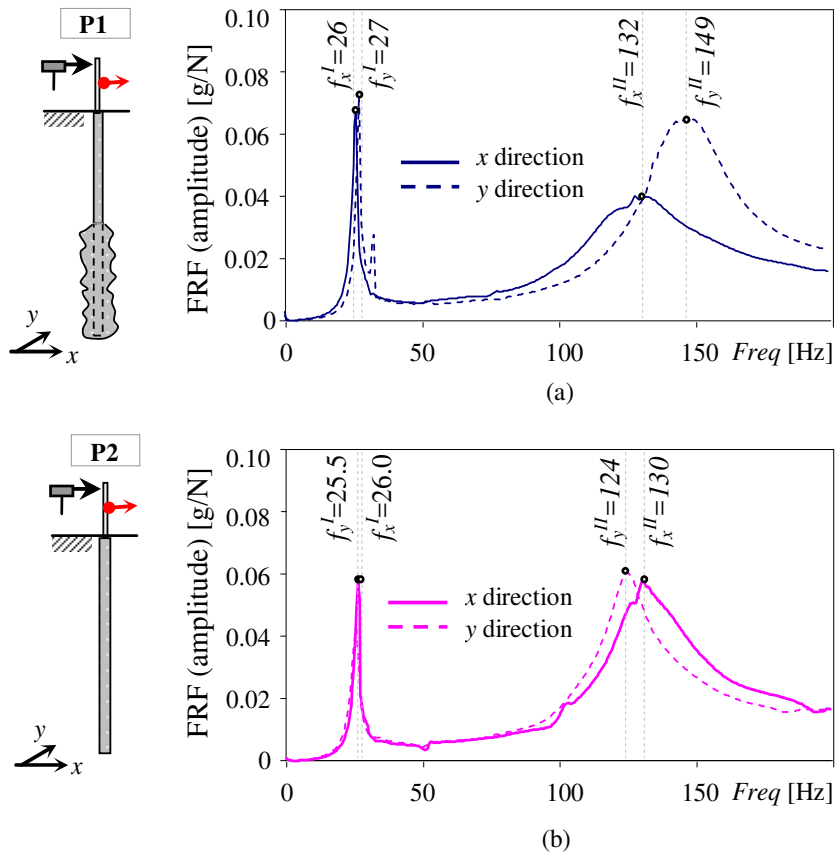


Figure 5-6 Results of ILTs for (a) injected micropiles, and (b) simply grouted micropiles, along x and y direction in configuration B

Table 5-3 Fundamental frequencies and damping of single micropiles via ILTs, for the first two modes identified (configuration B)

		P1		P2	
		x	y	x	y
I mode	Fundamental frequency f_I	26	27	26	25.5
	Damping ξ_I	0.030	0.022	0.031	0.044
II mode	Fundamental frequency f_{II}	131.5	148.5	130	124
	Damping ξ_{II}	0.154	0.095	0.094	0.071

Configuration C

By exploiting the pipe extension it is also possible to increase the level of energy exerted by the impact, and to better investigate the behaviour of the strain gages embedded in the soil. In this case, impacts are applied along the direction relevant for the strain gauge signals, i.e. x axis for P1 and y axis for P2.

Raw signals recorded at each strain gage are reported in Figure 5-7 for P1 and in Figure 5-8 for P2. Depths of strain gages, also provided in legend, are relative to the effective depth of the sensors (indirectly measured after the installation of the micropiles, by measuring the effective height of the towering part).

In Figure 5-9 and Figure 5-10 profiles of natural frequencies and damping obtained by means of peak picking method for P1 and P2 are shown.

Some observations arise:

- As it may be guessed, noise of SGs signals increases with depth.
- For both piles, natural frequency detectable from the first SGs signals is quite unstable; furthermore it slightly increases within the 1st meter but, after this shift, it remains constant with depth. Despite the presence of two close resonance peaks for some of the estensimetric signals, the fundamental frequencies of the first mode of vibration obtained from accelerometers in configuration B are in accordance with those obtained from configuration C.
- Amplitude of signals relevant for the first two SGs (placed within the first 20 cm in depth) show an exceptionally high value; since this behaviour can be found in all the instrumented piles (including the inclined micropile) when subjected to impact load, this phenomenon should not be neglected. Possible explanations of this behaviour are a partial debonding at the interface between the reinforcement bar (on which SGs are installed) alongside with heterogeneous characteristics of the soil in the shallower centimetres.
- Damping of this particular system is quite difficult to determine via peak picking method, especially for signals relevant for P1 which often show two very close peaks; this leads for P1 to particularly higher values of damping within the first 60 centimetres; however, from a first estimate, it appears that below the 1st meter for the simply grouted pile P2 damping is generally higher than that identified for P1, and tends to increase with depth.

In order to explain the latter point, Stockwell transform of signals acquired at different depth for a given impact load are represented in Figure 5-11 in order to follow the evolution of the dynamic properties with time.

From time histories of SGs placed at increasing depths, it can be observed that micropile vibrates around a deformed position, which can be thought as a sort of rigid rotation induced by the imperfect application of the impulse load. Micropile is subjected to two simultaneous movements: in fact it tends to return back to its original position with a “slow” movement, and in the meantime it undergoes flexural vibrations around a deformed position.

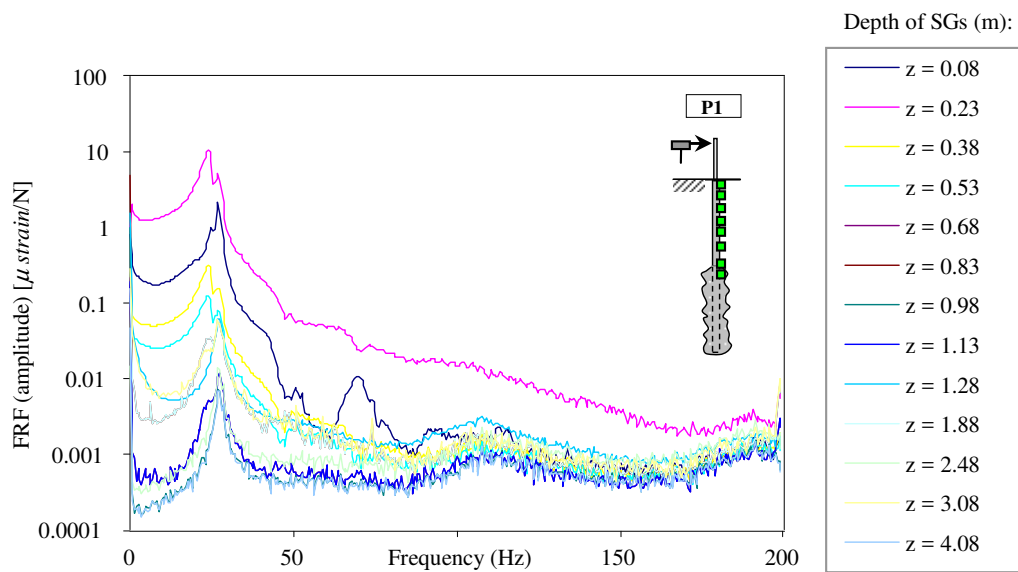


Figure 5-7 Results of ILTs for P1 at difference depth (strain gage signals)

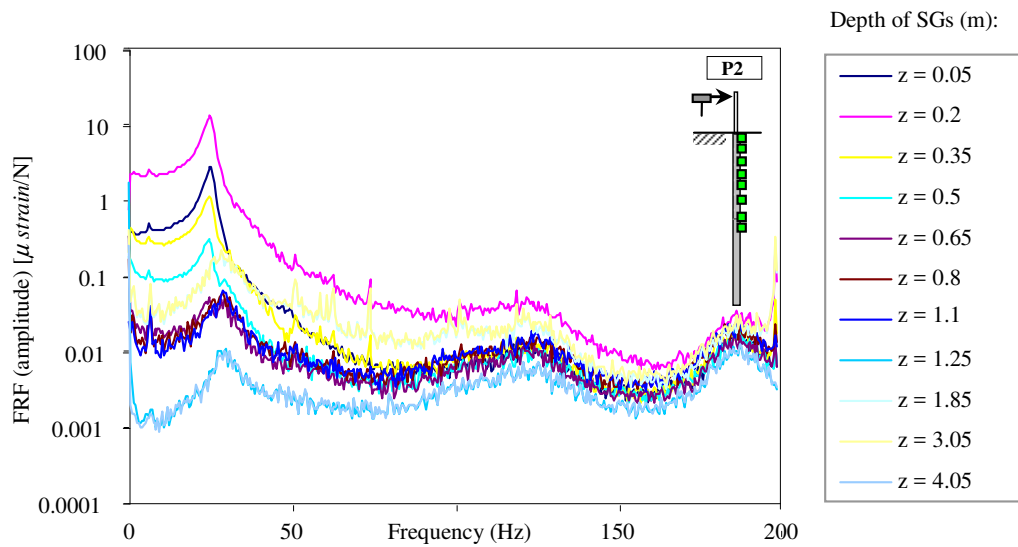


Figure 5-8 Results of ILTs for P2 at difference depth (strain gage signals)

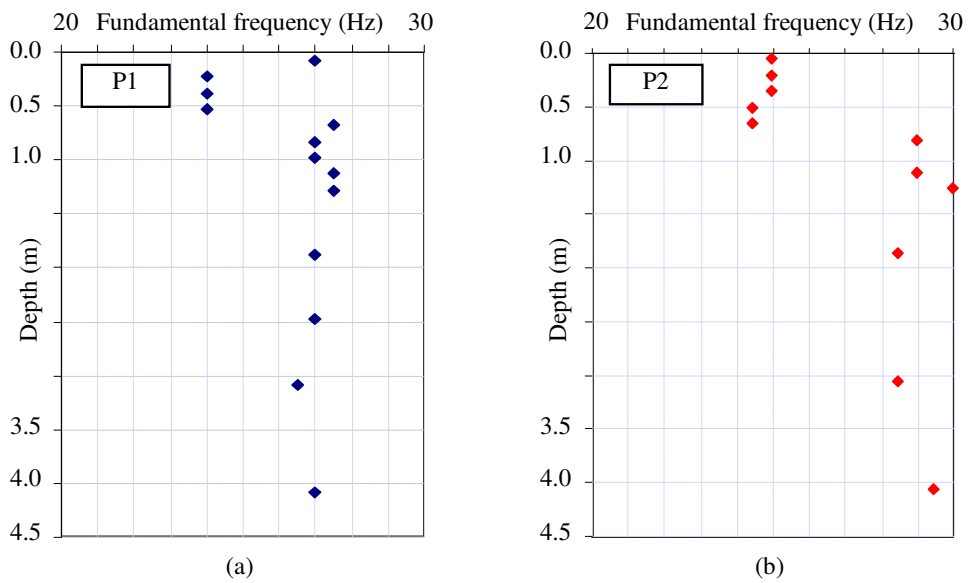


Figure 5-9 First fundamental frequency evaluated from strain gauges signals for P1 (a) and P2 (b)

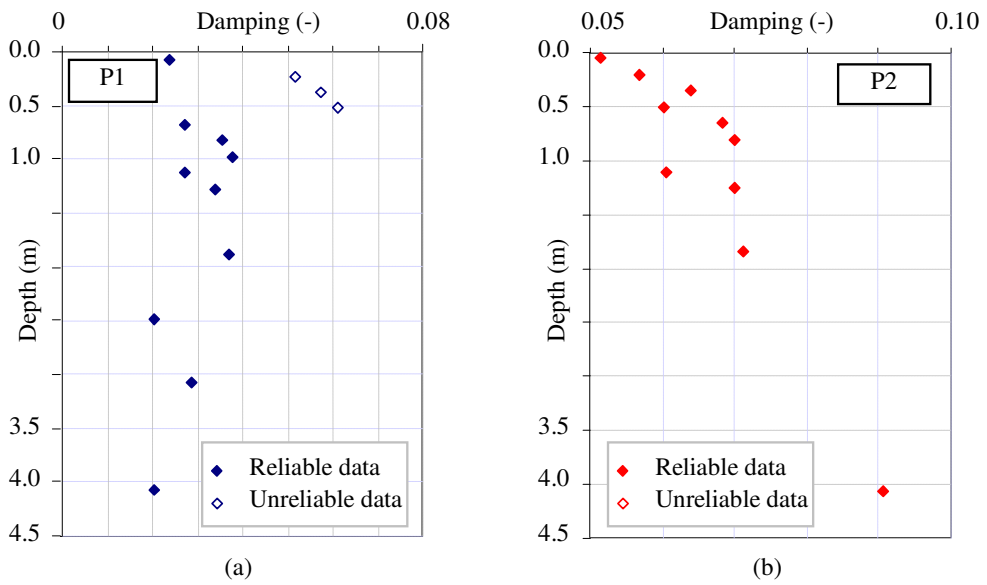


Figure 5-10 Damping evaluated from strain gauges signals for P1 (a) and P2 (b)

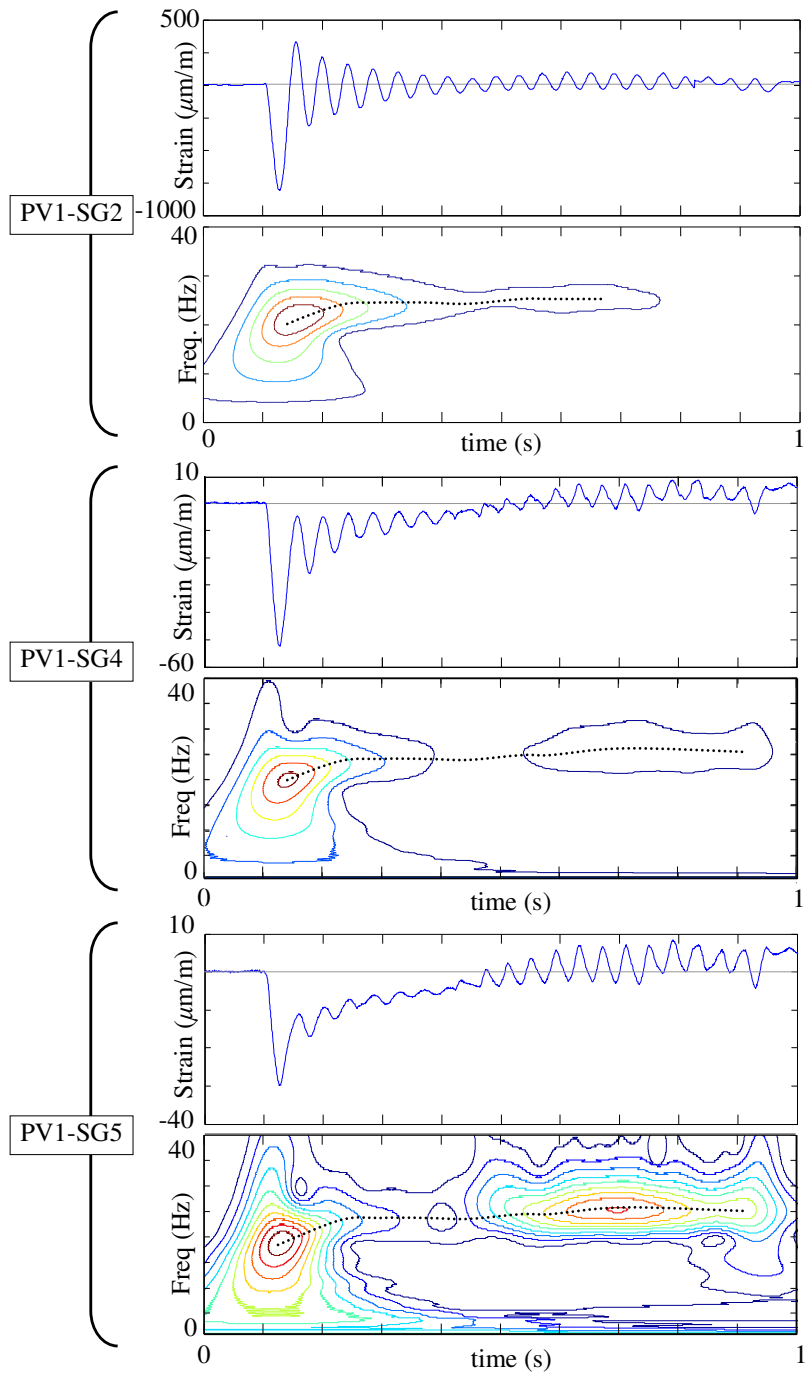


Figure 5-11 Time histories and Stockwell transform of 3 strain gage signals

From contours in the time-frequency domain relevant for S-transforms of signals it can be seen that the frequency of the vibration changes as the “return” movement proceeds. In the traditional FRF transform of each signal (i.e. Figure 5-7) this generates two close peaks, but S-transform reveals that each of them is related to a different part of the signal. Figure 5-12 tries to give simplified interpretations of the observed phenomenon. In the first part, the pile is deformed, and this probably induces a superficial, maybe partially reversible, debonding on the rear side of the micropile between the pile and the soil, and/or between the reinforcement bar and the surrounding grout, which is more likely, due to bad conditions of the superficial grout and to the fact that the bar is smooth and doesn’t facilitate the adherence with the grout; a superficial detachment between the bar and the grout has been observed, indeed. Conceptually the system can be schematically seen as a pile with compression-only Winkler springs on both sides. In the first instants, when the pile is deformed, superficial springs are partially detached (or not-working) on one side. Then the slow movement which brings the pile to its original position proceeds and, in a transitional position, the pile is slightly deformed on the other side. In this case the pile partially recovers some lateral restraints, and the portion of pile not ideally attached to springs is shorter than at the beginning, so that the system is a little stiffer and the fundamental frequency related to this part of the vibration is slightly higher. Moreover the second (higher) frequency gets more evident with depth, since the imposed initial deformation (and its consequences in terms of lateral restraints) is more significant in the superficial portion of the pile. On the contrary, the second strain gage (the first shown in Figure 5-11) is representative of a situation in which the bar is completely detached from the surrounding grout and recover substantially doesn’t take place. In practice, the inertia of the section at SG2 can be considered that of the bar filled with grout. This is in accordance with the high value of amplitude observed for this strain gage signal.

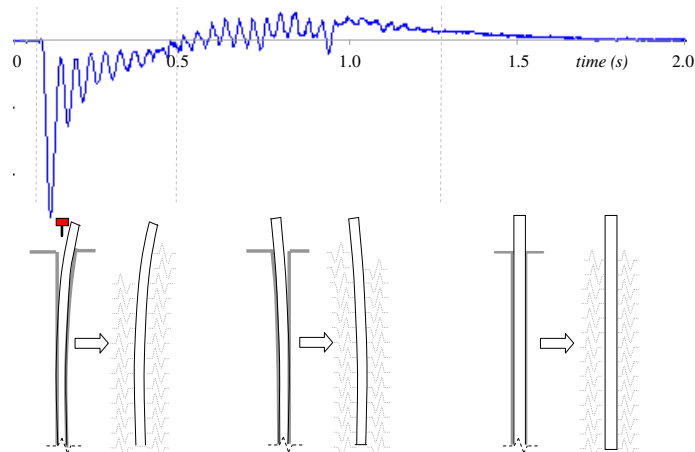


Figure 5-12 Schematic interpretation of SGs signals during impact load tests

Finally, in Figure 5-13 an approximated view of the modal shape for both P1 and P2 is depicted, within the first portion of the pile. For the determination of deformed shaped the following steps have been performed:

1. Calculation of FRFs of strains, and averaging among at least 10 impacts
2. Determination of strains profile at resonance from real or imaginary part of averaged FRFs at all the investigated positions
3. Fitting of curvature profile (in this case, a smoothing spline is adopted), as that shown, normalized with respect to maximum value, in Figure 5-13 a;
4. Double integration of curvature profile to obtain displacement values, shown in Figure 5-13 a, normalized with respect to maximum value.

It should be noted that, since the resonant frequency changes depending on the depth of the strain gage, the value chosen for the representation of the first bending mode has been identified on the basis of the SGs located within 0.75 m from the ground surface, where most of the deformation concentrates.

Profile of normalized curvatures and displacement for P1 and P2 are qualitatively similar.

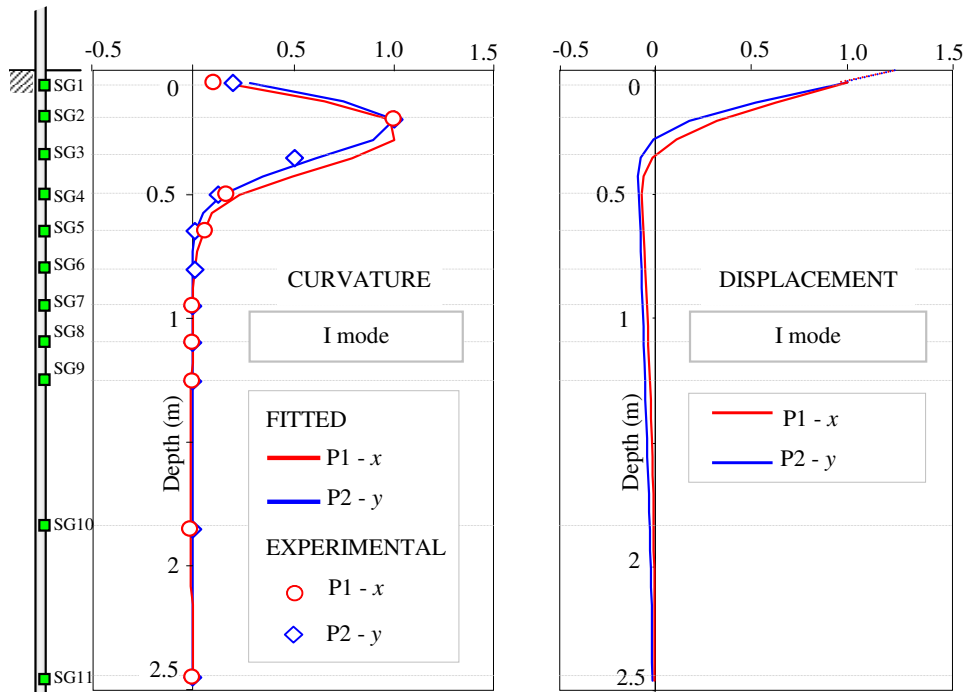


Figure 5-13 Normalized values close to the first resonance of (a) curvature (experimental and fitted values); (b) deformed shape for P1 and P2.

Impedance functions of single vertical micropiles

In the framework of *sub-structuring* approaches for the resolution of SSI problems, impedance functions are one of the essential components required for computing the response of pile-supported structures. Impedance function represents the complex stiffness of the soil–micropile system under dynamic loads. The real part reflects the stiffness of the soil–pile system, while the imaginary part represents the combined effect of radiation damping and material damping of micropile and soil.

Here, the horizontal impedance of the soil–micropiles system is determined as the ratio, in the frequency domain, between the impact load applied at the pile head along a direction orthogonal to the pile axis (in configuration A) and the resulting displacement at the pile head along the same direction. Displacements are derived from the recorded accelerometer signals by means of a double discrete integration in the time domain, and suitable filtering procedures. In Figure 5-14 (a, b) the real and imaginary parts of the experimental horizontal impedance of the whole system, for both P1 and P2, are shown over a wide frequency range. Curves are obtained by averaging among 10 impacts, and shadowed parts of the graphs represent the frequency ranges in which results are unstable. For both P1 and P2, the real part crosses zero at the first flexural frequency of the system and, within the range interested by the resonance of the system, the experimental stiffness ordinate exhibits reductions while damping increases with frequency. It can also be observed that the curves relevant for the injected and the non-injected micropile have similar trends. However, P1 shows a stiffer behaviour with respect to P2, along the entire range of frequency investigated, and the different value of the first flexural frequency with respect to P2 is identifiable through the comparison between the points of intersection with zero; moreover, trend of imaginary part seems more regular than that relevant for P2.

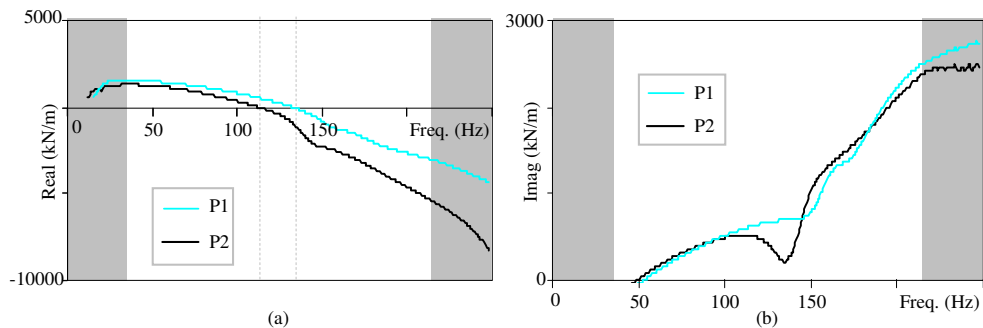


Figure 5-14 Experimental impedance functions of single vertical micropiles: real (a) and imaginary (b) parts of P1 and P2

5.2.3. Two-way cyclic loading

In the present section behaviour of simply grouted pile P2, and injected pile P1 under horizontal monotonic and cyclic loading is presented.

Monotonic load test (first branch)

The lateral monotonic field load tests are representative of the horizontal response of micropiles in free (pinned) head conditions. The load is applied in increments such that the relative displacement registered by the lower micropile head transducer L2 is about 0.5 mm for P2 and 1 mm for P1. When a total displacement of 12.5 mm is reached at L2, the corresponding load is held for 10 min, and the unloading is carried out. The approximate rotation of the micropile head is also obtained from the measures of the 2 aligned displacements, as shown in Figure 5-15.

In Figure 5-16, Figure 5-17, and Figure 5-18 the load-head displacement and load-head rotation curves for both micropiles are reported. The branch of the curve relative to the loading represents the original backbone curve (termed BKB in the sequel), and it is followed by the branch relative to the unloading (ULD).

From the observation of BKB curves it appears clearly that the behaviour of the injected micropile is comparable to that of the non injected micropile, but a higher force level is required to obtain the same displacement. This is also proven by the fact that when the *two-in-one* procedure was performed for the testing of P1, the displacement of P2 was kept monitored and, under the same force, P2 underwent displacements about 2 times higher than that experienced by P1.

It is important to point out that for both micropiles a gap opened during the loading test, (Figure 5-19). For both micropiles the maximum gap opening was of about 12-15 mm at the end of the loading step, with a depth of at least 10 cm (however it was very difficult to measure). During the unloading only a partial recovery of the gap occurred. Also permanent cracks in the shallower centimetres of the surrounding soil and in the superficial portion of grout were still evident at the end of the test.

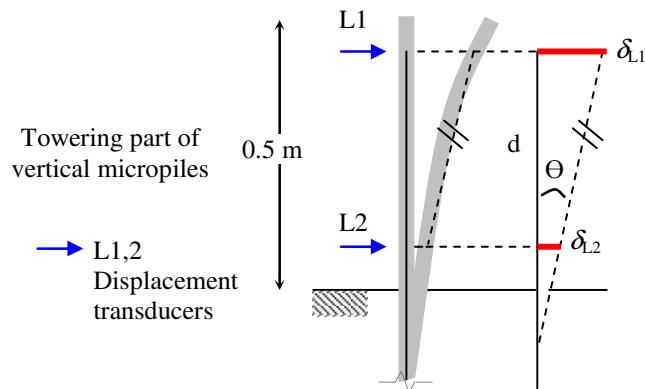


Figure 5-15 Derivation of simplified micropile head rotation

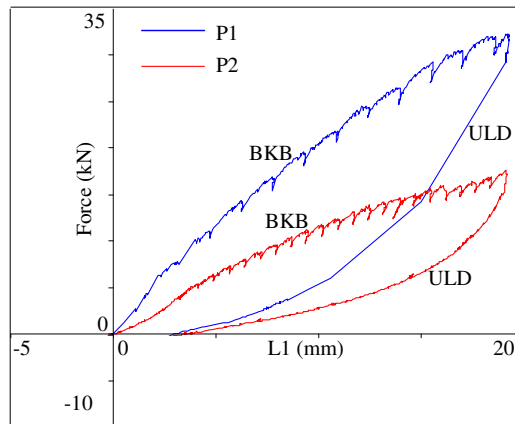


Figure 5-16 L1, pile head displacement for micropiles P1 and P2 for the monotonic load

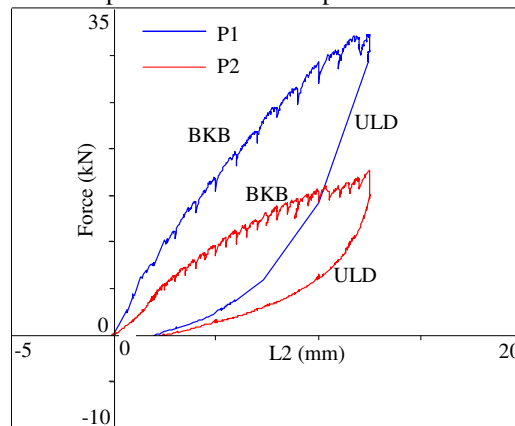


Figure 5-17 L2, pile head displacement for micropiles P1 and P2 for the monotonic load

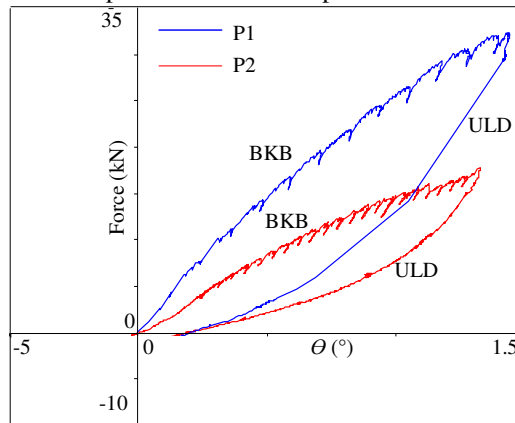


Figure 5-18 Θ , approximated head rotation for P1 and P2 for the monotonic load



Figure 5-19 Gap at the end of the first loading cycle on P1

In Figure 5-20 profiles of strains for pile P2¹ are reported, at increasing loading level; it appears clearly that at low loading level, strains obtained from the strain gages just below the ground have very high value, probably due to debonding between the reinforcement bar and the surrounding grout. As already suggested, this phenomenon can be attributed to weathering of the superficial grout as well as to lack of adherence between the reinforcement and the grout.

Moreover the scattering of the SGs data with the increase of the load proves that the pile suffered plasticization from the first loading steps of the test. In fact, for a linear pile in soft soil, it can easily be guessed that the depth of maximum bending moment (and of maximum strain) increases with the load intensity. In this case, on the contrary, due to small tensile resistance of the grout, the section suffered partialization that could have contributed to an unclear distribution of bending stresses with the increase of the loading.

Moreover, the progressive development of the gap opened between the grout and the soil from the surface to an uncertain depth could have contributed in different ways to shaping the strain distribution.

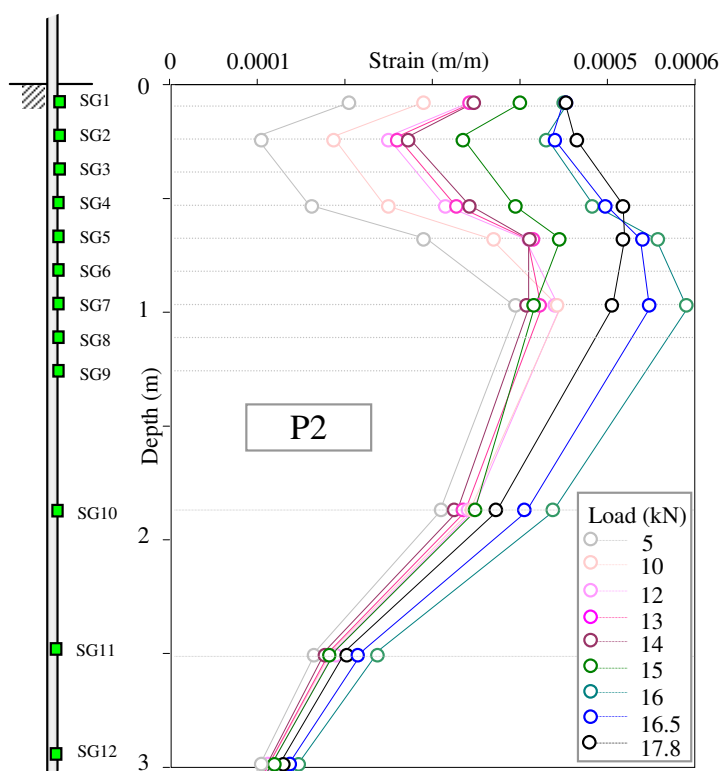


Figure 5-20 Strains profile at different loading levels

¹ Strain gages results for pile P1 have not been reported due to the lower quality of most of the data acquired during this test; further elaborations are needed.

Lateral 2-way cyclic load tests

Two-way cyclic loading procedure was adopted herein (i.e., the load was applied in a direction and reversed all the way in the other direction with the same amplitude). 3 cycles are applied for pile P2 and 5 for pile P1. Each cycle is carried out until the displacement measured by the lower transducer is equal to 12.5 mm.

Figure 5-21, Figure 5-22 and Figure 5-23 illustrate the load-deflection curves for the cyclic lateral load tests performed on both the micropiles for all the load cycles.

Some considerations immediately arise:

- Dealing with the load reversal, the load-displacement behaviour for both piles is symmetrical. It means that the gap previously opened during the first loading branch closes, and another gap develops on the other side of the pile.
- The reloading that follows the first cycle has a completely different appearance, as a consequence of the gap arisen in the previous loading cycle, and to the recompression occurred during the loading reversal. In particular, the slope of the first reloading curve (II cycle) is initially flat (the soil contribution to the stiffness is limited due to the soil-pile detachment) then it progressively grows when the contact between the soil and the pile is recovered, and finally it almost reaches the first BKB curve. The succeeding cycles are very similar to the II one.
- For all the cycles, it appears clearly that the stiffness of the micropiles varies with the load. Furthermore, for the same loading segment the corresponding stiffness varies with the number of cycles.

Taking cue from the latter consideration, the stiffness of the micropiles for each load cycle can be approximated by the slope of the load-deflection curve in different displacement-load step, i.e.

$$K_S = \frac{F_{\max} - F_{\min}}{y_{\max} - y_{\min}} \quad (13)$$

being K_S the micropile head stiffness for each step, F_{\max} and F_{\min} the maximum and minimum applied load for each step in which the BKB curve is divided, and y_{\max} and y_{\min} the corresponding pile head deflections. In particular, each BKB curve is divided into 5 segments, corresponding to a displacement increment equal to 2.5 mm.

The degradation of the pile head stiffness can be related to the number of cycles by means of a degradation parameter, β :

$$\frac{K_S^N}{K_S^1} = N^{-\beta_s} \quad (14)$$

that can also be expressed as

$$\log\left(\frac{K_S^N}{K_S^1}\right) = -\beta_s \log(N) \quad (15)$$

Where $K_{S,1}$ and $K_{S,N}$ are the stiffness value in cycles 1 and N , for the force-displacement range S . In a *log-log* graph β_s represents the slope of the fitting line.

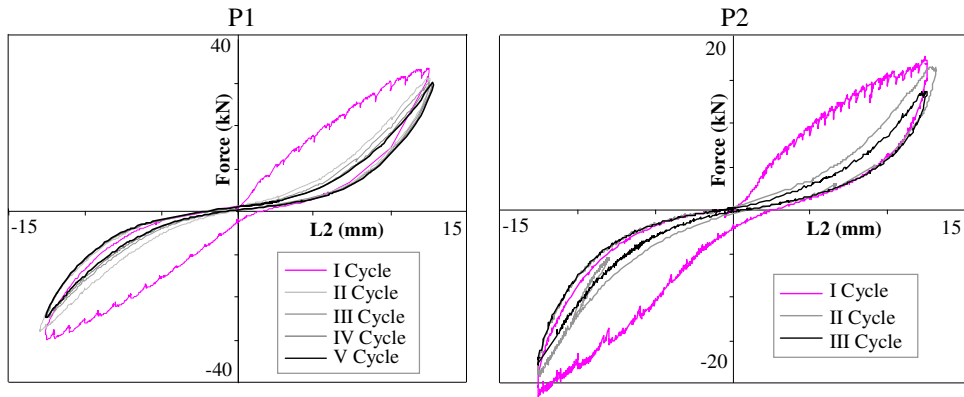


Figure 5-21 L2, pile head displacement for vertical micropiles over cycles

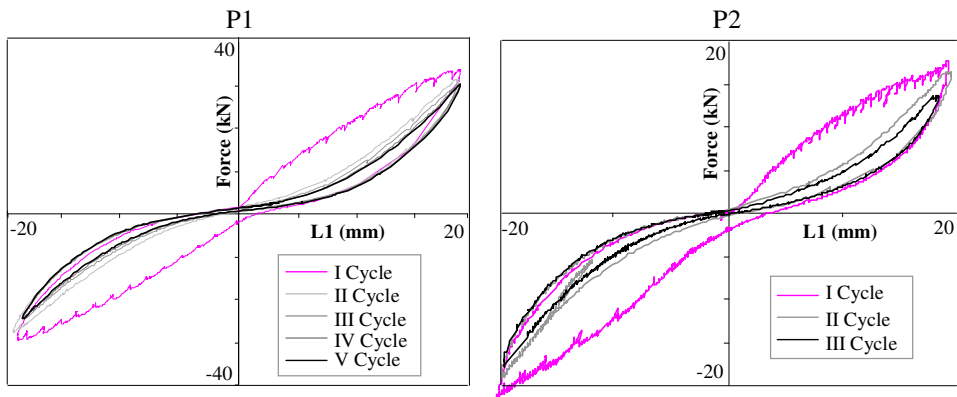


Figure 5-22 L1 pile head displacement for vertical micropiles over cycles

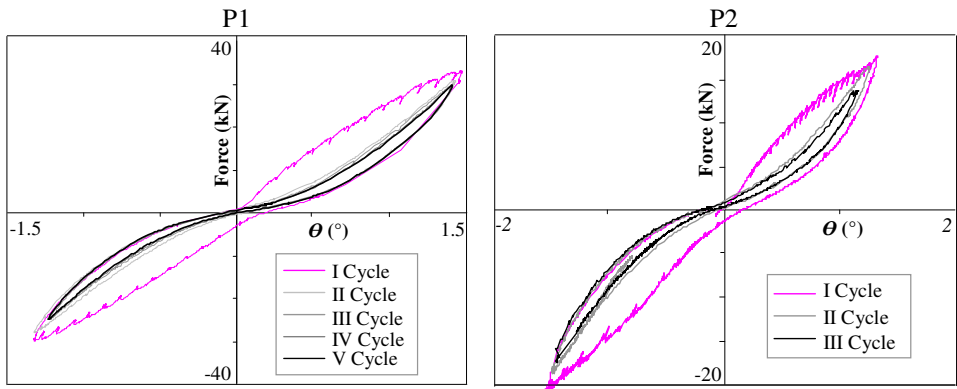


Figure 5-23 θ , micropile head rotation for vertical micropiles over cycles

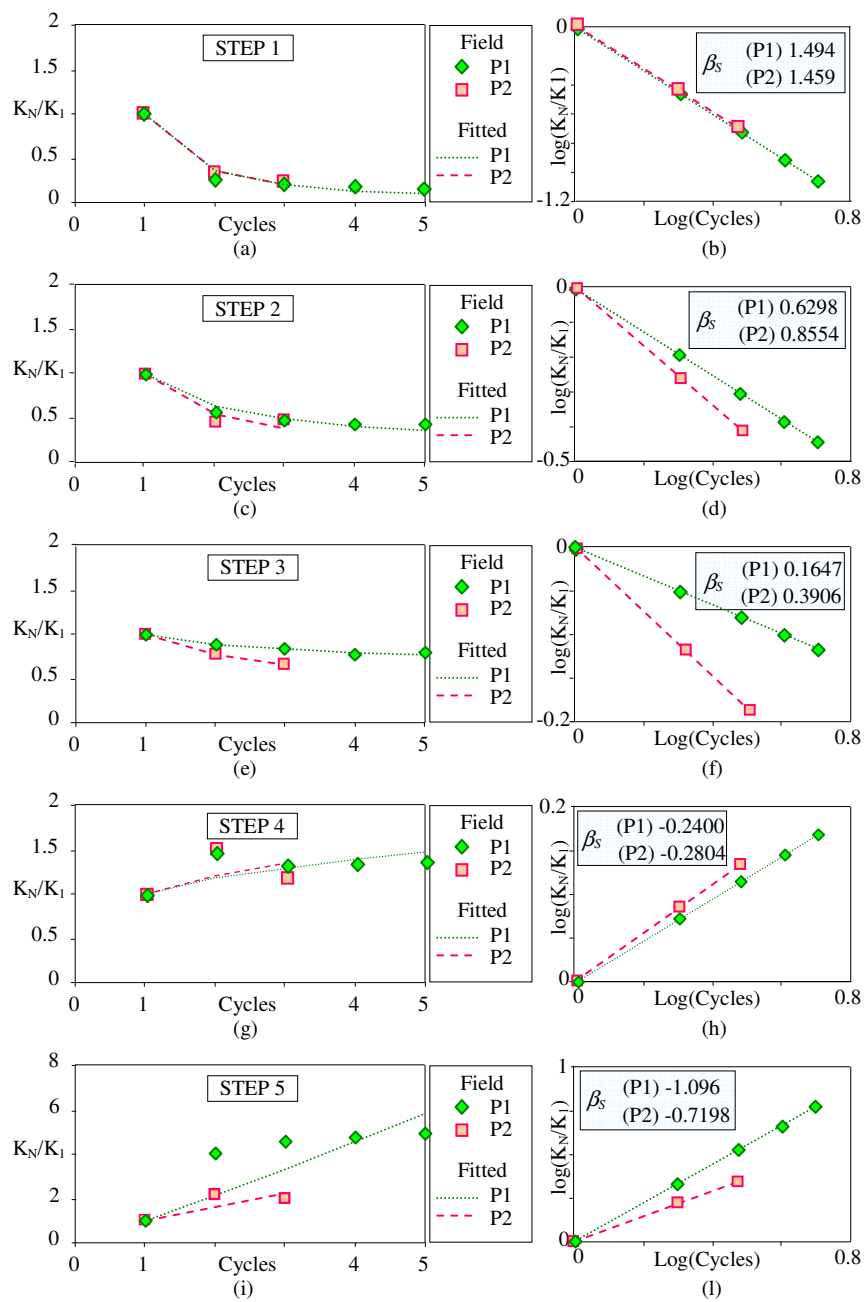


Figure 5-24 Stiffness ratio vs. number of cycles and corresponding degradation parameter (slope of the fitting line in the log-log graph) at increasing displacement step: (a, b) step 1; (c, d) step 2; (e, f) step 3; (g, h) step 4; (i, l) step 5

From Figure 5-24 some consideration can be drawn:

- For P1 and P2 from step 1 to 3 (up to pile head displacement = 7.5 mm) the slope of the curve in the log-log representation is negative, and it is representative of a degrading behaviour. However, with the increasing of the number of cycles N, the ratio K_N/K_1 tends to stabilize, approaching a sort of *shakedown* conditions, as described by Matlock, 1970.
- On the contrary, for step 4 and 5, the slope of the curve in the log-log representation is positive, indicating a hardening behaviour. Again, as the number of cycles increases, the value of the ratio K_N/K_1 tends to stabilize.
- The behaviour of the simply grouted pile is analogous to that of the injected micropiles; in particular, values of β_s for step 1 (small strain range) are substantially identical, as shown synthetically in Figure 5-25. As the pile head displacement increases, the difference between P1 and P2 in term of β_s increases until the hardening response occurs. At $y = 0.8Y_{max}$ β_s is again very similar for P1 and P2 while at the maximum displacement, the difference is quite evident (β_s is higher for P1 than for P2).

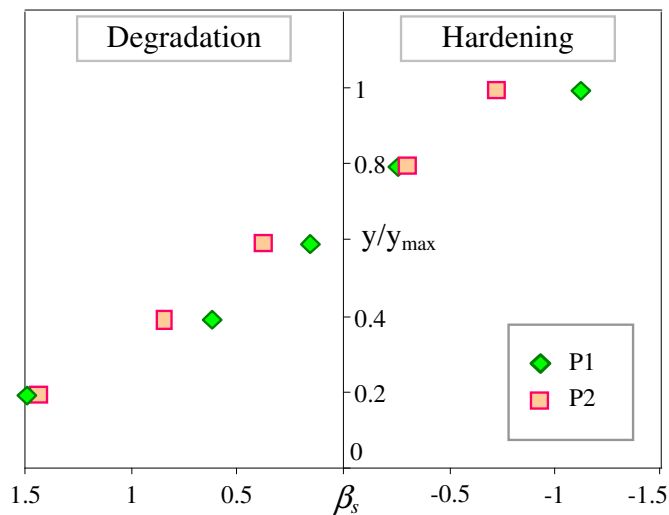


Figure 5-25 Trend of β_s for different values of the ratio y/y_{max} , for P1 and P2

5.2.4. Free Vibration Tests

In order to investigate the dynamic properties of the single vertical micropiles under high forces, free vibration tests have been performed on both P1 and P2. Given the high level of the forces under which the system is investigated, the traditional frequency-domain representations based on Fourier Transform, such as PSD of FRF, are not suitable. In fact, as shown in Figure 5-26, a, b for a specific input, time histories of acceleration and displacement change their features throughout time, and therefore, their characteristics in the frequency domain should be investigated point by point. This can be done via Stockwell Transform (Figure 5-26c), thanks to which it is possible to see that the first resonance frequency decreases as the time passes; this can be attributed to the widening and deepening of the gap as a result of the oscillation of the pile, as well as to the degradation of properties of grout and surrounding soil in the shallower portion of the soil pile system. In Figure 5-27 the temporal progression of the local spectrum at discrete temporal points is shown, as a proof of the evolution of the frequency response with time. Accordingly, by comparing the half power bandwidth, it's evident that the damping tends to decrease as a result of the progressive separation between the pile and the soil. In Appendix A.1 and A.2 time histories of displacements and accelerations, as well as S-Transform relative to P1 and P2 for all tested force level are shown.

Other important considerations stem from the results of SGs reported in Figure 5-28, Figure 5-29, Figure 5-30 and Figure 5-31. In particular Figure 5-28 and Figure 5-30 represent results relevant for deformations immediately before the release (quasi-static strains) for the first (a) and second (b) series of snap back tests, for P1 and P2, respectively. Alongside, Figure 5-29 and Figure 5-30 represents deformations at the end of the free vibration test (residual strains) for the first (a) and second (b) series of snap back tests, for P1 and P2, respectively. Before the execution of each test, strain and displacement measurements are set to zero.

Some observations can be drawn:

- Very superficial SGs gives quite very noisy data due to local damages for all the steps performed. Again, it can be attributed to partial reinforcement-grout debonding, weathering of shallower material, mechanical damages due to previous testing procedures within the first centimetres.
- Nonetheless, it is possible to recognize that for P1 deformations are evident within the 1st m while for P2 they get deeper along the shafts. Furthermore, for P2 (simply grouted micropiles) strains reach higher values, even doubled with respect to P1 for some force level.
- As a tendency, for both micropiles there is a general increment of deformation with the increasing of force level and this can be recognized in both test series.
- Residual deformations are evident after tests on P1 in the top 75 cm, and in P2 in the 1st m from the top; in particular, especially dealing with the strains registered after the 2nd series, it is evident that the depth at which residual strains are recognizable increases with the increase of the loading force level.

Finally, Figure 5-32 and Figure 5-33 shows the results of ambient vibration tests in term of PSD performed before and after the execution of free vibration tests on P1 and P2 respectively. The comparison between the two subsequent situations, summarized in Table

5-4, provides an efficient indicator of the variation in terms of fundamental frequency due to high force intensity dynamic loading. The technique is also able to identify the different behaviour along the principal horizontal directions: although relevant in both directions, the degradation of fundamental frequency is more pronounced in the direction along which tests are performed (x for P1, y for P2). Even after the high force intensity testing procedures, P1 is stiffer than P2 in both directions.

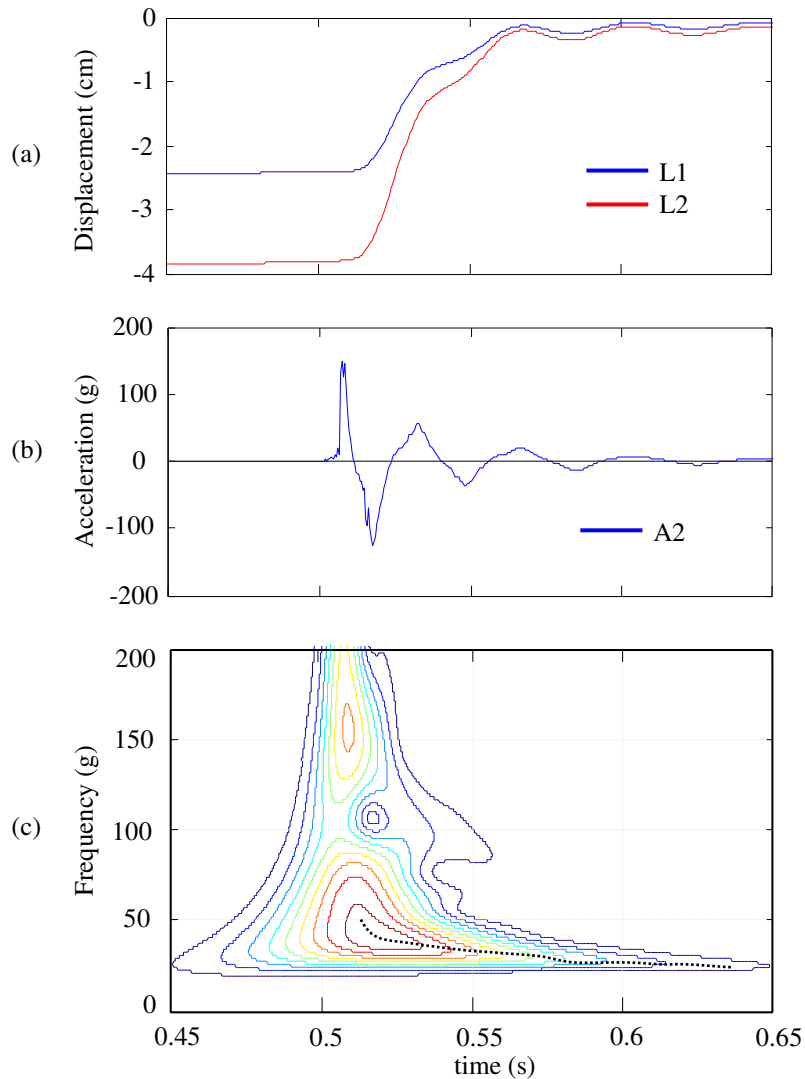


Figure 5-26 Displacements (a) and acceleration (b) time histories registered during a free vibration tests (F4-T2) on micropile P2; (c) S-Transform of acceleration.

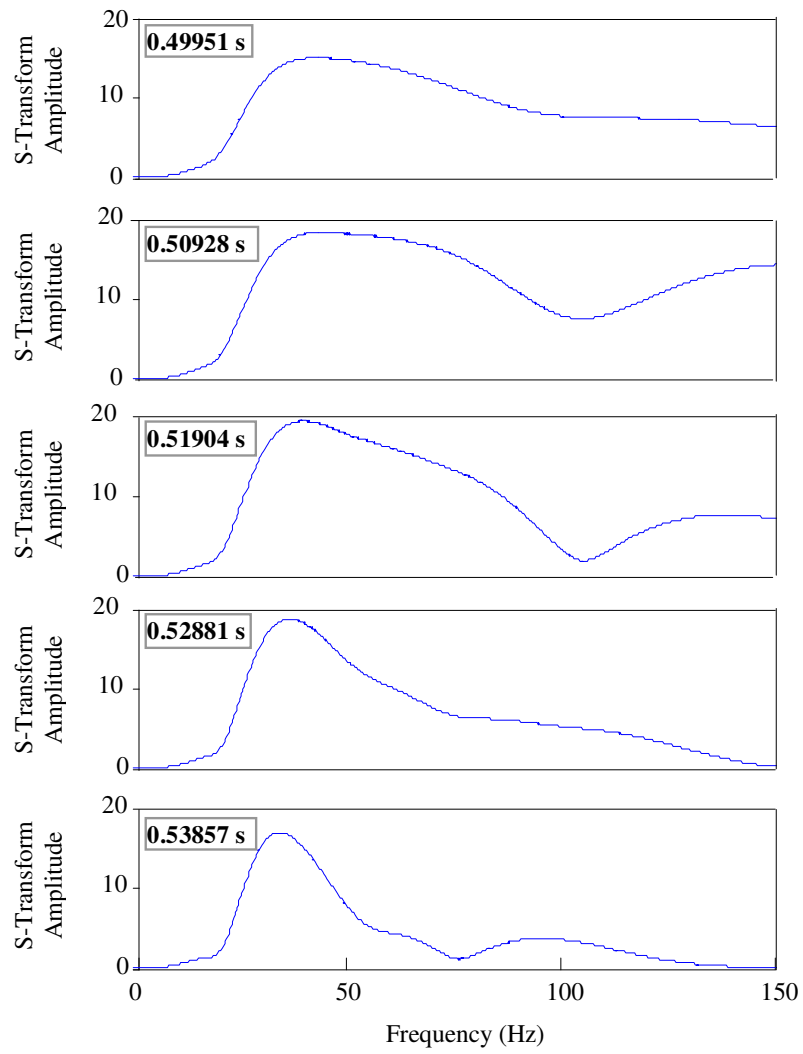


Figure 5-27 Variation with time of local spectrum

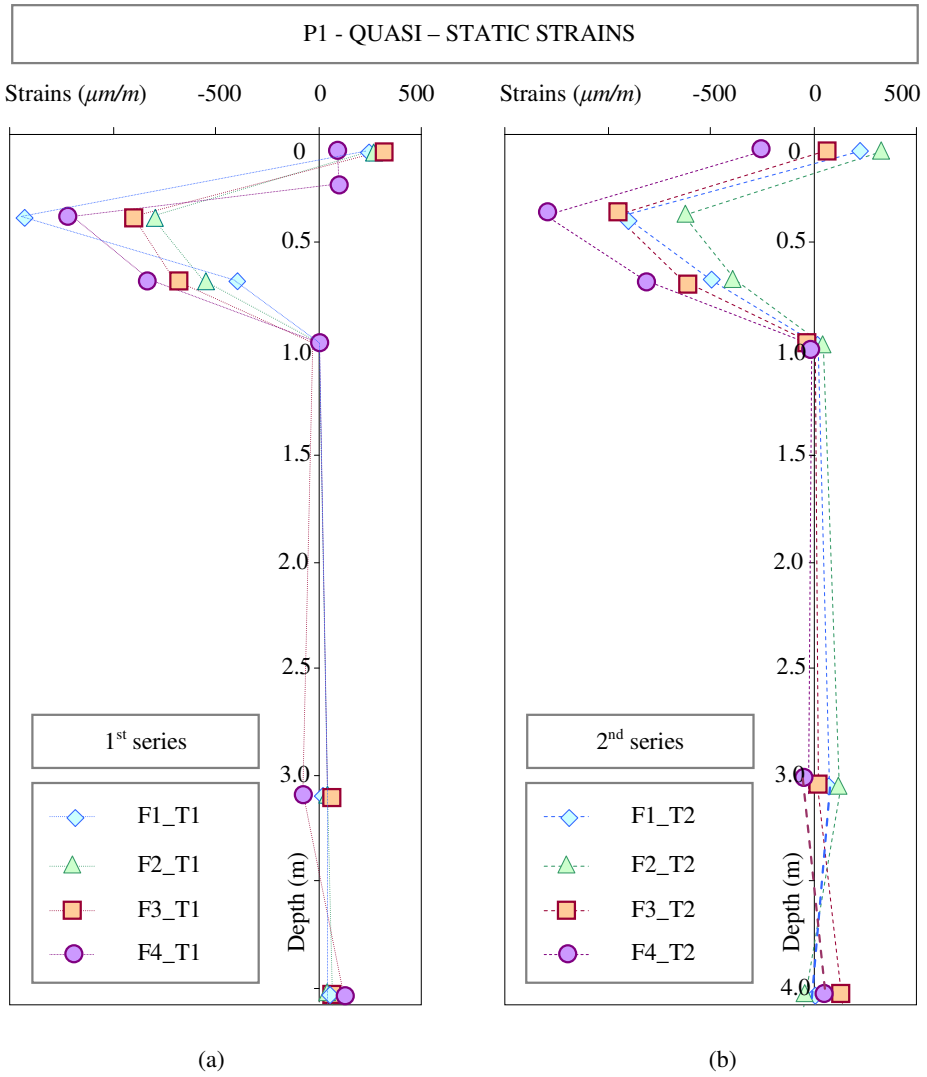


Figure 5-28 Profile of strains just before the release for the 4 force levels in (a) 1st series and (b) 2nd series (pile P1)

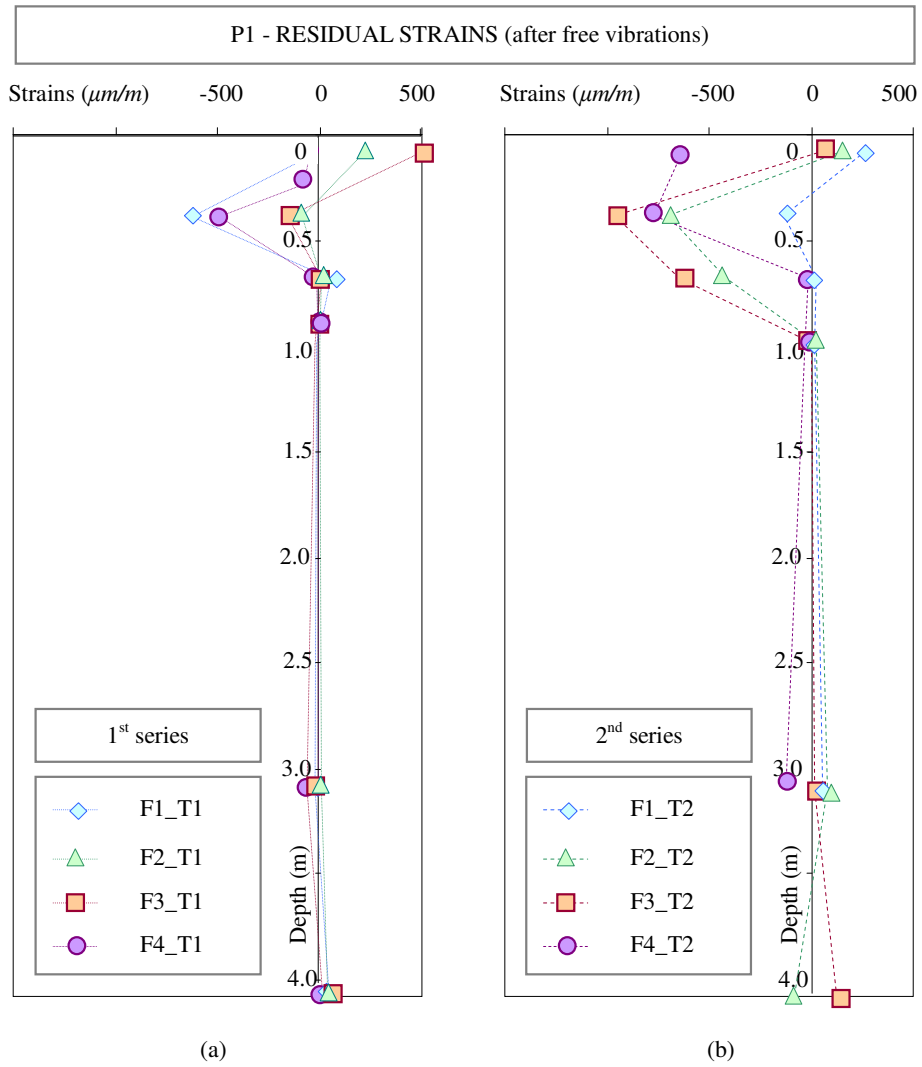


Figure 5-29 Profile of strains at the end of the free vibrations test for the 4 force levels in (a) 1st series and (b) 2nd series (pile P1)

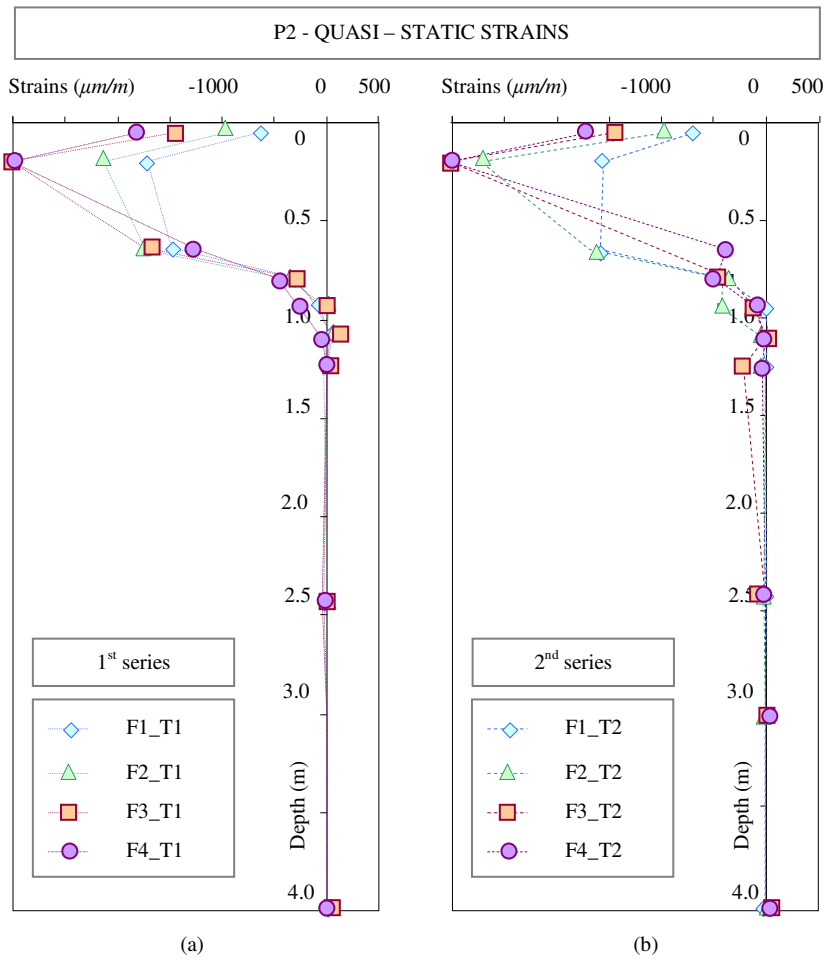


Figure 5-30 Profile of strains just before the release for the 4 force levels in (a) 1st series and (b) 2nd series (pile P2)

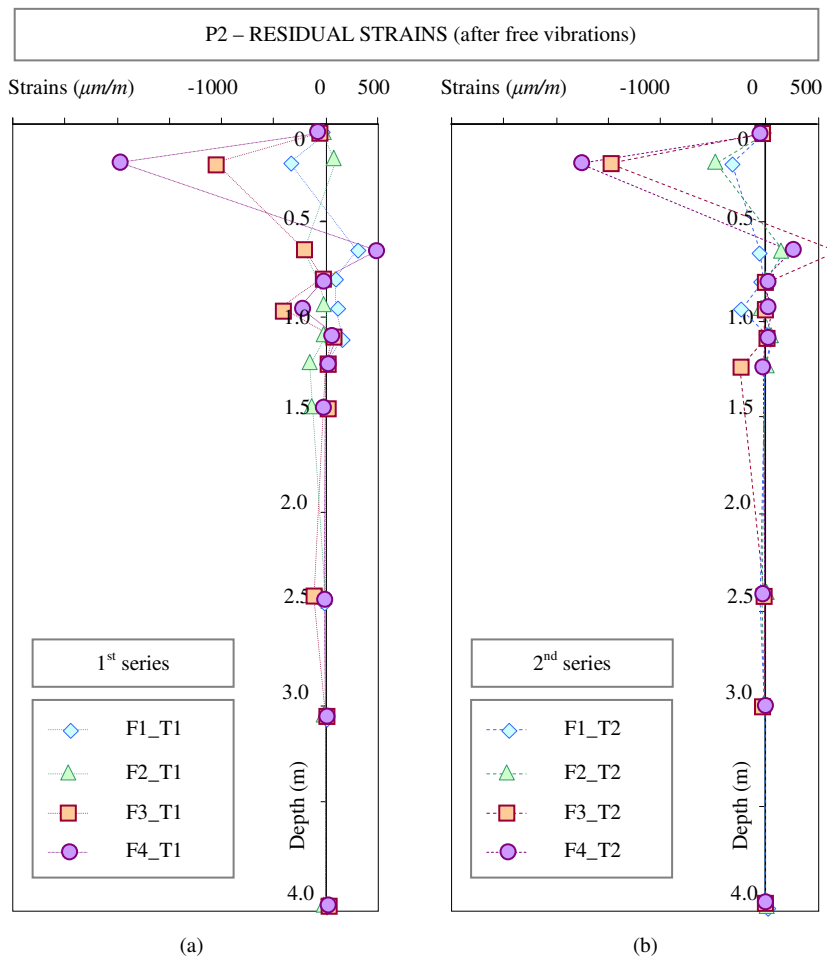


Figure 5-31 Profile of strains at the end of the free vibrations test for the 4 force levels in (a) 1st series and (b) 2nd series (pile P2)

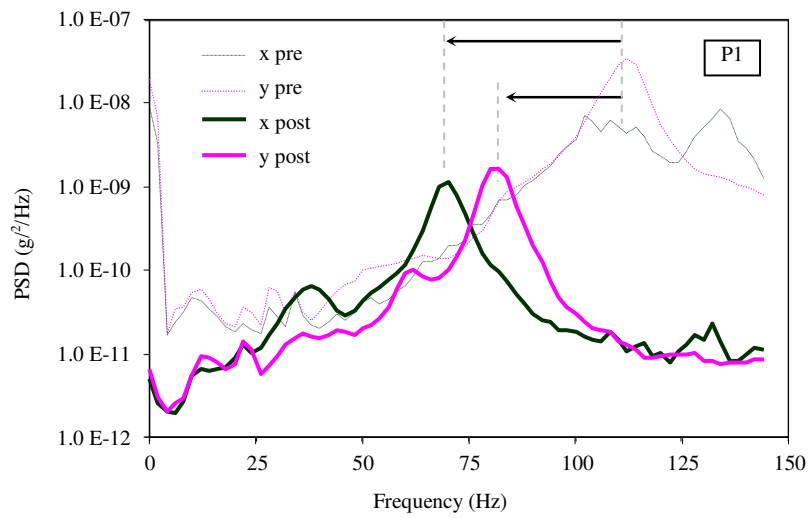


Figure 5-32 Investigation via ambient vibration tests of the residual dynamic properties after free vibration tests on P1 (x and y axis)

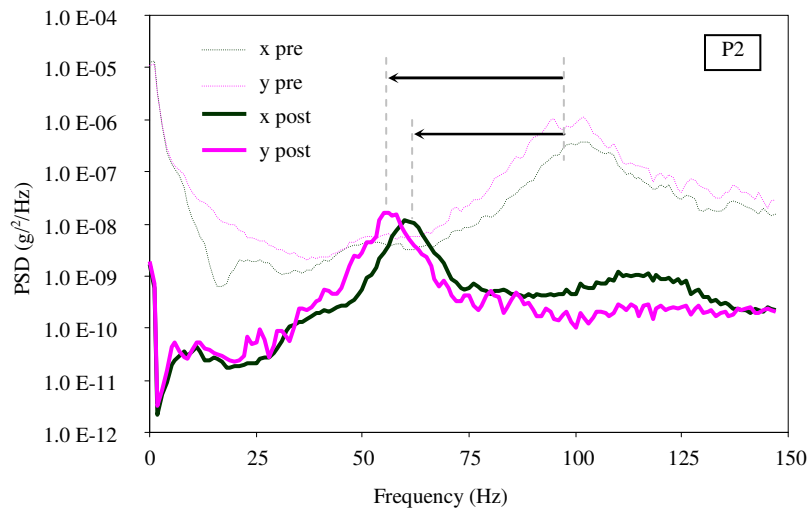


Figure 5-33 Investigation via ambient vibration tests of the residual dynamic properties after free vibration tests on P2 (x and y axis)

Table 5-4 Fundamental frequencies of P1 and P2 before and after snap back tests

	P1		P2	
	x	y	x	y
Before Snap Back	108 Hz	114 Hz	102 Hz	102 Hz
Post Snap Back	70 Hz	82 Hz	61 Hz	57 Hz

5.3. Micropiles group

Different techniques are adopted for the investigation of the dynamic behaviour of inclined micropiles group under different loading conditions and increasing loading level.

5.3.1. Ambient vibration Tests

Ambient vibration tests performed with accelerometers on the cap doesn't provide very good results, while those performed with geophones are clearer (since they are much more sensitive). In Figure 5-34 one of the ambient vibration tests performed with geophones is shown. In particular, since the instruments are extremely sensitive, results are shown in terms of ratio between the spectrum obtained on the cap and that obtained on the ground, in order to identify the fundamental frequency of the foundation system.

Some considerations stem out:

- The fundamental frequency in the x direction is lower than that observed in the y direction (along which micropiles are inclined); moreover the amplitude ratio of the first peak identified in x direction is higher than that obtained in the y direction.
- From spectral ratio along vertical direction, it can be seen that translational modes seems coupled to rocking motions; a pure rocking motion cannot be identified in the frequency range investigated.

Results relevant for other configurations are reported in Appendix A.3. However in order to obtain more precise information on the behaviour of the group in the small strain range, also impact load tests results are presented and compared with ambient vibration tests data.

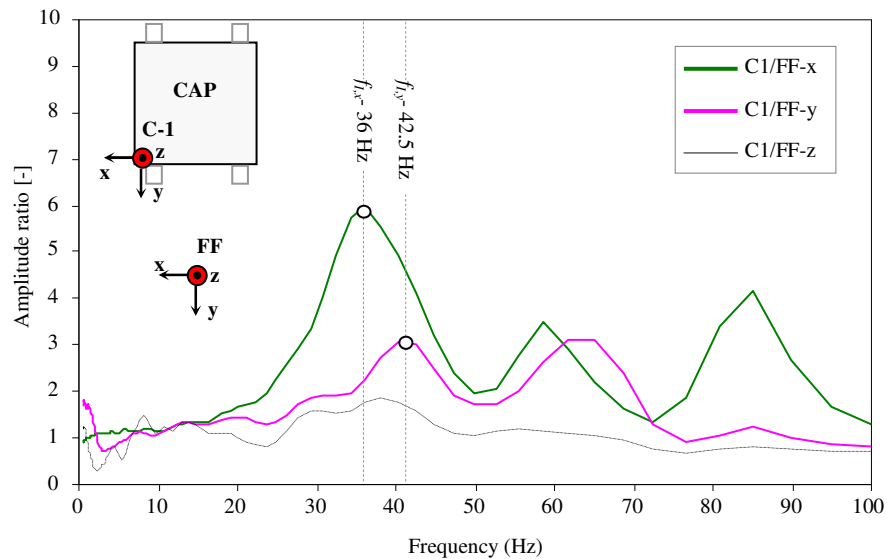


Figure 5-34 Results of Ambient Vibration Tests on micropiles group

5.3.2. Impact Load Tests

In Figure 5-35 a, b most significant results of ILTs on micropiles group are shown. Responses of two accelerometers in the direction of loading and one in the vertical direction (relevant for the recognition of rocking motion) are shown in terms of FRFs. Dynamic properties are also summarized in Table 5-5.

Some observation can be made:

- As a confirmation of what observed thanks to AVTs, dealing with the first (flexural) mode of vibration, the behaviour of the micropiles group along the direction of micropiles inclination is significantly stiffer; furthermore, it is more damped in the direction of inclination.
- Fundamental frequencies are slightly higher than those measured with AVTs; this can be partly attributed to different quantity acquired (acceleration vs. velocity) and test typology, but more probably it is due to the fact that ILTs and AVTs were performed in August 2016, respectively before and immediately after a violent earthquake and its aftershocks struck central Italy (Wikipedia, *Terremoto del Centro Italia del 2016*), probably inducing a decrease of the dynamic stiffness of the system.

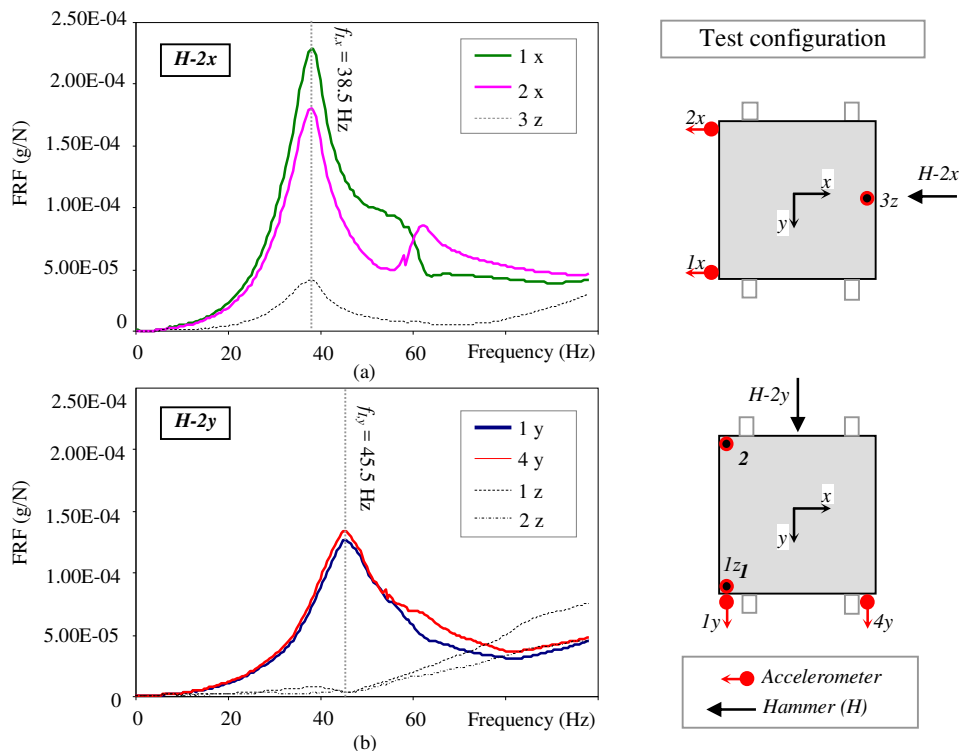


Figure 5-35 Results of ILTs on micropiles group: (a) along x and (b) y direction

Table 5-5 Fundamental frequencies and damping of micropiles group via ILTs

Direction Accelerometer	x		y	
	1x	2x	1y	4y
Fundamental frequency f_1 (Hz)	38.5	38.5	45.5	45.5
Damping ξ_1	0.103	0.096	0.127	0.133

- At about 60 Hz a roto-traslational mode can be identified (rotation in the x-y plane around node 1).
- Finally, there is an evidence of coupling between the translational and the rocking mode of vibration along x direction (i.e. for the flexural frequency, also the signal relevant for the vertical direction registered at the edges of the cap shows a peak). Contrarily to what is expected due to kinematic loading (i.e. the rocking behaviour associated to translational mode for inclined piles group is higher than that expected with vertical piles), the coupling in the y axis appears to be absent. In truth a little valley can be recognized. This can be attributed to the fact that the rocking behaviour associated to the translational mode is *out-of-phase* to that induced by the inertial loading.

In order to understand the last point it can be useful to shortly glance at the mechanism for undertaking inertial forces in vertical and inclined piles group. Conceptually, stress and strains developed under inertial forces should be added to those generated because of kinematic forces, when present (i.e. in the case of seismic loading). It is worth remembering that the main sources of kinematic interaction straining in vertical and battered piles are the existence of an abrupt change in stiffness between two consecutive soil layers (in this case the maximum bending moment is localized at the interface between the two layers and it is substantially independent from pile inclination) and the constraint imposed by the rigid pile cap (in this case the maximum bending moment is located at the pile head). For what regards inertial forces a rough difference can be identified in the response of the batter foundation subjected to horizontal loading or to moment. As shown in Figure 5-36, when dealing with horizontal loading the vertical groups develops a pair of shear forces and then bending moment due to the rotation fixity of the cap. Axial forces are negligible. On the other hand, a horizontal shear force on the cap of a batter piles group produces both shear and axial forces in each pile. The arrows of the shear force vectors describe qualitatively the rotation of the cap, since lateral pile deformation exceeds that imposed by the axial forces. When the overturning moment is the dominating load, vertical piles are subjected to a pair of axial forces that undertake most of this load, alongside with head moments that develop because of pile fixity to the cap. On the other hand, batter piles undertake moment mainly by bending and, consequently, a significant cap rotation takes place.

It is important to point out that in the case of batter group subjected to horizontal load the rotation of the pile cap is *out-of phase* with the one of the supported structure, while when batter group is subjected to overturning moment cap rotation and structure are *in-phase*.

With reference to the situation reproduced with the experimental tests, since horizontal impacts are given at the top of the cap, the head of the piles are subjected to both overturning moment and horizontal forces. By conceptually applying the superposition principle, one can guess that the contribution to the rotation induced by shear force and that induced by the bending moment (shear force \times height of the cap) are *in-phase* for the

direction in which piles behave as vertical, while along the direction in which piles are inclined the two contributions to rotations are mutually *out-of-phase*, and apparently this results in a *valley* in the FRF graphs. In results obtained from ambient vibration tests the roto-traslational coupling is more evident in the *y-z* plane, and this can be explained by thinking that the (ambient) excitation is not of inertial nature.

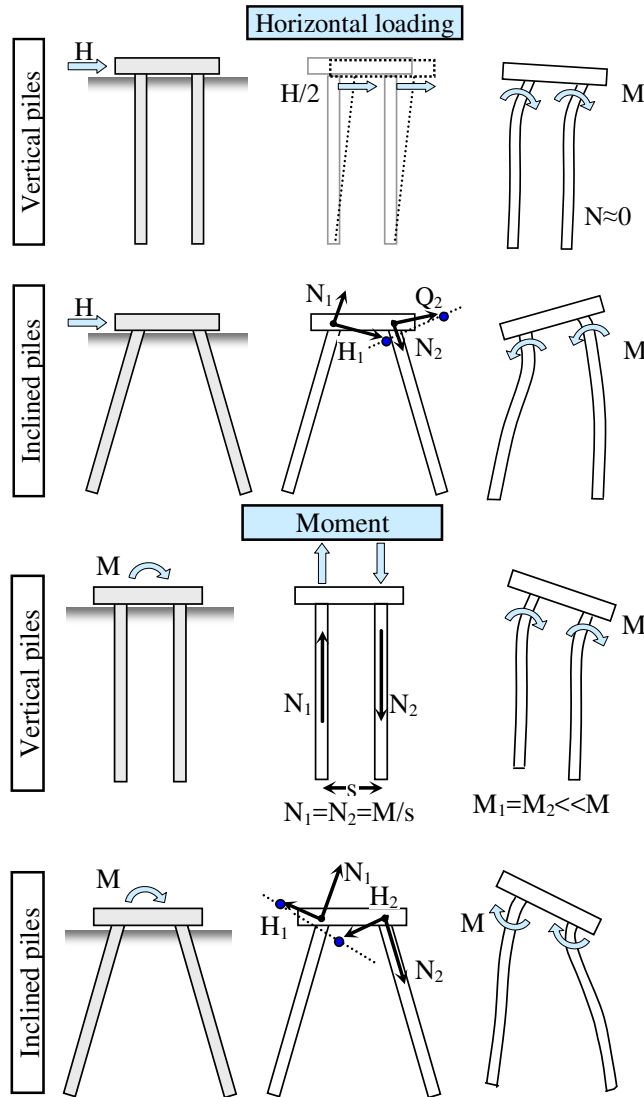


Figure 5-36 Mechanism for undertaking horizontal loading and moment of inertial origin, in vertical and inclined piles groups. Vectors indicate forces imposed by the cap on the piles while dashed lines correspond to the virtual location of the cap if the axial displacements of the piles are ignored.

Impedance functions of micropiles group

As already mentioned, the determination of impedance functions is an important issue in SSI analysis. It is important to point out that the dynamic pile group behaviour is substantially different from that of a single pile, and its impedance cannot be simply predicted by superimposing the impedances of its members since piles belonging to a group are not only affected by their individual loads, but also, for instance, by additional loads transferred through the soil from the neighbouring piles (*pile-soil-pile* interaction). Properties relevant for pile-soil-pile interaction phenomena are, in general, frequency-dependent complex quantities.

Here, the horizontal impedance of the soil–micropiles group system is determined as the ratio, in the frequency domain, between the impact load applied on the cap along global x and y directions and the resulting displacement of the cap along the same direction. Displacements are derived from the recorded accelerometer signals by means of a double discrete integration in the time domain, and suitable filtering procedures. In Figure 5-37 (a, b) the real and imaginary parts of the experimental horizontal impedance of the whole system, along both x and y axes, are shown over a wide frequency range. Curves are obtained by averaging among 5 impacts, and shadowed parts of the graphs represent the frequency ranges in which results are unstable. For both directions, the real part crosses zero at the first flexural frequency of the system along that direction and, within the range interested by the resonance of the system, the experimental stiffness ordinate exhibits a general reduction while damping increases with frequency up to about 90-100 Hz.

It can also be observed that the curves relevant for the two directions have similar trends. However, the group is stiffer in the direction along which micropiles are inclined, for almost the entire frequency range investigated, and the different values of the first flexural frequency along the two orthogonal directions can be identified through the comparison between the points of intersection with zero; moreover, the system appears to be more damped along the direction of micropiles inclination in the entire frequency range.

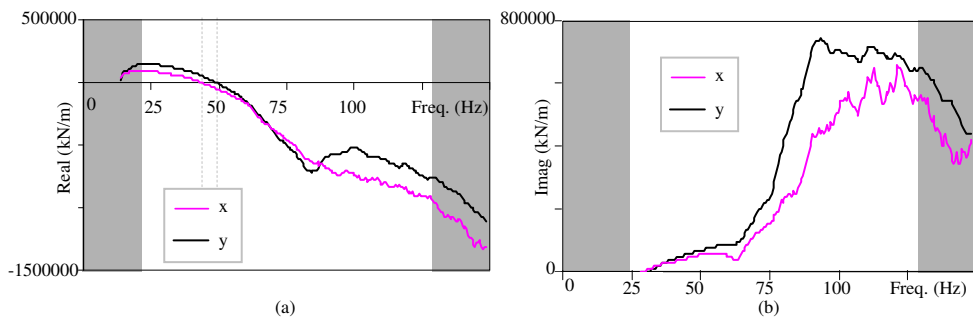


Figure 5-37 Experimental impedance functions of micropiles group: real (a) and imaginary (b) parts along x and y directions

5.3.3. Forced Vibration Tests

In Figure 5-38 and Figure 5-39 results of stepped sine tests in terms of acceleration along the direction of loading are presented. In particular point-by-point FRF functions are depicted, relevant to tests performed with increasing values of $K(\alpha)$. Fundamental frequencies obtained from stepped sine tests in both directions are summarized in Table 5-6.

Several considerations stem out:

- Even from the first force level, the natural frequency of the first translational mode is lower than that observed by means of ILTs, in both directions. This can be partially related to the fact that the mass of the shaker wasn't included during previous impact load tests.
- The first translational mode along the direction of micropiles inclination is found for a frequency that is higher than that obtained for the orthogonal direction; at the same time the first mode is more damped in that direction.
- With the increasing of the loading level natural frequency associated to the first and second mode tends to decrease. However, FRF are increasingly less damped with the increasing of the loading level (probably due to the opening of a gap at micropiles-soil interface) and show a peculiar appearance characterized by a sharp peak with an asymmetrical base.
- While in the y direction the value of fundamental frequency diminishes significantly at each different $K(\alpha)$ test, along the x direction it tends to stabilize at about 14.5 Hz.
- From a phenomenological point of view the achievement of the resonance condition is associated with the development of a radial zone, all around micropiles, in which several phenomena of degradation take place (gap, superficial cracks etc...) as shown in Figure 5-40.

In Figure 5-41 a comparison is proposed between two identical tests performed sequentially. It can be noted that the achievement of resonance in the second test is substantially different in the second test, with a characteristics *shark tail* shape. This is due to the fact that the system has changed after the first resonance, degrading its dynamic properties. When the load path is performed for the second time, the peak is less steep until it reaches the new condition of resonance. Then, the curve falls down abruptly.

From Figure 5-42 and Figure 5-43 the same phenomenon identified by means of impact load test, likely the coupling between the translational and the rocking mode of vibration along x direction, and the absence of coupling in the direction of micropiles inclination, is clearly evident (results are provided for $K(\alpha) = 0.9 \text{ N/Hz}^2$). Even in this case, the behaviour can be attributed to the application of an inertial force at the top of the cap.

More results are reported in Appendix A.4.

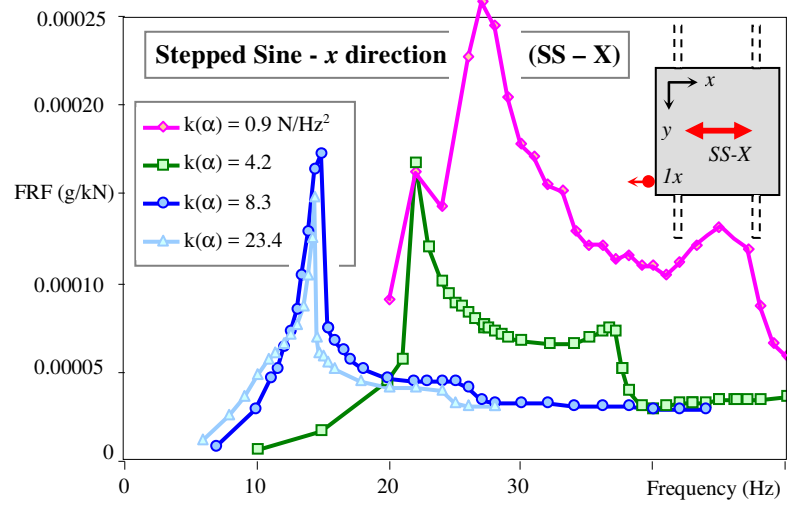


Figure 5-38 Results of Stepped Sine tests along x axis for increasing value of $K(\alpha)$

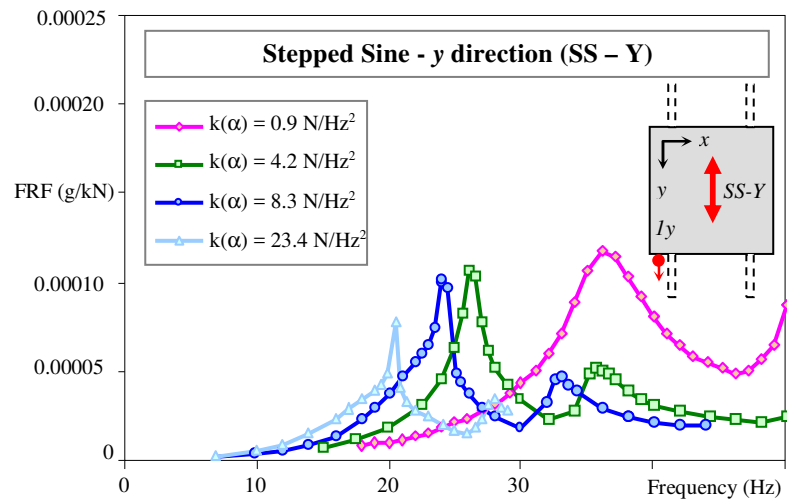


Figure 5-39 Results of Stepped Sine tests along y axis for increasing value of $K(\alpha)$

Table 5-6 Fundamental frequencies of micropiles group from stepped sine tests

Configuration	$K(\alpha) = 0.9 \text{ N/Hz}^2$	4.2 N/Hz^2	8.3 N/Hz^2	23.4 N/Hz^2
Dir. x	27 Hz	22 Hz	14.9 Hz	14.4 Hz
Dir. y	36 Hz	26.6 Hz	24.4 Hz	20.5 Hz



Figure 5-40 Superficial soil cracks around the pile

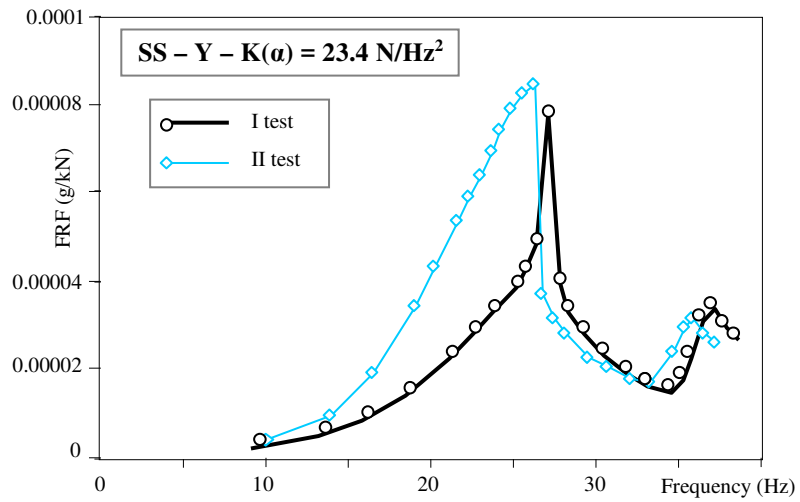


Figure 5-41 Effect of repetition of the same stepped sine tests ($K(\alpha) = 23.4 \text{ N/Hz}^2$, y axis)

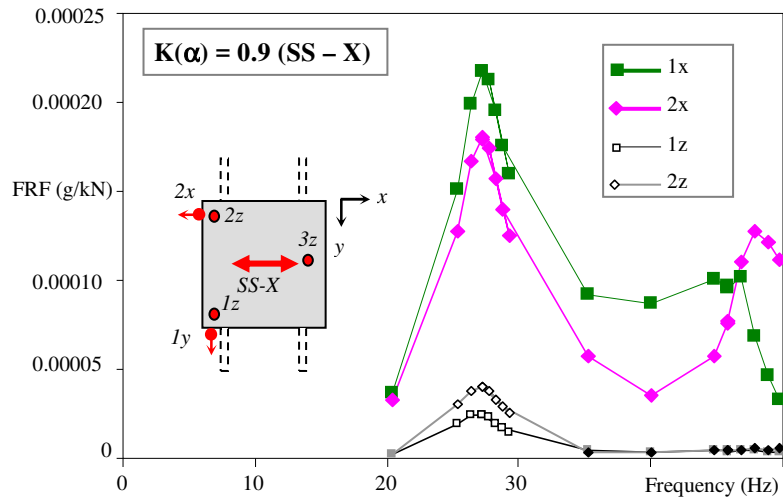


Figure 5-42 Results of Stepped Sine tests along x axis for increasing value of in terms of horizontal and vertical accelerations

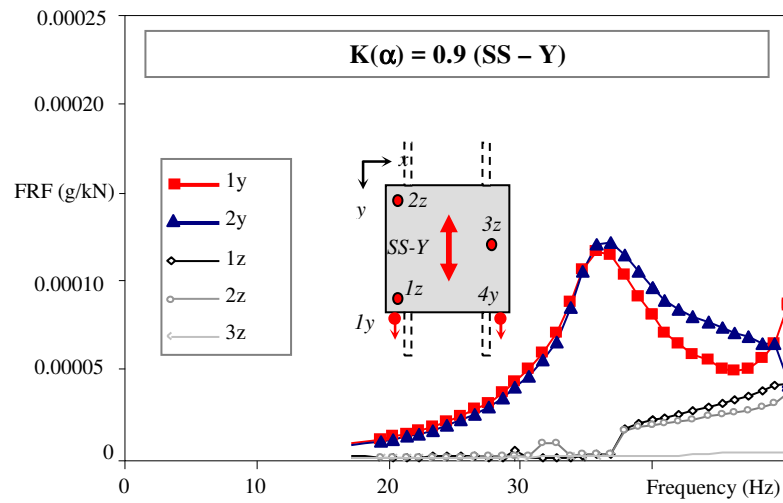


Figure 5-43 Results of Stepped Sine tests along y axis for increasing value of in terms of horizontal and vertical accelerations

Finally, Figure 5-44 shows the results of impact load tests in term of FRF performed after the execution of forced vibration tests with $K(\alpha) = 0.9 \text{ N/Hz}^2$ (first test) and $K(\alpha) = 23.8 \text{ N/Hz}^2$ (last test) along x and y direction. The comparison between the two subsequent situations, summarized in Table 5-7, provides an efficient indicator of the variation in terms of fundamental frequency and damping due to high force intensity dynamic loading. Although relevant in both directions, the degradation in terms of variation of fundamental frequency is more pronounced in the direction along which piles are inclined. Moreover, along the same direction a significant variation of damping is observed. Accordingly, under dynamic loading with high force intensity, degradation (mainly related to the opening of a gap at the interface between micropiles and surrounding soil) seems to be more pronounced if micropiles are inclined.

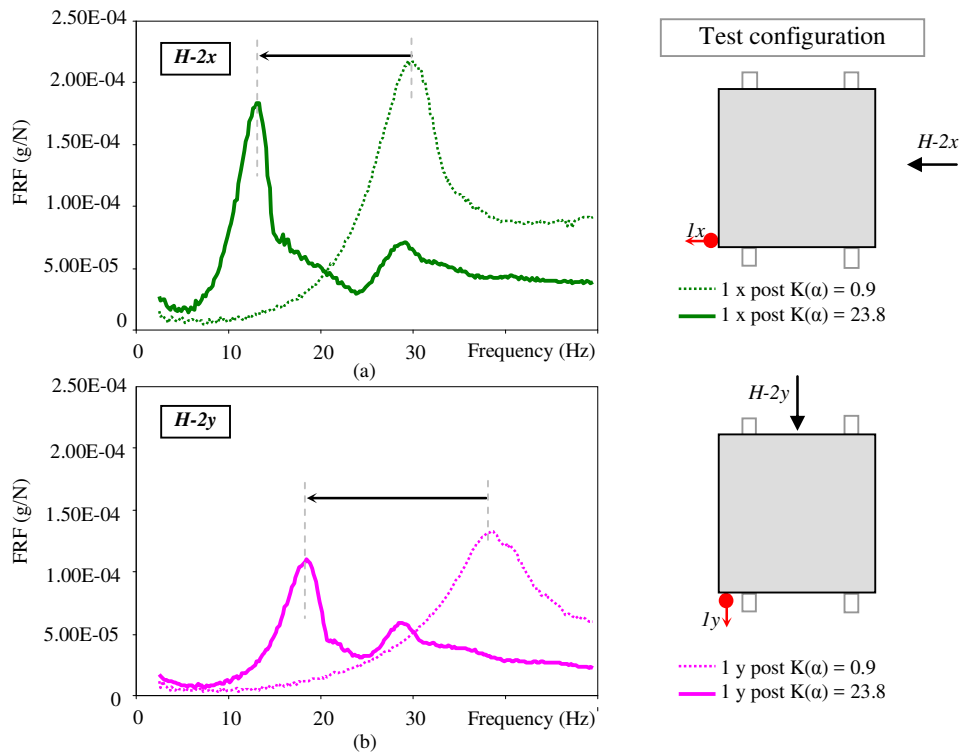


Figure 5-44 Investigation via impact load tests of the residual dynamic properties after forced vibration tests on micropiles group along x (a) and y (b) direction

Table 5-7 Fundamental frequencies of the group along x and y directions before and after forced vibration tests

	post $K(\alpha) = 0.9$		post $K(\alpha) = 23.4$	
	x	y	x	y
Fundamental frequency	29.6 Hz	38.6 Hz	13.4 Hz	18.6 Hz
Damping	0.100	0.102	0.104	0.073

Chapter 6.

Soil-Micropile Interaction Modelling

6.1. Introduction

Experimental results obtained during the experimental campaign are an essential instrument to calibrate both theoretical methods and 3-D Finite Element (FE) models. In this study, different numerical models are adopted to fit the experimental results. In particular the analytical approach of Dezi et al. (2016) for the 3D modelling of the kinematic interaction of vertical and inclined pile groups was here properly adapted to simulate the impact load tests on single micropiles and inclined micropile groups. Furthermore two 3D FE models were developed in ABAQUS, to reproduce the linear and non-linear phenomena occurred during impact load tests and free-vibration tests on vertical micropiles.

6.2. Analytical model

The model proposed by Dezi et al. (2009) allows performing the kinematic and inertial interaction analysis of pile group foundations in horizontally layered soils evaluating the soil-foundation impedances and the motion at the foundation level necessary to perform the inertial interaction analysis. A recent updating (Dezi et al., 2016) allows accounting for inclined piles. The latter was adopted, with proper modifications, to simulate numerically the test results. In the following the model is synthetically recalled; a short description of the adopted modifications is also provided.

6.2.1. Recall on the model

The problem is formulated in the frequency domain so that the forces and displacements reported are implicitly assumed to be the Fourier Transforms of the corresponding quantities expressed in the time domain.

A generic group of n circular piles, with same diameter but different rake angles, is considered. A right-handed global reference system $\{0; x_1, x_2, z\}$ is considered as shown in Figure 6-1(a). Piles are embedded in a horizontally layered soil profile constituted by horizontal infinite layers, independent of each other. It is assumed that during the motion no gaps arise between piles and soil.

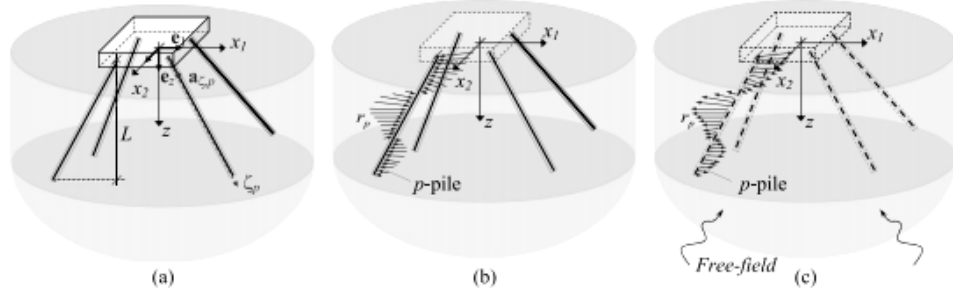


Figure 6-1(a) Pile group with inclined piles; (b) foundation subjected to interaction forces and (c) soil subjected to propagating seismic waves and interaction forces

The orientation of the generic p -th pile, assumed to be an Euler–Bernoulli beam, is defined by the unit vector $\mathbf{a}_{\zeta,p}$ of the pile longitudinal axis ζ_p . For simplicity, the projection of the pile length on the vertical axis z is equal to L , for all piles. The actual length of the generic p -th pile can thus be derived as

$$\zeta_p = (\mathbf{a}_{\zeta,p} \cdot \mathbf{e}_z)^{-1} z = \beta_p z \quad (6.1)$$

considering $z = L$. In Equation (6.1) \mathbf{e}_z is the unit vector of the vertical axis of the global reference system. The local reference system $\{0'; \xi_1, \xi_2, \zeta\}_p$ of the p -th pile is identified by the orthonormal basis

$$\mathbf{a}_{\zeta,p} \quad (6.2)$$

$$\mathbf{a}_{2,p} = \mathbf{e}_z \times \mathbf{a}_{\zeta,p} \quad (6.3)$$

$$\mathbf{a}_{1,p} = \mathbf{a}_{2,p} \times \mathbf{a}_{\zeta,p} \quad (6.4)$$

where $\mathbf{a}_{1,p}$ and $\mathbf{a}_{2,p}$ are the unit vectors of the local ζ_1 and ζ_2 axes, respectively. Being ω the circular frequency, the pile displacements at depth z in the global reference system can be described in the frequency domain by the complex-valued vector

$$\mathbf{u}^T(\omega; z) = [\mathbf{u}_1^T \cdots \mathbf{u}_p^T \cdots \mathbf{u}_n^T] \quad (6.5)$$

that collects displacements measured at the axis of the n piles constituting the group. Each subvector $\mathbf{u}_p(\omega; z)$, referring to the p -th pile, contains the displacement components u_{p1} , u_{p2} and u_{p3} along directions x_1 , x_2 and z , respectively. According to the Euler–Bernoulli model, strains are described by the pile curvatures on planes orthogonal to ζ_i and by the overall normal strain; these are grouped in the vector

$$\mathbf{D}\mathbf{R}\mathbf{u}^T(\omega; z) = [\tilde{\mathbf{D}}\mathbf{R}_1\mathbf{u}_1^T \cdots \tilde{\mathbf{D}}\mathbf{R}_p\mathbf{u}_p^T \cdots \tilde{\mathbf{D}}\mathbf{R}_n\mathbf{u}_n^T] \quad (6.6)$$

obtained by applying a differential operator $\tilde{\mathbf{D}}$ to displacements of the generic p -th pile according to

$$\tilde{\mathbf{D}}\mathbf{R}_p\mathbf{u}_p^T(\omega; z) = \left[-\frac{\partial^2}{\partial \zeta^2} (\mathbf{R}_p\mathbf{u}_p \cdot \mathbf{a}_{2,p}) \cdots \frac{\partial^2}{\partial \zeta^2} (\mathbf{R}_p\mathbf{u}_p \cdot \mathbf{a}_{1,p}) \cdots \frac{\partial}{\partial \zeta} (\mathbf{R}_p\mathbf{u}_p \cdot \mathbf{a}_{\zeta,p}) \right]^T \quad (6.7)$$

where \mathbf{R} is the rotation matrix that allows expressing the local displacements of each pile starting from the relevant global displacement, by assembling submatrices

$$\mathbf{R}_p \mathbf{u} = \begin{bmatrix} \mathbf{e}_1 \cdot \mathbf{a}_{1,p} & \mathbf{e}_1 \cdot \mathbf{a}_{2,p} & \mathbf{e}_1 \cdot \mathbf{a}_{\zeta,p} \\ \mathbf{e}_2 \cdot \mathbf{a}_{1,p} & \mathbf{e}_2 \cdot \mathbf{a}_{2,p} & \mathbf{e}_2 \cdot \mathbf{a}_{\zeta,p} \\ \mathbf{e}_z \cdot \mathbf{a}_{1,p} & \mathbf{e}_z \cdot \mathbf{a}_{2,p} & \mathbf{e}_z \cdot \mathbf{a}_{\zeta,p} \end{bmatrix}^T \quad (6.8)$$

relevant to each pile of the group. As shown in Figure 6-1(b), piles are subjected to distributed interaction lateral forces whose resultants are collected in the vector

$$\mathbf{r}^T(\omega; z) = [\mathbf{r}_1^T \cdots \mathbf{r}_p^T \cdots \mathbf{r}_n^T] \quad (6.9)$$

constituted by subvectors \mathbf{r}_p , each one containing components \mathbf{r}_{p1} , \mathbf{r}_{p2} and \mathbf{r}_{p3} along directions x_1 , x_2 and z , respectively. At dynamic conditions, inertia forces $\omega^2 \mathbf{M}\mathbf{u}(\omega; z)$ arise, where

$$\mathbf{M} = \rho_p A \begin{bmatrix} \mathbf{I} & \cdots & \mathbf{0} & \cdots & \mathbf{0} \\ \vdots & & \vdots & & \vdots \\ \mathbf{0} & \cdots & \mathbf{I} & \cdots & \mathbf{0} \\ \vdots & & \vdots & & \vdots \\ \mathbf{0} & \cdots & \mathbf{0} & \cdots & \mathbf{I} \end{bmatrix} \quad (6.10)$$

is the mass matrix of the group, ρ_p and A are the density and the cross-sectional area of the pile, respectively, and \mathbf{I} is the identity matrix of order 3. By assuming a linear behaviour for piles, the stress resultants are given by

$$\mathbf{s}(\omega; z) = \mathbf{KDRu}(\omega; z), \quad (6.11)$$

where

$$\mathbf{K} = \begin{bmatrix} \mathbf{K}_1 & \cdots & \mathbf{0} & \cdots & \mathbf{0} \\ \vdots & & \vdots & & \vdots \\ \mathbf{0} & \cdots & \mathbf{K}_p & \cdots & \mathbf{0} \\ \vdots & & \vdots & & \vdots \\ \mathbf{0} & \cdots & \mathbf{0} & \cdots & \mathbf{K}_n \end{bmatrix} \quad (6.12)$$

is the stiffness matrix of the pile group, obtained by assembling submatrices

$$\mathbf{K}_p = E \begin{bmatrix} I & 0 & 0 \\ 0 & I & 0 \\ 0 & 0 & A \end{bmatrix} \quad (6.13)$$

in which E is the material Young's modulus and I is the moment of inertia of the pile cross section.

The equilibrium condition of the pile group may be expressed in weak form by the Lagrange–D'Alembert principle that provides the following equation:

$$\int_0^L \mathbf{BKDRu}(\omega; z) \cdot \mathbf{DR}\hat{\mathbf{u}}(z) dz - \int_0^L \mathbf{r}(\omega; z) \hat{\mathbf{u}}(z) dz - \omega^2 \int_0^L \mathbf{BMu}(\omega; z) \cdot \hat{\mathbf{u}}(\omega; z) dz = 0 \quad \forall \hat{\mathbf{u}} \neq \mathbf{0} \quad (6.14)$$

where \mathbf{B} is the matrix containing the Jacobians of the coordinate transformations in Equation (6.1).

The compatibility condition between the pile and soil displacements may be expressed, under the assumption of perfect adherence at the soil pile interface (no gap), by the integral expression

$$\mathbf{u}(\omega, z) = \mathbf{u}_{ff}(\omega, z) - \int_0^L \mathbf{D}(\omega, \kappa, z) \mathbf{r}(\omega, \kappa) d\kappa \quad (6.15)$$

which equates the piles displacement (left-hand side) to the soil displacement at the piles locations (right-hand side); the latter is obtained from the superposition of the free-field motion \mathbf{u}_{ff} and the displacements induced by the pile–soil–pile interactions (Figure 6-1(c)). Like for pile displacements, the free-field motion is described by vector

$$\mathbf{u}_{ff}^T(\omega, z) = [\mathbf{u}_{1,ff}^T \dots \mathbf{u}_{p,ff}^T \dots \mathbf{u}_{n,ff}^T] \quad (6.16)$$

The kernel of equation (6.15) is the complex valued matrix

$$\mathbf{D}(\omega, \kappa, z) = \begin{bmatrix} \mathbf{D}_{11} & \dots & \mathbf{D}_{1q} & \dots & \mathbf{D}_{1n} \\ \vdots & & \vdots & & \vdots \\ \mathbf{D}_{p1} & \dots & \mathbf{D}_{pq} & \dots & \mathbf{D}_{pn} \\ \vdots & & \vdots & & \vdots \\ \mathbf{D}_{n1} & \dots & \mathbf{D}_{nq} & \dots & \mathbf{D}_{nn} \end{bmatrix}, \quad (6.17)$$

obtained by assembling submatrices $\mathbf{D}_{pq}(\omega; \kappa, z)$, which contain the elastodynamic Green's functions expressing the soil displacements at the location of the p -th pile at depth z , due to a time-harmonic unit point load acting at the location of the q -th pile at depth κ . Equation (6.15) allows modelling the pile–soil–pile dynamic interaction phenomena and the radiation problem once the Green's functions are defined. Because the problem is fully coupled, all components of the \mathbf{D}_{pq} matrices are theoretically non-zero. The problem is here simplified making use of the Baranov's hypothesis, i.e. assuming that the soil is constituted by infinite independent horizontal layers. Accordingly, the kernel of (6.15) takes the following form:

$$\mathbf{D}(\omega, \kappa, z) = \tilde{\mathbf{D}}(\omega, z) \delta(z - \kappa) \quad (6.18)$$

where $\delta(z-\kappa)$ is the Dirac's delta function and $\tilde{\mathbf{D}}(\omega, z)$ contains the elastodynamic Green's functions, which describe the dynamics of the infinite layer at depth z . In particular, component of matrix $\tilde{\mathbf{D}}_{pq}$ are expressed by

$$\tilde{\mathbf{D}}_{pq}(\omega, z) = \Lambda_{pq}^T(z) \Psi_{pq}(\omega, z) \Lambda_{pq}(z) \mathcal{D}(\omega, z) \quad (6.19)$$

where $\mathcal{D}(\omega, z)$ is a dynamic compliance matrix whose components are the displacements of the application point of a unit harmonic force. This can be view as the sum of the shaft component $\mathcal{D}_s(\omega, z)$ and base component $\mathcal{D}_b(\omega, z)$, according to

$$\mathcal{D}(\omega, z) = \mathcal{D}_s(\omega, z) + \delta(z-L)\mathcal{D}_b(\omega, z) \quad (6.20)$$

where

$$\mathcal{D}_\alpha(\omega) = \begin{bmatrix} \frac{k_{h\alpha}(\omega) - i\omega c_{h\alpha}(\omega)}{k_{h\alpha}^2(\omega) + \omega^2 c_{h\alpha}^2(\omega)} & 0 & 0 \\ 0 & \frac{k_{h\alpha}(\omega) - i\omega c_{h\alpha}(\omega)}{k_{h\alpha}^2(\omega) + \omega^2 c_{h\alpha}^2(\omega)} & 0 \\ 0 & 0 & \frac{k_{v\alpha}(\omega) - i\omega c_{v\alpha}(\omega)}{k_{v\alpha}^2(\omega) + \omega^2 c_{v\alpha}^2(\omega)} \end{bmatrix} \quad (6.21)$$

being $\alpha = s, b$.

In this paper, elastodynamic solutions proposed by Dobry et al. (1982) and by Roesset and Angelides (1980) are adopted for the horizontal and vertical stiffnesses, respectively.

$$k_h = 1.67 E_s \left(\frac{E_p}{E_s} \right)^{-0.053} \quad (6.22)$$

$$k_v = 0.6 E_s \left(1 + \frac{1}{2} \sqrt{\frac{\omega d}{V_s}} \right) \quad (6.23)$$

Where E_s and E_p are the soil and pile Young's modulus, d is the pile diameter and V_s the soil shear wave velocity. For damping coefficient, formulas proposed by Gazetas and Dobry (1984) are adopted; these have been derived by considering a pile section with unit thickness subjected to either vertical or horizontal steady-state vibrations under plane-strain conditions. The pile is assumed to have an equivalent square cross section, and each side of the square emits waves only in the associated truncated quarter plane; in particular, vertical oscillations produce shear waves propagating in all the quarter planes, while horizontal oscillations induce compression–extension waves in the two quarter planes perpendicular to the direction of loading and shear waves in the two quarter planes along the direction of loading. By including the material hysteretic damping, the following expressions have been adopted:

$$c_h(\omega) = \frac{1}{2} \pi d \rho V_s \left\{ \operatorname{Re} \left[-i \frac{H_1^{(2)} \left(\frac{\pi \omega d}{8 V_s} \right)}{H_0^{(2)} \left(\frac{\pi \omega d}{8 V_s} \right)} \right] + \frac{V_c}{V_s} \operatorname{Re} \left[-i \frac{H_1^{(2)} \left(\frac{\pi \omega d}{8 V_s} \right)}{H_0^{(2)} \left(\frac{\pi \omega d}{8 V_s} \right)} \right] \right\} + 2\xi \frac{k_h}{\omega} \quad (6.24)$$

$$c_v(\omega) = \pi d \rho V_s \operatorname{Re} \left[-i \frac{H_1^{(2)} \left(\frac{\pi \omega d}{8 V_s} \right)}{H_0^{(2)} \left(\frac{\pi \omega d}{8 V_s} \right)} \right] + 2\xi \frac{k_v}{\omega} \quad (6.25)$$

In which $H_0^{(2)}$ and $H_1^{(2)}$ are the zero order and first order Hankel functions of second kind, ρ , is the soil density and ξ is the material hysteretic damping. Moreover V_c is the velocity of the compression extension waves that may be assumed to propagate with the Lysmer's apparent velocity V_{La} , accounting for the unrealistic condition of perfect constraint provided in the near field by the two lateral boundaries. At very shallow depths, Equation (6.24) may overpredict the damping coefficient as the presence of the ground surface (stress free) facilitates the development of surface waves, which propagate with velocities closer to V_s than to V_{La} . For this reason, Gazetas and Dobry (1984) suggest to use velocity V_s for all the four quarter planes at depth less than $2.5d$, in order to approximately account for this effect. Hence, near the ground surface Equation ((6.24) is substituted by

$$c_h(\omega) = \pi d \rho V_s \operatorname{Re} \left(-i \frac{H_1^{(2)}\left(\frac{\pi \omega d}{8V_s}\right)}{H_0^{(2)}\left(\frac{\pi \omega d}{8V_s}\right)} \right) + 2\xi \frac{k_h}{\omega} \quad (6.26)$$

The displacement attenuation from point j to point i (Figure 6-2) of the layer is expressed by matrix $\Lambda_{pq}^T \Psi_{pq} \Lambda_{pq}$ where

$$\Psi_{pq}(\omega) = \begin{bmatrix} \psi_0(\omega, s_{pq}) & 0 & 0 \\ 0 & \psi_{\pi/2}(\omega, s_{pq}) & 0 \\ 0 & 0 & \psi_v(\omega, s_{pq}) \end{bmatrix} \quad (6.27)$$

Contains the attenuation functions for points located along lines, passing through the application point, parallel and orthogonal to the source displacement, and

$$\Lambda_{pq} = \begin{bmatrix} (x_j - x_i) s_{pq}^{-1} & (y_j - y_i) s_{pq}^{-1} & 0 \\ (y_i - y_j) s_{pq}^{-1} & (x_j - x_i) s_{pq}^{-1} & 0 \\ 0 & 0 & 1 \end{bmatrix} \quad (6.28)$$

is a geometric matrix in which s_{ij} is the distance between the axis of the i -th pile, of coordinates (x_i, y_i) , and the axis of the j -th pile, of coordinates (x_j, y_j) .

Attenuation functions are obtained from the works of Makris and Gazetas (1992), and Mylonakis and Gazetas (1998), which provides the following expressions:

$$\psi_0(\omega, s_{pq}) = \frac{H_0^{(2)}\left(\frac{s\omega}{V_{La}\sqrt{1+2i\xi}}\right)}{H_0^{(2)}\left(\frac{\omega d}{2V_{La}\sqrt{1+2i\xi}}\right)} \approx \left(\frac{d}{2s_{pq}}\right)^{\frac{1}{2}} e^{-(\xi+i)\left(s_{pq} - \frac{d}{2}\right)\frac{\omega}{V_c}} \quad (6.29)$$

$$\psi_{\pi/2}(\omega, s_{pq}) = \psi_v(\omega, s_{pq}) = \frac{H_0^{(2)}\left(\frac{s\omega}{V_s \sqrt{1+2i\xi}}\right)}{H_0^{(2)}\left(\frac{\omega d}{2V_s \sqrt{1+2i\xi}}\right)} \approx \left(\frac{d}{2s_{ij}}\right)^{\frac{1}{2}} e^{-(\xi+i)\left(s_{ij}-\frac{d}{2}\right)\frac{\omega}{V_s}} \quad (6.30)$$

Concerning the base components, impedances are evaluated assuming that the pile base behaves as a rigid disk on the 'surface' of the underlying homogeneous half space. By assuming that vertical and horizontal stiffness at the pile tip are uncoupled, the projection of the pile base on the horizontal plane is considered, and the stiffness and damping coefficients are evaluated by means of expressions proposed by Veletsos and Verbic (1973) for the surface rigid disk:

$$k_{hb}(\omega) = \frac{4G\tilde{d}}{2-\nu} \left[\bar{k}_h \left(\frac{\omega\tilde{d}}{2V_s}, \nu \right) \right] \quad (6.31)$$

$$k_{vb}(\omega) = \frac{2G\tilde{d}}{1-\nu} \left[\bar{k}_v \left(\frac{\omega\tilde{d}}{2V_s}, \nu \right) \right] \quad (6.32)$$

$$c_{hb}(\omega) = \frac{4G\tilde{d}}{2-\nu} \left[\frac{\tilde{d}}{2V_s} \bar{c}_h \left(\frac{\omega\tilde{d}}{2V_s}, \nu \right) \right] + 2\xi \frac{k_{hb}(\omega)}{\omega} \quad (6.33)$$

$$c_{vb}(\omega) = \frac{2G\tilde{d}}{1-\nu} \left[\frac{\tilde{d}}{2V_s} \bar{c}_v \left(\frac{\omega\tilde{d}}{2V_s}, \nu \right) \right] + 2\xi \frac{k_{vb}(\omega)}{\omega} \quad (6.34)$$

where $\bar{k}_h, \bar{c}_h, \bar{k}_v, \bar{c}_v$ are frequency dependent dimensionless function of the soil Poisson's ratio, ν , and \tilde{d} is the diameter of the rigid disk, which is equivalent to the pile base projection.

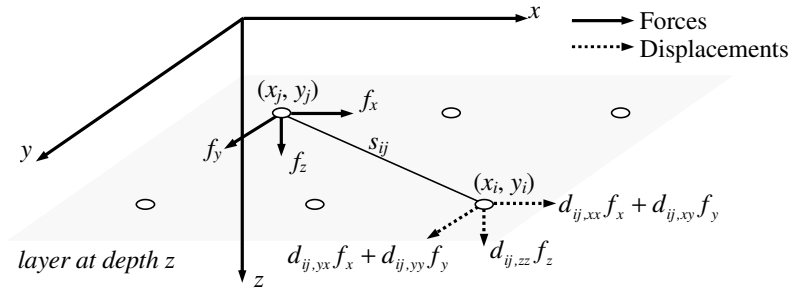


Figure 6-2 Displacements at point *i* due to forces applied at point *j*

For values of $a_0 = \omega \tilde{d} / V_s$ smaller than 1 (which is typical in earthquake engineering) the following values may be assumed:

$$\bar{k}_h = \bar{k}_v \approx 1 \quad (6.35)$$

$$\bar{c}_h \approx 0.58 \text{ and} \quad (6.36)$$

$$\bar{c}_v \approx 0.85 \quad (6.37)$$

However, according to Equation (6.18), (6.15) transforms into

$$\mathbf{u}(\omega, z) = \mathbf{u}_{ff}(\omega, z) - \tilde{\mathbf{D}}(\omega, z) \mathbf{r}(\omega, z) \quad (6.38)$$

from which pile-soil-pile interaction forces can be obtained as:

$$\mathbf{r}(\omega, z) = -\tilde{\mathbf{D}}^{-1}(\omega, z) [\mathbf{u}(\omega, z) - \mathbf{u}_{ff}(\omega, z)] \quad (6.39)$$

The global balance condition can thus be expressed as

$$\begin{aligned} \int_0^L \mathbf{BKDRu}(\omega, z) \cdot \mathbf{DR}\hat{\mathbf{u}}(z) dz + \int_0^L \tilde{\mathbf{D}}^{-1} \mathbf{u}(\omega, z) \cdot \hat{\mathbf{u}}(z) dz - \omega^2 \int_0^L \mathbf{BMu}(\omega, z) \cdot \hat{\mathbf{u}}(\omega, z) dz \\ = \int_0^L \tilde{\mathbf{D}}^{-1} \mathbf{u}_{ff}(\omega, z) \cdot \hat{\mathbf{u}}(z) dz \quad \forall \hat{\mathbf{u}} \neq \mathbf{0} \end{aligned} \quad (6.40)$$

the solution of which is obtained numerically, considering a finite element procedure in the displacement based approach. Piles are divided into E finite elements of length L_e , and the local displacements within the elements are expressed by interpolating those at the end nodes. In the global reference system, nodal displacements of the e -element of the p -th pile having nodes h and k are collected in the vector

$$\tilde{\mathbf{d}}_p^e(\omega) = [\mathbf{u}_h \quad \Phi_h \quad \mathbf{u}_k \quad \Phi_k] \quad (6.41)$$

where \mathbf{u}_i ($i = h, k$) groups components u_{i1}, u_{i2}, u_{i3} along the x_1, x_2 and z axes, respectively, while Φ_i ($i = h, k$) collects rotations $\phi_{i1}, \phi_{i2}, \phi_{i3}$ around x_1, x_2 and z .

Local pile displacements within the elements are interpolated by means of equation

$$\mathbf{R}_p \mathbf{u}_p(z; \omega) \cong \mathbf{N}_p(z) \mathbf{L}_p \mathbf{d}_p^e(\omega) \quad (6.42)$$

where

$$\mathbf{N}_p(z) = \begin{bmatrix} n_1 & 0 & 0 & 0 & n_2 & 0 & n_3 & 0 & 0 & 0 & n_4 & 0 \\ 0 & n_1 & 0 & -n_2 & 0 & 0 & 0 & n_3 & 0 & -n_4 & 0 & 0 \\ 0 & 0 & n_5 & 0 & 0 & 0 & 0 & 0 & n_6 & 0 & 0 & 0 \end{bmatrix} \quad (6.43)$$

is the matrix of the interpolating polynomials, in which n_1, n_2, n_3 are third order polynomials approximating transverse displacements, while n_5 and n_6 are first order polynomials interpolating longitudinal displacements.

Moreover

$$\mathbf{L}_p = \begin{bmatrix} \mathbf{R}_p & 0 & 0 & 0 \\ 0 & \mathbf{R}_p & 0 & 0 \\ 0 & 0 & \mathbf{R}_p & 0 \\ 0 & 0 & 0 & \mathbf{R}_p \end{bmatrix} \quad (6.44)$$

is the rotation matrix, which allows expressing the local displacements of the element end nodes starting from the global ones. Vector containing the displacements of the n piles of the group in (6.5) is thus approximated in the form

$$\mathbf{u}(z; \omega) \cong \mathbf{R}^T \mathbf{N}(z) \mathbf{L} \mathbf{d}^e(\omega) \quad (6.45)$$

where $\mathbf{d}^e(\omega)$ is the vector grouping the nodal displacements of all the piles, while \mathbf{N} and \mathbf{L} are overall matrices obtained by assembling contributions of all the piles, likely:

$$\mathbf{N}(z) = \begin{bmatrix} \mathbf{N}_1 & \cdots & \mathbf{0} & \cdots & \mathbf{0} \\ \vdots & & \vdots & & \vdots \\ \mathbf{0} & \cdots & \mathbf{N}_p & \cdots & \mathbf{0} \\ \vdots & & \vdots & & \vdots \\ \mathbf{0} & \cdots & \mathbf{0} & \cdots & \mathbf{N}_n \end{bmatrix}, \quad (6.46)$$

$$\mathbf{L} = \begin{bmatrix} \mathbf{L}_1 & \cdots & \mathbf{0} & \cdots & \mathbf{0} \\ \vdots & & \vdots & & \vdots \\ \mathbf{0} & \cdots & \mathbf{L}_p & \cdots & \mathbf{0} \\ \vdots & & \vdots & & \vdots \\ \mathbf{0} & \cdots & \mathbf{0} & \cdots & \mathbf{L}_n \end{bmatrix}. \quad (6.47)$$

Thus, the global balance condition can be rewritten as

$$\begin{aligned} & \sum_{e=1}^E \int_0^{L_e} \mathbf{B} \mathbf{K} \mathbf{D} \mathbf{N} \mathbf{L} \mathbf{d}^e \cdot \mathbf{D} \mathbf{N} \mathbf{L} \hat{\mathbf{d}}^e dz + \sum_{e=1}^E \int_0^{L_e} \tilde{\mathbf{D}}^{-1} \mathbf{R}^T \mathbf{N} \mathbf{L} \mathbf{d}^e \cdot \mathbf{R}^T \mathbf{N} \mathbf{L} \hat{\mathbf{d}}^e dz \\ & - \omega^2 \sum_{e=1}^E \int_0^{L_e} \mathbf{B} \mathbf{M} \mathbf{R}^T \mathbf{N} \mathbf{L} \mathbf{d}^e \cdot \mathbf{R}^T \mathbf{N} \mathbf{L} \hat{\mathbf{d}}^e dz = \sum_{e=1}^E \int_0^{L_e} \tilde{\mathbf{D}}^{-1} \mathbf{u}_{ff} \cdot \mathbf{N} \mathbf{R}^T \mathbf{N} \mathbf{L} \mathbf{d}^e \hat{\mathbf{d}}^e dz \quad \forall \hat{\mathbf{d}}^e \neq \mathbf{0} \end{aligned} \quad (6.48)$$

By properly assembling the node displacement in a unique displacement vector $\mathbf{d}(\omega)$, standard considerations allow obtaining the complex linear equation system

$$(\bar{\mathbf{K}}_p - \omega^2 \bar{\mathbf{M}} + \bar{\mathbf{K}}_s) \mathbf{d} = \mathbf{f} \quad (6.49)$$

in which

$$\bar{\mathbf{K}}_p = \sum_{e=1}^E \int_0^{L_e} (\mathbf{D} \mathbf{N} \mathbf{L})^T \mathbf{B} \mathbf{K} (\mathbf{D} \mathbf{N} \mathbf{L}) dz \quad (6.50)$$

$$\bar{\mathbf{M}} = -\omega^2 \sum_{e=1}^E \int_0^{L_e} (\mathbf{R}^T \mathbf{N} \mathbf{L})^T \mathbf{B} \mathbf{M} (\mathbf{R}^T \mathbf{N} \mathbf{L}) dz \quad (6.51)$$

$$\bar{\mathbf{K}}_S = \sum_{e=1}^E \int_0^{L_e} (\mathbf{R}^T \mathbf{N} \mathbf{L})^T \tilde{\mathbf{D}}^{-1} (\mathbf{R}^T \mathbf{N} \mathbf{L}) dz \quad (6.52)$$

$$\mathbf{f} = \sum_{e=1}^E \int_0^{L_e} (\mathbf{R}^T \mathbf{N} \mathbf{L})^T \tilde{\mathbf{D}}^{-1} \mathbf{u}_{ff} dz \quad (6.53)$$

are the global stiffness and mass matrix of the piles, the global impedance matrix of soil and the vector of external loads due to the free-field motion, respectively.

The rigid connection at the pile heads is imposed introducing a rigid constraint and defining a master node with six generalised displacement components (Figure 6-3), collected in the vector

$$\mathbf{d}_r^T(\omega) = [U_1 \quad U_2 \quad U_z \quad \Phi_1 \quad \Phi_2 \quad \Phi_z] \quad (6.54)$$

are the global stiffness and mass matrices of the piles, the global impedance matrix of the soil and the vector of external load due to the free filed motion, respectively.

Since piles of a group are generally connected by a rigid cap, a master node, having six additional generalized displacement components, is introduced for the rigid cap. By suitably defining the geometric matrix \mathbf{A} , the nodal displacements of the piles may be expressed as

$$\mathbf{d}(\omega) = \mathbf{A} \begin{bmatrix} \mathbf{d}_F \\ \mathbf{d}_E \end{bmatrix} \quad (6.55)$$

where \mathbf{d}_F and \mathbf{d}_E group together the displacements of the cap and of the embedded piles, respectively.

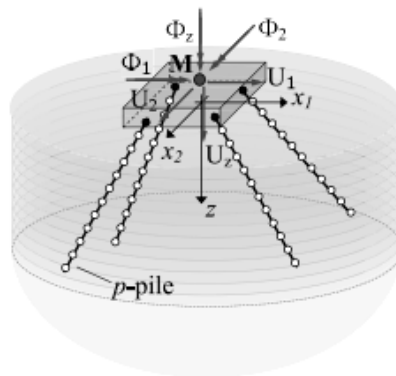


Figure 6-3 Pile group model

Taking (6.55) into account, and substituting it into Equation (6.49), the complex-valued foundation impedance matrix is obtained:

$$\begin{bmatrix} \mathbf{Z}_{FF} & \mathbf{Z}_{FE} \\ \mathbf{Z}_{EF} & \mathbf{Z}_{EE} \end{bmatrix} \begin{bmatrix} \mathbf{d}_F \\ \mathbf{d}_E \end{bmatrix} = \begin{bmatrix} \mathbf{f}_F \\ \mathbf{f}_E \end{bmatrix} \quad (6.56)$$

where

$$\begin{bmatrix} \mathbf{Z}_{FF} & \mathbf{Z}_{FE} \\ \mathbf{Z}_{EF} & \mathbf{Z}_{EE} \end{bmatrix} = \mathbf{A}^T (\overline{\mathbf{K}}_P - \omega^2 \overline{\mathbf{M}}_P + \overline{\mathbf{K}}_S) \mathbf{A} \quad (6.57)$$

$$\begin{bmatrix} \mathbf{f}_F \\ \mathbf{f}_E \end{bmatrix} = \mathbf{A}^T \mathbf{f} \quad (6.58)$$

Once pile displacements are evaluated, the stress resultants in the p -th pile may be calculated from Equation (6.11) that, accounting for the approximation of displacements (6.45), yields

$$s(\omega; z) = \mathbf{KDN}(z) \mathbf{L} \mathbf{d}^e(\omega) \quad (6.59)$$

By simply manipulating Equation (6.56) the complex-valued foundation impedance matrix

$$\mathfrak{S}(\omega) = (\mathbf{Z}_{FF} - \mathbf{Z}_{FE} \mathbf{Z}_{EE}^{-1} \mathbf{Z}_{EF}) \quad (6.60)$$

and the complex-valued motion at the foundation level

$$\mathbf{d}_F(\omega) = \mathfrak{S}^{-1} [\mathbf{f}_F - \mathbf{Z}_{FE} \mathbf{Z}_{EE}^{-1} \mathbf{f}_E] \quad (6.61)$$

may be obtained. The procedure furnishes the frequency-dependent foundation impedances, namely the forces necessary to induce time-harmonic unit displacements at the master node, and the motion of the master node due to the application of free-field displacements. These, according to the substructure approach, are essential quantities for the inertial interaction analysis of the superstructure.

In the framework of the substructure method, Equation (6.60) defines the force–displacement relationships that allow accounting for the soil–foundation system compliance in the structural analysis, while Equation (6.61) defines the seismic input motion for the structural analysis. This accounts for both the amplification due to the site response and the filtering effect exerted by the foundation. It can also be applied when the loading is of inertial nature, such as an impact or a harmonic load applied at the pile head.

Classical elastodynamic solutions available in the literature were adopted for the definition of earlier matrices. However, it should be mentioned that Green's functions obtained also by other formulations may be implemented, accounting for new developments in the research. As an example, more recent solution of dynamic stiffness of flexible piles have been obtained by Shadlou and Bhattacharya (2015), who calibrate spring and dashpot coefficients obtained from a rigorous two-dimensional elastodynamic solution starting from results of finite element analyses where 3D soil–pile interaction phenomena are naturally included. Beside, experimentally derived expressions can also be implemented.

6.2.2. Adaptation of the model for test simulations

With respect to the original formulation, the above described procedure, implemented in MATLAB environment, has been herein adapted to properly take into account the specific conditions of the problem under study.

In particular:

- The loading conditions have been properly applied to the micropile; in particular the time-varying inertial load constituted by the impact of the hammer has been applied to the towering part of the pile.
- The variations with depth of the cross section of the micropile have been taken into account by considering the homogenized cross-sectional properties reported in Table 4-3.
- The injections are taken into account by considering an equivalent diameter evaluated on the basis of the volume of injected grout.
- Both soil and piles have been accurately discretized in order to catch the dynamic behaviour in a sufficiently large range of frequencies.
- In the small strain range the lack of perfect adherence between the reinforcement and the surrounding weathered grout has been taken into account by considering a decrement of radiation damping.

The procedure has been firstly specialized to reproduce impact load tests on single vertical micropiles and then also impact load tests on micropiles group were modeled.

Figure 6-4 schematically depicts the model adopted to simulate the single micropile problem, and its main properties. In the sequel, relevant information about the modeling of soil and micropile are reported.

Soil

It is worth pointing out that the best fit with experimental data is obtained, after some trial analyses, by considering that the profile of V_s varies linearly with depth, starting from a value of 115 m/s at surface (such profile is suggested by empirical correlations based on CPT data). However, the average shear wave velocity is taken equal to 180 m/s in the top 10 m, coherently with the results of geophysical surveys (see §4.2.2). Other soil properties required for the visco-elastic dynamic analysis are simply deduced from standard geotechnical characterization.

With reference to the soil, the height of each sublayers in which the soil is discretized is selected small enough to satisfy the required level of precision. Moreover, the size satisfies the criterion recommended for proper wave transmission. Kuhlemeyer and Lysmer (1973) showed that for accurate representation of wave transmission through a model, the spatial element size, Δh , must be smaller than approximately one-tenth to one-eighth of the wavelength associated with the highest frequency component of the input wave:

$$\Delta h \leq \frac{\lambda}{10} \quad (6.62)$$

where λ is the wavelength associated with the highest frequency component that contains appreciable energy. Therefore, in order to represent accurately a travelling wave of a given

frequency about 10 nodes per wavelength are required. Employing less than 10 nodes can introduce numerical damping since the peaks of the wave may not be well captured.

Since the input travels along the pile, and then radiates into the soil, the required height of each sublayer in which the soil is discretized depends on the frequency content of the input as well as on the mechanical characteristics of the media.

Denoting with V the velocity of the wave crossing a homogeneous medium, the maximum size of mesh Δh can be expressed by the following relationship:

$$\Delta h < \frac{\lambda}{10} = \frac{V}{10f_{\max}} \quad (6.63)$$

where f_{\max} is about 200 Hz (from the Fourier Spectrum of the Impact Load) and V is the shear wave velocity in the shallower portion of soil.

Micropile

Micropiles P1 and P2 are modelled as *beam* element. Micropiles have several cross sectional variations:

- the towering part, which is constituted by a reinforcement bar filled with grout;
- the embedded simply grouted portion (constituted by the reinforcement bar, filled and surrounded by grout);
- the embedded portion interested by injections, considered similarly to the previous simply grouted part but with a different grout section (defined according to the principle of the equivalent diameter).

Accordingly, linear elastic generalized sections have been realized, the properties of which are obtained by means of homogenisation procedure (coherently with Table 4-3). Obviously, the latter cross section is present only in the injected micropiles.

Particular care has been put in definition of the height of the towering part, since small variations of this parameter can potentially induce high modifications of the final results especially in terms of fundamental frequency of the system. The pile is discretized to catch the required frequency contribution and accordingly with the dimension of the soil mesh.

The analytical model has been also adopted to simulate the behaviour of the micropiles group in the small strain range; in particular, impact load tests along x and y directions have been reproduced.

Figure 6-5 schematically depicts the model adopted to simulate the inclined micropiles group, and its main properties. Soil properties and sublayers height are the same adopted for single micropile models. Again, cross sections of injected micropiles are defined according to Table 4-3.

The inclination of the micropiles reproduces the real condition (i.e. inclination along y direction). The presence of the cap is simulated by introducing an infinitely rigid beam element, having the mass of the cap concentrated at the height of the centroid and loaded at the top with the corresponding hammer loading time history. The lack of contact between the cap and the soil is simulated by considering the top portion of pile embedded in soil with null shear wave velocity and excluding radiation damping.

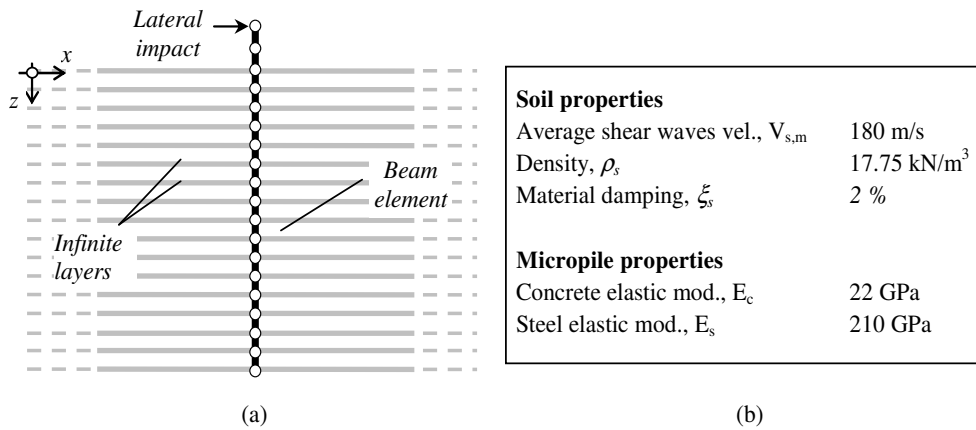


Figure 6-4(a) Schematic representation of the analytical model used to reproduce impact tests and (b) main properties of soil and micropile

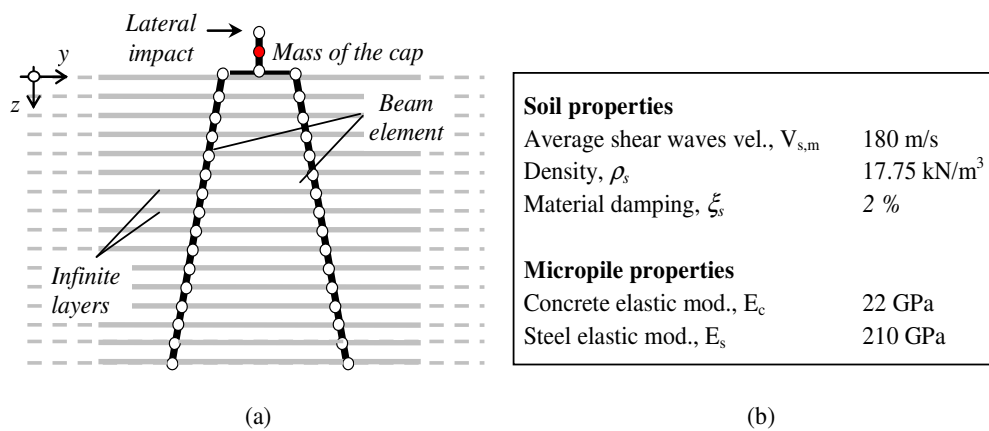


Figure 6-5 (a) Schematic representation of the analytical model used to reproduce impact tests on the inclined micropile group and (b) main properties of soil and micropiles

6.2.3. Results of impact load tests on single vertical micropiles

Figure 6-6 and Figure 6-7 show the comparison in terms of FRF of acceleration and acceleration time histories at the micropile head for one of the impact load test performed on P1 and P2, in configuration A and B, respectively. A good accordance between the experimental and analytical data can be found for both micropiles. In particular, the first and, for configuration B, the second vibration modes of the soil-pile system are correctly described. Therefore, it can be stated that the model, despite the simplifying hypothesis on the soil behavior and on the injected portion of the micropiles, is reasonably capable to catch the dynamic response of the system in the small strains range, in terms of fundamental frequency, damping and amplitude.

Figure 6-8 shows the comparison in terms on real part of FRF of strains; it should be kept in mind that, since the level of strain is very low for this particular loading typology and the frequency of the system is very high, it is often difficult to interpret the strain gages signal with depth. Furthermore, the response of the shallower strain gages is influenced by several factor (i.e. partial debonding between reinforcement and grout, differences between the characteristics of the very shallow soil layer with the underlying silty soil, noise, etc..).

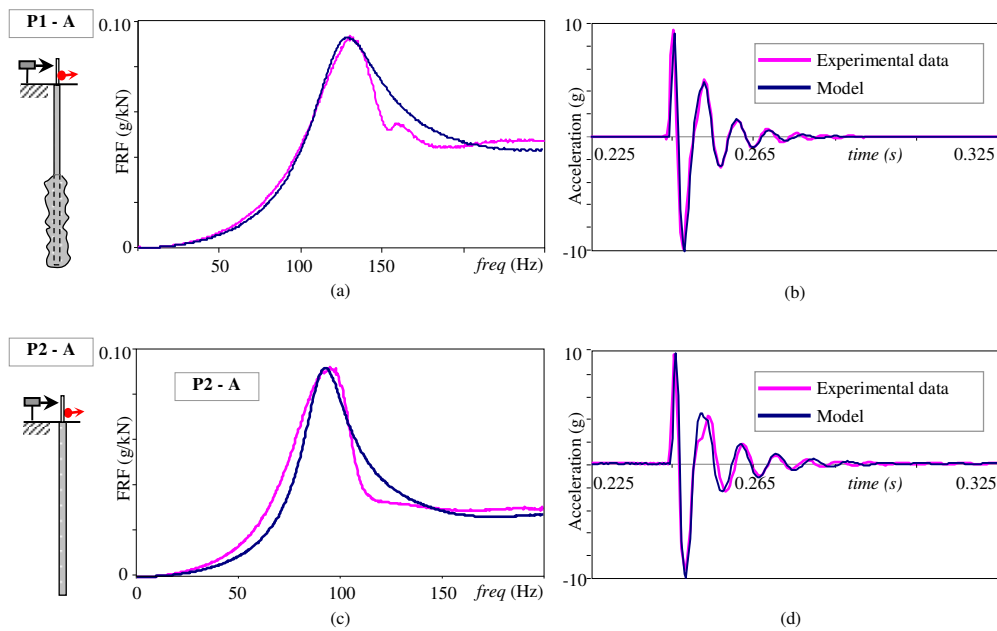


Figure 6-6 Configuration A: comparison between experimental and analytical results for an impact load in frequency domain (FRF of micropile head acceleration) and time domain (time history) on P1 (a, b) and P2 (c,d)

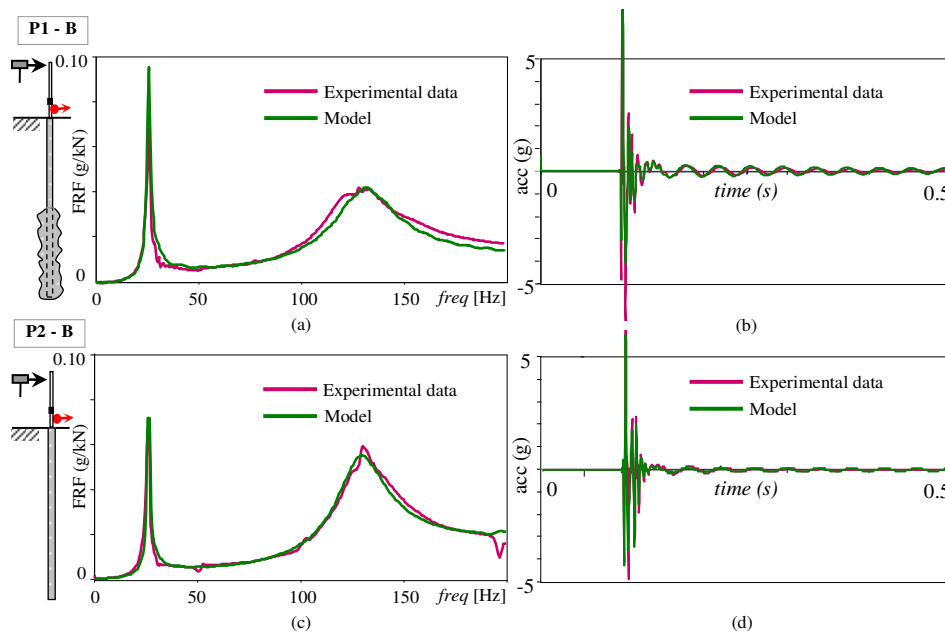


Figure 6-7 Configuration B: comparison between experimental and analytical results for an impact load in frequency domain (FRF of micropile head acceleration) and time domain (time history) on P1 (a, b) and P2 (c, d)

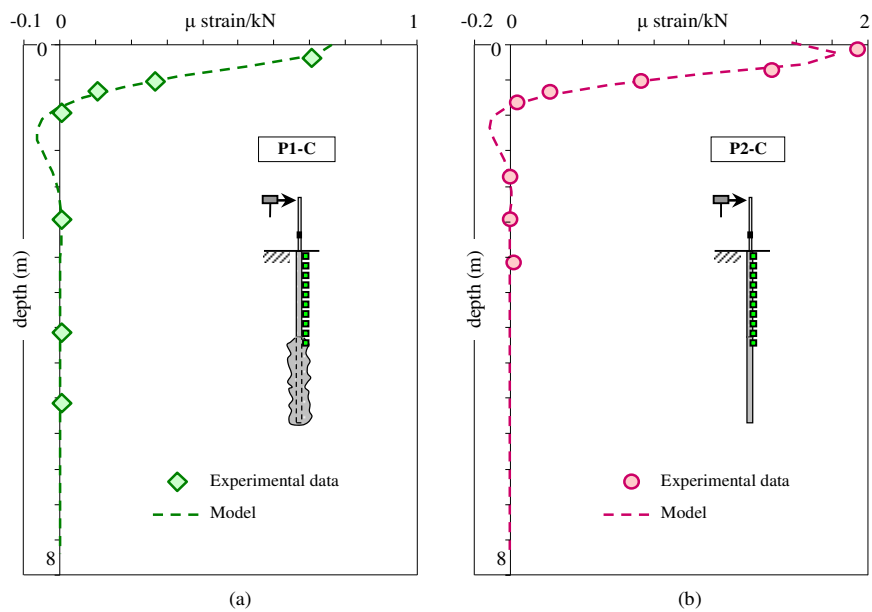
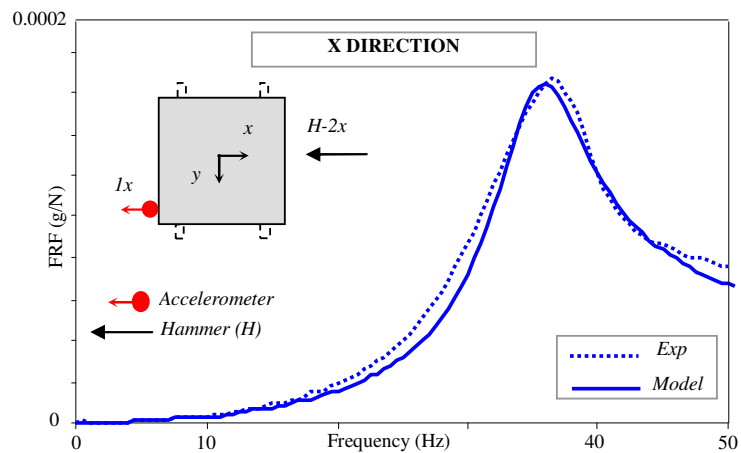


Figure 6-8 Configuration C: comparison between experimental and analytical deformation profiles at the first fundamental frequency, due to impact load test for P1 (a) and P2 (b)

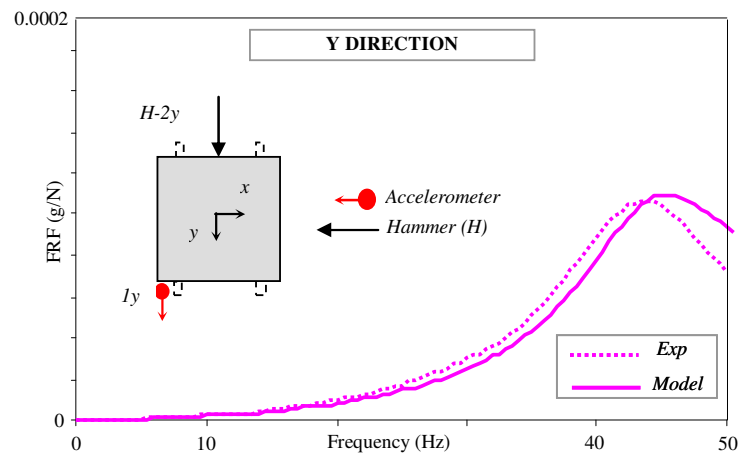
6.2.4. Results of impact load tests on micropiles group

Figure 6-9 show the comparison in terms of FRFs of acceleration acquired on the cap for two of the impact load tests configurations performed along x and y direction on the micropiles group.

A good accordance between the experimental and analytical data can be found for both directions. Therefore, it can be stated that the model, if well calibrated, is able to satisfactorily reproduce the behavior of the foundation system even when a certain angle of inclination is considered.



(a)



(b)

Figure 6-9 Comparison between experimental results of impact load tests on micropiles group and analytical simulation along x (a) and y (b) directions

6.2.5. Analytical and experimental impedance functions

The horizontal impedance functions derived experimentally via ILTs are compared with those obtained by means of the dynamic soil–pile interaction approach illustrated in the previous sections.

Figure 6-10 shows the comparison between experimental and theoretical impedance functions for the single vertical micropiles P1 (a) and P2 (b) in terms of real and imaginary parts. Figure 6-11 shows the same comparison for micropiles group along x and y directions. It is noteworthy that in all the analysed cases a good agreement between the experimental results and the theoretical predictions is found within a significant frequency range, which largely covers the system resonance. At frequencies far from the system resonance the accordance between the experimentally and theoretically derived impedance functions is lower mostly due to scattering of experimental results.

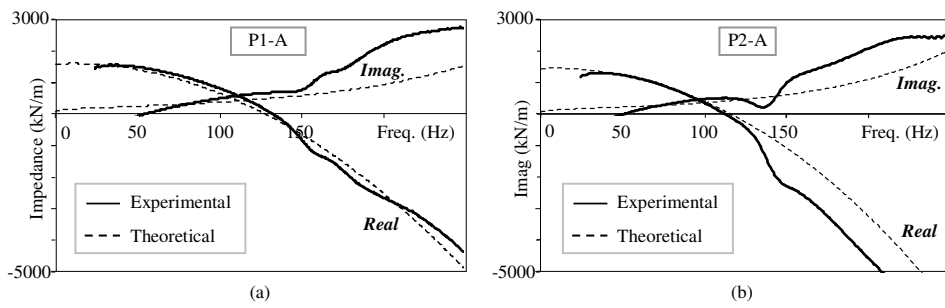


Figure 6-10 Experimental and theoretical impedance functions (real and imaginary parts) for the single vertical micropiles for P1 (a) and P2 (b)

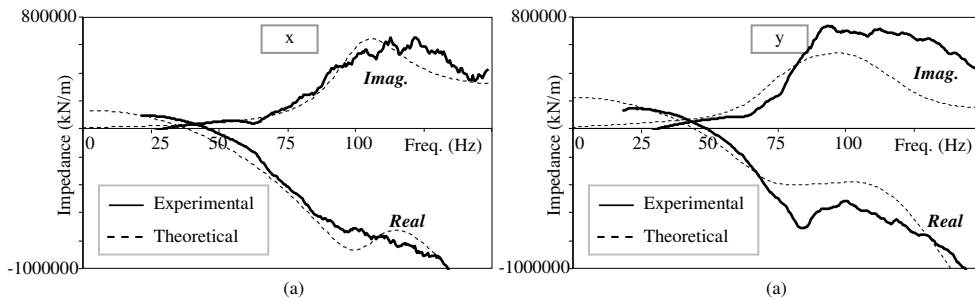


Figure 6-11 Experimental and theoretical impedance functions (real and imaginary parts) for the micropiles group along x (a) and y (b) directions

6.3. ABAQUS model

Two different 3D Finite Element models have been realized with the computer code ABAQUS: one has been adopted to simulate impact load tests, while the other to simulate the non linear phenomena connected to snap back testing. Thus the former will be referred to as *linear* model, while the second one as *non linear* model. In the following sections the pile and soil properties, their mutual interaction, boundary conditions, mesh size and methods of load application, are discussed with reference to both models.

6.3.1. Linear model

The realization of the 3D linear model has been possible thanks to a calibration based on the experimental results obtained from the impact load tests in configuration A, B and C. Each configuration has been reproduced by means of a specific model, which differs from the others only for the presence of the pipe extension rigidly connected to the reinforcement bar, and/or the height of the impact load. However, the main geometric and mechanical characteristics remain the same for all the linear models realized. A schematic view of the general model is provided in Figure 6-12, alongside with the main mechanical properties adopted for the soil and the micropile.

All the models have been realized through two separated parts: the micropile and the soil, the specific characteristics of which will be described in the sequel.

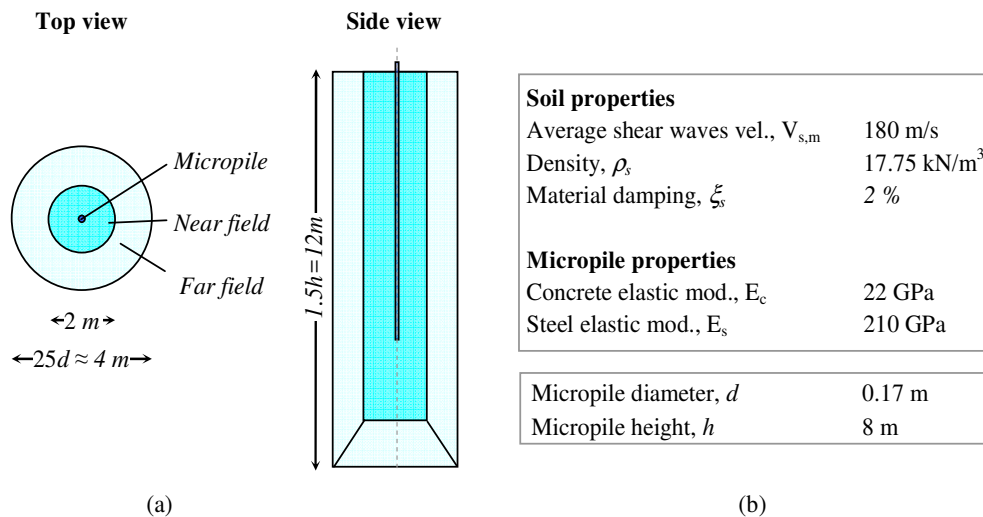


Figure 6-12 Schematic view of the 3D FE linear model (a) and main geotechnical properties of soil and micropile (b)

Micropile

The micropile is modelled as a 1D element (*wire*). The modelling of micropiles resembles what described for the analytical model of Dezi et al. In particular, since micropiles (especially the injected ones) have several cross-sectional variations, the wire has been suitably partitioned to obtain the three distinct sections already described in § 6.2.2:

- the towering part, constituted by a reinforcement bar filled with grout;
- the embedded simply grouted portion;
- the embedded portion interested by injections, considered similarly to the previous simply grouted part but with a different grout section.

Particular care has been put in definition of the height of the towering part, since small variations of this parameter can potentially induce high modifications of the final results especially in terms of fundamental frequency of the system. Accordingly, linear elastic generalized sections have been realized, the properties of which are obtained by means of homogenisation procedure (coherently with Table 4-3). The pile is discretized to catch the required frequency contribution and accordingly with the dimension of the soil mesh; linear elements of type B31 are adopted.

Soil

As shown in Figure 6-12, the soil domain has been idealized as a cylinder with an overall height of 12 m (i.e. 1.5 times the height of the pile) and a diameter about 25 times that of the micropile (≈ 4 m). Those dimensions have been chosen on the basis of preliminary analyses. In the centre of the soil domain, a hole with diameter consistent with that of the micropile sections is realized. It should be noted that the soil domain is the same for all the impact load configurations analysed and that the average mechanical properties of the soil are those adopted for the previously described analytical model; in particular, the linear variation of the elastic modulus with depth is realized by considering many progressively stiffer horizontal layers, each one characterized by a constant Young modulus. In order to account for the dissipative behaviour of the soil under dynamic loading conditions, Rayleigh damping is introduced in the linear FE model. The Rayleigh damping matrix [C] can be expressed as a linear combination of the mass matrix and stiffness matrix:

$$[C]=\alpha[M]+\beta[K] \quad (6.64)$$

The damping ration corresponding to the i -th mode of vibration of the system can be accordingly expressed as:

$$\xi_i = \frac{\alpha}{2\omega_i} + \frac{\beta\omega_i}{2}, \quad i=1,\dots,N \quad (6.65)$$

Thus, the parameters α and β can be set such that a target value of the damping factor is achieved for two modes of vibration only. In particular, denoting with ω_i and ω_j the circular frequencies of two vibration modes and with $\bar{\xi}$ the desired damping factor for both modes, the parameters α and β can be obtained as follows:

$$\alpha = \bar{\xi} \frac{2\omega_i\omega_j}{\omega_i + \omega_j}, \quad (6.66)$$

$$\beta = \bar{\xi} \frac{2}{\omega_i + \omega_j}. \quad (6.67)$$

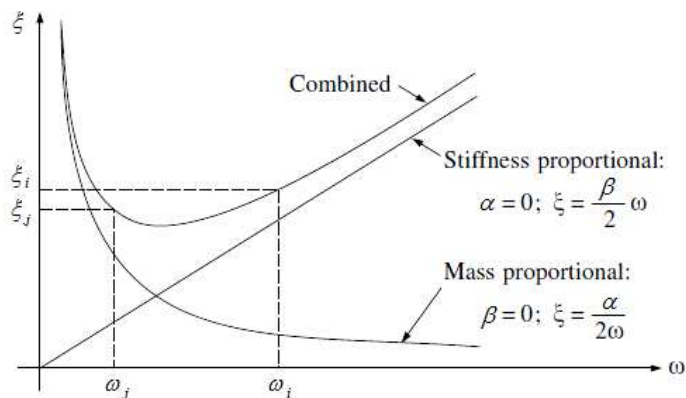


Figure 6-13 Relationship between damping ratio and frequency (for Rayleigh damping)

According to Equation (6.65), the damping factor ζ , which is equal to $\bar{\zeta}$ for ω equal to ω_i and ω_j , varies with the natural frequency of vibration of the system. In particular, the damping ratio contribution corresponding to the mass proportional damping $\alpha[M]$ is inversely proportional to the frequency while the damping ratio contribution corresponding to the stiffness proportional damping $\beta[K]$ increases proportionally with the frequency (Figure 6-13). It is noteworthy that all the N modes of vibration contribute to the dynamic response, although usually only a limited number of modes significantly affect the response. Thus, neither of these two types of damping would be suitable for use with an MDOF system in which the frequencies of the significant modes span a wide range because the relative amplitudes of the different modes would be seriously distorted by inappropriate damping ratios. For this reason, particular care must be posed in selecting the values of ω_i , ω_j and ζ . In common practice, it is recommended that ω_j generally be taken as the fundamental frequency of the MDOF system and that ω_i be set among the higher frequencies of the modes that contribute significantly to the dynamic response. This ensures that the desired damping ratio is obtained for these two modes. Modes with frequencies between the two specified frequencies are characterized by lower values of damping ratio, while modes with frequencies greater than ω_j will have damping ratios that increase above ζ_j linearly with frequency. In conclusion, the vibration modes with high frequencies are significantly damped due to the associated high values of the damping ratio.

For this application, the damping of the system is calibrated by selecting ω_i , ω_j and ζ on the basis of the results of impact load tests.

Meshing criteria aim at obtaining an as much as possible structured mesh (it can be obtained by partitioning horizontally and radially the soil domain) and assuring a sufficient number of nodes per wavelength. Moreover the soil domain is divided into an inner portion (2 m in diameter) constituted by *structured* C3D8R elements, while the outer portion (with an external diameter of 4 m) is modelled by means of infinite elements CIN3D8 (Figure 6-14) that are used to address the *quiet* conditions at the boundary, and that will be described more extensively in the sequel.

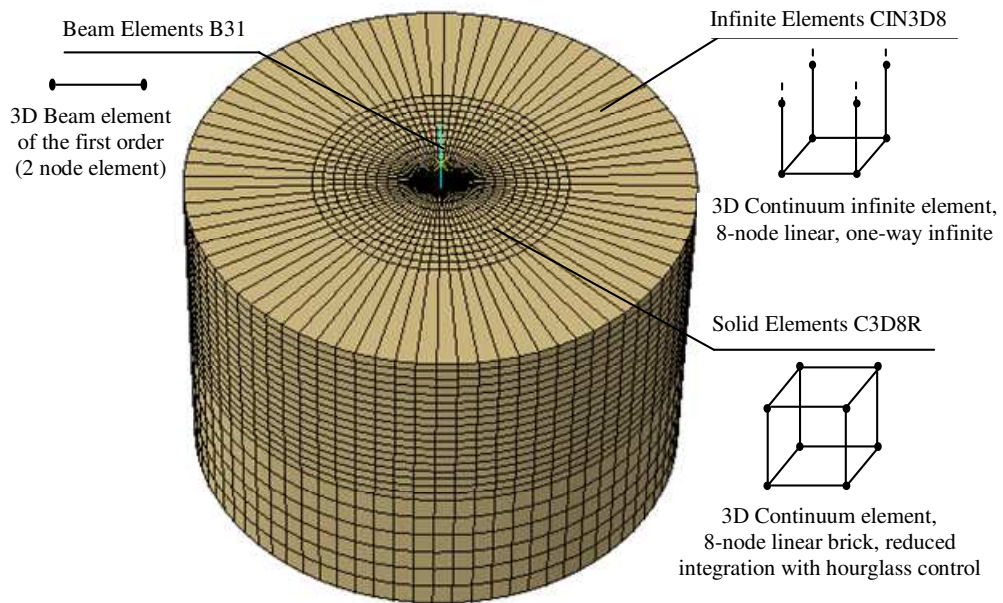


Figure 6-14 Schematic view of the model calibrated on impact load tests, and of element used for pile, soil and quiet boundaries

Infinite elements

The choice of realistic boundary conditions is an important issue that must be addressed in the dynamic soil-foundation interaction analysis. The unbounded or infinite medium can be approximated by extending the finite element mesh to a far distance, where the influence of the surrounding medium on the region of interest is considered small enough to be neglected. This approach needs experimentation with mesh sizes and assumed boundary conditions at the truncated edges of the mesh and is not always reliable. The issue is of particular concern in dynamic analysis, when the boundary of the mesh may reflect energy back into the region being modelled. Moreover, because of limited computational resources, the computational domain must be kept small enough so that the FE analysis can be performed in a reasonable amount of time. A better approach is to use the so called *infinite elements*, which are defined over semi-infinite domains with suitably chosen decay functions. Abaqus provides first- and second-order infinite elements that are based on the work of Zienkiewicz et al. (1983) for static response and of Lysmer and Kuhlemeyer (1969) for dynamic response. The elements are used in conjunction with standard finite elements, which model the area around the region of interest, with the infinite elements modelling the far-field region.

The dynamic response of the infinite elements is based on consideration of plane body waves travelling orthogonally to the boundary. Again, it is assumed that the response adjacent to the boundary is of small enough amplitude so that the medium responds in a linear elastic fashion. The equilibrium equation is

$$-\rho \ddot{\mathbf{u}} + \frac{\partial}{\partial \mathbf{x}} \cdot \boldsymbol{\sigma} = 0, \quad (6.68)$$

where ρ is the material's density, $\ddot{\mathbf{u}}$ is the material particle acceleration, $\boldsymbol{\sigma}$ is the stress, and \mathbf{x} is position.

Introducing the Lamé's constants in the equilibrium equation, under the hypothesis of small strains, provides the governing equation for the motion

$$\rho \ddot{u}_i = G \frac{\partial^2 u_i}{\partial x_i \partial x_j} + (\lambda + G) \frac{\partial^2 u_j}{\partial x_i \partial x_j}, \quad (6.69)$$

where index notation has been used for simplicity.

We consider plane waves travelling along the x -axis. Two body wave solutions of this form exist for this equation. One describes plane, longitudinal (“*push*”) waves, which have the form

$$u_x = f(x \pm c_p t), \quad u_y = u_z = 0 \quad (6.70)$$

where, by substitution in the governing equation, one can find that the wave speed, c_p , is

$$c_p = \sqrt{\frac{\lambda + 2G}{\rho}}. \quad (6.71)$$

The other solution of this form is the “shear” wave solution

$$u_y = f(x \pm c_s t), \quad u_x = u_z = 0 \quad (6.72)$$

or

$$u_z = f(x \pm c_s t), \quad u_x = u_y = 0 \quad (6.73)$$

where—again by substitution in the governing equation—it can be obtained

$$c_s = \sqrt{\frac{G}{\rho}}. \quad (6.74)$$

In each case the solution $f(x-ct)$ represents waves moving in the direction of increasing x , while $f(x+ct)$ represents waves moving in the direction of decreasing x .

Now consider a boundary at $x = L$ of a medium modelled by finite elements in $x < L$. A distributed damping on this boundary is now introduced, such that

$$\sigma_{xx} = -d_p \dot{u}_x, \quad (6.75)$$

$$\sigma_{xy} = -d_s \dot{u}_y, \quad (6.76)$$

$$\sigma_{xz} = -d_s \dot{u}_z, \quad (6.77)$$

where the damping constants d_p and d_s have to be chosen to avoid reflection of longitudinal and shear wave energy back into the medium in $x < L$. Plane, longitudinal waves approaching the boundary have the form $u_x = f_1(x - c_p t)$, $u_y = u_z = 0$. If they are reflected at all as plane, longitudinal waves, their reflection will travel away from the boundary in some form $u_x = f_2(x + c_p t)$, $u_y = u_z = 0$. Since the problem is linear, superposition provides the total displacement $f_1 + f_2$, with corresponding stresses $\sigma_{xx} = (\lambda + 2G)(f_1' + f_2')$, all other $\sigma_{ij} = 0$, and velocity $\dot{u}_x = -c_p(f_1' - f_2')$. For this solution to satisfy the damping behaviour introduced on the boundary at $x = L$ requires

$$(\lambda + 2G - d_p c_p) f_1' + (\lambda + 2G + d_p c_p) f_2' = 0. \quad (6.78)$$

We can, therefore, ensure that $f_2 = 0$ (so that $f_2' = 0$) for any f_1 by choosing

$$d_p = \frac{\lambda + 2G}{c_p} = \rho c_p. \quad (6.79)$$

A similar argument for shear waves provides

$$d_s = \rho c_s. \quad (6.80)$$

These values of boundary damping are built into the infinite elements in Abaqus. From the above discussion we see that they transmit all normally impinging plane body waves exactly (provided that the material behaviour close to the boundary is linear elastic). General problems involve non-plane body waves that do not impinge on the boundary from an orthogonal direction and may also involve Rayleigh surface waves and Love waves. Nevertheless, these “quiet” boundaries work quite well even for such general cases, provided that they are arranged so that the dominant direction of wave propagation is orthogonal to the boundary or, at free surfaces and interfaces where Rayleigh or Love waves are of concern, they are orthogonal to the surface (see, for example, Cohen and Jennings, 1983). As the boundaries are “quiet” rather than silent (perfect transmitters of all waveforms), and because the boundaries rely on the solution adjacent to them being linear elastic, they should be placed some reasonable distance from the region of main interest. In addition the node numbering for infinite elements must be defined such that the first face is the face that is connected to the finite element part of the mesh. It should be noted that the infinite element nodes that are not part of the first face are treated differently in explicit dynamic analysis than in other procedures. These nodes are located away from the finite element mesh in the infinite direction. The location of these nodes is not meaningful for explicit analysis, and loads and boundary conditions must not be specified using these nodes in explicit dynamic procedures. In other procedures these outer nodes are important in the element definition and can be used in load and boundary condition definitions.

Except for explicit procedures, the basis of the formulation of the solid medium elements is that the far-field solution along each element edge that stretches to infinity is centred about an origin, called the “pole.” For example, the solution for a point load applied to the boundary of a half-space has its pole at the point of application of the load. It is important to choose the position of the nodes in the infinite direction coherently with respect to the pole. The second node along each edge pointing in the infinite direction must be positioned so that it is twice as far from the pole as the node on the same edge at the boundary between the finite and the infinite elements (Figure 6-15a). In addition to this length consideration, the second nodes in the infinite direction must be defined such that the element edges in the infinite direction do not cross over, which would give non-unique mappings ((Figure 6-15b).

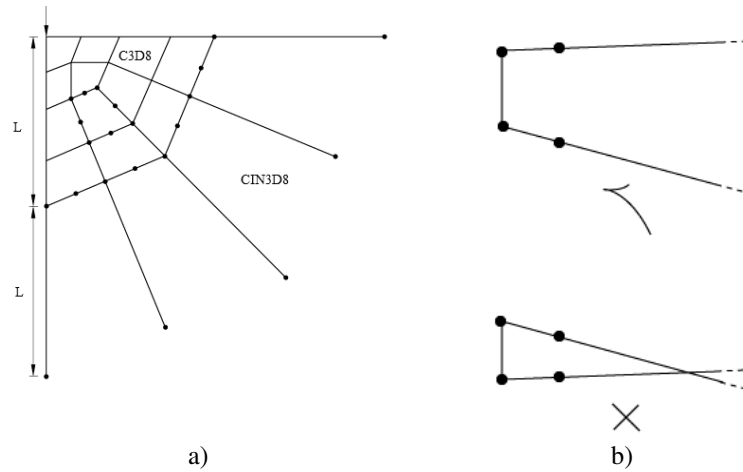


Figure 6-15 Infinite Element: a) positioning of the second node; b) examples of an acceptable and an unacceptable two-dimensional infinite element

In direct-integration implicit dynamic response analysis, steady-state dynamic frequency domain analysis, matrix generation, super-element generation, and explicit dynamic analysis, infinite elements provide “quiet” boundaries to the finite element model through the effect of a damping matrix; the stiffness matrix of the element is suppressed. The elements do not provide any contribution to the eigenmodes of the system. The elements maintain the static force that was present at the start of the dynamic response analysis on this boundary; as a consequence, the far-field nodes in the infinite elements will not displace during the dynamic response.

During dynamic response analysis following static preload (as is common in geotechnical applications), the traction provided by the infinite elements to the boundary of the finite element mesh consists of the constant stress obtained from the static response with the quiet boundary damping stress added. Since the elements have no stiffness during dynamic analysis, they allow a net rigid body motion to occur, which is usually not a significant effect.

Summarizing, infinite elements:

- can be adopted in boundary value problems defined in unbounded domains or problems in which the region of interest is small in size compared to the surrounding medium;
- are usually used in conjunction with finite elements;
- a solid section definition is used to define the section properties of infinite elements, that can have linear behaviour only;
- provide stiffness in static solid continuum analyses, while provide “quiet” boundaries to the finite element model in dynamic (direct integration-implicit and explicit) analyses.

Interface

The interaction between micropiles and soil in the linear model is modelled by means of a tie constraint around the pile surface. This approach is expected to reproduce the conditions of the impact load test, due to the low strain induced into the soil. However, the use of the tie constraint may provide unrealistic results, especially for tests with greater load (i.e. free vibration tests) since it would neglect the gapping arising between the pile and the soil.

Mesh

The size of the elements employed for discretizing the domain plays a crucial role in the assessment of the true solution of problem with a FE model. A finer mesh results in a better approximation to the true solution, however it comes at the expense of computational time. With reference to the soil, grids size is selected small enough to satisfy the required level of precision. Moreover, the size satisfies the criterion recommended for proper wave transmission. Kuhlemeyer and Lysmer (1973) showed that for accurate representation of wave transmission through a model, the spatial element size, Δh , must be smaller than approximately one-tenth to one-eighth of the wavelength associated with the highest frequency component of the input wave:

$$\Delta h \leq \frac{\lambda}{10} \quad (6.81)$$

where λ is the wavelength associated with the highest frequency component that contains appreciable energy. Therefore, in order to represent accurately a travelling wave of a given frequency about 10 nodes per wavelength are required. Employing less than 10 nodes can introduce numerical damping since the peaks of the wave may not be well captured.

Since the input travels along the pile, and then radiates into the soil, the mesh size depends on the frequency content of the input as well as on the mechanical characteristic of the media. Denoting with V the velocity of the wave crossing a homogeneous medium, the maximum size of mesh Δh can be expressed by the following relationship:

$$\Delta h < \frac{\lambda}{10} = \frac{V}{10f_{\max}} \quad (6.82)$$

where f_{\max} is about 200 Hz (from the Fourier Spectrum of the Impact Load) and V_s is the shear wave velocity in the shallower portion of soil.

Load and step procedure

The impact load is applied by means of a concentrated load. The choice of time integration method for the resolution of the dynamic problem is a non trivial problem. Abaqus allows adopting two different resolution schemes, a Direct Integration Implicit procedure, and a Dynamic Explicit procedure.

In order to perform the simulations for this study, the implicit integration scheme turn out to be more efficient, and provides more stable results; thus it has been adopted to simulate both impact load tests and snap back tests.

6.3.2. Non-linear model

During the free vibration tests performed on vertical single micropiles, non linear response of the soil-micropile system have been observed, together with the development of a gap between the micropile and the surrounding soil interface which strongly modifies the dynamic behaviour of the system. To reproduce such phenomenon the adoption of visco-elastic behaviour for the soil and the hypothesis of perfect bonding at the pile –soil interface are inappropriate. For this reason, a more refined 3D FE model has been developed, including elasto-plastic behaviour of the soil, and an interface element able to reproduce contact, separation and slip between the foundation element and the soil. The non linear model has been developed on the basis of the linear model calibrated on impact load test results on pile P2. However, undrained elasto-plastic behaviour is adopted in the portion of soil close to the pile and contact elements are used at the interface between the micropile and the soil. With respect to the linear model the height of the soil domain has been reduced as much as possible to limit the computational cost. Moreover, symmetry conditions are exploited (only one-half of the soil and micropile domain are considered). A schematic view of the general model is provided in Figure 6-16, alongside with the main mechanical properties adopted for the soil and the micropile.

Micropile

The adoption of an interface with contact properties does not permit the simultaneous adoption of solid elements for the soil and wire elements for the pile. Therefore, the grout inside and outside the reinforcement bar of the micropile have been modelled as a 3D element (C3D8R) while the reinforcement bar is modelled by means of a membrane element (often used to represent thin surfaces in space that offer strength in the plane of the element but have no bending stiffness such as thin stiffening components in solid structures, such as a reinforcing layer in a continuum). In this case, M3D4R, a three-dimensional, 4-node membrane element with reduced integration, is used. For simplicity in the interpretation of final results, a perfect bonding between the components of micropile (confined grout, membrane, and unconfined grout) is considered. Material properties are simulated *as-they-are*, with no necessity of homogenisation, but the elastic modulus of external unconfined grout is reduced by 10% to account for widespread degradation. The model is depicted in Figure 6-17.

Soil

For the non-linear model the soil domain has a toroidal cross-section divided into three concentric rings: the outer diameter is constituted by infinite elements (CIN3D8) with the same properties described for the linear model; it is adjacent to the middle ring, made by linear elastic elements (C3D8R), while the core, that is in contact with the pile, is constituted by 3D continuous elements (C3D8R), with an elasto-plastic behaviour. In particular, the Mohr-Coulomb plasticity is adopted combined with the linear elastic material model. A view of the soil model is presented in Figure 6-18. Details about the Mohr-Coulomb model implemented in ABAQUS are provided in Appendix A5.

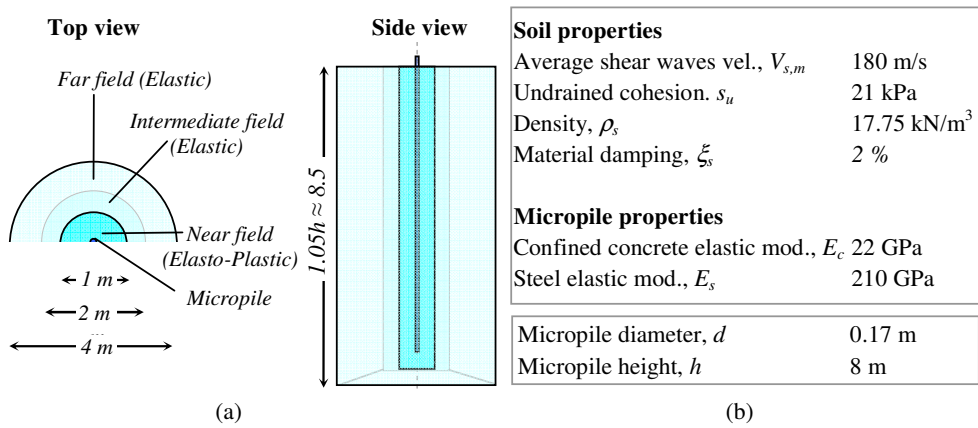


Figure 6-16 Schematic view of the 3D FE nonlinear model (a) and main geotechnical properties of soil and micropile (b)

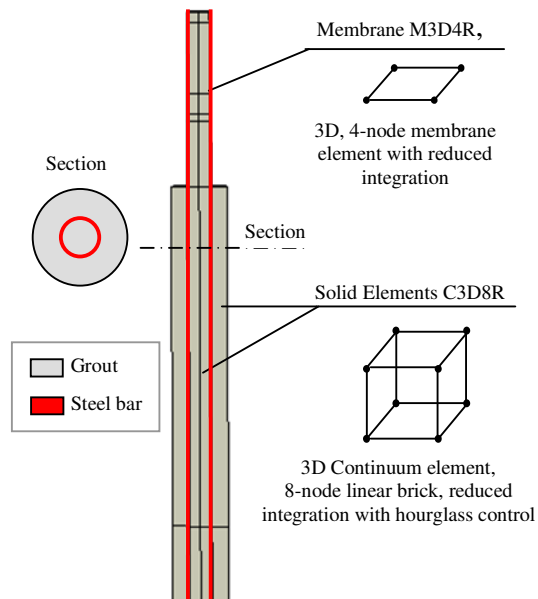


Figure 6-17 Pile domain in non-linear model

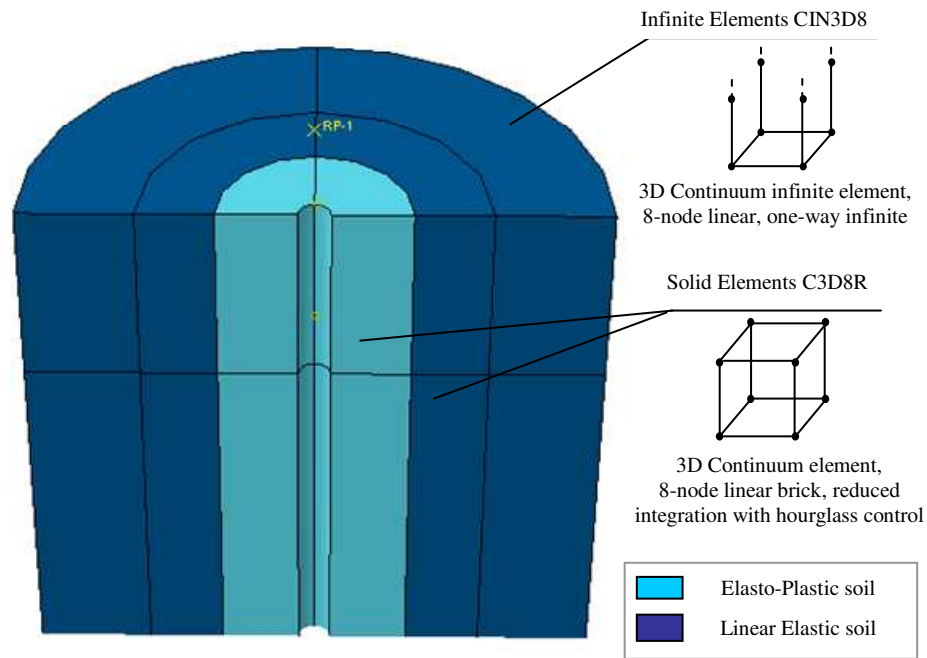


Figure 6-18 Soil domain in non-linear model

Interface

The interaction between micropiles and elasto-plastic portion of soil in the non linear model is realized by means of a contact constraint between the pile surface (master surface) and the soil surface (slave surface). The interaction between contacting surfaces consists of two components: one normal to the surfaces and one tangential to the surfaces. The tangential component consists of the relative motion (sliding) of the surfaces and, eventually, frictional shear stresses. In the non linear model a frictionless contact with no bonding for the tangential behaviour has been adopted, while the rule exploited for the behaviour normal to the surface is the so called *hard* contact behaviour. The distance separating two surfaces is called the clearance. The contact constraint is applied when the clearance between two surfaces becomes zero. There is no limit in the contact formulation on the magnitude of contact pressure that can be transmitted between the surfaces. The surfaces separate when the contact pressure between them becomes zero or negative, and the constraint is removed. This behaviour, referred to as “hard” contact, is the default contact behavior in Abaqus and is summarized in the contact pressure-clearance relationship shown in Figure 6-19. Such relationship minimizes the penetration of the slave surface (soil) into the master surface (pile) at the constraint locations and does not allow the transfer of tensile stress across the interface.

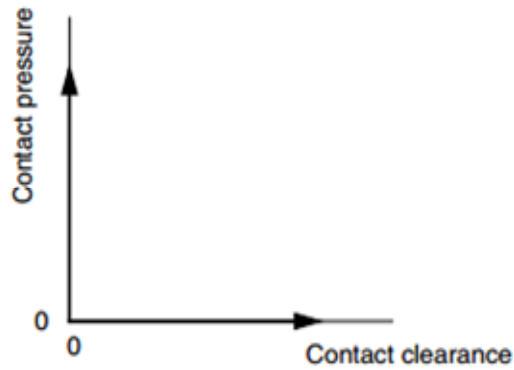


Figure 6-19 Contact pressure-clearance relationship for “hard” contact

Mesh

With respect to linear model, the mesh is radially and vertically less refined with the exception of the 1st m from the micropile head. This choice has been driven by the awareness that the fundamental frequency of the system is less than that obtained in the linear case, by the need for the reduction of the computational time, and finally by the fact that too small elements in plastic analyses can induce local convergence errors.

Load and Step Procedure

The load is divided into three steps:

- The *initial* step: in which boundary conditions are applied to the system;
- The *loading* step: during which the loading is applied to the pile, in a *quasi-static* manner (as during the snap back test)
- The *unloading* step: immediately after the release, during which the system turns back to its equilibrium position by means of free vibrations.

In the loading step the duration has been reduced with respect to the effective one, due to computational costs; however the loading time have been kept long enough to let the system deform in a realistic manner.

Analyses are executed according to Dynamic, Implicit procedure.

6.3.3. Results of numerical simulation of impact load tests

The linear model has been adopted to simulate the response of single vertical micropiles to impact load tests, in the three different configurations tested:

- configuration A: ILTS on micropiles without pipe extension, low impact intensity

- configuration B: ILTS on micropiles with pipe extension, low impact intensity
- configuration C: ILTS on micropiles with pipe extension, higher impact intensity

For Configuration A and B the signal of the accelerometer at the micropile head is acquired, while for configuration C strain gauges signals along the shaft are registered. Therefore, for configuration A and B the comparison between the numerical model and the field data is shown in terms of absolute value of FRF of acceleration registered at the micropile head and corresponding time histories of acceleration (Figure 6-20 and Figure 6-21), while for configuration C the real values of FRFs calculated on strains at increasing depth, close to the resonance frequency of the system, are shown in Figure 6-22. All analyses are performed considering, for each configuration, a specific impact among the corresponding set in x direction. The choice has fallen on the impact record that provides results closest to the average experimental FRF.

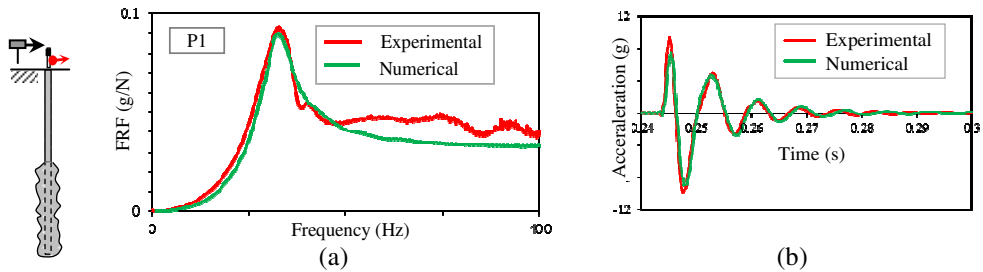


Figure 6-20 Comparison between experimental and simulated FRF of impact load test (a) and corresponding acceleration time history (b) for P1 in configuration A

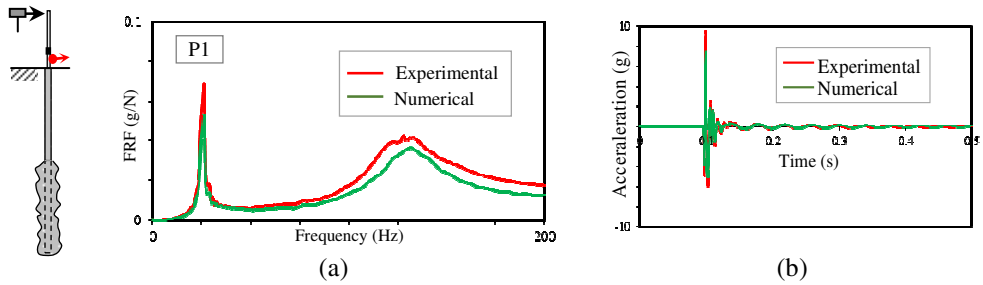


Figure 6-21 Comparison between experimental and simulated FRF of impact load test (a) and corresponding acceleration time history (b) for P1 in configuration B

The numerical model is able to describe the experimental results in term of amplitude damping and fundamental frequencies. Thanks to the mesh refinement in the surroundings of the micropile, the comparison is acceptable up to 200 Hz, and even the second mode of vibration identified with configuration B is correctly described. Moreover, from the comparison shown in Figure 6-22 it can be seen that the model is also able to describe the profile of deformations with depth.

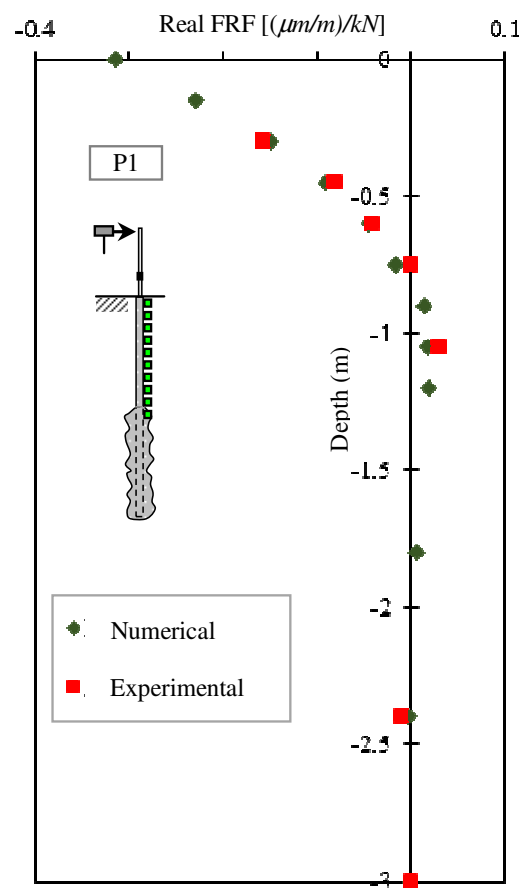


Figure 6-22 Comparison between experimental and simulated strain profile close to resonance at 25 Hz in terms of real component of FRF at increasing depth, for P1

6.3.4. Results of numerical simulation of free vibration tests

The non linear model has been adopted to simulate the snap tack test performed on micropile P2, at the lowest force level (experiment F1_P1).

This choice has been driven by two considerations:

1. Snap back tests on P1 and P2 were realized after the 2-way cyclic loading tests (that have provoked the opening of a gap between the micropile and the surrounding soil). In particular, for what concerns P2, snap back tests were carried out about a month after cyclic load tests, so that a recovery occurred in the soil (even thanks to several episodes of rain). On the contrary, for pile P1 the interval between cyclic load tests and snap back tests was much shorter and results of snap back experiments cannot be considered completely independent from cyclic load tests.
2. Since non linear phenomena, including the opening of a gap at the interface between the micropile and the soil, occurred even during the test performed at the lowest force level (F1_P1) and considering that F1_P1 was the first carried out among the set of free vibration experiments (so it can be considered more representative of the *virgin* behaviour of the system), the non linear model has been calibrated on the experimental data obtained from F1_P1 experiment on P2.

As already explained, the numerical model developed for the simulation of free vibration tests includes a loading phase, during which the pile is pulled towards the hydraulic jack until the shear pin breaks, and a second phase, just after the release, which reproduce the free vibrations with which the micropile tries to turn back to its original position.

In Figure 6-23 different frames of the simulation are portrayed for the test performed on P2, at the first level of force. Colours refer to value of displacements magnitude.

During the loading phase (Figure 6-23 a, b) a gap develops in the rear side of the pile (with respect to the verse of loading) and its dimensions progressively increase with the increasing of the loading; after the abrupt release due to the failure of the calibrated pin, the micropile starts to vibrate and a gap develops even in the front side of the pile (as observed during experimental tests).

The comparison in terms of displacement (Figure 6-24) reached in the quasi-static phase is satisfying, since the maximum quasi-static displacement registered by the transducer nearer to the ground level is 7.8 mm, while the corresponding simulated displacement is 7.3 mm.

In Figure 6-25 the experimental response of the accelerometer is compared with the simulated results. Results are comparable in terms of amplitude and oscillatory behaviour, even if simulated results are affected by numerical scattering.

More refined constitutive model for the soil and the interface will be taken into account in the next future; however, the good accordance between the model and the experimental results are such that the adopted modelling techniques can be considered up-and-coming for the description of the same system under severe dynamic events of inertial and kinematic nature.

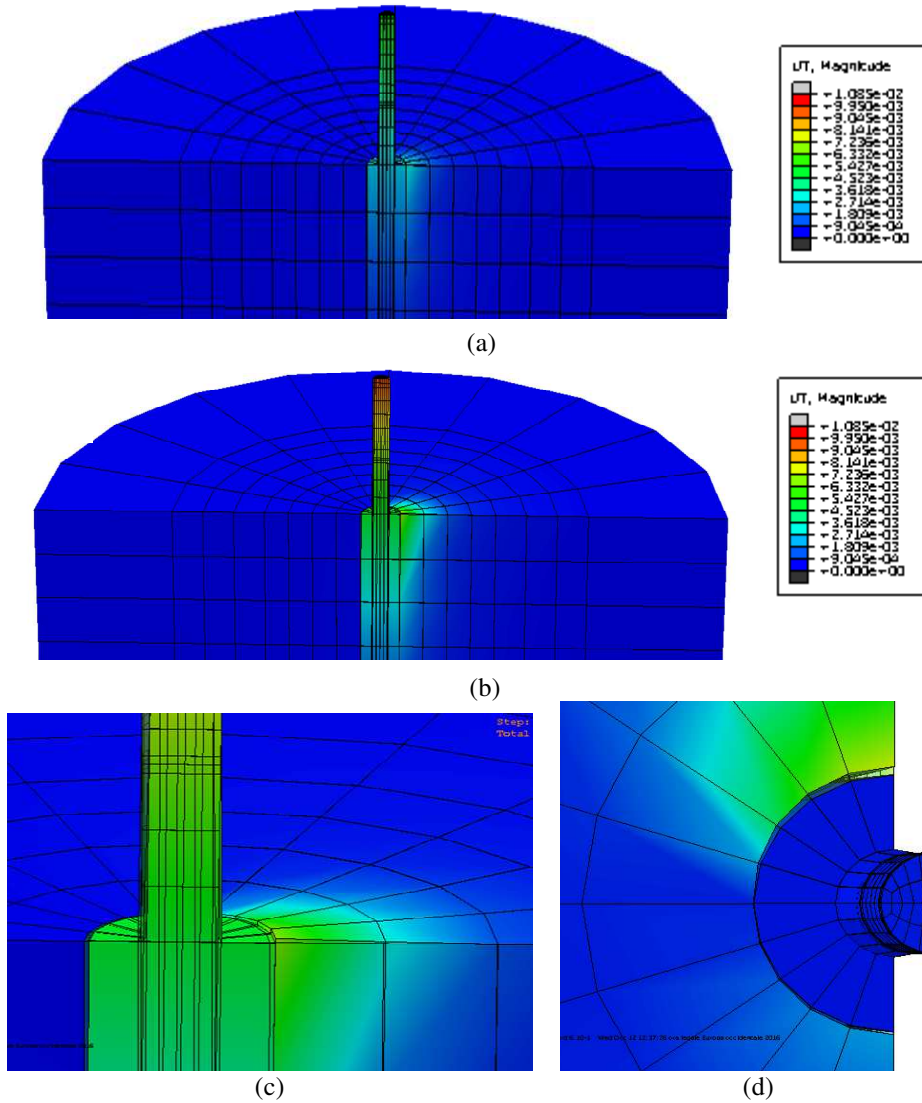


Figure 6-23 Subsequent steps of a simulated free vibration test (F1_P1 on micropile P2): (a) initial moments of the loading step; (b) advanced phase of the loading; (c) detail of the detachment between soil and micropile; (d) view from the top of the free vibrations after the release, with double side detachment.

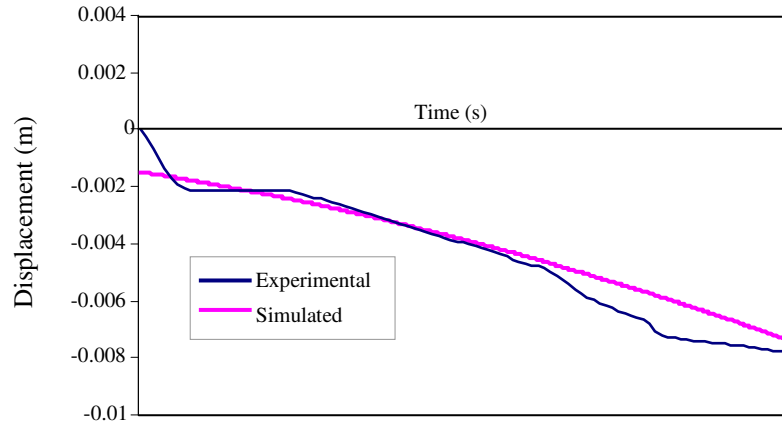


Figure 6-24 Comparison between numerical and experimental result in terms of displacement registered at the pile head in the quasi static-loading phase

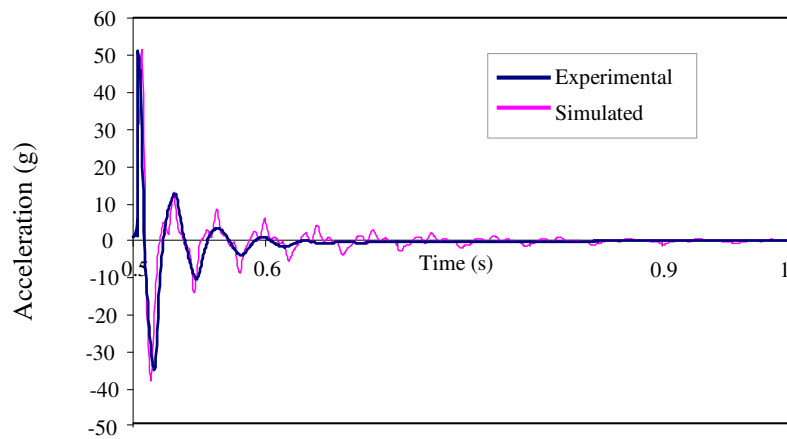


Figure 6-25 Comparison between numerical and experimental result in terms of acceleration registered at the pile head after the release

Chapter 7.

Main Conclusions

This work describes an extensive experimental program of full-scale field tests performed on two single vertical micropiles in free head conditions, and on a group of four inclined micropiles connected at the head by a concrete cap, embedded into alluvial soils. Five of the six micropiles were completed with high pressure injections, a technique traditionally adopted to improve the bearing capacity. A single vertical micropile was left simply grouted, to allow a comparison with the behaviour of the injected vertical micropile.

Piles were permanently instrumented with strain gauges along the shaft; moreover, several other transducers were adopted depending on the test typology. The performed dynamic tests included ambient vibration tests and impact load tests, in the low force intensity range, snap back testing on vertical micropiles and forced vibration tests on the inclined micropiles group in the high force intensity level range. Furthermore, two-way cyclic loading tests were performed on the single vertical micropiles to investigate their cyclic behaviour.

Some of the results were compared with those obtained with numerical models: in particular, a 3-D model for the kinematic and inertial interaction analysis of pile groups was employed for comparison in the linear and linear-equivalent strain range. For this purpose, the model was modified and specialized to simulate the impact load tests on vertical and inclined micropiles of the experimental campaign. Moreover, two different 3-D finite element models were developed with a general purpose Finite Element computer code. The first model was developed to simulate impact load tests, while the second has been calibrated to reproduce, in a computationally efficient manner, the results of snap back testing on single vertical micropiles, including the detachment at the interface between the micropile and the soil that has been identified during snap back tests.

Many observations come from the present work:

- High-pressure injections, aside from improving the bearing capacity to vertical loads, also increase the fundamental frequency of the system (with respect to not injected micropiles); contrarily to simply grouted micropile, for the injected micropiles a different behaviour along x and y axis can be identified (i.e. a variation of fundamental frequency up to 10-15% depending on the load configuration and the mode of vibration excited); moreover, the horizontal stiffness of the injected micropile head to static and cyclic load is significantly higher than that of the simply grouted micropile.
- By comparing the behaviour of the group along x and y axis, it can be observed that inclination of micropiles, although limited, significantly influences the dynamic stiffness of the micropiles group; with a variation of

fundamental frequency along the two orthogonal directions of about 25%. Moreover, differences due to inclination have been identified in the characteristics of the rocking-translational coupling induced by inertial dynamic loading.

- During high intensity force level tests (dynamic and cyclic) on both single micropiles and micropiles group, several phenomena related to non-linearity manifested (i.e. gap at the soil-micropile, radial cracks in the soil, materials degradation). In association with the opening of the gap, a substantial change in the dynamic stiffness and cyclic behaviour occurred.
- For the investigated micropiles group degradation due to high force intensity dynamic tests is slightly more pronounced in the direction along which micropiles are inclined (45% along x axis vs 48% along y axis, in terms of variation of fundamental frequency).
- The ability of numerical models developed for dynamic interaction of traditional piles to reproduce the results obtained experimentally on micropiles has been proved. A FE model able to reproduce the development of the main non-linear phenomena observed during in-situ tests on single vertical micropiles has also been developed. The comparison between experimental and numerical results is promising.
- The experimental work hereinafter described comprises several techniques for the dynamic identification of systems. To the author knowledge those techniques have never been applied to investigate full scale micropile-soil systems and the results are encouraging.

The extensive experimental study has produced numerous data, some of which still require further processing. Moreover, the modelling techniques can be improved to consider the effect of high pressure injections on the surrounding soil, the materials degradation, more refined conditions at the interface as well as complex constitutive soil models.

The obtained experimental data can also be considered as a starting point for the development of new simplified modelling approaches, able to take into account the effects of execution techniques, real interfaces behaviour, and micropiles inclination under dynamic and cyclic loading conditions.

Finally, the obtained results represent a key issue for the optimization of injected micropiles design and execution.

References

Abd Elaziz, A.Y., El Naggar, M.H., 2014. Group behaviour of hollow-bar micropiles in cohesive soils. *Canadian Geotechnical Journal* 51, 1139–1150. doi:10.1139/cgj-2013-0409

A.F.P.S. 1990 - French association for earthquake engineering, n.d. Recommendations for the redaction of rules relative to the structures and installations built in regions prone to earthquake.

Allotey, N., El Naggar, M.H., 2008. Generalized dynamic Winkler model for nonlinear soil–structure interaction analysis. *Canadian Geotechnical Journal* 45, 560–573. doi:10.1139/T07-106

Alpan, I., 1973. The dynamic response of pile foundations to lateral forces, in: *Proceedings of the 5th World Conference on Earthquake Engineering*. Rome, Italy. pp. 256–71.

Angelides, D.C., Roesset, J.M., 1981. Nonlinear lateral dynamic stiffness of piles. *Journal of Geotechnical and Geoenvironmental Engineering* 107.

Ashford, S.A., Rollins, K.M., Lane, J.D., 2004. Blast-Induced Liquefaction for Full-Scale Foundation Testing. *Journal of Geotechnical and Geoenvironmental Engineering* 130, 798–806. doi:10.1061/(ASCE)1090-0241(2004)130:8(798)

ASTM, n.d. D3966M - 07(2013)e1, Standard Test Methods for Deep Foundations Under Lateral Load.

Banerjee, P.K., Davies, T.G., n.d. 13. Analysis of some reported case histories of laterally loaded pile groups, in: *Numerical Methods in Offshore Piling*. pp. 101–108.

Banerjee, P., Sen, R., 1987. Dynamic behavior of axially and laterally loaded piles and pile groups. *Dynamic behaviour of foundations and buried structures* 3, 95–133.

Berger, E., Mahi, S.A., Pyke, R., 1977. Simplified Method For Evaluating Soil-Pile-Structure Interaction Effects. *Offshore Technology Conference*. doi:10.4043/2954-MS

Blaney, G., Kausel, E., Roesset, J., n.d. Roesset. JM (1976).“ Dynamic Stiffness of Piles,” in: *Proc. 2nd Int. Conf. on Num. Methods in Geomechanics*, Virginia Polytechnic and State Univ., Blackburg. June. pp. 1001–1009.

Blaney, G.W., O'Neill, M.W., 1989. Dynamic lateral response of a pile group in clay.

Blaney, G.W., O'Neill, M.W., 1986. Analysis of dynamic laterally loaded pile in clay. *Journal of geotechnical engineering* 112, 827–840.

Blaney, G.W., O'Neill, M.W., 1986. Measured Lateral Response of Mass on Single Pile in Clay. *Journal of Geotechnical Engineering* 112, 443–457. doi:10.1061/(ASCE)0733-9410(1986)112:4(443)

Bogard, D., Matlock, H., 1983. Procedures for analysis of laterally loaded pile groups in soft clay, in: *Geotechnical Practice in Offshore Engineering*. ASCE, pp. 499–535.

Boominathan, A., Ayothiraman, R., 2007. An experimental study on static and dynamic bending behaviour of piles in soft clay. *Geotechnical and Geological Engineering* 25, 177–189. doi:10.1007/s10706-006-9102-7

Brown, D.A., Morrison, C., Reese, L.C., 1988. Lateral Load Behavior of Pile Group in Sand. *Journal of Geotechnical Engineering* 114, 1261–1276. doi:10.1061/(ASCE)0733-9410(1988)114:11(1261)

Brown, D.A., Reese, L.C., O'Neill, M.W., 1987. Cyclic Lateral Loading of a Large - Scale Pile Group. *Journal of Geotechnical Engineering* 113, 1326–1343. doi:10.1061/(ASCE)0733-9410(1987)113:11(1326)

Bruce, D.A., DiMillio, A.F., Juran, I., 1995. Introduction to micropiles: an international perspective, in: *Geotechnical Special Publication*. ASCE, pp. 1–26.

Bruce, D., Juran, I., 1997. Drilled and grouted micropiles: state-of-practice review, volume ii: design.

Cairo, R, Dente, G. and Troncone, A. 1999. Cone model for a pile foundation embedded in a soil layer, in *Earthquake Resistant Engineering Structures, Vol. 2*, (Ed. G. Oliveto and C.A. Brebbia), WIT Press, Southampton, 565-574.

Carbonari, S., Morici, M., Dezi, F., Gara, F., Leoni, G., 2017. Soil-structure interaction effects in single bridge piers founded on inclined pile groups. *Soil Dynamics and Earthquake Engineering* 92, 52–67.

Carbonari, S., Morici, M., Dezi, F., Leoni, G., 2016. Analytical evaluation of impedances and kinematic response of inclined piles. *Engineering Structures* 117, 384–396. doi:10.1016/j.engstruct.2016.03.027

Chen, Y.-J., Lee, Y.-H., 2010. Evaluation of lateral interpretation criteria for drilled shaft capacity. *Journal of geotechnical and geoenvironmental engineering* 136, 1124–1136.

Cohen, M., and P. C. Jennings, *Silent Boundary Methods for Transient Analysis (in Computational Methods for Transient Analysis)*, Ed. T. Belytschko and T. R. J. Hughes, Elsevier, 1983.

Comodromos, E.M., Bareka, S.V., 2005. Evaluation of negative skin friction effects in pile foundations using 3D nonlinear analysis. *Computers and Geotechnics* 32, 210–221.

Crouse, C., Cheang, L., 1987. Dynamic testing and analysis of pile-group foundations, in: *Dynamic Response of Pile Foundations—Experiment, Analysis and Observation*. ASCE, pp. 79–98.

Davies, T., Budhu, M., 1986. Non-linear analysis of laterally loaded piles in heavily overconsolidated clays. *Geotechnique* 36, 527–538.

Dezi, F., Carbonari, S., Leoni, G., 2010. Kinematic bending moments in pile foundations. *Soil Dynamics and Earthquake Engineering* 30, 119–132.

Dezi, F., Carbonari, S., Leoni, G., 2010. Static equivalent method for the kinematic interaction analysis of single piles. *Soil Dynamics and Earthquake Engineering* 30, 679–690. doi:10.1016/j.soildyn.2010.02.009

Dezi, F., Carbonari, S., Leoni, G., 2009. A model for the 3D kinematic interaction analysis of pile groups in layered soils. *Earthquake Engineering & Structural Dynamics* 38, 1281–1305. doi:10.1002/eqe.892

Dezi, F., Carbonari, S., Morici, M., 2016a. A numerical model for the dynamic analysis of inclined pile groups: A Numerical Model for the Dynamic Analysis of Inclined Pile Groups. *Earthquake Engineering & Structural Dynamics* 45, 45–68. doi:10.1002/eqe.2615

Dezi, F., Gara, F., Roia, D., 2016b. Linear and Nonlinear Dynamic Response of Piles in Soft Marine Clay. *Journal of Geotechnical and Geoenvironmental Engineering* 04016085. doi:10.1061/(ASCE)GT.1943-5606.0001580

Dezi, F., Gara, F., Roia, D., 2013. Experimental study of near-shore pile-to-pile interaction. *Soil Dynamics and Earthquake Engineering* 48, 282–293. doi:10.1016/j.soildyn.2013.01.025

Dezi, F., Gara, F., Roia, D., 2012. Dynamic response of a near-shore pile to lateral impact load. *Soil Dynamics and Earthquake Engineering* 40, 34–47. doi:10.1016/j.soildyn.2012.04.002

Dezi, F., Poulos, H., 2016. Kinematic Bending Moments in Square Pile Groups. *International Journal of Geomechanics* 04016066. doi:10.1061/(ASCE)GM.1943-5622.0000747

Dobry, R., Gazetas, G., 1988. Simple method for dynamic stiffness and damping of floating pile groups. *Géotechnique* 38, 557–574. doi:10.1680/geot.1988.38.4.557

- Dobry, R., Vicente, E., O'Rourke, M., Roesset, M., 1982. Horizontal stiffness and damping of single piles. *Journal of Geotechnical and Geoenvironmental Engineering* 108, 439–458.
- Dunnivant, T.W., O'Neill, M.W., 1989. Experimental p - y Model for Submerged, Stiff Clay. *Journal of Geotechnical Engineering* 115, 95–114. doi:10.1061/(ASCE)0733-9410(1989)115:1(95)
- Ehlers G., 1942. The effect of soil flexibility on vibrating systems, *Beton und Eisen*, 41, 197-203.
- El-Marsafawi, H., Han, Y.C., Novak, M., 1992. Dynamic Experiments on Two Pile Groups. *Journal of Geotechnical Engineering* 118, 576–592. doi:10.1061/(ASCE)0733-9410(1992)118:4(576)
- El-Marsafawi, H., Kaynia, A.M., Novák, M., 1992. The superposition approach to pile group dynamics, in: *Piles Under Dynamic Loads*. ASCE, pp. 114–135.
- El Naggar, M.H., Novak, M., 1994. Non-linear model for dynamic axial pile response. *Journal of geotechnical engineering* 120, 308–329.
- El Naggar, M., Novak, M., 1995. Nonlinear lateral interaction in pile dynamics. *Soil Dynamics and Earthquake Engineering* 14, 141–157.
- Eurocode, E., 1994. Structures in seismic regions. Part 5: Foundations, retaining structures, and geotechnical aspects. Commission of the European Communities, Brussels.
- Ewins, D.J., 1984. *Modal testing: theory and practice*. Research studies press Letchworth.
- Fan, K., Gazetas, G., 1991. Seismic response of single piles and pile groups.
- Feagin, L.B., 1937. Lateral pile-loading tests. *Transactions of the American Society of Civil Engineers* 102, 236–254.
- FHWA NHI-05-039 Micropile design and construction, Reference manual, 2005.
- Fleming, K., Weltman, A., Randolph, M., Elson, K., 2008. *Piling Engineering*, Third Edition. Taylor & Francis.
- Focht, J.A., Koch, K.J., 1973. Rational Analysis of the Lateral Performance of Offshore Pile Groups. *Offshore Technology Conference*. doi:10.4043/1896-MS
- Frank, R., 2006. Forever the French National Project on Micropiles. 14th Prague Geotechnical Lecture, 22nd May.

Fuse, Y., Ashihara, E., Kikuchi, T., Goto, Y., 1992. Vibration test of bridge pier with large-scale group-pile foundation. Presented at the Proceedings of the 10th world Conference of Earthquake Engineering, Madrid, Spain.

Gazetas, G., 1991. Foundation Vibrations, in: Fang, H.-Y. (Ed.), *Foundation Engineering Handbook*. Springer US, Boston, MA, pp. 553–593.

Gazetas, G., Dobry, R., 1984a. Simple radiation damping model for piles and footings. *Journal of Engineering Mechanics* 110, 937–956.

Gazetas, G., Dobry, R., 1984b. Horizontal Response of Piles in Layered Soils. *Journal of Geotechnical Engineering* 110, 20–40. doi:10.1061/(ASCE)0733-9410(1984)110:1(20)

Gazetas, G., Makris, N., 1991. Dynamic pile-soil-pile interaction. Part I: Analysis of axial vibration. *Earthquake Engineering & Structural Dynamics* 20, 115–132.

Gazetas, G., Fan, K., Kaynia, A., 1993. Dynamic response of pile groups with different configurations. *Soil Dynamics and Earthquake Engineering* 12, 239–257.

Geological sheet 293, Osimo [WWW Document], n.d. URL http://www.isprambiente.gov.it/Media/carg/293_OSIMO/Foglio.html (accessed 4.11.16).

Geosystems, 2011. Description of full scale tests conducted and data obtained in the three phases of tests conducted for the US Military in Baltimore, MD. Federal Highway Administration, Order DTFH61-02-P-00162, Requisition/Reference.

Gerolymos, N., Giannakou, A., Anastasopoulos, I., Gazetas, G., 2008. Evidence of beneficial role of inclined piles: observations and summary of numerical analyses. *Bulletin of Earthquake Engineering* 6, 705–722. doi:10.1007/s10518-008-9085-2

Giannakou, A., Gerolymos, N., Gazetas, G., Tazoh, T., Anastasopoulos, I., 2010. Seismic Behavior of Batter Piles: Elastic Response. *Journal of Geotechnical and Geoenvironmental Engineering* 136, 1187–1199. doi:10.1061/(ASCE)GT.1943-5606.0000337

Grib, S., 1975. Behaviour of Pile Foundations Under Horizontal Seismic Action. Presented at the Proceedings of the 5th European Conference of Earthquake Engineering, Istanbul.

Guillaume, P., De Sitter, G., Jordaens, P.J., Devriendt, C., 2013. Damping estimation of an offshore wind turbine on a monopile foundation. *IET Renewable Power Generation* 7, 401–412. doi:10.1049/iet-rpg.2012.0276

Hafez, D., Turan, A., El Naggar, H., Sangiuliano, T., n.d. Seismic response of group of micropiles considering pile-cap connectivity conditions. DFI 11th International workshop on micropiles, Milan, Italy.

Halling, M.W., Womack, K.C., Muhamad, I., Rollins, K.M., 2000. Vibrational testing of a full-scale pile group in soft clay, in: Proc. 12th World Conference on Earthquake Engineering, Auckland. Paper.

Hansen, R.J., Engineering, M.I. of T.D. of C., Study, M.I. of T.C. for A.E., 1970. Seismic Design for Nuclear Power Plants. M.I.T. Press.

Hibbett, Karlsson, Sorensen, 1998. ABAQUS/standard: User's Manual. Hibbett, Karlsson & Sorensen.

Holloway, D., Moriwaki, Y., Finno, R., Green, R., 1981. Lateral load response of a pile group in sand, in: Proceedings of the Second International Conference on Numerical Methods in Offshore Piling, pp. 441–456.

Imamura, A., Hijikata, K., Tomii, Y., Nakai, S., Hasegawa, M., 1996. An experimental study on nonlinear pile–soil interaction based on forced vibration tests of a single pile and a pile group, in: Proceedings, 11th World Conference on Earthquake Engineering.

Jennings, D.N., Thurston, S.J., Edmonds, F.D., 1986. Static and dynamic lateral loading of two piles, in: Proc. N Z National Roads Board Road Research Unit. Presented at the Bridge Design and Research Seminar, RRU Bulletin, Auckland, pp. 29–38.

Juran, I., Benslimane, A., Hanna, S., 2001. Engineering analysis of dynamic behavior of micropile systems. Transportation Research Record 91–106.

Kagawa, T., 1983. Dynamic Lateral Pile - Group Effects. Journal of Geotechnical Engineering 109, 1267–1285. doi:10.1061/(ASCE)0733-9410(1983)109:10(1267)

Kausel, E., 1988. Local Transmitting Boundaries. Journal of Engineering Mechanics 114, 1011–1027. doi:10.1061/(ASCE)0733-9399(1988)114:6(1011)

Kausel, E., 1974. Forced Vibrations of Circular Foundations on Layered Media, Soils publication. Massachusetts Institute of Technology.

Kaynia, A., 1982. Dynamic stiffness and seismic response of pile groups. MIT-CE-R82-03.

Kaynia, A.M., Novak, M., 1992. Response of pile foundations to rayleigh waves and obliquely incident body waves. Earthquake Engineering & Structural Dynamics 21, 303–318. doi:10.1002/eqe.4290210403

Khalili-Tehrani, P., Ahlberg, E.R., Rha, C., Lemnitzer, A., Stewart, J.P., Taciroglu, E., Wallace, J.W., 2014. Nonlinear Load-Deflection Behavior of Reinforced Concrete Drilled Piles in Stiff Clay. Journal of Geotechnical and Geoenvironmental Engineering 140, 04013022. doi:10.1061/(ASCE)GT.1943-5606.0000957

Kim, J., Brungraber, R., 1976. Full-scale lateral load tests of pile groups. *Journal of the Soil Mechanics and Foundations Division* 102, 87–105.

Kim, J., Brungraber, R., Singh, L., 1979. Pile cap soil interaction from full-scale lateral load tests. *Journal of the Soil Mechanics and Foundations Division* 105, 643–653.

Kishishita, T., Saito, E., Miura, F., 2000. Dynamic-response characteristics of structures with micropile foundation system, in: 12th World Conference on Earthquake Engineering, Auckland, New Zealand. pp. 1–8.

Kobori, T., Miura, K., Nakazawa, M., Hijikata, K., Miyamoto, Y., Moroi, T., Kobayashi, Y., 1991. Study on dynamic characteristics of a pile group foundation.

Kooijman, A., 1989. Comparison of an elasto–plastic quasi three-dimensional model for laterally loaded piles with field tests. *Numerical models in geomechanics-NUMOG III* 675–682.

Kramer, S., 1991. Behavior of piles in full-scale, field lateral loading tests. Final report.

Kuhlemeyer, R., 1979. Static and dynamic laterally loaded floating piles. *Journal of Geotechnical and Geoenvironmental Engineering* 105.

Kuhlemeyer, R.L., 1979. Vertical vibration of piles. *Journal of Geotechnical and Geoenvironmental Engineering* 105.

Laefer, D., 1999. Geotechnical Procedures for at-Risk and in-Distress Structures, in: Sickels-Taves, L. (Ed.), *The Use of and Need for Preservation Standards in Architectural Conservation*. ASTM International, 100 Barr Harbor Drive, PO Box C700, West Conshohocken, PA 19428-2959, pp. 211–211–15.

Lam, I.P., Cheang, L., 1995. Dynamic soil-pile interaction behavior in submerged sands, in: *Earthquake-Induced Movements and Seismic Remediation of Existing Foundations and Abutments*. ASCE, pp. 110–135.

Lewis, K., Gonzalez, L., 1985. Finite element analysis of laterally loaded drilled piers in clay, in: *Proceedings of 12th International Conference on Soil Mechanics and Foundation Engineering*, Rio de Janeiro. pp. 1201–4.

Lizzi, F., n.d. First patent on root piles and reticulated root piles.

Lu, X., Li, P., Chen, B., Chen, Y., 2005. Computer simulation of the dynamic layered soil pile structure interaction system. *Canadian geotechnical journal* 42, 742–751.

Lysmer, J., Kuhlemeyer, R.L., *Transportation, I. of, Engineering, T., University of California, B.S.M., Laboratory, B.M.R., University of California, B.G.E.G., 1969. Finite Dynamic Model for Infinite Media, Reprint (University of California). Department of Civil*

Engineering, University of California, Institute of Transportation and Traffic Engineering, Soil Mechanics Laboratory.

Makris, N., Badoni, D., 1995. Seismic response of pile groups under oblique-shear and Rayleigh waves. *Earthquake Engineering & Structural Dynamics* 24, 517–532. doi:10.1002/eqe.4290240405

Makris, N., Gazetas, G., 1992. Dynamic pile-soil-pile interaction. Part II: Lateral and seismic response. *Earthquake engineering & structural dynamics* 21, 145–162.

Mascardi, C., 1982. Design criteria and performance of micropiles, in: *Symposium on Soil and Rock Improvement Techniques Including Geotextiles. Reinforced Earth and Modern Piling Methods*, Bangkok, Paper D-3.

Matlock, H., 1970. Correlations for design of laterally loaded piles in soft clay. *Offshore Technology in Civil Engineering's Hall of Fame Papers from the Early Years* 77–94.

Matlock, H., Ingram, W.B., Kelley, A.E., Bogard, D., 1980. Field Tests Of The Lateral-Load Behavior Of Pile Groups In Soft Clay. *Offshore Technology Conference*. doi:10.4043/3871-MS

Meimon, Y., Baguelin, F., Jezequel, J., 1986. Pile group behaviour under long time lateral monotonic and cyclic loading, in: *Proceedings, Third International Conference on Numerical Methods in Offshore Piling*, Inst. Francais Du Petrole, Nantes, France. pp. 285–302.

Menetrey, P., Willam, K., 1995. Triaxial failure criterion for concrete and its generalization. *ACI structural Journal* 92, 311–318.

Mindlin, R.D., 1936. Force at a Point in the Interior of a Semi-Infinite Solid. *Physics* 7, 195. doi:10.1063/1.1745385

Ministero delle Infrastrutture, 2008. *Norme tecniche per le costruzioni*. D. M. 14/01/2008 14.

Misra, A., Oberoi, R., Kleiber, A., 1999. Micropiles for seismic retrofitting of highway interchange foundation, in: *IWM99, Proceedings of Second International Workshop on Micropiles*. pp. 215–223.

Mitwally, H., Novak, M., 1987. Response of Offshore Towers with Pile Interaction. *Journal of Engineering Mechanics* 113, 1065–1084. doi:10.1061/(ASCE)0733-9399(1987)113:7(1065)

Mizuno, H., Iiba, M., 1992. Dynamic effects of backfill and piles on foundation impedance, in: *Proceedings of the 10th World Conference of Earthquake Engineering*, Madrid, Spain. pp. 1823–8.

Mylonakis, G., Gazetas, G., 2000. Seismic soil-structure interaction: beneficial or detrimental? *Journal of Earthquake Engineering* 4, 277–301. doi:10.1080/13632460009350372

Mylonakis, G., Gazetas, G., 1998. Vertical Vibration and Additional Distress of Grouped Piles in Layered Soil. *Soil and Foundations* 38, 1–14.

Mylonakis, G., Nikolaou, A., Gazetas, G., 1997. Soil-pile-bridge seismic interaction: kinematic and inertial effects. Part I: soft soil. *Earthquake engineering & structural dynamics* 26, 337–359.

Nogami, T., 1979. Dynamic group effect of multiple piles under vertical vibration, in: *Engineering Mechanics*. ASCE, pp. 750–754.

Nogami, T., Konagai, K., 1988. Time Domain Flexural Response of Dynamically Loaded Single Piles. *Journal of Engineering Mechanics* 114, 1512–1525. doi:10.1061/(ASCE)0733-9399(1988)114:9(1512)

Nogami, T., Konagai, K., 1987. Dynamic Response of Vertically Loaded Nonlinear Pile Foundations. *Journal of Geotechnical Engineering* 113, 147–160. doi:10.1061/(ASCE)0733-9410(1987)113:2(147)

Nogami, T., Novak, M., 1976. Soil-pile interaction in vertical vibration. *Earthquake Engineering & Structural Dynamics* 4, 277–293. doi:10.1002/eqe.4290040308

Nogami, T., Otani, J., Konagai, K., Chen, H., 1992. Nonlinear Soil - Pile Interaction Model for Dynamic Lateral Motion. *Journal of Geotechnical Engineering* 118, 89–106. doi:10.1061/(ASCE)0733-9410(1992)118:1(89)

Novak, M., 1974. Dynamic Stiffness and Damping of Piles. *Canadian Geotechnical Journal* 11, 574–598. doi:10.1139/t74-059

Novak, M., Nogami, T., 1977. Soil-pile interaction in horizontal vibration. *Earthquake Engineering & Structural Dynamics* 5, 263–281.

Novak, M., Sharnouby, B.E., 1984. Evaluation of Dynamic Experiments on Pile Group. *Journal of Geotechnical Engineering* 110, 738–756. doi:10.1061/(ASCE)0733-9410(1984)110:6(738)

Novak, M., Sheta, M., 1980. Approximate approach to contact effects of piles. *Dynamic response of pile foundations: analytical aspects* 53–79.

O'Neill, M., Dunnavant, T., 1985. An evaluation of the behaviour and Analysis of laterally loaded piles Groups, Research report NUHCE 85-11. University of Houston, 177p.

O'Neill, M.W., Gazioglu, S.M., 1984. An evaluation of ρ -y relationships in clays. University of Houston, Department of Civil Engineering.

Ousta, R., Shahrour, I., 2001. Three-dimensional analysis of the seismic behaviour of micropiles used in the reinforcement of saturated soil. *International Journal for Numerical and Analytical Methods in Geomechanics* 25, 183–196. doi:10.1002/nag.124

Padrón, L.A., Aznárez, J.J., Maeso, O., Santana, A., 2010. Dynamic stiffness of deep foundations with inclined piles. *Earthquake Engineering & Structural Dynamics* n/a–n/a. doi:10.1002/eqe.1000

Pearlman, S.L., Wolosick, J.R., 1993. Pinpiles for seismic rehabilitation of bridges. Presented at the 10th international bridge conference, Pittsburg, Pennsylvania.

Penzien, J., Scheffey, C.F., Parmelee, R.A., 1964. Seismic analysis of bridges on long pile. *Journal of the Engineering Mechanics Division* 90, 223–254.

Petrovski, J., Jurukovski, D., 1974. Static and dynamic test of piles under horizontal load.

Poulos, H.G., 1982. Single pile response to cyclic lateral load. *Journal of Geotechnical and Geoenvironmental Engineering* 108.

Poulos, H.G., 1971a. Behavior of laterally loaded piles II. Pile groups. *Journal of Soil Mechanics & Foundations Div* 97, 733–751.

Poulos, H.G., 1971b. Behavior of laterally loaded piles I. Single piles. *Journal of Soil Mechanics & Foundations Div* 97, 711–731.

Poulos, H.G., Davis, E.H., 1980. *Pile foundation analysis and design*, Series in geotechnical engineering. Wiley, New York.

Poulos, H.G., Randolph, M.F., 1983. Pile Group Analysis: A Study of Two Methods. *Journal of Geotechnical Engineering* 109, 355–372. doi:10.1061/(ASCE)0733-9410(1983)109:3(355)

Priestly, N., Singh, J., Youd, T., Rollins, K., 1991. Costa Rica earthquake of April 22, 1991: reconnaissance report. Earthquake Engineering Research Institute, Oakland.

Puri, V.K., Prakash, S., 1992. Observed and predicted response of piles under dynamic loads, in: *Piles under Dynamic Loads*. ASCE, pp. 153–169.

Ramberg, W., Osgood, W. R., 1943. Description of stress–strain curves by three parameters. Technical Note No. 902, National Advisory Committee For Aeronautics, Washington DC.

Randolph, M., 1980. PIGLET: a computer program for the analysis and design of pile groups under general loading conditions. University of Cambridge, Department of Engineering.

Randolph, M.F., 1981. The response of flexible piles to lateral loading. *Géotechnique* 31, 247–259. doi:10.1680/geot.1981.31.2.247

Reese, L., Cox, W., Koop, F., 1975. Field Testing and Analysis of Laterally Loaded Piles on Stiff Clay. The Offshore Technology Conference. doi:10.4043/2312-MS

Reese, L.C., Welch, R.C., 1975. Lateral loading of deep foundations in stiff clay. *Journal of Geotechnical and Geoenvironmental Engineering* 101.

Reese, L., Wright, S., Aurora, R., 1984. Analysis of a Pile Group Under Lateral Loading, in: Langer, J., Mosley, E., Thompson, C. (Eds.), *Laterally Loaded Deep Foundations: Analysis and Performance*. ASTM International, 100 Barr Harbor Drive, PO Box C700, West Conshohocken, PA 19428-2959, pp. 56–56–16.

Richards, T.D., Rothbauer, M.J., 2004. Lateral loads on pin piles (micropiles), in: *GeoSupport 2004: Drilled Shafts, Micropiling, Deep Mixing, Remedial Methods, and Specialty Foundation Systems*. ASCE, pp. 158–174.

Roesset, J., Angelides, D., 1980. 10. Dynamic stiffness of piles, in: *Numerical Methods in Offshore Piling*. Thomas Telford Publishing, pp. 75–81.

Rollins, K.M., Olsen, R.J., Egbert, J.J., Jensen, D.H., Olsen, K.G., Garrett, B.H., 2006. Pile spacing effects on lateral pile group behavior: load tests. *Journal of geotechnical and geoenvironmental engineering* 132, 1262–1271.

Rollins, K.M., Peterson, K.T., Weaver, T.J., 1998. Lateral load behavior of full-scale pile group in clay. *Journal of Geotechnical and Geoenvironmental Engineering* 124, 468–478.

RP2A-WSD, A., 2000. Recommended practice for planning, designing and constructing fixed offshore platforms—working stress design—, in: *Twenty-*

Sadek, M., Isam, S., 2004. Three-dimensional finite element analysis of the seismic behavior of inclined micropiles. *Soil Dynamics and Earthquake Engineering* 24, 473–485. doi:10.1016/j.soildyn.2004.02.002

Sadek, M., Shahrour, I., 2006. Influence of the head and tip connection on the seismic performance of micropiles. *Soil Dynamics and Earthquake Engineering* 26, 461 – 468. doi:http://dx.doi.org/10.1016/j.soildyn.2005.10.003

- Sa'don, N.M., 2012. Full scale static and dynamic lateral loading of a single pile. ResearchSpace@ Auckland.
- Scott, R., Tsai, C., Steussy, D., Ting, J., 1982. Full-scale dynamic lateral pile tests, in: 14th Annual Offshore Technology Conference. pp. 435–450.
- SeismoSoft, S., 2010. SeismoStruct, A computer program for static and dynamic nonlinear analysis of framed structures. Available from URL: www.seismosoft.com.
- Shadlou, M., Bhattacharya, S., 2014. Dynamic stiffness of pile in a layered elastic continuum. *Géotechnique* 64, 303–319. doi:10.1680/geot.13.P.107
- Shahrour, I., Juran, I., 2004. Seismic behaviour of micropile systems. *Ground Improvement* 8, 109–120. doi:10.1680/grim.8.3.109.41118
- Shahrour, I., Sadek, M., Ousta, R., 2001. Seismic Behavior of Micropiles used as Foundation Support Elements: Three-Dimensional Finite Element Analysis. *Transportation Research Record: Journal of the Transportation Research Board* 84–90.
- Shamouby, B.E., Novak, M., 1984. Dynamic Experiments with Group of Piles. *Journal of Geotechnical Engineering* 110, 719–737. doi:10.1061/(ASCE)0733-9410(1984)110:6(719)
- Sheta, M., Novak, M., 1982. Vertical vibration of pile groups. *Journal of Geotechnical and Geoenvironmental Engineering* 108.
- Shimomura, Y., Ikeda, Y., Ogushi, Y., Nakamura, M., Arai, T., 2004. Aging effects on dynamic soil spring of pile foundations based on forced vibration tests, in: *Proceedings of the 13th World Conference on Earthquake Engineering, Vancouver*.
- Stevens, J., Audibert, J., others, 1979. Re-examination of py curve formulations, in: *Offshore Technology Conference. Offshore Technology Conference*.
- Stockwell, R.G., Mansinha, L., Lowe, R., 1996. Localization of the complex spectrum: the S transform. *IEEE transactions on signal processing* 44, 998–1001.
- Structural Engineers Association of California, 1991. Reflections on the October 17, 1989 Loma Prieta earthquake, Chapter 6 Structural Pounding. *Ad Hoc Earthquake Reconnaissance*.
- Takeda T, Sozen M A, Nielsen N N., 1970. Reinforced concrete response to simulated earthquakes. *Journal of the Structural Division ASCE*; 96(12): 2557-2573.
- Taylor, G.E., Gularte, F.B., Gularte, G.G., 1998. Seismic retrofit of Fourth Street & Riverside viaducts with micropiles, in: *Soil Improvement for Big Digs. ASCE*, pp. 313–325.

Ting, J.M., 1987. Full-scale cyclic dynamic lateral pile responses. *Journal of Geotechnical engineering* 113, 30–45.

Tombari, A., Capatti, M.C., Dezi, F., El Naggar, M.H., 2013. The Influence of Soil Non-Linearity on the Seismic Response of Bridge Structures Supported on Extended Pile Shafts, in: *Proceedings of the 6th International Conference on Earthquake Geotechnical Engineering (ICEGE6) - Istanbul, Turkey*.

Trochanis, A., Bielak, J., Christiano, P., 1988. A three-dimensional nonlinear study of piles leading to the development of a simplified model (No. R-88-176). Dept. of Civil Engineering.

Trochanis, A.M., Bielak, J., Christiano, P., 1991. Three - Dimensional Nonlinear Study of Piles. *Journal of Geotechnical Engineering* 117, 429–447. doi:10.1061/(ASCE)0733-9410(1991)117:3(429)

Tuzuki, M., Inada, O., Yamaguchi, M., Yahata, K., Naito, Y., Kitamura, E., 1992. Field testing and analysis of dynamic loaded pile group, in: *Proc. 10th World Conf. On Earthquake Eng. pp. 1787–1790*.

Veletsos, A.S., Verbič, B., 1973. Vibration of viscoelastic foundations. *Earthquake Engineering & Structural Dynamics* 2, 87–102. doi:10.1002/eqe.4290020108

Walker, J., Cox, E., 1966. Design of pier foundations for lateral loads. *Transactions of the ASAE* 9, 417–4420.

Whitman, R., 1970. *Soil-structure interaction*. Massachusetts Inst. of Tech., Cambridge.

Wikipedia, 2016. Terremoto del Centro Italia del 2016 — Wikipedia, L'enciclopedia libera.

Wolf, J.P., 1987. *Soil-structure-interaction analysis in time domain*. AA Balkema Publishers, United States.

Wolf, J.P., 1985. *Dynamic soil-structure interaction*, Prentice-Hall international series in civil engineering and engineering mechanics. Prentice-Hall, Englewood Cliffs, N.J.

Wolf, J. P., 1994. *Foundation Vibration Analysis using Simple Physical Models*, Prentice-Hall Inc., Englewood Cliffs, New Jersey.

Wolf, J.P., Meek, J.W., Song, C., 1992. Cone models for a pile foundation, in: *Piles Under Dynamic Loads-Sessions Proceedings/ASCE National Convention*.

Wolf, J. P., Meek, J. W., 1994. Dynamic stiffness of foundation on layered soil halfspace using cone frustums, *Earthquake Engineering and Structural Dynamics*, 1079-1095.

Wolf, J., Von Arx, G., 1978. Impedance function of a group of vertical piles, in: *From Volume I of Earthquake Engineering and Soil Dynamics—Proceedings of the ASCE Geotechnical Engineering Division Specialty Conference, June 19-21, 1978, Pasadena, California*. Sponsored by Geotechnical Engineering Division of ASCE in Cooperation With:

Wong, J., *The seismic behaviour of micropiles (Master)*. Washington State University, WA, USA.

Wong, P.C.-W., Kulhawy, F.H., Ingraffea, A.R., 1989. Numerical modeling of interface behavior for drilled shaft foundations under generalized loading, in: *Foundation Engineering: Current Principles and Practices*. ASCE, pp. 565–579.

Wu, G., Finn, W., 1997. Dynamic nonlinear analysis of pile foundations using finite element method in the time domain. *Canadian Geotechnical Journal* 34, 44–52. doi:10.1139/t96-088

Wu, G., Finn, W.D.L., 1997. Dynamic elastic analysis of pile foundations using finite element method in the frequency domain. *Canadian Geotechnical Journal* 34, 34–43. doi:10.1139/cgj-34-1-34

Yamane, T., Nakata, Y., Otani, Y., 2000. Efficiency of micropile for seismic retrofit of foundation system, in: *12th World Conference on Earthquake Engineering, Auckland, New Zealand*. pp. 1–8.

Yang, J., McManus, K.J., Berrill, J.B., 2000. Kinematic soil-micropile interaction, in: *12th World Conference on Earthquake Engineering, Auckland, New Zealand*. pp. 1–8.

Yegian, M., Wright, S.G., 1973. Lateral Soil Resistance Displacement Relationships for Pile Foundation in Soft clays. *Offshore Technology Conference*. doi:10.4043/1893-MS

Zelenko, B.H., Bruce, D.A., Schoenwolf, D.A., Traylor, R.P., 1998. Micropile Application for Seismic Retrofit Preserves Historic Structure in Old San Juan, Puerto Rico, in: *Grouts and Grouting: A Potpourri of Projects*. ASCE, pp. 43–62.

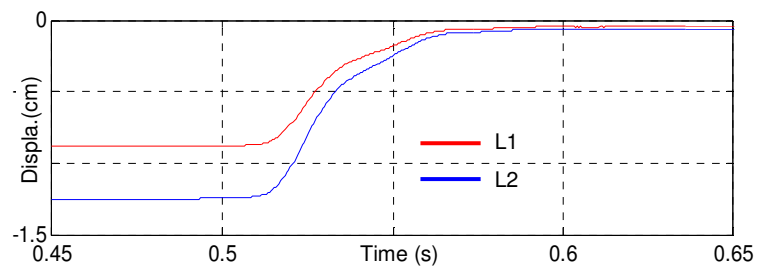
Zienkiewicz, O., Chang, C., Bettess, P., 1980. Drained, undrained, consolidating and dynamic behaviour assumptions in soils. *Geotechnique* 30, 385–395.

Appendix A.

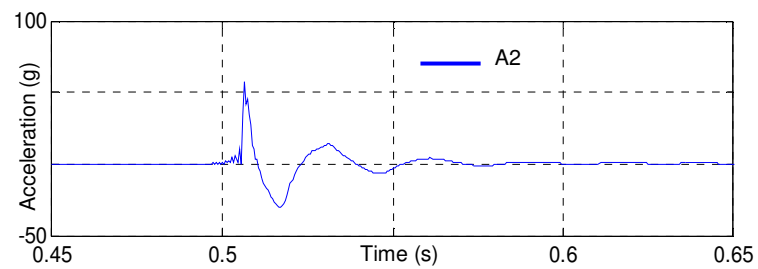
Experimental Data

A.1. Free Vibration Tests on P1

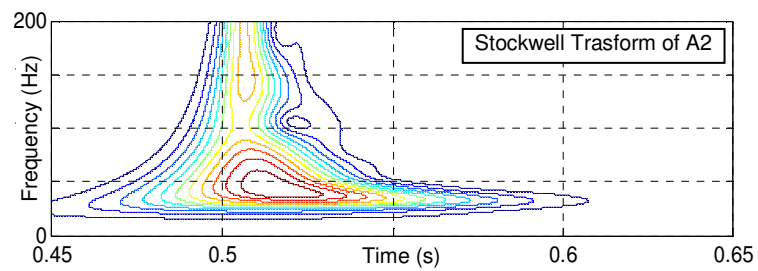
Displacements (a) and acceleration (b) time histories registered during free vibration test F1-T1 on micropile P1; (c) S-Transform of acceleration.



(a)

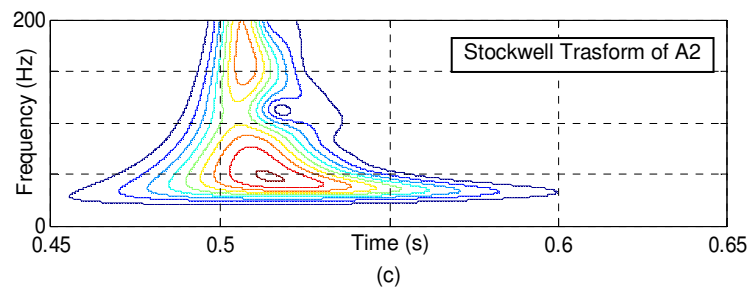
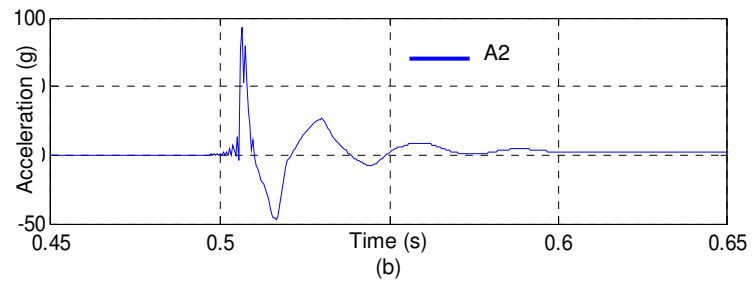
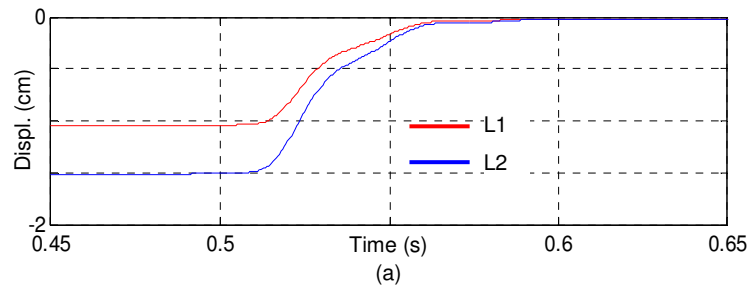


(b)

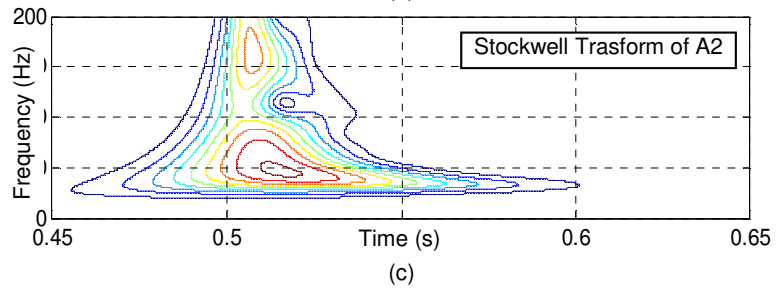
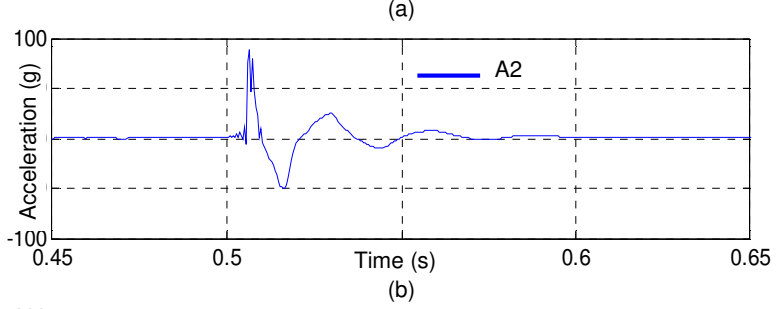
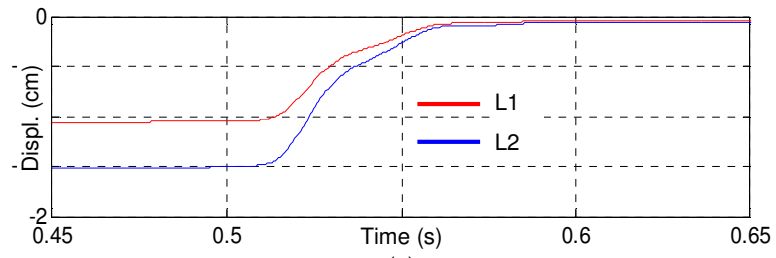


(c)

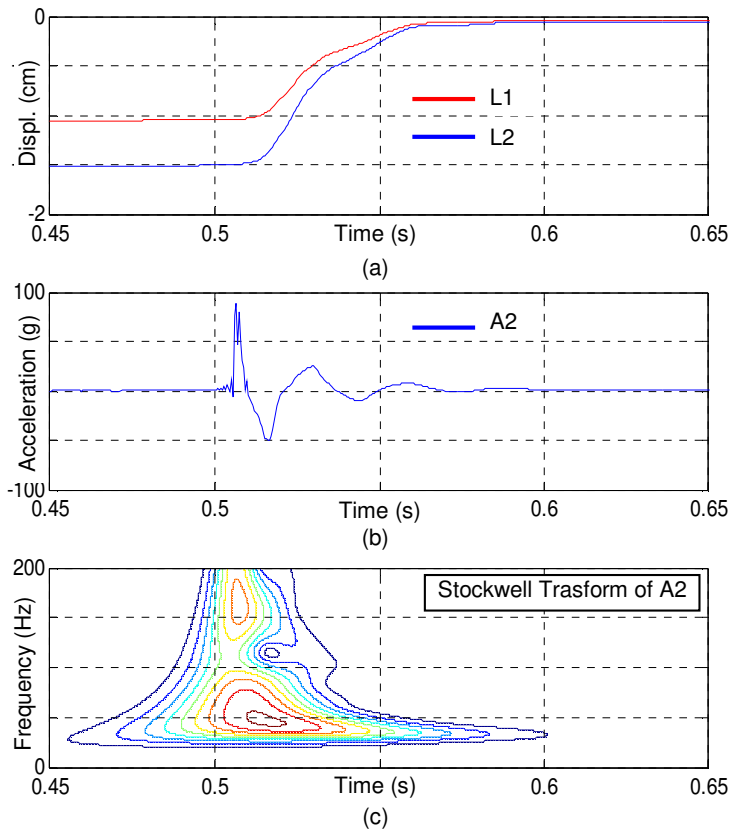
Displacements (a) and acceleration (b) time histories registered during free vibration test F2-T1 on micropile P1; (c) S-Transform of acceleration.



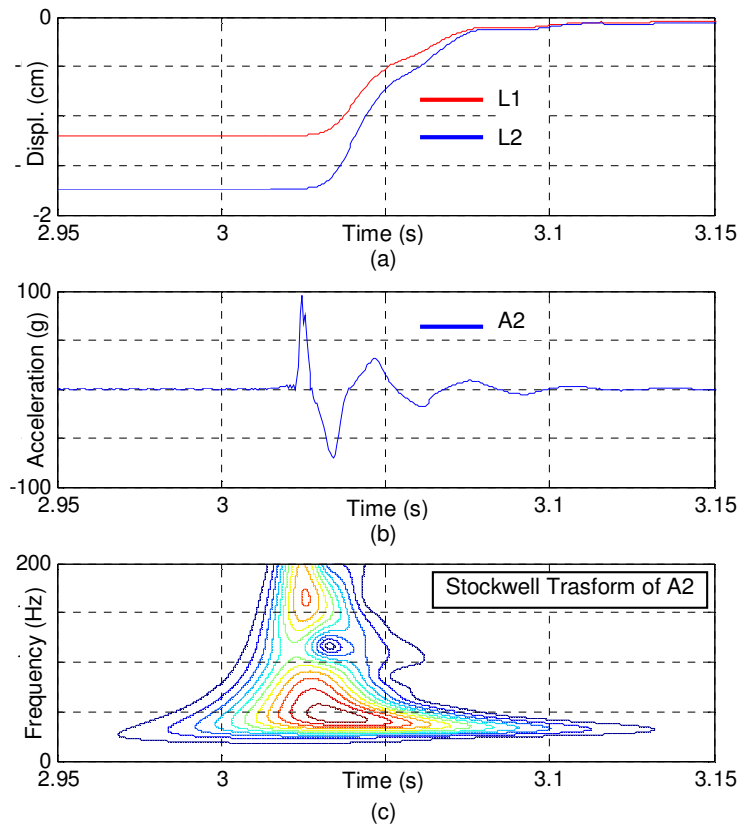
Displacements (a) and acceleration (b) time histories registered during free vibration test F2-T2 on micropile P1; (c) S-Transform of acceleration.



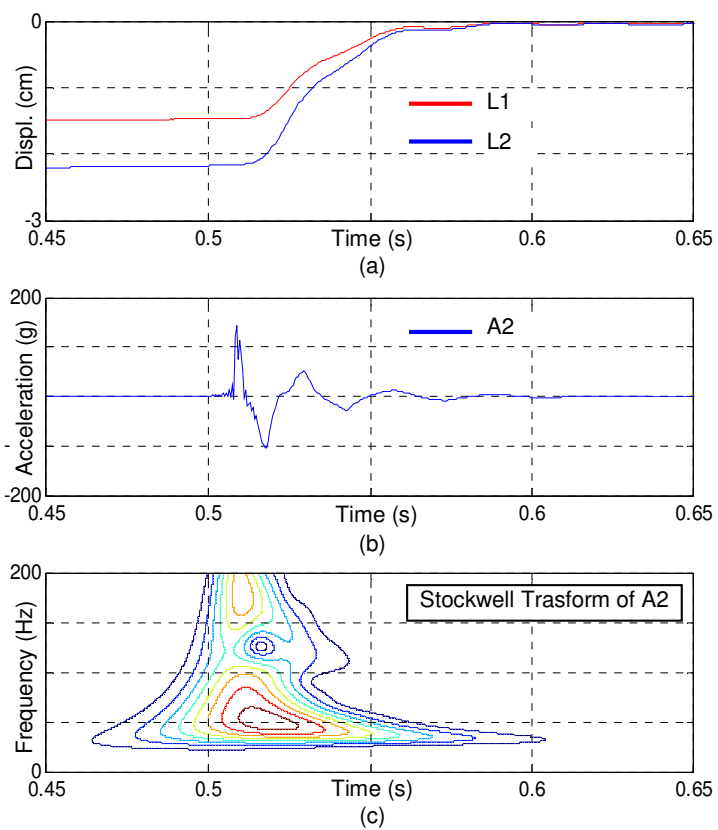
Displacements (a) and acceleration (b) time histories registered during free vibration test F3-T1 on micropile P1; (c) S-Transform of acceleration.



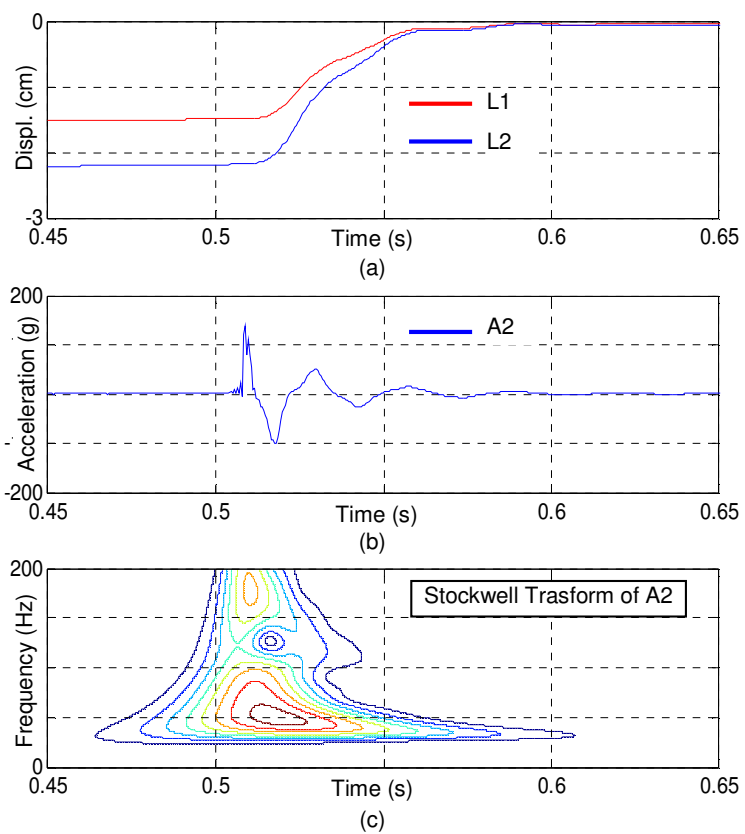
Displacements (a) and acceleration (b) time histories registered during free vibration test F3-T2 on micropile P1; (c) S-Transform of acceleration.



Displacements (a) and acceleration (b) time histories registered during free vibration test F4-T1 on micropile P1; (c) S-Transform of acceleration.

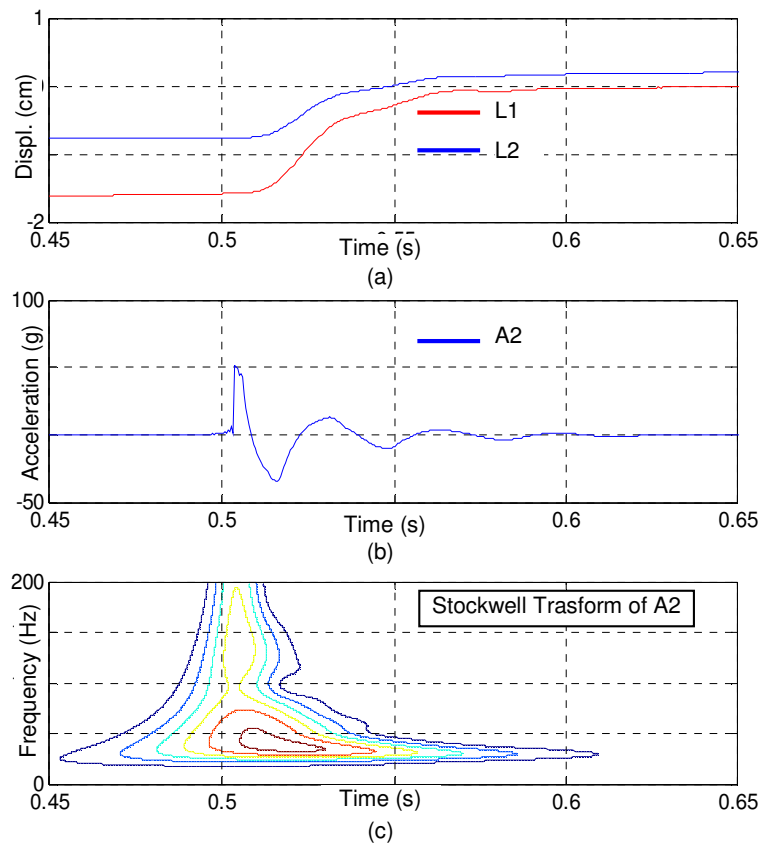


Displacements (a) and acceleration (b) time histories registered during free vibration test F4-T2 on micropile P1; (c) S-Transform of acceleration.

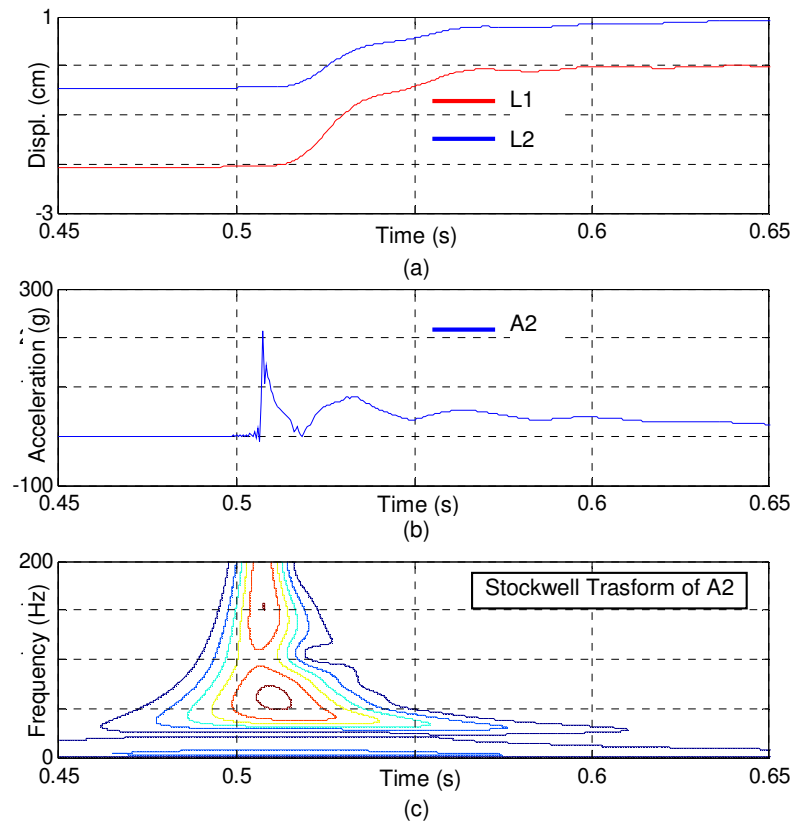


A.2. Free Vibration Tests on P2

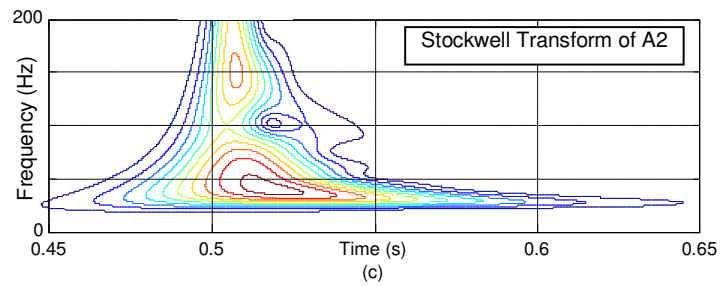
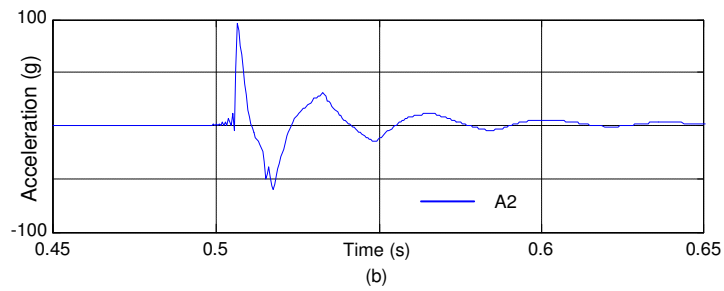
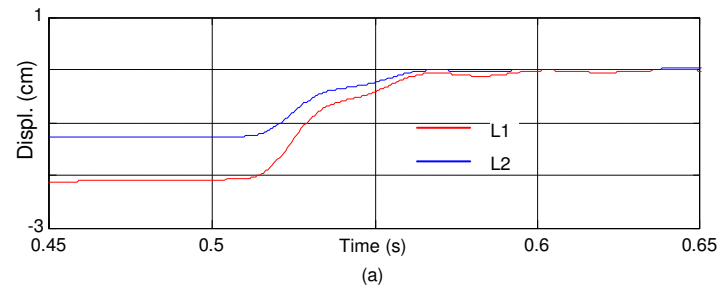
Displacements (a) and acceleration (b) time histories registered during free vibration test F1-T1 on micropile P2; (c) S-Transform of acceleration.



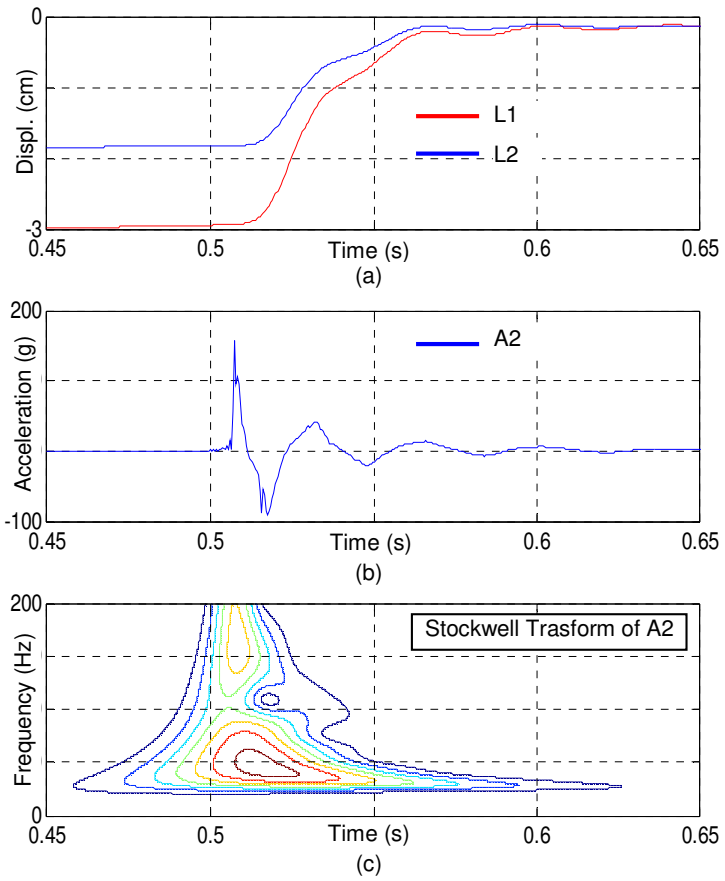
Displacements (a) and acceleration (b) time histories registered during free vibration test F1-T2 on micropile P2; (c) S-Transform of acceleration.



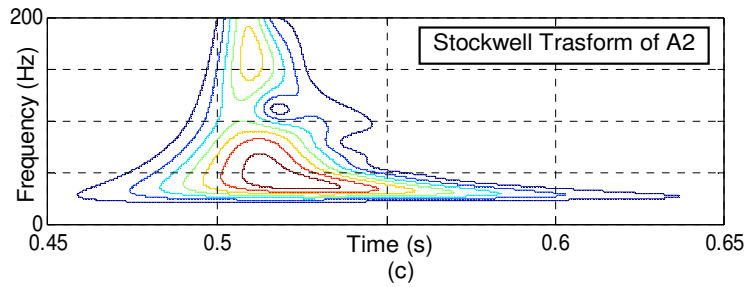
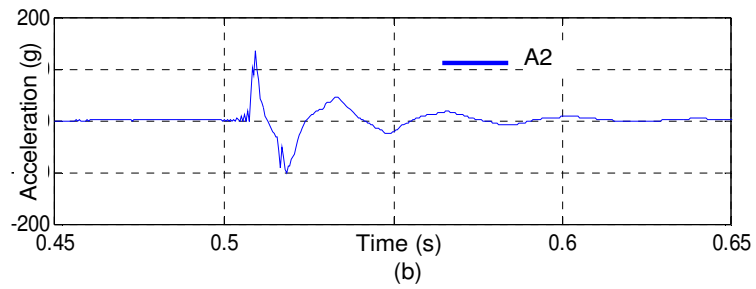
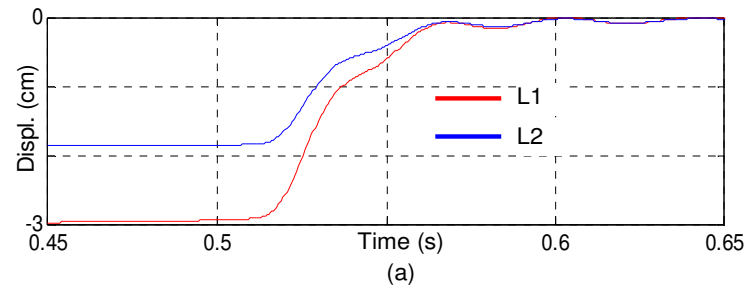
Displacements (a) and acceleration (b) time histories registered during free vibration test F2-T2 on micropile P2; (c) S-Transform of acceleration.



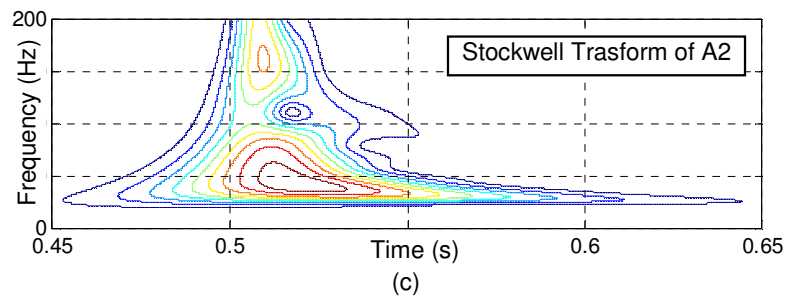
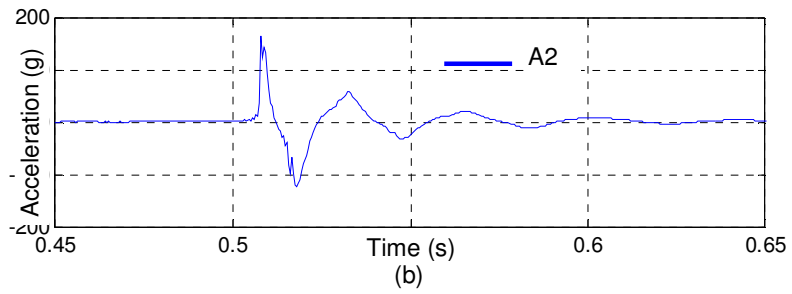
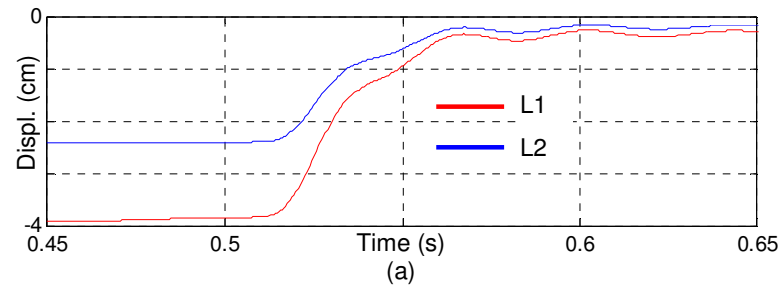
Displacements (a) and acceleration (b) time histories registered during free vibration test F3-T1 on micropile P2; (c) S-Transform of acceleration.



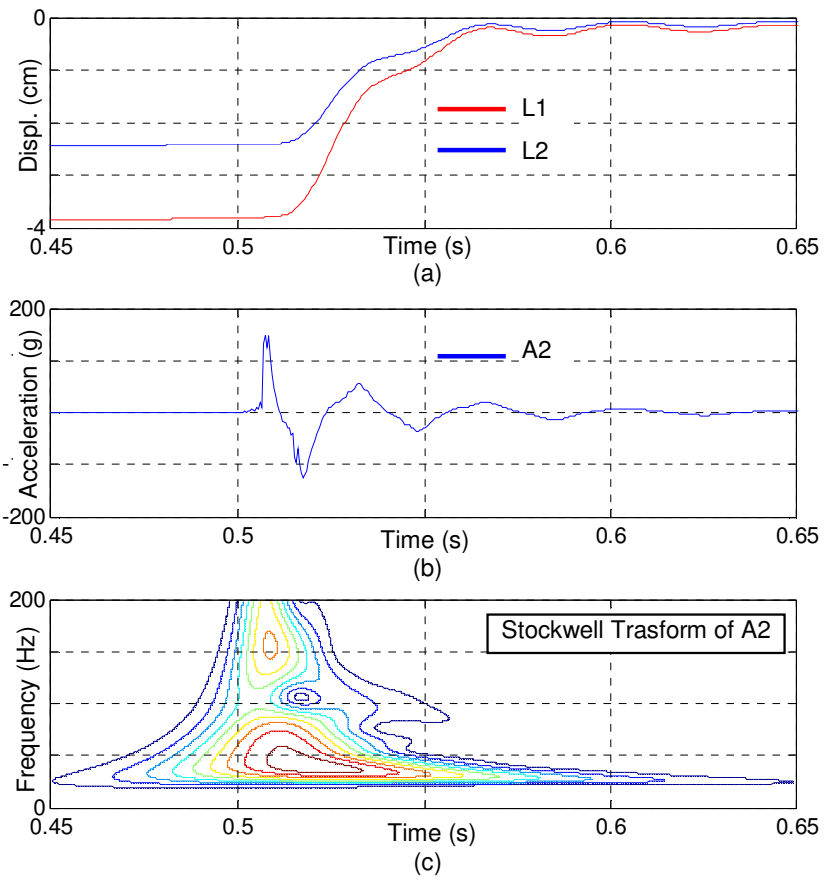
Displacements (a) and acceleration (b) time histories registered during free vibration test F3-T2 on micropile P2; (c) S-Transform of acceleration.



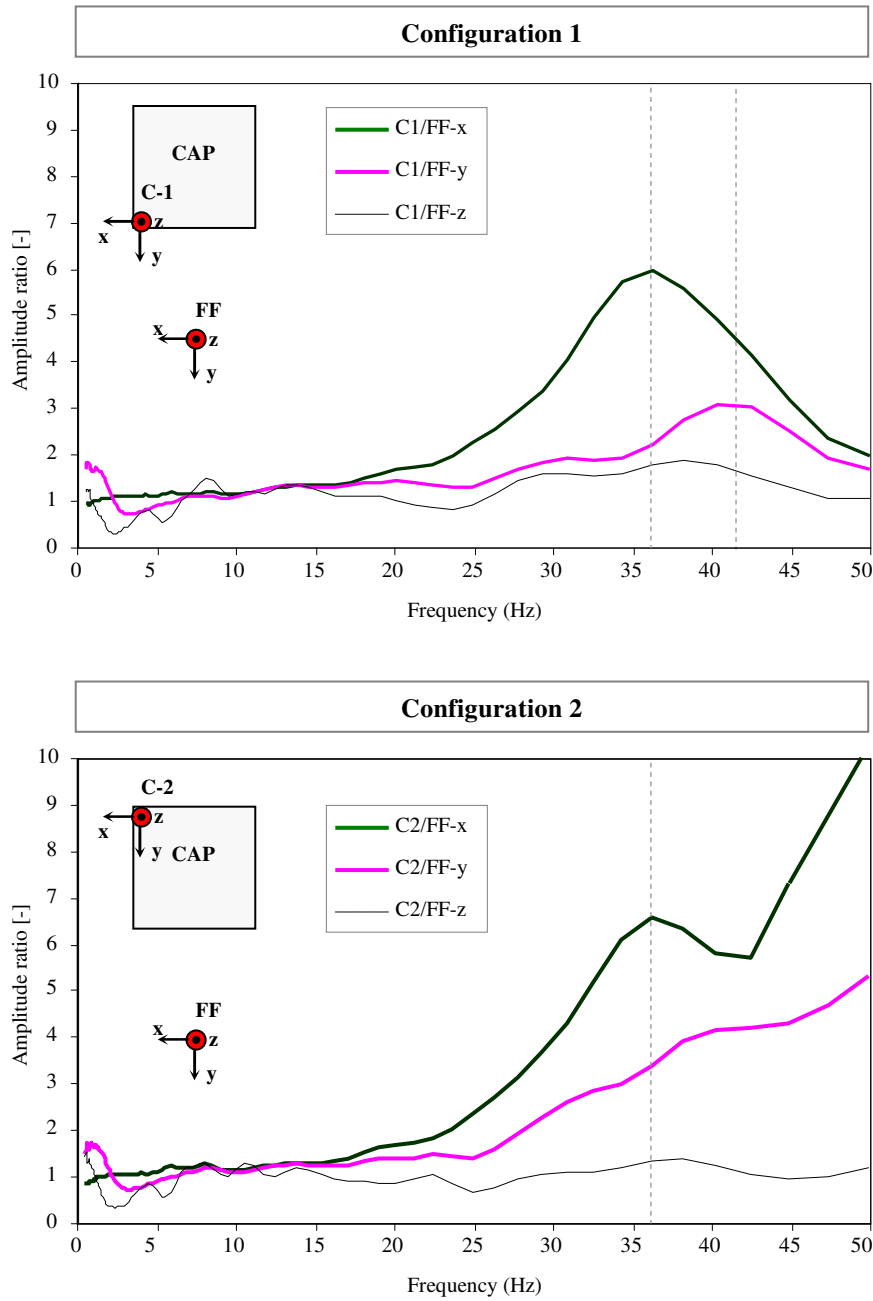
Displacements (a) and acceleration (b) time histories registered during free vibration test F4-T1 on micropile P2; (c) S-Transform of acceleration.

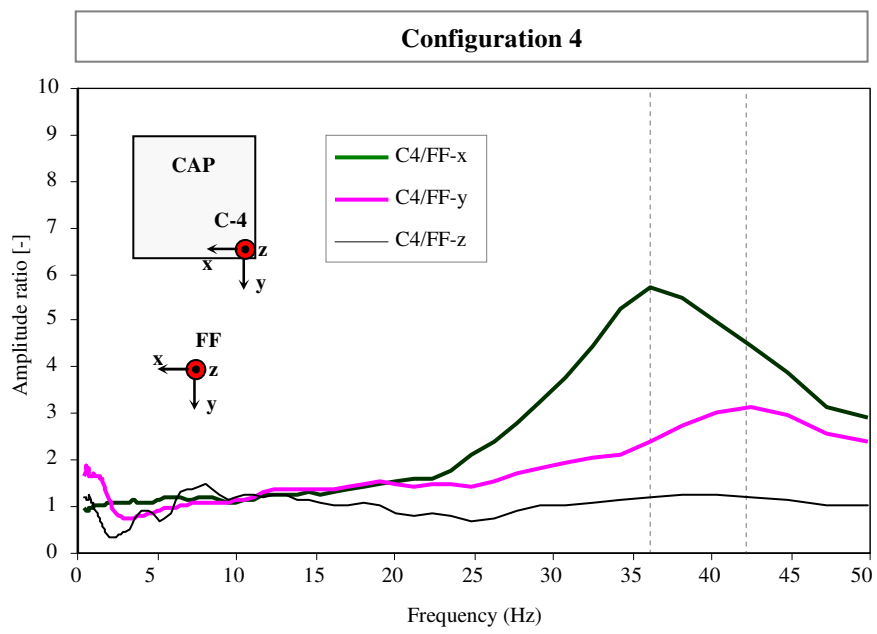
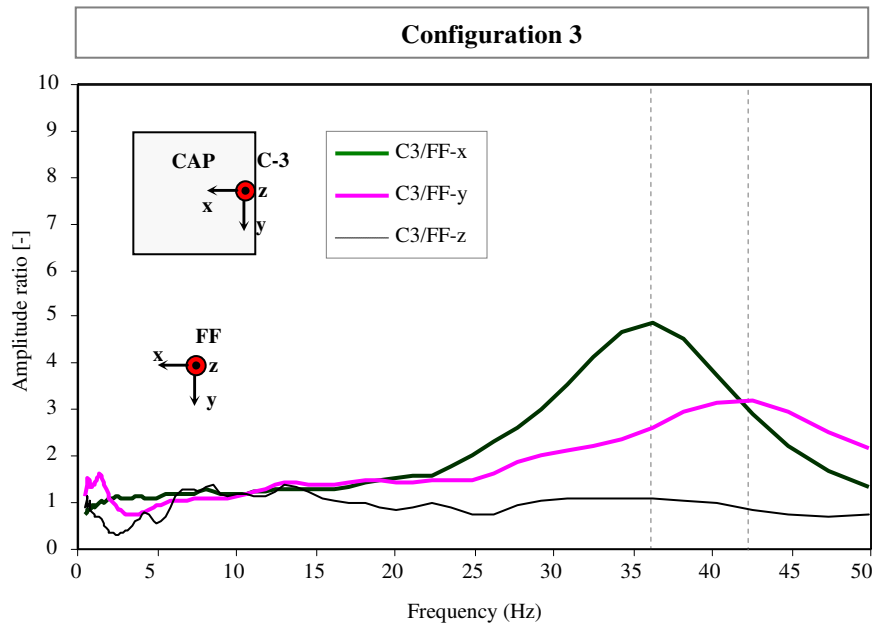


Displacements (a) and acceleration (b) time histories registered during free vibration test F4-T2 on micropile P2; (c) S-Transform of acceleration.

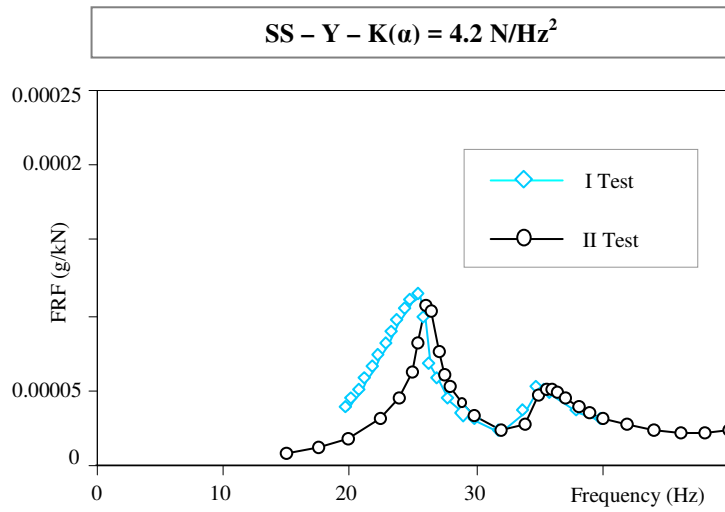
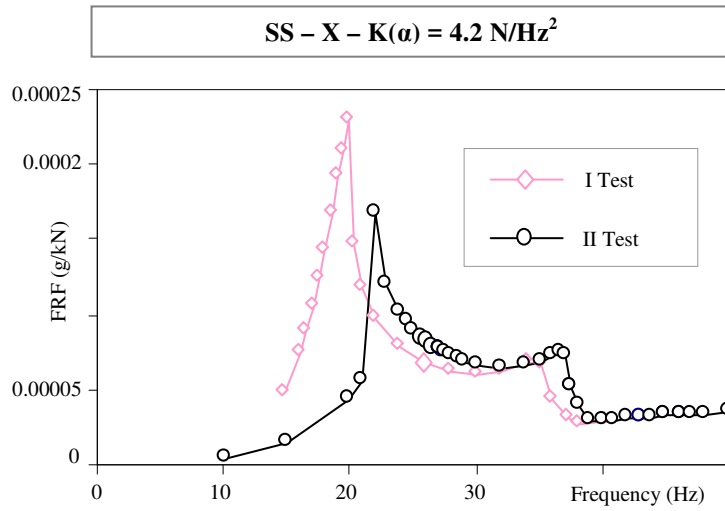


A.3. Ambient Vibration Test on inclined micropile group

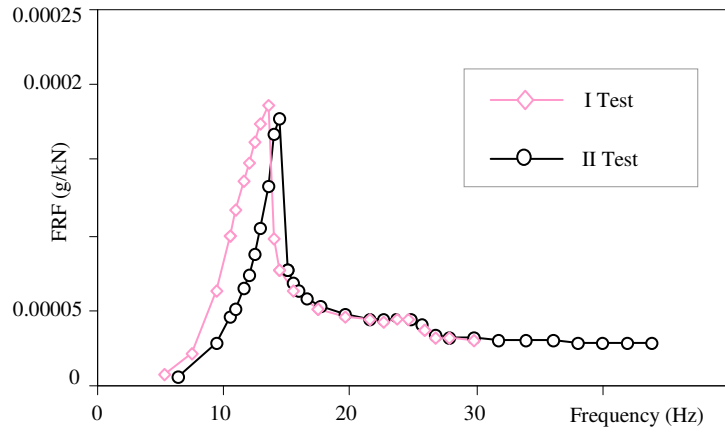




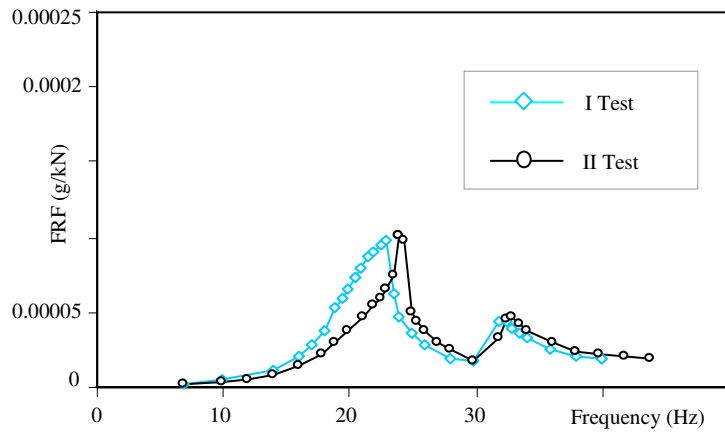
A.4. Repetitions of Stepped Sine tests on micropiles group



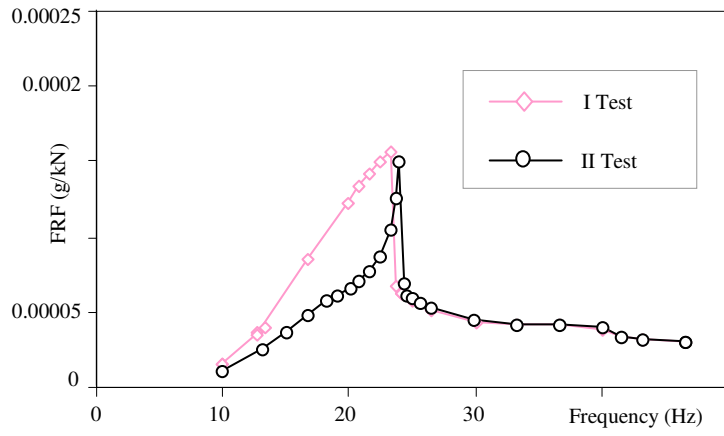
SS - X - $K(\alpha) = 8.3 \text{ N/Hz}^2$



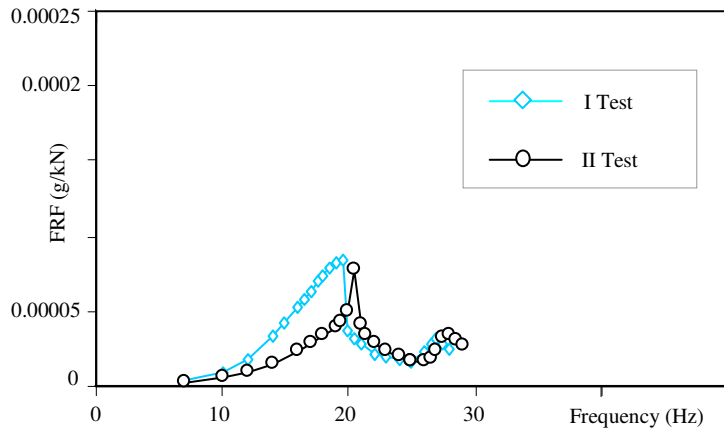
SS - Y - $K(\alpha) = 8.3 \text{ N/Hz}^2$



SS - X - $K(\alpha) = 23.4 \text{ N/Hz}^2$



SS - Y - $K(\alpha) = 23.4 \text{ N/Hz}^2$



A.5. Mohr Coulomb criterion in ABAQUS

The Mohr-Coulomb criterion assumes that yield occurs when the shear stress on any point in a material reaches a value that depends linearly on the normal stress in the same plane. The Mohr-Coulomb model (Figure A-1) is based on plotting Mohr's circle for states of stress at yield in the plane of the maximum and minimum principal stresses. The yield line is the best straight line that touches these Mohr's circles. Therefore, the Mohr-Coulomb model is defined by

$$\tau = c - \sigma \tan \phi \quad (\text{A.1})$$

where σ is negative in compression. From Mohr's circle,

$$\tau = s \cos \phi \quad (\text{A.2})$$

$$\sigma = \sigma_m + s \sin \phi. \quad (\text{A.3})$$

Substituting for τ and σ , multiplying both sides by $\cos \phi$, and reducing, the Mohr-Coulomb model can be written as

$$s + \sigma_m \sin \phi - c \cos \phi = 0, \quad (\text{A.4})$$

where

$$s = \frac{1}{2}(\sigma_1 - \sigma_3) \quad (\text{A.5})$$

is half of the difference between the maximum principal stress, σ_1 , and the minimum principal stress, σ_3 (and is, therefore, the maximum shear stress),

$$\sigma_m = \frac{1}{2}(\sigma_1 + \sigma_3) \quad (\text{A.6})$$

is the average of the maximum and minimum principal stresses, and ϕ is the friction angle.

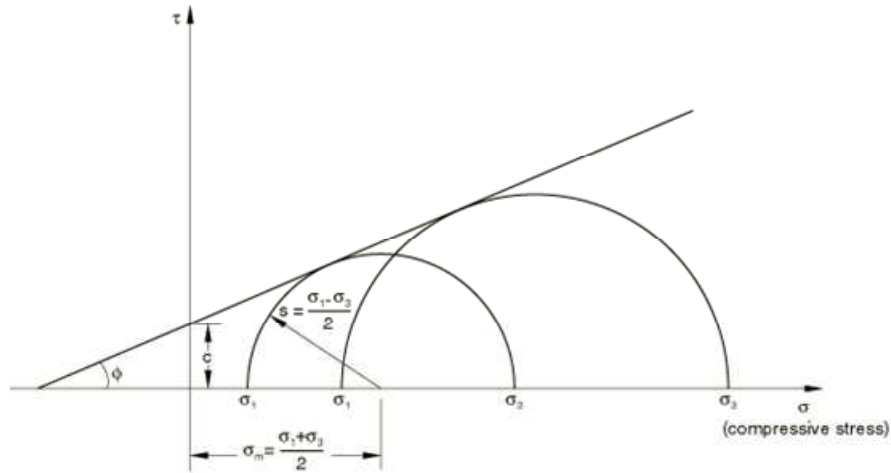


Figure A-1. Mohr Coulomb Yield Model

For general states of stress the model is more conveniently written in terms of three stress invariants as

$$F = R_{mc}q - p \tan \phi - c = 0, \quad (\text{A.7})$$

where

$$R_{mc}(\Theta, \phi) = \frac{1}{\sqrt{3} \cos \phi} \sin\left(\Theta + \frac{\pi}{3}\right) + \frac{1}{3} \cos\left(\Theta + \frac{\pi}{3}\right) \tan \phi, \quad (\text{A.8})$$

ϕ is the slope of the Mohr-Coulomb yield surface in the p - $R_{mc}q$ stress plane, which is commonly referred to as the friction angle of the material and can depend on temperature and predefined field variables; c is the cohesion of the material; and Θ is the deviatoric polar angle defined as

$$\cos(3\Theta) = \left(\frac{r}{q}\right)^3, \quad (\text{A.9})$$

$$p = -\frac{1}{3} \text{trace}(\boldsymbol{\sigma}), \quad (\text{A.10})$$

is the equivalent pressure stress,

$$q = \sqrt{\frac{3}{2}(\mathbf{S} : \mathbf{S})}, \quad (\text{A.11})$$

is the Mises equivalent stress,

$$r = \left(\frac{9}{2} \mathbf{S} \cdot \mathbf{S} : \mathbf{S}\right)^{\frac{1}{3}}, \quad (\text{A.12})$$

is the third invariant of deviatoric stress, and

$$\mathbf{S} = \boldsymbol{\sigma} + p\mathbf{I}, \quad (\text{A.13})$$

is the deviatoric stress.

The friction angle, ϕ , controls the shape of the yield surface in the deviatoric plane as shown in Figure A-2. The tension cutoff surface is shown for a meridional angle of $\Theta = 0$. The friction angle range is $0^\circ < \phi < 90^\circ$. In the case of $\phi = 0$ the Mohr-Coulomb model reduces to the pressure-independent Tresca model with a perfectly hexagonal deviatoric section. In the case of $\phi = 90^\circ$ the Mohr-Coulomb model reduces to the ‘‘tension cut-off’’ Rankine model with a triangular deviatoric section and $R_{mc} = \infty$ (this limiting case is not permitted within the Mohr-Coulomb model described here).

Isotropic cohesion hardening is assumed for the hardening behavior of the Mohr-Coulomb yield surface. The hardening curve must describe the cohesion yield stress as a function of plastic strain and, possibly, temperature and predefined field variables. In defining this dependence at finite strains, ‘‘true’’ (Cauchy) stress and logarithmic strain values should be given. An optional tension cutoff hardening (or softening) curve can be specified. Rate dependency effects are not accounted for in this plasticity model. The flow potential, for the Mohr-Coulomb yield surface is chosen as a hyperbolic function in the meridional stress plane and the smooth elliptic function proposed by Menétrey and Willam (1995) in the deviatoric stress plane. Since the plastic flow is nonassociated in general, the use of this

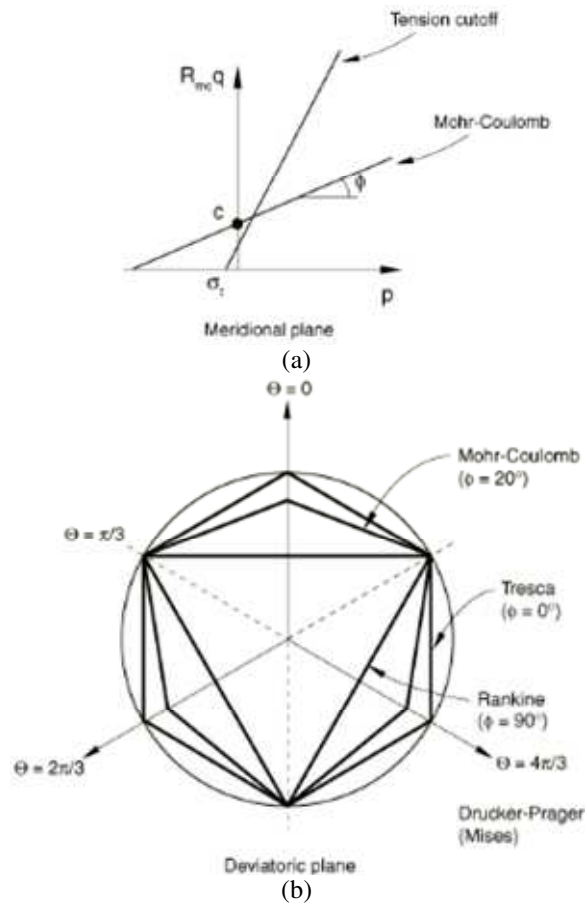


Figure A-2 Mohr-Coulomb and tension cutoff surfaces in meridional (a) and deviatoric (b) planes

Mohr-Coulomb model generally requires the unsymmetric matrix storage and solution scheme in Abaqus/Standard.
 For the present application, a pressure-independent Tresca Model is adopted.